Uncovering atrial fibrillation complexity: from signals to (bio)markers

Roeliene Starreveld - Brand

ISBN 978-94-6421-241-9
Lay-out and design Daniëlle Balk | www.persoonlijkproefschrift.nl
Printing Ipskamp Printing | proefschriften.net

Uncovering Atrial Fibrillation Complexity:

From signals to (bio)markers

Complexiteit van boezemfibrilleren ontrafeld:

van signalen naar (bio)markers

Proefschrift

ter verkrijging van de graad van doctor aan de

Erasmus Universiteit Rotterdam

op gezag van de

rector magnificus

Prof. dr. F.A. van der Duijn Schouten

en volgens besluit van het College voor Promoties.

De openbare verdediging zal plaatsvinden op

Woensdag 31 maart om 10.30 uur

Roeliene Starreveld - Brand

geboren te Hengelo (Overijssel)

Erasmus University Rotterdam

Promotiecommissie

Promotoren:	Prof. dr. N.M.S. de Groot
	Prof. dr. B.J.J.M. Brundel
Overige leden:	Prof. dr. F. Zijlstra
	Prof. dr. A.J.J.C. Bogers
	Prof. dr. A. Alings

Financial support by the Dutch Heart Foundation for the publication of this thesis is gratefully acknowledged. The research described in this thesis was supported by a grant of the Dutch Heart Foundation (DHF 14728).

Financial support by Medical Delta for publication of this thesis is gratefully acknowledged. The research described in this thesis was performed in the framework of the Medical Delta Cardiac Arrhythmia Lab.

List of contents

Chapter 1	**General introduction and outline of this thesis** Roeliene Starreveld	9
Chapter 2	**Atrial fibrillation fingerprinting; spotting bio-electrical markers to early recognize atrial fibrillation by the use of a bottom-up approach (AFFIP): rationale and design** Roeliene Starreveld, Paul Knops, Kennedy S. Ramos, Maarten C. Roos-Serote, Ad J.J.C. Bogers, Bianca J.J.M. Brundel, Natasja M.S. de Groot *Clinical Cardiology. 2020 Jun;43(6):546-552*	27
Chapter 3	**Direction- and rate-dependent fractionation during atrial fibrillation persistence: unmasking cardiac anisotropy?** Roeliene Starreveld, Natasja M.S. de Groot *Journal of Cardiovascular Electrophysiology. 2020 Aug;31(8):2206-2209*	43
Chapter 4	**Anatomical hotspots of fractionated electrograms in the left and right atrium: do they exist?** Roeliene Starreveld, Lisette J.M.E. van der Does, Natasja M.S. de Groot *Europace. 2019 Jan;21(1):60-72*	53
Chapter 5	**The impact of filter settings on morphology of unipolar fibrillation potentials** Roeliene Starreveld, Paul Knops, Maarten C. Roos-Serote, Charles Kik, Ad J.J.C. Bogers, Bianca J.J.M. Brundel, Natasja M.S. de Groot *Journal of Cardiovascular Translational Research. 2020 Dec;13(6):953-964*	83
Chapter 6	**Classification of sinus rhythm single potential morphology in patients with mitral valve disease** Mathijs S. van Schie, Roeliene Starreveld, Maarten C. Roos-Serote, Yannick J.H.J. Taverne, Frank R.N. van Schaagen, Ad J.J.C. Bogers, Natasja M.S. de Groot *Europace. 2020 Oct;22(10):1509-1519*	105
Chapter 7	**Do atrial fibrillation episodes affect sinus rhythm voltage fingerprints in patients with mitral valve disease?** Mathijs S. van Schie, Roeliene Starreveld, Ad J.J.C. Bogers, Natasja M.S. de Groot *Europace. 2021 Jan:euaa336*	125
Chapter 8	**Unipolar atrial electrogram morphology from an epicardial and endocardial perspective** Lisette J.M.E. van der Does, Paul Knops, Christophe P. Teuwen, Corina Serban, Roeliene Starreveld, Eva A.H. Lanters, Elisabeth M.J.P. Mouws, Charles Kik, Ad J.J.C. Bogers, Natasja M.S. de Groot *Heart Rhythm. 2018 Jun;15(6):879-887*	145

Chapter 9 **Detection of endo-epicardial asynchrony in the atrial wall using one-sided unipolar and bipolar electrograms** 171

Lisette J.M.E. van der Does, Roeliene Starreveld, Rohit K. Kharbanda, Paul Knops, Charles Kik, Ad J.J.C. Bogers, Natasja M.S. de Groot

Submitted

Chapter 10 **The impact of obesity on early postoperative atrial fibrillation burden** 195

Corina Serban, John T. Arinze, Roeliene Starreveld, Eva A.H. Lanters, Ameeta Yaksh, Charles Kik, Yalin Acardag, Paul Knops, Ad J.J.C. Bogers, Natasja M.S. de Groot

Journal of Thoracic and Cardiovascular Surgery. 2020 Mar;159(3):930-938

Chapter 12 **Biomarkers to non-invasively determine the atrial fibrillation progression phenotype: a bridge to individualized ablative therapy?** 215

Roeliene Starreveld, Natasja M.S. de Groot

Heart Rhythm. 2018 Aug;15(8):1138-1139

Chapter 13 **Daily supplementation of L-glutamine in atrial fibrillation patients: the effect on heat shock proteins and metabolites** 221

Roeliene Starreveld, Kennedy S. Ramos, Agnes J.Q.M. Muskens, Bianca J.J.M. Brundel, Natasja M.S. de Groot

Cells. 2020 Jul;9(7):1729

Chapter 14 **General discussion** 249

Roeliene Starreveld

Chapter 15 **English summary** 271

Roeliene Starreveld

Chapter 16 **Nederlandse samenvatting** 281

Roeliene Starreveld

1

General introduction

Roeliene Starreveld

Atrial fibrillation (AF) is the most common sustained cardiac arrhythmia affecting worldwide about 33.5 million individuals[1]. Its exact pathophysiology, however, remains incompletely understood and there still is no curative therapy. AF occurs when a chaotic pattern of rapid electrical activity in the atria suppresses or replaces the normal sinus mechanism, resulting in ineffective rapid atrial contractions and a nearly 5-fold increased risk of stroke[2, 3]. Unfortunately, treatment modalities for AF such as anti-arrhythmic drug therapy, electrical cardioversion and ablative therapy are only moderately effective and frequently exhibit high AF recurrence rates. This chapter introduces the challenging world of AF, including its etiology and the search for optimal treatment strategies.

The growing epidemic of atrial fibrillation

Risk of developing AF strongly increases with age (*Figure 1*) and the presence and severity of underlying heart disease, particularly congestive heart failure and valvular disease.[4]

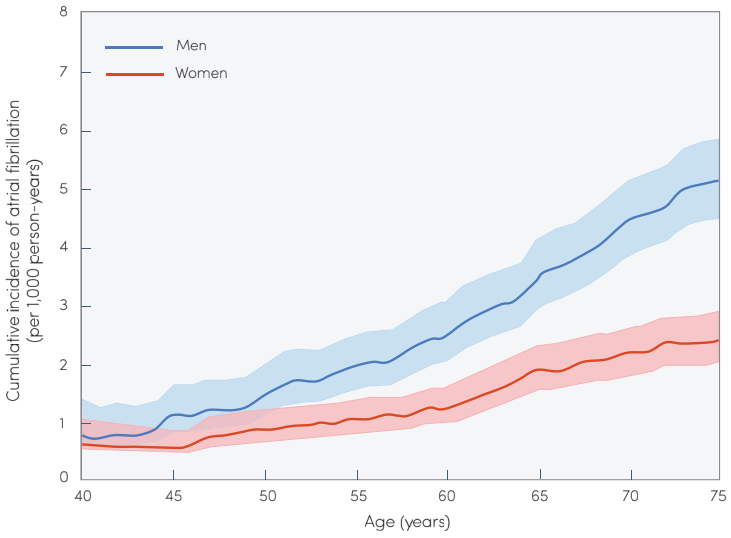

Figure 1 – The increasing incidence of atrial fibrillation with age. The plot shows the cumulative incidence of atrial fibrillation per 1,000 person-years in men (blue line) and women (red line), with the respective 95% confidence intervals (shaded areas), as reported in a large Dutch cohort study. Modified from Vermond et al.[5]

Due to the constantly increasing life expectancy worldwide, incidence of AF has progressively increased in the past decades. Currently, men and women of 40 years and older have a risk of about 25% of developing AF during their life.[6] Worldwide prevalence of AF in persons aged 60 to 65 years is about 1% and increases up to

10% in persons older than 80 years.[4] Based on projections, it is estimated that the total number of AF patients in the Netherlands will rise to approximately half a million in 2050 (95% CI: 0.42-0.74), with more than 75% being 75 years and older.[7]

Though not confined to any limitations, AF is more prevalent in men than in women (age-adjusted prevalence of 5.96 per 1000 versus 3.73 per 1000, respectively[1]) and in obese patients than in non-obese patients (3.8-5.8% excess risk of AF for every unit of body mass index (BMI) increase[8]). About 25% of patients undergoing bypass surgery and 40% of patients undergoing valvular surgery develop new-onset AF.[9] Commonly associated conditions furthermore include hypertension, diabetes and sleep-disordered breathing.[4] All these numbers clearly evince the growing epidemic of AF and emphasize the need for a better understanding of its pathophysiology.

Atrial fibrillation: chaos above order

In normal heart rhythm, electrical activation of the heart is initiated at the sinus node in the right atrium with rates between 60 and 100 per minute, and regularly spreads through the atrial myocardium towards the atrioventricular (AV) node and via the His-Purkinje fibers to the ventricles of the heart. During AF there is no coordinated electric activity, as multiple areas of atrial myocardium depolarize simultaneously and independently, with rates up to 600 times per minute (*Figure 2*). Propagation towards the ventricles of the heart is reduced by the AV node, yet the ventricular rate can be more than 200 times per minute. Diagnosis of AF entails a surface electrocardiogram demonstrating continuous atrial activation (no distinct p-waves) and irregular ventricular rate (R-R interval).

Symptoms commonly accompanying AF are high resting heart rate, irregular palpitations, dizziness, shortness of breath, decreased exercise intolerance and/or chest pain. Nevertheless, some patients lack any symptoms while having AF and can remain undiagnosed for years (so-called 'silent AF'). In contrast to ventricular arrhythmias, AF usually only has little negative hemodynamic effect and short-term prognosis of AF is therefore rather good. On the long-term however, the rapid heart rates and ineffective atrial contractions during AF can cause heart failure and stasis of blood provoking stroke, leading to an increased risk of all-cause mortality.[3, 10] To reduce clotting of blood, AF patients with additional risk factors for stroke, such as age ≥ 65 years, history of heart failure, hypertension, stroke, vascular disease or diabetes are required to use oral anticoagulants.[11, 12]

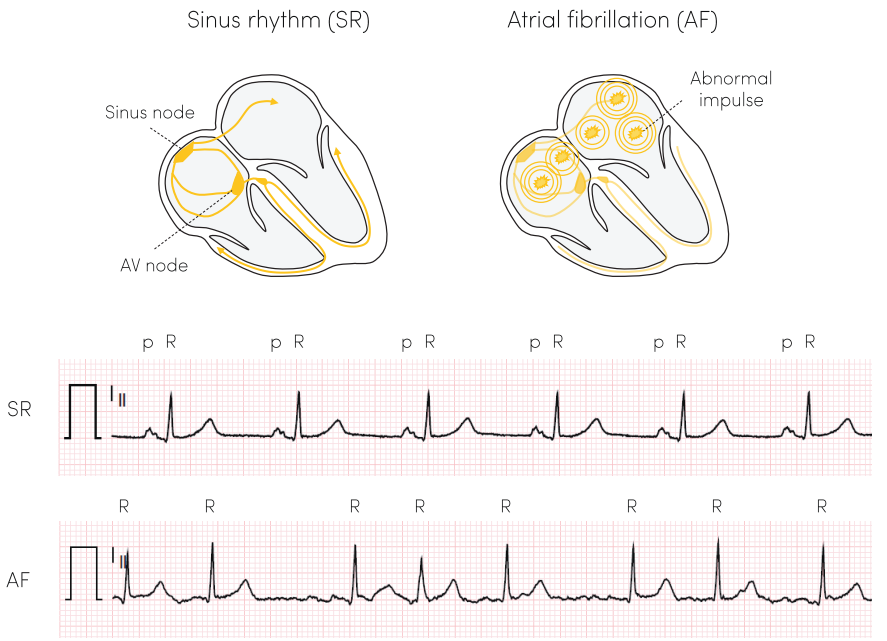

Figure 2 - Electrical conduction in normal sinus rhythm and during atrial fibrillation. *Upper panel:* during sinus rhythm (left), electrical activity is regularly initiated at the sinus node and spreads through the right atria towards the AV node and via the His-Purkinje fibers towards the ventricles of the heart. Activation of the atria during atrial fibrillation (right) is chaotic due to abnormal impulses within both atria, and consequently activation of the ventricles is distorted. *Lower panel:* rhythm registration of sinus rhythm (top) with p-waves and a regular R-R interval. The rhythm registration during atrial fibrillation (bottom) shows no distinct p-waves and an irregular R-R interval.

In most patients, AF progresses from short, infrequent and self-terminating episodes to longer and more frequent episodes that require intervention to terminate the arrhythmia. Four clinical profiles are commonly used to distinguish the different AF patterns according to duration of AF episodes: (1) *paroxysmal AF*: AF that terminates spontaneously or with intervention within seven days of onset; (2) *persistent AF*: AF that persists beyond seven days; (3) *long-standing persistent AF*: continuous AF lasting for more than 12 months; (4) *permanent AF*: presence of AF that is accepted by the patient and physician and for which no further attempts are taken to restore sinus rhythm.[12, 13] In general, success rates of therapy gradually decline with progression of AF. Primarily in symptomatic, paroxysmal AF patients, initially a rhythm control strategy is chosen aimed at restoring and maintaining sinus rhythm. This strategy firstly combines anti-arrhythmic drug therapy with medication that lowers the heart rate. If this fails to restore sinus rhythm, electrical cardioversion is used to reset the heart to its regular rhythm. Usage of pharmacological therapy is impeded by severe side effects, such as nausea, dizziness, headache, visual

blurring and gastrointestinal conditions, as well as proarrhythmogenicity.[14] In addition, AF recurs within one year in up to 70% of patients while on anti-arrhythmic medication[14] and in up to 67% of patients after electrical cardioversion[15]. Since Haïssaguerre in 1998 firstly described triggers in the pulmonary veins initiating AF[16], catheter ablation eliminating such ectopic activity by freezing or burning has found widespread use. Ablative therapy seemed promising, but many patients still have recurrences or require multiple ablation procedures. After a single procedure, AF recurs in about 35% of patients within one year, in 44% of patients within three years and in 49% of patients within five years, in comparison to 14%, 21% and 22% of patients after multiple procedures, respectively.[17] Ablation therapy is more successful in patients with paroxysmal AF than in patients with persistent AF (AF recurrence 46% vs. 58% at 5-year follow-up, respectively).[17] These numbers accentuate the limited efficacy of currently available therapies for AF and the need for new mechanistic insights. As up to 15% of patients with paroxysmal AF progress to persistent AF within one year[18], the importance of timely recognition of AF should also not be underestimated.

Pathophysiology of atrial fibrillation

In general, AF is caused by interaction between an initiating trigger and an underlying atrial substrate maintaining the arrhythmia. The trigger is usually an atrial extrasystolic beat. The proximal sleeves of the pulmonary veins are a common source of these ectopic triggers, yet other atrial regions can also be involved. Ectopic activity can be enhanced by increased automaticity of atrial issue, triggered activity due to delayed afterdepolarizations and mechanical stress, e.g. due to (acute) stretch of the atrial wall.[19] Development of the underlying atrial substrate that ease maintenance of AF is multifactorial. Ageing and underlying cardiac conditions (e.g. hypertension and ischemia) facilitate remodeling on long-term (years), whereas the so-called process of 'AF begets AF' (i.e. arrhythmia-induced remodeling) commences within hours after AF onset.[20] Presence of AF itself provokes electrical, functional and structural changes in atrial tissue that promote both initiation and maintenance of the arrhythmia.[21] This process aids the progressive nature of AF, going from a 'trigger-driven' arrhythmia in which atrial extrasystoles trigger self-terminating episodes of AF to a 'substrate-driven' arrhythmia in which remodeled tissue expedites perpetuation of AF. The vicious cycle of atrial remodeling is illustrated in *Figure 3* and discussed in more detail in the next paragraph.

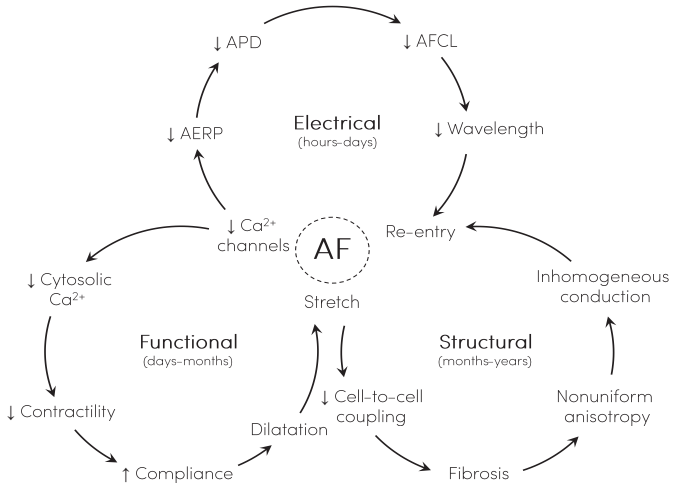

Figure 3 – Atrial fibrillation begets atrial fibrillation. Presence of atrial fibrillation (AF) induces electrical, functional and structural changes that in turn promote initiation and maintenance of AF. Downregulation of L-type Ca^{2+} channels is considered the primary cause for electrical and functional remodeling, whereas stretch as a result of functional (contractile) changes stimulates structural remodeling of atrial tissue. Shortening of the wavelength, as a result of the reduction in atrial effective refractory period (AERP) and atrial fibrillation cycle length (AFCL), and increased inhomogeneous conduction, due to fibrosis-induced nonuniform anisotropy, allows for re-entry to maintain. APD, action potential duration. Modified from Allessie et al.[21]

Atrial remodeling and atrial fibrillation persistence

Remodeling on electrical, functional and structural level jointly form the vicious cycle of atrial remodeling and AF persistence. The pioneering animal studies of Morillo et al. and Wijffels et al. firstly described AF-induced electrical remodeling, showing reduction in atrial effective refractory period (AERP; -15% and -45%, respectively) within hours after AF onset.[20, 22]

This process is primarily due to inactivation of L-type Ca^{2+} ion channels during AF[23, 24], inducing shortening of the atrial action potential duration (APD) and loss of physiological rate adaptation, as confirmed in humans [25-27]. The shortening of APD in turn facilitates shortening of the atrial fibrillation cycle length (AFCL), generally considered a surrogate for local tissue refractoriness[28], and decreases the wavelength of the fibrillatory waves, allowing for more disorganized AF. In addition, downregulation of Ca^{2+} channels induces abnormalities in cellular Ca^{2+} load (i.e. calcium overload), which can provoke delayed afterdepolarizations and triggered activity.[19] Electrical remodeling thereby enhances both the arrhythmogenic substrate as well as formation of triggers and thereby progressively increases vulnerability to develop and maintain AF. Importantly, these AF-induced electrical changes have been shown completely reversible when sinus rhythm is restored,

even after prolonged periods of AF (months to years).[20, 29] Recurrence of AF after successful cardioversion can therefore not be explained based on electrical remodeling alone.

Alongside electrical remodeling, the AF-induced reduction in Ca^{2+} channels also promotes functional remodeling[30]. The reduction in Ca^{2+} channels decreases activation of the contractile apparatus and triggers myolysis of sarcomeres, leading to decreased contractility of the atrial tissue.[31] Consequently, compliance increases and dilatation of the atria commences.[32] In turn, atrial cardiomyocytes become stretched, setting the stage for structural remodeling.

On cellular level, stretch of atrial cardiomyocytes can induce cellular hypertrophy, dedifferentiation, derailed proteostasis, altered cell-to-cell coupling and extracellular matrix remodeling, forming fibroblastic and collagenous depositions.[21, 33-36] In addition, due to cardiomyocyte and sarcomeric stress, several profibrotic (growth) factors are secreted that synergistically increase fibroblast proliferation (e.g. angiotensin II and transforming growth factor-β_1).[19] The altered cell-to-cell coupling in combination with formation of (mainly longitudinal) fibrosis between myocardial fibers facilitates nonuniform anisotropy, leading to discontinuous and inhomogeneous conduction.[37-39] Likewise, inhomogeneous conduction favors re-entry and consequently AF.[39] Aside from its evident role in formation of the arrhythmogenic substrate, structural remodeling also facilitates induction of spontaneous ectopic activity due to coupling of fibroblast and cardiomyocytes.[40] While electrical and functional remodeling commence within days, structural remodeling is a much slower process that builds up in months to years. On short-term, structural changes caused by AF are irreversible, and can be considered physiological adaptation of the atria to chronic Ca^{2+} overload and metabolic stress.[21]

These coinciding mechanisms of electrical, functional and structural remodeling all maintain the process of 'AF begets AF' and lead to persistence of AF. Although the relation between AF and remodeling is well established, considerable progress still has to be made in understanding its precise paths and interactions.

Uncovering electrical markers of atrial fibrillation: cardiac mapping

By placing electrodes at the surface of the heart, transmembrane currents that are generated through depolarization of cardiomyocytes can be measured. The recorded electrical potentials reflect the time, direction and complexity of atrial activation near the recording electrode. The process of identifying the temporal and spatial distributions of myocardial electrical potentials during a particular heart

rhythm is called 'cardiac mapping'.[41] Cardiac mapping can aid in understanding arrhythmogenesis of AF by visualizing atrial activation patterns and electrical abnormalities. Common mapping techniques include endocardial and epicardial mapping, measuring electrical potentials from the inner and outer surface of the heart, respectively. Both techniques have its strengths and weaknesses.

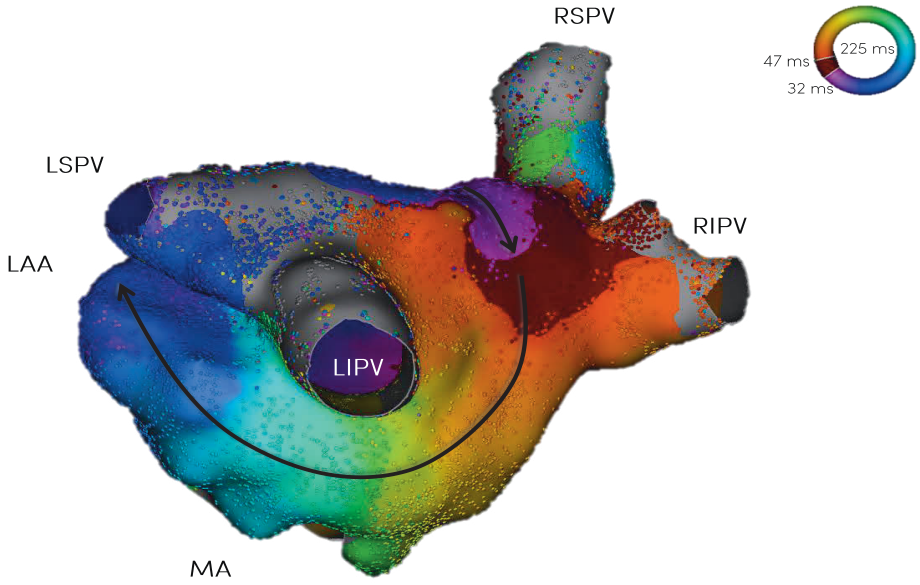

Figure 4 – Three-dimensional endocardial activation map of the left atrium during atrial tachycardia. This activation map was acquired with the RHYTHMIA HDx™ mapping system using a 64-polar basket mapping catheter and displays the macro-reentrant circuit (black arrow) at a posterolateral view. LAA, left atrium appendage; LIPV, left inferior pulmonary vein; LSPV, left superior pulmonary vein; MA, mitral annulus; RIPV, right inferior pulmonary vein; RSPV, right superior pulmonary vein.

Endocardial mapping uses long and flexible catheters that are advanced from the femoral vein or artery to the atria, so that the procedure is minimally invasive. In turn, the small catheters are limited in size and number of electrodes. Commonly used electrophysiological catheters contain 4-20 electrodes, although newer, deployable catheters can contain up to 64 electrodes (i.e., basket catheters). Activation maps are reconstructed by software that links the location of the catheter in space to the recorded electrograms obtained from different locations throughout both atria (*Figure 4*). Epicardial mapping can only be performed during open-chest cardiac surgery, yet uses arrays with up to 192 electrodes that are placed on the outer surface of the heart. Using larger electrodes increases spatial resolution of the reconstructed activation maps and thereby facilitates more detailed visualization of activation patterns and electrical abnormalities, such as conduction blocks (*Figure 5*).

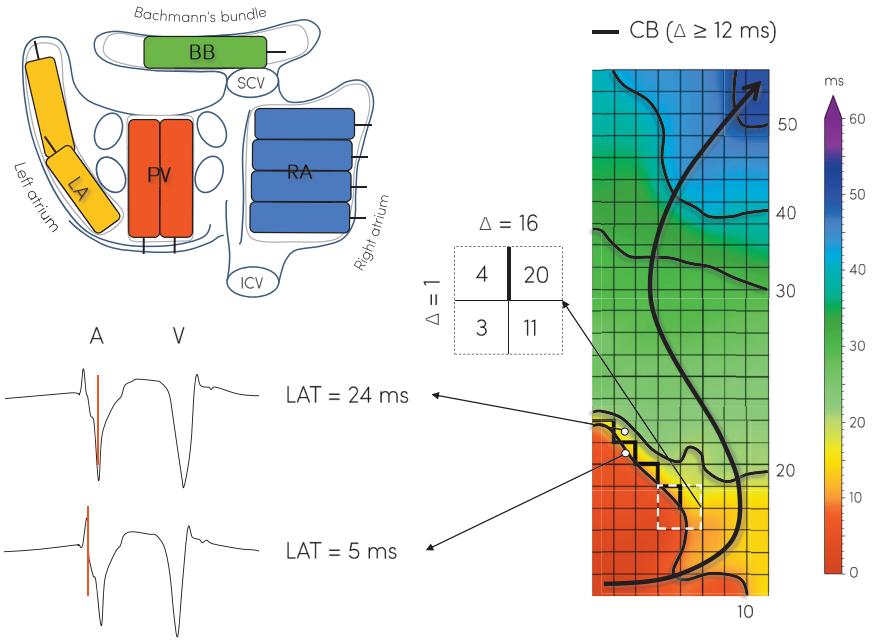

Figure 5 – Epicardial high-resolution mapping. Recordings are made following a pre-defined scheme, covering the entire epicardial surface of the left and right atrium (LA, RA). A high-resolution activation map can be derived by annotating local activation times (LAT) of the obtained electrograms, and conduction abnormalities such as conduction block (CB) can be visualized. The black arrow indicates the main trajectory of activation. BB, Bachmann's bundle; ICV, inferior caval vein; PV, pulmonary veins; SCV, superior caval vein.

Whereas epicardial mapping enables access to Bachmann's bundle, the interatrial septum and the myocardial sleeves of the pulmonary veins – all regarded as potential arrhythmogenic structures [42-44] – can only be reached during endocardial mapping.

Unipolar and bipolar electrograms

Cardiac mapping can be performed using either unipolar or bipolar electrode configurations. In unipolar recordings, the recording electrode is positioned at the site of interest and is connected to a remote electrode (i.e., the indifferent or reference electrode) that is positioned distant from the heart. In turn, bipolar recordings are obtained by connecting two electrodes at the site of interest, usually close together. In both cases, the resulting electrograms are the net difference between the two electrodes. Extracellular currents of thousands of cardiac cells underneath and surrounding the recording electrode(s) are visualized in these electrograms. As the depolarization wave approaches and then passes the recording electrode, a unipolar electrogram is biphasic: a positive peak is denoted while the wavefront is approaching, a sudden drop to zero when the

wavefront is underneath the electrode, and a negative peak as the wavefront is passing by. The bipolar electrogram is the result of subtracting two unipolar electrograms at adjacent sites, thus the initial peak in bipolar recordings coincides with depolarization beneath the recording electrode. As far-field potentials and noise are almost similar at adjacent electrodes, subtraction filters out interferences and only displays local activity. This important advantage is the primary reason why bipolar electrograms have clinically often been preferred above unipolar measurements.[45, 46] Nevertheless, in contrast to unipolar electrograms, morphology of bipolar electrograms is affected by direction of wavefront propagation, interelectrode spacing, electrode size and the orientation of the recording electrode relative to the tissue.[45, 46] Whereas detection of the local activation time in unipolar recordings (i.e., the maximum negative slope of the potential) can be distorted by farfield signals, interpretation of bipolar electrogram morphology is more complicated and factor-dependent. As such, both unipolar or bipolar recordings have its strengths and weaknesses, and provide complimentary information.

Morphology of electrograms

Signal morphology of especially unipolar electrograms reflect underlying activation and conduction processes. In contrast to a biphasic unipolar electrogram that reflects homogeneous conduction, multiple positive and negative peaks in the unipolar electrogram (i.e., fractionation) arise from action potentials in cardiomyocytes that are out of phase.[47] The local asynchronous activation in these fractionated potentials can be due to spatial dispersion in refractory periods, nonuniform tissue anisotropy owing to a low number of electrical side-to-side connections (electrical remodeling) or pathological mechanisms such as the presence of insulating collagenous septa between atrial muscle bundles (structural remodeling). Thereby, studying atrial electrogram morphology could aid in revealing the substrate of AF (*Figure 6*). Fractionated potentials have been linked to abnormal conduction and arrhythmogenicity in patients with AF.[47, 48]

Analysis of signal morphology also comprises measurement of the amplitude, which is determined by the volume of cardiac tissue that is activated simultaneously. As such, low-amplitude signals have been linked to asynchronous activation due to e.g. interstitial fibrosis and decreased side-to-side coupling, and could reflect the substrate of AF.[49] In addition, remodeling-induced dissociation between the epicardial and endocardial wall can be an important factor contributing to persistence of AF.[50] Asynchrony in epicardial and endocardial propagating waves could give rise to differences in electrogram morphology at the epi- en endocardial side, which can only be visualized using simultaneous endo- and epicardial cardiac mapping. Although cardiac mapping techniques offer unique insights into the pathophysiological basis of AF, the procedure is invasive and is not suitable (yet) for diagnosis of AF in daily clinical practice.

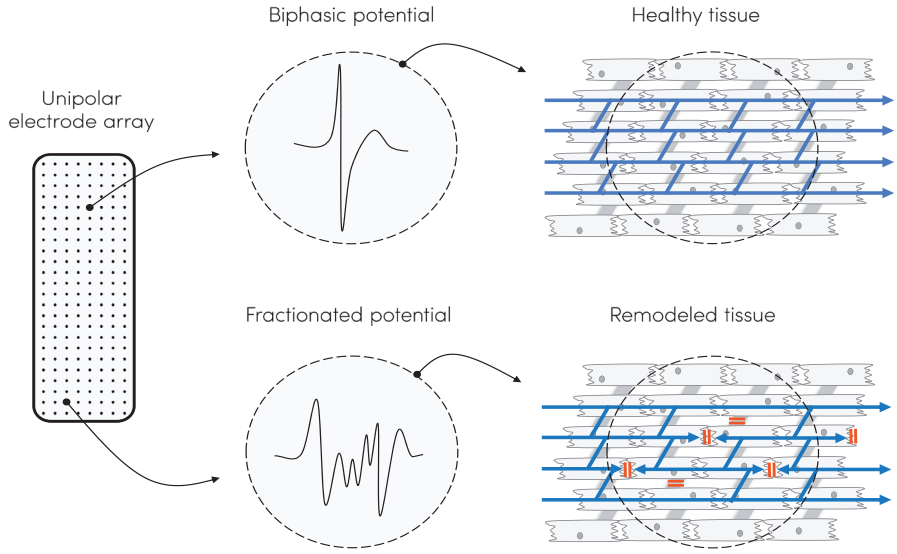

Figure 6 – Unipolar electrogram morphology reflects the arrhythmogenic substrate. *Left:* array with 192 unipolar electrodes that is placed on the epicardial surface during open-chest cardiac surgery. *Middle*: examples of biphasic and fractionated potentials that are measured. *Right:* the tissue underlying the recording electrode, as reflected in the measured potential. Biphasic unipolar potentials reflect homogeneous conduction in healthy anisotropic tissue, whereas fractionated potentials reflect asynchronous activation and inhomogeneous conduction in remodeled (nonuniform anisotropic) tissue.

Biological markers of atrial fibrillation

Blood-based biomarkers could be of great value in diagnosis and treatment of AF, since they are easy to obtain with minimal harm for the patient. As mentioned earlier, derailment of protein homeostasis promotes structural remodeling, favoring progression and persistence of AF. Recently discovered factors contributing to derailment of protein homeostasis are impairment of heat shock proteins (HSPs)[34, 35, 51, 52], autophagy[53], loss of sarcomeric and microtubule proteins[54, 55], mitochondrial dysfunction[56] and activation of DNA damage[57]. Effectiveness of pharmacological therapy could greatly increase when therapeutic agents would be directed at these drivers of structural damage during AF.

Thesis outline

This thesis aims to characterize electrophysiological and structural alterations underlying onset and persistence of AF in patients undergoing cardiac surgery.

The rationale and design of our unique methodology, aiming at identifying bio-electrical markers of AF, is discussed in **Chapter 2**. The next chapters focus on electrical markers underlying AF onset and persistence. **Chapter 3** demonstrates the phenomenon of direction- and rate-dependent fractionation and illustrates its morphological manifestations in a 76-year old longstanding persistent AF patient. Whether anatomical hotspots of fractionated electrograms exist in the left and right atrium is reviewed in **Chapter 4**. The impact of filtering on morphology of unipolar AF potentials is investigated and described in **Chapter 5**. In patients undergoing mitral valve surgery, morphology of single, non-fractionated potentials is investigated and discussed in **Chapter 6**. Voltage fingerprints of unipolar potentials and the impact of prior AF episodes are outlined in **Chapter 7**. Contribution of asynchronous activation of the epicardial and endocardial layers to pathophysiology of AF is discussed in **Chapter 8** and **Chapter 9**. Electrogram morphology of both endocardial and epicardial electrograms and their differences are described in **Chapter 8**, whereas **Chapter 9** focusses on whether unipolar or bipolar electrograms are better suited to detect epi-endocardial asynchrony. **Chapter 10** and **Chapter 11** focus on postoperative AF, discussing the impact of obesity on postoperative AF burden and the incidence and characteristics of postoperative AF in adult bicuspid aortic valve patients, respectively.

The second part of the thesis focusses on biological markers of AF. The editorial in **Chapter 12** emphasizes the opportunity for biomarkers within the treatment chain of AF. The clinical study performed in **Chapter 13** investigates the effect of daily supplementation of L-glutamine in patients, specifically on heat shock proteins and metabolites.

Implications of these findings and future perspectives are discussed in **Chapter 14**. An English and Dutch summary of this thesis are provided in **Chapter 15** and **Chapter 16**, respectively.

References

1. Chugh SS, Havmoeller R, Narayanan K, Singh D, Rienstra M, Benjamin EJ, Gillum RF, Kim YH, McAnulty JH, Jr., Zheng ZJ, Forouzanfar MH, Naghavi M, Mensah GA, Ezzati M, Murray CJ. Worldwide epidemiology of atrial fibrillation: A global burden of disease 2010 study. *Circulation*. 2014;129:837-847
2. Kannel WB, Wolf PA, Benjamin EJ, Levy D. Prevalence, incidence, prognosis, and predisposing conditions for atrial fibrillation: Population-based estimates. *Am J Cardiol*. 1998;82:2N-9N
3. Wolf PA, Abbott RD, Kannel WB. Atrial fibrillation as an independent risk factor for stroke: The framingham study. *Stroke*. 1991;22:983-988
4. Zimetbaum P. Atrial fibrillation. *Ann Intern Med*. 2017;166:ITC33-ITC48
5. Vermond RA, Geelhoed B, Verweij N, Tieleman RG, Van der Harst P, Hillege HL, Van Gilst WH, Van Gelder IC, Rienstra M. Incidence of atrial fibrillation and relationship with cardiovascular events, heart failure, and mortality: A community-based study from the netherlands. *J Am Coll Cardiol*. 2015;66:1000-1007
6. Lloyd-Jones DM, Wang TJ, Leip EP, Larson MG, Levy D, Vasan RS, D'Agostino RB, Massaro JM, Beiser A, Wolf PA, Benjamin EJ. Lifetime risk for development of atrial fibrillation: The framingham heart study. *Circulation*. 2004;110:1042-1046
7. Krijthe BP, Kunst A, Benjamin EJ, Lip GY, Franco OH, Hofman A, Witteman JC, Stricker BH, Heeringa J. Projections on the number of individuals with atrial fibrillation in the european union, from 2000 to 2060. *Eur Heart J*. 2013;34:2746-2751
8. Wong CX, Sullivan T, Sun MT, Mahajan R, Pathak RK, Middeldorp M, Twomey D, Ganesan AN, Rangnekar G, Roberts-Thomson KC, Lau DH, Sanders P. Obesity and the risk of incident, post-operative, and post-ablation atrial fibrillation: A meta-analysis of 626,603 individuals in 51 studies. *JACC Clin Electrophysiol*. 2015;1:139-152
9. D'Agostino RS, Jacobs JP, Badhwar V, Fernandez FG, Paone G, Wormuth DW, Shahian DM. The society of thoracic surgeons adult cardiac surgery database: 2019 update on outcomes and quality. *Ann Thorac Surg*. 2019;107:24-32
10. Stewart S, Hart CL, Hole DJ, McMurray JJ. A population-based study of the long-term risks associated with atrial fibrillation: 20-year follow-up of the renfrew/paisley study. *Am J Med*. 2002;113:359-364
11. Lip GY, Nieuwlaat R, Pisters R, Lane DA, Crijns HJ. Refining clinical risk stratification for predicting stroke and thromboembolism in atrial fibrillation using a novel risk factor-based approach: The euro heart survey on atrial fibrillation. *Chest*. 2010;137:263-272
12. Kirchhof P, Benussi S, Kotecha D, Ahlsson A, Atar D, Casadei B, Castella M, Diener HC, Heidbuchel H, Hendriks J, Hindricks G, Manolis AS, Oldgren J, Popescu BA, Schotten U, Van Putte B, Vardas P, Group ESCSD. 2016 esc guidelines for the management of atrial fibrillation developed in collaboration with eacts. *Eur Heart J*. 2016;37:2893-2962
13. Calkins H, Hindricks G, Cappato R, Kim YH, Saad EB, Aguinaga L, Akar JG, Badhwar V, Brugada J, Camm J, Chen PS, Chen SA, Chung MK, Cosedis Nielsen J, Curtis AB, Davies DW, Day JD, d'Avila A, de Groot NMS, Di Biase L, Duytschaever M, Edgerton JR, Ellenbogen KA, Ellinor PT, Ernst S, Fenelon G, Gerstenfeld EP, Haines DE, Haissaguerre M, Helm RH, Hylek E, Jackman WM, Jalife J, Kalman JM, Kautzner J, Kottkamp H, Kuck KH, Kumagai K, Lee R, Lewalter T, Lindsay BD, Macle L, Mansour M, Marchlinski FE, Michaud GF, Nakagawa H, Natale

A, Nattel S, Okumura K, Packer D, Pokushalov E, Reynolds MR, Sanders P, Scanavacca M, Schilling R, Tondo C, Tsao HM, Verma A, Wilber DJ, Yamane T, Document R. 2017 hrs/ehra/ecas/aphrs/solaece expert consensus statement on catheter and surgical ablation of atrial fibrillation. *Europace*. 2018;20:e1-e160

14. Waks JW, Zimetbaum P. Antiarrhythmic drug therapy for rhythm control in atrial fibrillation. *J Cardiovasc Pharmacol Ther*. 2017;22:3-19
15. Fetsch T, Bauer P, Engberding R, Koch HP, Lukl J, Meinertz T, Oeff M, Seipel L, Trappe HJ, Treese N, Breithardt G, Prevention of Atrial Fibrillation after Cardioversion I. Prevention of atrial fibrillation after cardioversion: Results of the pafac trial. *Eur Heart J*. 2004;25:1385-1394
16. Haissaguerre M, Jais P, Shah DC, Takahashi A, Hocini M, Quiniou G, Garrigue S, Le Mouroux A, Le Metayer P, Clementy J. Spontaneous initiation of atrial fibrillation by ectopic beats originating in the pulmonary veins. *N Engl J Med*. 1998;339:659-666
17. Ganesan AN, Shipp NJ, Brooks AG, Kuklik P, Lau DH, Lim HS, Sullivan T, Roberts-Thomson KC, Sanders P. Long-term outcomes of catheter ablation of atrial fibrillation: A systematic review and meta-analysis. *J Am Heart Assoc*. 2013;2:e004549
18. Kerr CR, Humphries KH, Talajic M, Klein GJ, Connolly SJ, Green M, Boone J, Sheldon R, Dorian P, Newman D. Progression to chronic atrial fibrillation after the initial diagnosis of paroxysmal atrial fibrillation: Results from the canadian registry of atrial fibrillation. *Am Heart J*. 2005;149:489-496
19. Nattel S, Burstein B, Dobrev D. Atrial remodeling and atrial fibrillation: Mechanisms and implications. *Circ Arrhythm Electrophysiol*. 2008;1:62-73
20. Wijffels MC, Kirchhof CJ, Dorland R, Allessie MA. Atrial fibrillation begets atrial fibrillation. A study in awake chronically instrumented goats. *Circulation*. 1995;92:1954-1968
21. Allessie M, Ausma J, Schotten U. Electrical, contractile and structural remodeling during atrial fibrillation. *Cardiovasc Res*. 2002;54:230-246
22. Morillo CA, Klein GJ, Jones DL, Guiraudon CM. Chronic rapid atrial pacing. Structural, functional, and electrophysiological characteristics of a new model of sustained atrial fibrillation. *Circulation*. 1995;91:1588-1595
23. Yue L, Feng J, Gaspo R, Li GR, Wang Z, Nattel S. Ionic remodeling underlying action potential changes in a canine model of atrial fibrillation. *Circ Res*. 1997;81:512-525
24. Bosch RF, Zeng X, Grammer JB, Popovic K, Mewis C, Kuhlkamp V. Ionic mechanisms of electrical remodeling in human atrial fibrillation. *Cardiovasc Res*. 1999;44:121-131
25. Attuel P, Childers R, Cauchemez B, Poveda J, Mugica J, Coumel P. Failure in the rate adaptation of the atrial refractory period: Its relationship to vulnerability. *Int J Cardiol*. 1982;2:179-197
26. Franz MR, Karasik PL, Li C, Moubarak J, Chavez M. Electrical remodeling of the human atrium: Similar effects in patients with chronic atrial fibrillation and atrial flutter. *J Am Coll Cardiol*. 1997;30:1785-1792
27. Boutjdir M, Le Heuzey JY, Lavergne T, Chauvaud S, Guize L, Carpentier A, Peronneau P. Inhomogeneity of cellular refractoriness in human atrium: Factor of arrhythmia? *Pacing Clin Electrophysiol*. 1986;9:1095-1100
28. Misier AR, Opthof T, van Hemel NM, Defauw JJ, de Bakker JM, Janse MJ, van Capelle FJ. Increased dispersion of "refractoriness" in patients with idiopathic paroxysmal atrial fibrillation. *J Am Coll Cardiol*. 1992;19:1531-1535
29. Yu WC, Lee SH, Tai CT, Tsai CF, Hsieh MH, Chen CC, Ding YA, Chang MS, Chen SA. Reversal of atrial electrical remodeling following cardioversion of long-standing atrial fibrillation in man.

Cardiovasc Res. 1999;42:470-476
30. Schotten U, Duytschaever M, Ausma J, Eijsbouts S, Neuberger HR, Allessie M. Electrical and contractile remodeling during the first days of atrial fibrillation go hand in hand. *Circulation*. 2003;107:1433-1439
31. Schotten U, Ausma J, Stellbrink C, Sabatschus I, Vogel M, Frechen D, Schoendube F, Hanrath P, Allessie MA. Cellular mechanisms of depressed atrial contractility in patients with chronic atrial fibrillation. *Circulation*. 2001;103:691-698
32. Schotten U, de Haan S, Neuberger HR, Eijsbouts S, Blaauw Y, Tieleman R, Allessie M. Loss of atrial contractility is primary cause of atrial dilatation during first days of atrial fibrillation. *Am J Physiol Heart Circ Physiol*. 2004;287:H2324-2331
33. De Jong AM, Maass AH, Oberdorf-Maass SU, Van Veldhuisen DJ, Van Gilst WH, Van Gelder IC. Mechanisms of atrial structural changes caused by stretch occurring before and during early atrial fibrillation. *Cardiovasc Res*. 2011;89:754-765
34. Brundel BJ, Henning RH, Ke L, van Gelder IC, Crijns HJ, Kampinga HH. Heat shock protein upregulation protects against pacing-induced myolysis in hl-1 atrial myocytes and in human atrial fibrillation. *J Mol Cell Cardiol*. 2006;41:555-562
35. Brundel BJ, Shiroshita-Takeshita A, Qi X, Yeh YH, Chartier D, van Gelder IC, Henning RH, Kampinga HH, Nattel S. Induction of heat shock response protects the heart against atrial fibrillation. *Circ Res*. 2006;99:1394-1402
36. Zhang D, Ke L, Mackovicova K, Van Der Want JJ, Sibon OC, Tanguay RM, Morrow G, Henning RH, Kampinga HH, Brundel BJ. Effects of different small hspb members on contractile dysfunction and structural changes in a drosophila melanogaster model for atrial fibrillation. *J Mol Cell Cardiol*. 2011;51:381-389
37. Spach MS. Anisotropy of cardiac tissue: A major determinant of conduction? *J Cardiovasc Electrophysiol*. 1999;10:887-890
38. Spach MS, Heidlage JF, Dolber PC, Barr RC. Changes in anisotropic conduction caused by remodeling cell size and the cellular distribution of gap junctions and na(+) channels. *J Electrocardiol*. 2001;34 Suppl:69-76
39. Spach MS, Josephson ME. Initiating reentry: The role of nonuniform anisotropy in small circuits. *J Cardiovasc Electrophysiol*. 1994;5:182-209
40. Miragoli M, Salvarani N, Rohr S. Myofibroblasts induce ectopic activity in cardiac tissue. *Circ Res*. 2007;101:755-758
41. Issa ZF, Miller JM, Zipes DP. *Clinical arrhythmology and electrophysiology : A companion to braunwald's heart disease*. 2019.
42. Teuwen CP, Yaksh A, Lanters EA, Kik C, van der Does LJ, Knops P, Taverne YJ, van de Woestijne PC, Oei FB, Bekkers JA, Bogers AJ, Allessie MA, de Groot NM. Relevance of conduction disorders in bachmann's bundle during sinus rhythm in humans. *Circ Arrhythm Electrophysiol*. 2016;9:e003972
43. Kharbanda RK, Ozdemir EH, Taverne Y, Kik C, Bogers A, de Groot NMS. Current concepts of anatomy, electrophysiology, and therapeutic implications of the interatrial septum. *JACC Clin Electrophysiol*. 2019;5:647-656
44. Roux N, Havet E, Mertl P. The myocardial sleeves of the pulmonary veins: Potential implications for atrial fibrillation. *Surg Radiol Anat*. 2004;26:285-289
45. Venkatachalam KL, Herbrandson JE, Asirvatham SJ. Signals and signal processing for the electrophysiologist: Part ii: Signal processing and artifact. *Circ Arrhythm Electrophysiol*. 2011;4:974-981
46. Venkatachalam KL, Herbrandson JE, Asirvatham SJ. Signals and signal processing for the electrophysiologist: Part i: Electrogram acquisition. *Circ Arrhythm Electrophysiol*. 2011;4:965-973

47. Konings KT, Smeets JL, Penn OC, Wellens HJ, Allessie MA. Configuration of unipolar atrial electrograms during electrically induced atrial fibrillation in humans. *Circulation*. 1997;95:1231-1241
48. Nademanee K, McKenzie J, Kosar E, Schwab M, Sunsaneewitayakul B, Vasavakul T, Khunnawat C, Ngarmukos T. A new approach for catheter ablation of atrial fibrillation: Mapping of the electrophysiologic substrate. *J Am Coll Cardiol*. 2004;43:2044-2053
49. Blandino A, Bianchi F, Grossi S, Biondi-Zoccai G, Conte MR, Gaido L, Gaita F, Scaglione M, Rametta F. Left atrial substrate modification targeting low-voltage areas for catheter ablation of atrial fibrillation: A systematic review and meta-analysis. *Pacing Clin Electrophysiol*. 2017;40:199-212
50. de Groot NM, Houben RP, Smeets JL, Boersma E, Schotten U, Schalij MJ, Crijns H, Allessie MA. Electropathological substrate of longstanding persistent atrial fibrillation in patients with structural heart disease: Epicardial breakthrough. *Circulation*. 2010;122:1674-1682
51. Hoogstra-Berends F, Meijering RA, Zhang D, Heeres A, Loen L, Seerden JP, Kuipers I, Kampinga HH, Henning RH, Brundel BJ. Heat shock protein-inducing compounds as therapeutics to restore proteostasis in atrial fibrillation. *Trends Cardiovasc Med*. 2012;22:62-68
52. Hu X, Li J, van Marion DMS, Zhang D, Brundel B. Heat shock protein inducer gga*-59 reverses contractile and structural remodeling via restoration of the microtubule network in experimental atrial fibrillation. *J Mol Cell Cardiol*. 2019;134:86-97
53. Wiersma M, Meijering RAM, Qi XY, Zhang D, Liu T, Hoogstra-Berends F, Sibon OCM, Henning RH, Nattel S, Brundel B. Endoplasmic reticulum stress is associated with autophagy and cardiomyocyte remodeling in experimental and human atrial fibrillation. *J Am Heart Assoc*. 2017;6
54. Brundel BJ, Ausma J, van Gelder IC, Van der Want JJ, van Gilst WH, Crijns HJ, Henning RH. Activation of proteolysis by calpains and structural changes in human paroxysmal and persistent atrial fibrillation. *Cardiovasc Res*. 2002;54:380-389
55. Zhang D, Wu CT, Qi X, Meijering RA, Hoogstra-Berends F, Tadevosyan A, Cubukcuoglu Deniz G, Durdu S, Akar AR, Sibon OC, Nattel S, Henning RH, Brundel BJ. Activation of histone deacetylase-6 induces contractile dysfunction through derailment of alpha-tubulin proteostasis in experimental and human atrial fibrillation. *Circulation*. 2014;129:346-358
56. Wiersma M, van Marion DMS, Wust RCI, Houtkooper RH, Zhang D, Groot NMS, Henning RH, Brundel B. Mitochondrial dysfunction underlies cardiomyocyte remodeling in experimental and clinical atrial fibrillation. *Cells*. 2019;8
57. Zhang D, Hu X, Li J, Liu J, Baks-Te Bulte L, Wiersma M, Malik NU, van Marion DMS, Tolouee M, Hoogstra-Berends F, Lanters EAH, van Roon AM, de Vries AAF, Pijnappels DA, de Groot NMS, Henning RH, Brundel B. DNA damage-induced parp1 activation confers cardiomyocyte dysfunction through nad(+) depletion in experimental atrial fibrillation. *Nat Commun*. 2019;10:1307

2

Atrial fibrillation fingerprinting; spotting bio-electrical markers to early recognize atrial fibrillation by the use of a bottom-up approach (AFFIP): rationale and design

Roeliene Starreveld
Paul Knops
Kennedy S. Ramos
Maarten C. Roos-Serote
Ad J.J.C. Bogers
Bianca J.J.M. Brundel
Natasja M.S. de Groot

Clinical Cardiology. 2020 Jun;43(6):546-552

Abstract

Background

The exact pathophysiology of atrial fibrillation (AF) remains incompletely understood and treatment of AF is associated with high recurrence rates. Persistence of AF is rooted in the presence of electropathology, defined as complex electrical conduction disorders caused by structural damage of atrial tissue. The Atrial Fibrillation Fingerprinting (AFFIP) study aims to characterize electropathology, enabling development of a novel diagnostic instrument to predict AF onset and early progression.

Hypotheses

History of AF, development of post-operative AF, age, gender, underlying heart disease and other clinical characteristics impact the degree of electropathology.

Methods

This study is a prospective observational study with a planned duration of 48 months. Three study groups are defined: 1) (longstanding) persistent AF patients, 2) paroxysmal AF patients and 3) patients without a history of AF, all undergoing open-chest cardiac surgery. Intra-operative high-resolution epicardial mapping is performed to identify the patient-specific electrical profile, whereas the patient-specific biological profile is assessed by evaluating proteostasis markers in blood samples and atrial appendage tissue samples. Post-operative continuous rhythm monitoring is performed for detection of early post-operative AF. Late post-operative AF (during five-year follow-up) is documented by either electrocardiogram or 24-hour Holter registration.

Results

The required sample size for this study is estimated at 447 patients. Up till now 105 patients were included, of whom 36 have a history of AF.

Conclusion

The AFFIP study will elucidate whether electrophysiological and structural characteristics represent a novel diagnostic tool, the AF Fingerprint, to predict onset and early progression of AF in cardiac surgery patients.

Introduction

Atrial fibrillation (AF) is the most common cardiac arrhythmia worldwide, and its incidence[1] and associated medical health care costs[2] continuously increase. Even though numerous predisposing factors for progression of AF have been identified, the exact pathophysiology remains incompletely understood and treatment of AF is associated with high recurrence rates. As disease progression from recurrent intermittent episodes to finally permanent AF is accompanied by a gradual increase in therapy failure, early recognition of AF is of prime importance. Persistence of AF is rooted in the presence of electropathology, which is defined as complex electrical conduction disorders caused by structural damage of atrial tissue. Therefore, early recognition of AF susceptibility in patients is necessary to halt electropathology and hence disease onset and progression. Although promising artificial intelligence applications are emerging[3], up till this day in clinical practice, AF is diagnosed with a surface electrocardiogram when a patient already suffers from AF. This rhythm registration cannot assess the degree of electropathology and thus the stage of AF which is essential for selection of the appropriate therapy. Hence, early recognition of AF and the start of effective treatment is seriously hampered. By characterizing electropathology, we aim to develop a novel diagnostic instrument to predict AF onset and early progression. We hypothesize that every patient has a unique biological and electrical signal profile that is influenced by age, gender and underlying heart disease. This bio-electrical profile is deduced from the ratio abnormal/normal electrical signals in the atria by utilizing a unique high-density atrial mapping approach and determination of proteostasis markers in tissue or blood samples related to structural damage. These outcomes are summarized in an AF Fingerprint.

Multi-site high density epicardial mapping has been used in multiple research protocols in Rotterdam (QUASAR study MEC 2010-054, HALT&REVERSE study MEC 2015-393), Leiden and Maastricht.[4-7] Since 2010 the mapping procedure is daily practice in the Erasmus Medical Center. Atrial conduction during both sinus rhythm (SR) and (induced) AF can be visualised to identify the patient-specific electrical profile. This alone however does not clarify electropathological changes on structural level that contribute to substrate for AF. Previous studies revealed that structural damage is caused by derailment of protein homeostasis due to loss of key modulators within the protein quality system.[8] Failure of protein quality control in AF involves impairment of heat shock proteins (HSPs)[9], autophagy[10], loss of sarcomeric and microtubule proteins[11, 12] and activation of DNA damage/PARP1/NAD axis[13], favoring progression of AF.

The AFFIP study combines electrophysiological and structural alterations into one AF Fingerprint (*Figure 1*). Electrophysiological data obtained from epicardial mapping during surgery are combined with proteostasis markers on one hand

and atrial tissue characteristics on the other hand. By comparing the bio-electrical AF Fingerprint of patients from different age groups, gender, history of AF, development of post-operative AF, underlying heart disease and other clinical characteristics, we hope to gain more insight in the mechanism underlying AF and the development of a substrate for AF. The findings will elucidate whether structural and electrophysiological characteristics represent a novel diagnostic tool, the AF Fingerprint, to predict onset and early progression of AF in cardiac surgery patients.

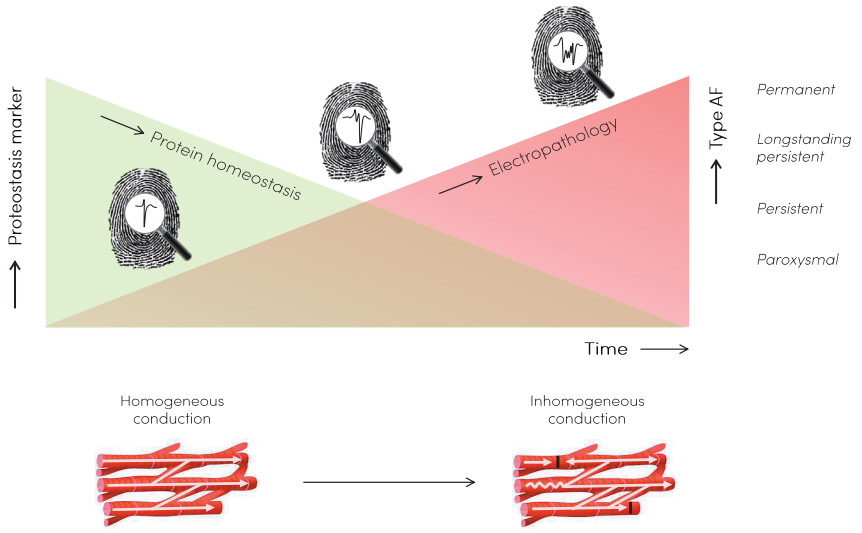

Figure 1 – Concept of the AFFIP study. The AFFIP study hypothesizes that every patient has a unique biological and electrical signal profile that is influenced by age, gender and heart disease. Intra-operative high-resolution epicardial mapping is performed to identify the patient-specific electrical profile, whereas the biological profile is assessed by evaluating proteostasis levels in blood samples and atrial appendage tissue samples. Derailment of protein homeostasis can lead to structural remodeling, favoring inhomogeneous conduction and progression of AF. We aim to develop a novel diagnostic tool, the bio-electrical AF Fingerprint, to predict onset and early progression of AF.

Methods

AFFIP is a prospective observational study, with a planned duration of 48 months. This study is carried out according to the principals of the Declaration of Helsinki and in accordance with the Medical Research involving Human Subjects Acts. The study is part of the HALT&REVERSE protocol which is approved by the Rotterdam local medical ethical committee (MEC-2014-393).

Study objectives

The primary study objectives are to test the correlation between the AF Fingerprint, revealing the degree of electropathology including e.g. patterns of activation and signal morphology, proteostasis levels and atrial tissue characteristics, clinical characteristics and onset and progression of AF in patients undergoing open-chest cardiac surgery.

Study population

Patients with structural heart disease scheduled for elective cardiac surgery are included. The study population consists of three study groups: patients with (longstanding) persistent AF (group 1), patients with paroxysmal AF (group 2) and patients without a history of AF (group 3) undergoing open-chest cardiac surgery. In line with the ESC guidelines, patients with documentation (ECG or ECG description) of self-terminating AF episodes up to 7 days, or with AF episodes cardioverted within 7 days are classified as paroxysmal AF. Patients with documentation of AF episodes longer than 7 days or longer than a year are classified as persistent and longstanding persistent AF, respectively. Patients are recruited at the Department of Cardiothoracic Surgery at the Erasmus Medical Center, Rotterdam, The Netherlands.

Prior to enrolling in the study, each patient is provided an oral and a written explanation of the study procedure. Written informed consent is obtained from all patients. Prior to cardiac surgery, blood samples are taken from all patients for determination of HSP levels (*Figure 2*). Patient characteristics (e.g. age, medical history, cardiovascular risk factors) are obtained from the patient's file.

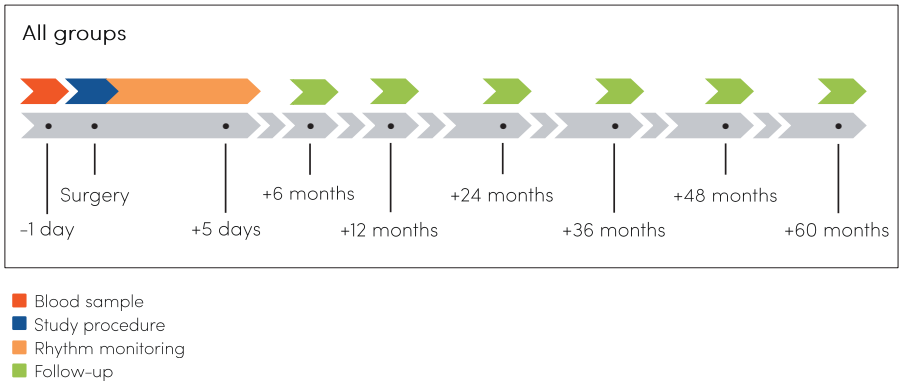

Figure 2 - Time course of the AFFIP study. A baseline blood sample (red bar) is obtained from all patients one day prior to surgery. During surgery, the study procedure (blue bar, epicardial mapping) is performed, followed by post-operative continuous rhythm monitoring (orange bar). Patients are consulted by phone at 6 months, 12 months and yearly up to 5 years after surgery for detection of late post-operative AF (green bars).

Inclusion criteria
In order to be eligible to participate in this study, a subject must meet all of the following criteria:
+ at least 18 years of age
+ structural heart disease (with or without history of AF)
+ scheduled for elective cardiac surgery

Exclusion criteria
A potential subject who meets any of the following criteria is excluded from participation in this study:
- hemodynamic instability
- emergency cardiac surgery
- redo-cardiac surgery

Additional details of entry criteria are listed in the *Supplemental material.*

Intra-operative mapping procedure
Epicardial mapping is performed during surgery. Patients are under full anesthesia and vital signs are monitored continuously throughout the procedure. Epicardial unipolar electrograms are recorded using a custom-made multi-site electrode array. Recordings are made at nine consecutive sites (right atrium 1-4, Bachmann's bundle, right and left pulmonary vein and left atrium 1-2), following a predefined mapping scheme (*Figure 2*) during SR (9 sites, 5 seconds/site), during pacing maneuvers for inducing AF (1 site, Bachmann's bundle), and in AF (9 sites, 10 seconds/site). Pacing is performed with atrial fixed rate pacing directly from the electrode or with a standard temporary pacemaker wire. If AF sustains at the end of the mapping procedure, SR is restored with 5-10J electrical cardioversion.

After introduction of the extra corporal circulation into the right atrium via the right atrial appendage (RAA) a tissue sample (approximately 10x10mm) is obtained from the incision site in all patients. In patients undergoing mitral valve surgery, the left atrial appendage (LAA) is also incised and a small tissue sample is excised. In patients undergoing surgical pulmonary vein isolation, a left sided procedure in patients with AF which includes amputation of the LAA, the LAA tissue is also studied.

Follow up
After procedure, the heart rhythm is continuously monitored until hospital discharge in order to detect early post-operative AF. Patients are also consulted by phone at 6 months, 12 months and yearly up to 5 years after surgery in order to detect late post-operative AF *(Figure 3*). If post-operative AF is suspected, documentation of electrocardiography, 24-hour Holter registration or a clinical discharge letter from peripheral hospitals are retrieved.

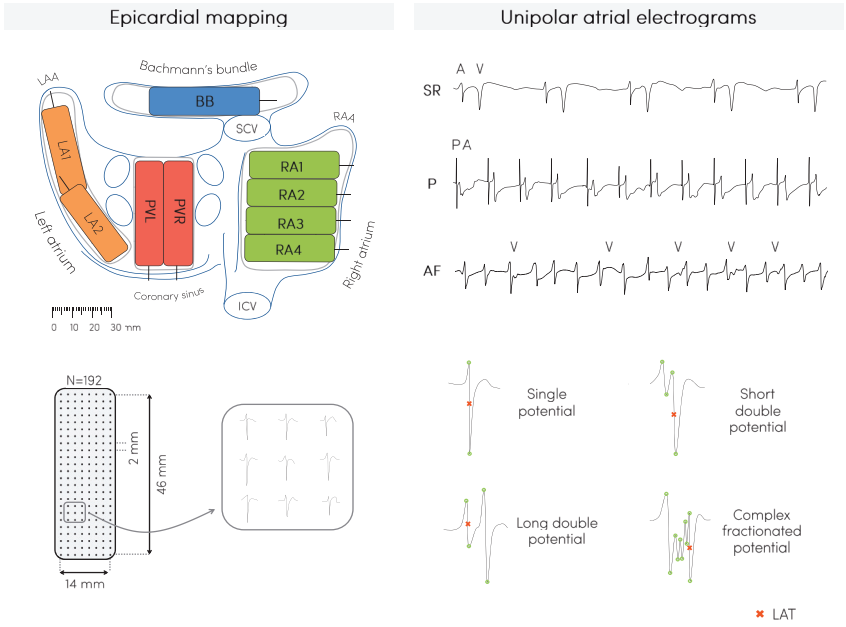

Figure 3 - Epicardial mapping to retrieve unipolar atrial electrograms. With the use of a 192 electrode array, the left atrium (LA), right atrium (RA), pulmonary vein (PV) area and Bachmann's Bundle (BB) are mapped following this predefined mapping scheme. Unipolar atrial electrograms are collected during sinus rhythm (SR), pacing maneuvers (P) and (electrically induced) atrial fibrillation (AF). Morphology of atrial potentials are subdivided into four categories: single potentials (one deflection), short double potentials (two deflections less than 15ms apart), long double potentials (two deflections 15ms or more apart) and complex fractionated potentials (three or more deflections). ICV = inferior caval vein, LAA = left atrial appendage, PVL = left pulmonary vein area, PVR = right pulmonary vein area, RAA = right atrial appendage, SCV = superior caval vein.

Tissue analysis

All obtained blood samples and atrial tissue samples are stored at -80oC until transport to the Amsterdam UMC, location VU Medical Center. Proteostasis markers include HSP27, HSP70, HSPA1A, HSPA5, HSPB1, HSPB5, HSPB6, HSPB7, HSPB8, HSPD1, α-SMA, LC3B-II, TIMP1, LOX3, MMP9, Galectin-3, NCAM, MT-ND1 and COX3, and are determined by commercially available ELISAs and Western blot analysis at the Department of Physiology of the Amsterdam UMC.

Main study parameters and endpoints

Primary endpoint of the study is development or recurrence of AF. Secondary endpoints include implantation of an atrial pacemaker or implantable cardioverter defibrillator. At present, no substudies are planned. Additional secondary endpoints are described in the *Supplemental material*. At present, no substudies are planned.

Deflections of the recorded atrial electrograms are detected semi-automatically in custom-made Python 3.6 software. In case of fractionated electrograms, the component with the steepest negative slope is taken as the local activation time (*Figure 3*). Electrograms with injury potentials and artifacts are excluded from analysis by consensus of two investigators. Signals are used to construct color-coded activation, conduction block, break-through wave, fractionation and voltage maps (*Figure 4*). Furthermore, the relation between patterns of activation, incidence of breakthrough waves, fractionation, fibrillation intervals, conduction abnormalities and voltage is studied and compared between the different atrial sites and atrial rhythms. Electrical changes as defined with the above-mentioned electrical parameters will be correlated with the pre-operative proteostasis levels, development of post-operative AF, sex, age and other clinical characteristics.

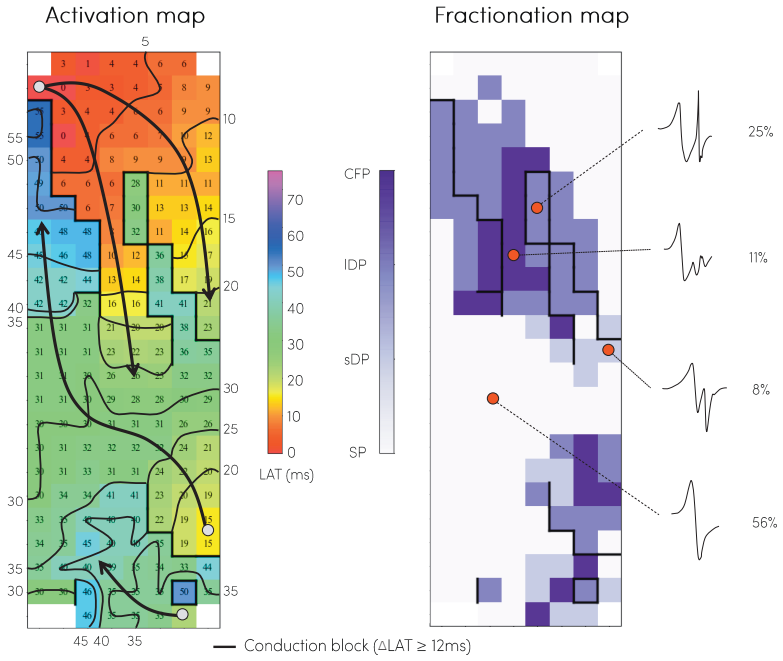

Figure 4 - Construction of the AF Fingerprint. The left panel shows an example of an activation map during electrically induced atrial fibrillation (AF) of the left pulmonary vein area in a patient undergoing coronary artery bypass grafting without a history of AF. Isochrones are drawn at 5ms, areas of conduction block (Δ local activation time (LAT) ≥ 12ms) are indicated by black bars and the origin of peripheral waves by grey dots. The arrows indicate main activation direction. The corresponding fractionation map is displayed in the right panel and shows the different types of atrial potential morphologies: single potentials (SP, one deflection), short double potentials (sDP, two deflections less than 15ms apart), long double potentials (IDP, two deflections 15ms or more apart) and complex fractionated potentials (CFP, three or more deflections). The maps are used to determine the incidence of e.g. fractionation and conduction block.

The primary hypothesis is that the degree of electropathology will be increased in patients with a history of AF and patients whom develop post-operative AF. Secondarily, we hypothesize that age, gender, underlying heart disease and other clinical characteristics impact the degree of electropathology.

Sample size calculation

Based upon our experience in prior mapping studies approximately 30% of patients develop early post-operative AF in the Erasmus MC[14], which is in correspondence with published literature[15].

There is no data on the proposed novel electrophysiological parameters and biomarkers, and calculation of the sample size is therefore at present not possible. However, we used data obtained from a pilot study containing 5 patients with and 5 patients without AF. With a p-value of 0.05 and a chosen power of 0.95 the required number is 135 per study group. An attrition rate of 10% increases this to 149 patients in each group. The required sample size for this study is therefore estimated at 447 patients. These calculations will be repeated after the first 50 patients in every group in order to adjust the sample size.

Statistical analysis

Associations between proteostasis markers, electrical signals and clinical patient outcomes are calculated using multivariate logistic regression and cox regression models. Log rank tests compare patient groups with different stages of AF. Continuous and categorical electrophysiological parameters are compared with respectively ANOVA and chi-square tests. For repeated biomarker measurements, joint modeling and mixed modeling analysis is used. ANOVA with Bonferroni adjustments corrects for analysis of multiple biomarkers.

Study organization

This multi-disciplinary study is carried out by dedicated teams, whom are responsible for the following tasks:

Translational Electrophysiology Research Unit of the Department of Cardiology at the Erasmus Medical Center, Rotterdam, The Netherlands: patient screening and recruitment, collection of electrophysiological data during intra-operative mapping procedure, collection of blood samples, patient follow-up, electrophysiological data analyses, statistical analyses

Department of Cardiothoracic Surgery at the Erasmus Medical Center, Rotterdam, The Netherlands: intra-operative mapping procedure and collection of atrial tissue samples during open-chest cardiac surgery

Atrial Fibrillation Research Unit of the Department of Physiology at the Amsterdam UMC, Amsterdam, The Netherlands: analysis of biological markers from tissue and blood samples

Trial Office of the Department of Cardiothoracic Surgery, Erasmus Medical Center, Rotterdam, The Netherlands: Data Safety Monitoring

Supervision and steering of these teams is done by prof. dr. Natasja M.S. de Groot, prof. dr. Bianca J.J.M. Brundel and prof. dr. Ad J.J.C. Bogers. Prof. dr. ir. Eric Boersma of the Department of Clinical Epidemiology at the Erasmus Medical Center, Rotterdam, The Netherlands, supervises all statistical analyses.

Results

The AFFIP study started in January 2017. The first patient enrolled on January 27, 2017, and up till now 105 patients were included (as of March 20, 2020), of whom 36 have a history of AF. Table 1 provides the preliminary baseline characteristics of all enrolled patients.

Table 1 – Preliminary baseline characteristics of enrolled patients (as of 20th of March 2020)

Number of patients	**105**
Male	70 (67%)
Age (years)	64 (54 – 71)
BMI	27.2 (24.6 – 30.1)
Underlying heart disease	
CABG	16 (15)
AVD	18 (16)
MVD	11 (10)
CABG + AVD	8 (8)
CABG + MVD	4 (4)
AVD + MVD	4 (4)
CHD	44 (42)
History of AF	36 (34)
Paroxysmal	20 (56)
Persistent	14 (39)
Longstanding persistent	2 (6)
Hypertension	48 (46)
Dyslipidemia	26 (25)
Diabetes mellitus	16 (15)

Values are presented as N (%) or median (25^{th} – 75^{th} percentile). AVD, aortic valve disease; BMI, body mass index; CABG, coronary artery bypass grafting; CHD, congenital heart disease; MVD, mitral valve disease.

Discussion

In clinical practice, AF is currently diagnosed with a surface electrocardiogram when a patient already suffers from AF. This rhythm registration cannot assess the degree of electropathology and thus the stage of AF which is essential for selection of the appropriate therapy. Hence, early recognition of AF and the start of effective treatment is seriously hampered. The AFFIP study aims to characterize electropathology, enabling development of a novel diagnostic instrument to predict AF onset and early progression. Electrophysiological data obtained from epicardial mapping during surgery are combined with proteostasis markers on one hand and atrial tissue characteristics on the other hand. The findings will elucidate whether electrophysiological and structural characteristics represent a novel diagnostic tool, the AF Fingerprint, to predict onset and early progression of AF in cardiac surgery patients.

References

1. Go AS, Hylek EM, Phillips KA, Chang Y, Henault LE, Selby JV and Singer DE. Prevalence of diagnosed atrial fibrillation in adults: national implications for rhythm management and stroke prevention: the AnTicoagulation and Risk Factors in Atrial Fibrillation (ATRIA) Study. *JAMA*. 2001;285:2370-5.
2. Wolf PA, Mitchell JB, Baker CS, Kannel WB and D'Agostino RB. Impact of atrial fibrillation on mortality, stroke, and medical costs. *Arch Intern Med*. 1998;158:229-234.
3. Attia ZI, Noseworthy PA, Lopez-Jimenez F, Asirvatham SJ, Deshmukh AJ, Gersh BJ, Carter RE, Yao X, Rabinstein AA, Erickson BJ, Kapa S and Friedman PA. An artificial intelligence-enabled ECG algorithm for the identification of patients with atrial fibrillation during sinus rhythm: a retrospective analysis of outcome prediction. *Lancet*. 2019;394:861-867.
4. Eckstein J, Maesen B, Linz D, Zeemering S, van Hunnik A, Verheule S, Allessie M and Schotten U. Time course and mechanisms of endo-epicardial electrical dissociation during atrial fibrillation in the goat. *Cardiovascular Research*. 2011;89:816-824.
5. Verheule S, Tuyls E, van Hunnik A, Kuiper M, Schotten U and Allessie M. Fibrillatory Conduction in the Atrial Free Walls of Goats in Persistent and Permanent Atrial Fibrillation. *Circ-Arrhythmia Elec*. 2010;3:590-U64.
6. Yaksh A. Atrial Fibrillation: to map or not to map? *Netherlands Heart Journal*. 2013.
7. Eckstein J, Zeemering S, Linz D, Maesen B, Verheule S, van Hunnik A, Crijns H, Allessie MA and Schotten U. Transmural Conduction Is the Predominant Mechanism of Breakthrough During Atrial Fibrillation Evidence From Simultaneous Endo-Epicardial High-Density Activation Mapping. *Circ-Arrhythmia Elec*. 2013;6:334-341.
8. Henning RH and Brundel BJJM. Proteostasis in cardiac health and disease. *Nat Rev Cardiol*. 2017;14:637-653.
9. Brundel BJ, Shiroshita-Takeshita A, Qi X, Yeh YH, Chartier D, van Gelder IC, Henning RH, Kampinga HH and Nattel S. Induction of heat shock response protects the heart against atrial fibrillation. *Circ Res*. 2006;99:1394-402.
10. Wiersma M, Meijering RAM, Qi XY, Zhang D, Liu T, Hoogstra-Berends F, Sibon OCM, Henning RH, Nattel S and Brundel B. Endoplasmic Reticulum Stress Is Associated With Autophagy and Cardiomyocyte Remodeling in Experimental and Human Atrial Fibrillation. *J Am Heart Assoc*. 2017;6.
11. Brundel BJ, Ausma J, van Gelder IC, Van der Want JJ, van Gilst WH, Crijns HJ and Henning RH. Activation of proteolysis by calpains and structural changes in human paroxysmal and persistent atrial fibrillation. *Cardiovasc Res*. 2002;54:380-9.
12. Zhang D, Wu CT, Qi X, Meijering RA, Hoogstra-Berends F, Tadevosyan A, Cubukcuoglu Deniz G, Durdu S, Akar AR, Sibon OC, Nattel S, Henning RH and Brundel BJ. Activation of histone deacetylase-6 induces contractile dysfunction through derailment of alpha-tubulin proteostasis in experimental and human atrial fibrillation. *Circulation*. 2014;129:346-58.
13. Zhang D, Hu X, Li J, Liu J, Baks-Te Bulte L, Wiersma M, Malik NU, van Marion DMS, Tolouee M, Hoogstra-Berends F, Lanters EAH, van Roon AM, de Vries AAF, Pijnappels DA, de Groot NMS, Henning RH and Brundel B. DNA damage-induced PARP1 activation confers cardiomyocyte dysfunction through NAD(+) depletion in experimental atrial fibrillation. *Nat Commun*. 2019;10:1307.

14. Yaksh A, Kik C, Knops P, van Ettinger MJ, Bogers AJ and de Groot NM. Early, de novo atrial fibrillation after coronary artery bypass grafting: Facts and features. *Am Heart J*. 2017;184:62-70.
15. Dobrev D, Aguilar M, Heijman J, Guichard JB and Nattel S. Postoperative atrial fibrillation: mechanisms, manifestations and management. *Nat Rev Cardiol*. 2019;16:417-436.

Supplemental material

Entry criteria

Only patients with ECG-documented AF were included in the paroxysmal or (longstanding) persistent AF groups. Patients with documentation of atrial flutter were excluded from participation in the study. Criteria for hemodynamic instability included usage of inotropic agents or vasopressors and/or presence of a cardiac assist device. Emergency cardiac surgery was defined as cardiac surgery within 24 hours. Patients with end stage renal failure requiring dialysis were also excluded from participation in the study.

Endpoints

Primary endpoint of the study is development or recurrence of documented AF. In line with the latest ESC guidelines, AF is defined as an episode of at least 30 seconds with absolutely irregular RR intervals and no discernible, distinct P waves.

Secondary endpoints include:

- implantation of atrial pacemaker
- implantation of implantable cardioverter defibrillator
- withdrawal of informed consent
- lost to follow-up (unreachable via contact details of the home doctor or hospital)
- decease (confirmed by hospital, home doctor or Dutch BRP register)

3

Direction- and rate-dependent fractionation during atrial fibrillation persistence: unmasking cardiac anisotropy?

Roeliene Starreveld
Natasja M.S. de Groot

Journal of Cardiovascular Electrophysiology. 2020 Aug;31(8):2206-2209

Abstract

This human case is the first to illustrate morphological manifestations of direction- and rate-dependent anisotropic conduction in high-resolution unipolar atrial potentials. Premature impulses induced low-amplitude, fractionated extracellular potentials with exceptionally prolonged durations in a 76-year old longstanding persistent AF patient, demonstrating direction-dependency of anisotropic conduction. An increased pacing frequency induced presence of similar fractionated potentials, reflecting rate-dependent anisotropy and inhomogeneous, slow transverse conduction. Pacing with different rates and from different sites could aid in identifying nonuniform anisotropic tissue and thus the substrate of AF.

Introduction

Due to the cable-like longitudinal arrangement of atrial myocardial fibers, electrical conduction is much faster in longitudinal direction than in transverse direction.[1] While cell geometry is a major determinant of anisotropy, mostly gap junction distribution determine whether propagation is continuous or discontinuous.[2] Altered gap junction distribution and formation of longitudinal collagenous septa between myocardial fibers result in discontinuous transverse propagation ("nonuniform anisotropy") and increased susceptibility to reentrant tachyarrhythmias such as atrial fibrillation (AF).[3, 4] In addition to gap junctions, myocytes can interact by ephaptic coupling, as shown in ventricular myocardium in experimental and modeling studies.[5, 6]

During nonuniform anisotropy, extracellular waveforms consist of more than one deflection (i.e. fractionation), caused by asynchronous firing of two or more groups of cells that are separated by areas in which there is diminished or no cell-to-cell electrical coupling in the path of propagation.[3] Extracellular waveform morphology can therefore be used to detect anisotropic structural discontinuities that are proarrhythmic, such as areas of slowed conduction due to grossly irregular discontinuous propagation.[3]

Importantly, anisotropy is not a static property of cardiac tissue, but can be modulated by alterations in gap junctional conductance (i.e. intercellular coupling), as demonstrated in multiple simulation and animal models.[1, 2, 7, 8] For example, Spach et al. demonstrated anisotropy to be rate-dependent, with higher pacing rates resulting in a lower transverse conduction velocity in relation to longitudinal conduction velocity.[2, 7] In addition, premature stimulation in nonuniform anisotropy resulted in decremental longitudinal conduction and block with zigzag transverse conduction, while this was not the case in uniform anisotropy (i.e. direction-dependency).[9]

Although described in experimental studies, clear examples of these phenomena in patient data are rare. In this paper we present a case in which both the rate- and direction-dependency of anisotropy is demonstrated in a 76-year old patient with longstanding persistent AF.

Case report

A 76-year old female with a history of longstanding persistent AF presented for mitral valve surgery and surgical radiofrequency ablation. During surgery – prior to commencement to extra-corporal circulation – epicardial mapping of the pulmonary vein (PV) area was performed with a 64-electrode spatula (mapping area 17.5x17.5 mm, interelectrode distances 2.5 mm) (*Figure 1*). A silver disc positioned

inside the thoracic cavity served as indifferent electrode. Unipolar signals were stored on a hard disk after amplification (gain 1000), filtering (bandwidth 1-500 Hz), sampling (1kHz) and analogue to digital conversion (12 bits). The patient presented in AF but was cardioverted to sinus rhythm (SR).

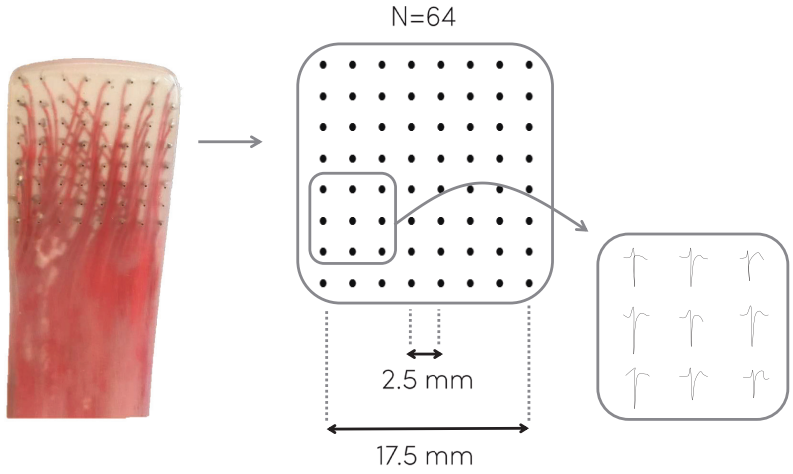

Figure 1 – Epicardial mapping using a 64-electrode spatula. With eight rows of eight unipolar electrodes, having an interelectrode distance of 2.5 mm, the spatula covers a mapping area of 17.5 x 17.5 mm. During epicardial mapping extracellular potentials of atrial tissue are recorded.

During SR, with the spatula on the caudal PV area, several premature atrial complexes (PACs) occurred. During these PACs, morphology of atrial potentials changed considerably (*Figure 2*). Whereas high-amplitude, single atrial potentials of short durations were observed during SR beats, PACs induced low-amplitude and multiphasic (i.e. fractionated) potentials, manifesting exceptional prolongation of potential duration.

After SR recordings, programmed electrical stimulation was performed using electrodes sutured to the right atrial appendage (RAA). With the spatula on the mid PV area, pacing was executed at cycle lengths of 600 ms, 500 ms and 333 ms (corresponding with 100 bpm, 120 bpm and 180 bpm, respectively). At a paced cycle length of 600 ms and 500 ms, high-amplitude, single atrial potentials with short durations were observed. In contrary, pacing at a cycle length of 333 ms induced low-amplitude, fractionated atrial potentials with prolonged durations (*Figure 3*).

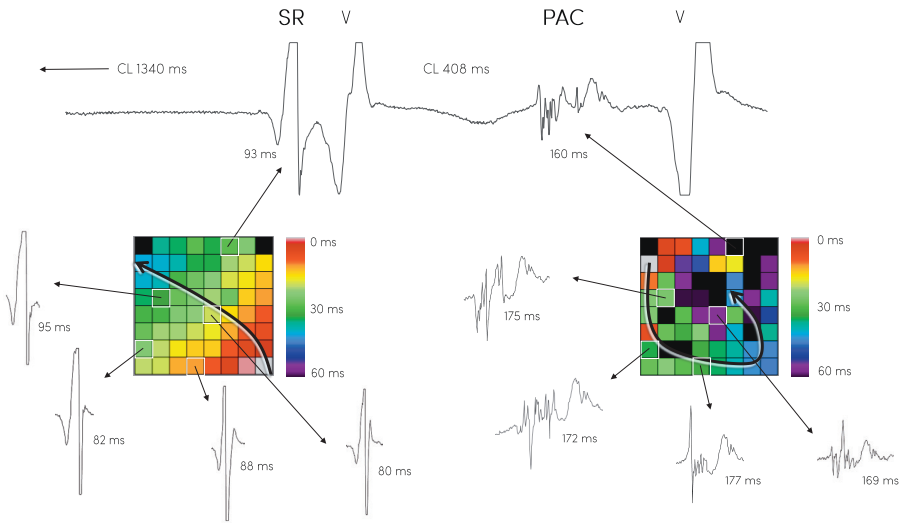

Figure 2 – Premature atrial complex (PAC) causes unidirectional longitudinal block with corresponding low-amplitude, fractionated potentials with long duration. At the top, the electrode 6 tracing demonstrates one sinus rhythm (SR) beat followed by a ventricular far-field complex (V), together with one PAC with subsequent ventricular activation. During recordings the spatula was placed on the caudal PV area. Color-coded activation maps of both the SR beat and PAC are shown. The SR impulse arises from the right-lower part of the mapping area and homogeneously propagates towards the left-upper part, whereas the PAC exhibits inhomogeneous and slow conduction around several lines of block (Δlocal activation time ≥ 12ms, visualized as thick white lines). The SR beat is characterized by high-amplitude, biphasic and smooth extracellular potentials with short duration (80-95 ms), whereas the PAC exhibits low-amplitude, multiphasic potentials with long duration (160-177 ms). CL = cycle length (i.e. coupling interval of consecutive atrial impulses).

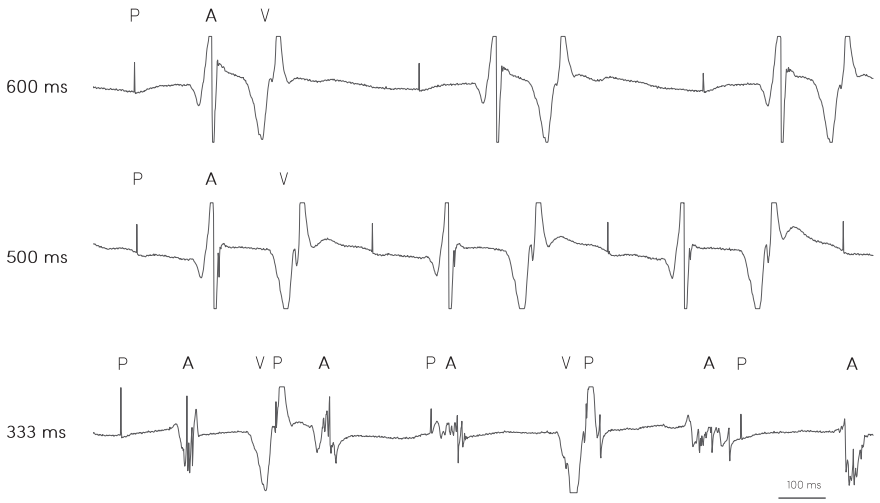

Figure 3 – Pacing at shorter cycle length induces multiphasic fractionated potentials, due to a lower transverse conduction velocity in relation to longitudinal conduction velocity. With the spatula on the mid PV area, pacing from the right atrial appendage was performed. Three unipolar tracings of electrode 10 are shown, corresponding with pacing cycle lengths of 600 ms, 500 ms and 333 ms (i.e. 100 bpm, 120 bpm and 180 bpm, respectively). In contrary to pacing at low rates, pacing at the highest rate (i.e. cycle length of 333 ms) induced low-amplitude, fractionated atrial potentials with prolonged durations. A = atrial complex, P = pacing, V = ventricular far-field complex.

Discussion

This case demonstrates direction- and rate-dependency of anisotropic conduction in the intact human heart and is the first to illustrate its morphological manifestations in high-resolution unipolar atrial potentials.

Premature impulses can cause unidirectional longitudinal block

In correspondence with the experimental studies of Spach et al.[3, 9], low-amplitude fractionated extracellular potentials with prolonged durations were observed during premature impulses in this patient, indicating slow propagation in association with unidirectional block. While one would expect smooth and biphasic extracellular atrial potentials in uniform anisotropic tissue[3], the observed irregular potentials with low-amplitude deflections and severely prolonged potential duration reveal the nonuniformity of anisotropic tissue in the PV area of this patient.

The coupling interval at which the premature impulse arrives is crucial for the course of propagation. In a canine study, Spach et al. showed that at a long

coupling interval (290 ms) both longitudinal and transverse propagation succeeded, whereas during stimulation within the refractory period (130 ms) both failed.[10] At short coupling intervals just above the refractory period (134 and 145 ms) propagation was decremental, showing longitudinal block without transverse conduction. At a coupling interval of 155 ms, decremental conduction and block occurred in the longitudinal direction with preserved transverse propagation, enabling reentry to occur. Spach concluded that only in the latter the premature stimulus was below the safety factor in the longitudinal direction, but above the threshold in the transverse direction, giving rise to longitudinal block with transverse conduction.[2, 8] This example also illustrated that propagation becomes decremental first in the direction having the highest conduction velocity (i.e. the longitudinal direction) with a corresponding long refractory period.[10] As illustrated in *Figure 2*, the SR beat arises from the right-lower part of the mapping area and homogeneously propagates towards the left-upper part, where the earliest activation of the PAC is seen. The relative short coupling interval of the premature impulse (408 ms) causes multiple areas of local conduction block (Δlocal activation time ≥12 ms), around which the wavefront slowly propagates. This also stresses the importance and impact of wavefront entrance and curvature for initiation of reentry, facilitated by the direction-dependency of nonuniform anisotropic tissue.

Increased pacing frequency decreases transverse conduction velocity

Animal studies have shown that the ratio between longitudinal and transverse conduction velocity (i.e. anisotropy ratio) is rate-dependent, with higher stimulation rates resulting in an increased anisotropy ratio due to a relative decrease in transverse conduction velocity.[2, 7] The sudden decay in transverse conduction velocity could not be accounted for by any changes in the action potential and was fully reversible upon decreases of pacing rate[7], and therefore must be due to a change in intercellular coupling (i.e. gap junctional conductance). Although all gap junctions regardless of directionality will be affected, longitudinal propagation velocity retains due to its relative insensitivity to decreases in coupling.[7, 11] Intercellular coupling is thus susceptible to modulation by rate, even within the course of a few action potentials.[2, 7] In our patient, an increase in pacing frequency induced presence of low-amplitude, multiphasic atrial potentials with long durations, which was likely caused by an increase in intercellular coupling resistance and led to inhomogeneous and slow transverse conduction. Partially similar findings were presented in bipolar recordings[12], although especially the potential duration delays observed within this case are exceptional.

Importantly, during premature stimulation both longitudinal and transverse conduction velocity decrease proportionally, whereas increasing the pacing frequency primarily induces an exponential decay of transverse conduction velocity.[2, 7] So although closely related, the sudden appearance of fractionated

potentials during premature impulses as well as during an increased pacing rate are caused by two distinct phenomena: the direction- and rate-dependency of anisotropic conduction, respectively.

Clinical importance

Pacing with different rates and from different sites could aid in identifying nonuniform anisotropic tissue and thus the substrate of AF. Furthermore, substrate-guided AF ablation techniques that are used in clinical practice – such as low-voltage ablation and ablation of complex fractionated atrial electrograms – use thresholds that do not take into account direction- and rate-dependency of (nonuniform) anisotropic tissue.

Conclusions

Premature impulses and an increased pacing rate induced low-amplitude, fractionated potentials with exceptional prolongation of potential duration. Pacing with different rates and from different sites could aid in identifying nonuniform anisotropic tissue and thus the substrate of AF.

References

1. Wit AL, Dillon SM, Coromilas J, Saltman AE and Waldecker B. Anisotropic reentry in the epicardial border zone of myocardial infarcts. *Ann N Y Acad Sci*. 1990;591:86-108.
2. Valderrabano M. Influence of anisotropic conduction properties in the propagation of the cardiac action potential. *Prog Biophys Mol Biol*. 2007;94:144-68.
3. Spach MS. Anisotropy of cardiac tissue: a major determinant of conduction? *J Cardiovasc Electrophysiol*. 1999;10:887-90.
4. Spach MS and Dolber PC. Relating extracellular potentials and their derivatives to anisotropic propagation at a microscopic level in human cardiac muscle. Evidence for electrical uncoupling of side-to-side fiber connections with increasing age. *Circ Res*. 1986;58:356-71.
5. Veeraraghavan R, Lin J, Hoeker GS, Keener JP, Gourdie RG and Poelzing S. Sodium channels in the Cx43 gap junction perinexus may constitute a cardiac ephapse: an experimental and modeling study. *Pflugers Arch*. 2015;467:2093-105.
6. Veeraraghavan R, Lin J, Keener JP, Gourdie R and Poelzing S. Potassium channels in the Cx43 gap junction perinexus modulate ephaptic coupling: an experimental and modeling study. *Pflugers Arch*. 2016;468:1651-61.
7. Spach MS, Kootsey JM and Sloan JD. Active modulation of electrical coupling between cardiac cells of the dog. A mechanism for transient and steady state variations in conduction velocity. *Circ Res*. 1982;51:347-62.
8. Delgado C, Steinhaus B, Delmar M, Chialvo DR and Jalife J. Directional differences in excitability and margin of safety for propagation in sheep ventricular epicardial muscle. *Circ Res*. 1990;67:97-110.
9. Spach MS, Dolber PC and Heidlage JF. Influence of the passive anisotropic properties on directional differences in propagation following modification of the sodium conductance in human atrial muscle. A model of reentry based on anisotropic discontinuous propagation. *Circ Res*. 1988;62:811-32.
10. Spach MS, Miller WT, 3rd, Geselowitz DB, Barr RC, Kootsey JM and Johnson EA. The discontinuous nature of propagation in normal canine cardiac muscle. Evidence for recurrent discontinuities of intracellular resistance that affect the membrane currents. *Circ Res*. 1981;48:39-54.
11. Jongsma HJ and Wilders R. Gap junctions in cardiovascular disease. *Circ Res*. 2000;86:1193-7.
12. Jadidi AS, Duncan E, Miyazaki S, Lellouche N, Shah AJ, Forclaz A, Nault I, Wright M, Rivard L, Liu X, Scherr D, Wilton SB, Sacher F, Derval N, Knecht S, Kim SJ, Hocini M, Narayan S, Haissaguerre M and Jais P. Functional nature of electrogram fractionation demonstrated by left atrial high-density mapping. *Circ Arrhythm Electrophysiol*. 2012;5:32-42.

4

Anatomical hotspots of fractionated electrograms in the left and right atrium: do they exist?

Roeliene Starreveld
Lisette J.M.E. van der Does
Natasja M.S. de Groot

Europace. 2019 Jan;21(1):60-72

Abstract

Aims

Targeting of complex fractionated electrograms (CFEs) in the atria is not yet beneficial in treating drug-refractory atrial fibrillation (AF). In order to gain insight into potential anatomical hotspots of fractionated electrograms a structured literature search was performed.

Methods

PubMed was searched for studies describing fractionation during human atrial electrophysiological measurements (N=565), of which 36 articles described the pre-ablation distribution of fractionated EGMs for the left atrium and/or right atrium in at least four regions.

Results

Fractionation was commonly found in high proportions within all regions of both atria, without clear preference for specific regions. Furthermore, no differences in the fractionation distribution between paroxysmal AF and persistent AF patients were observed.

Conclusion

Whilst atrial inhomogeneous conduction is widely believed to play a key role in AF initiation and perpetuation, different electrophysiological causes for fractionation and the influence of measurement properties complicate identification of the arrhythmogenic substrate. Thereby, simply targeting all CFEs would be short-sighted. Further research is warranted on how to distinguish "physiologic CFEs" from "pathologic CFEs", with only the latter reflecting potential targets for ablative therapy of AF.

Introduction

The search for a successful ablative strategy customized to the specific mechanisms of atrial fibrillation (AF) is an ongoing challenge. Even though AF represents the most commonly sustained cardiac arrhythmia worldwide, the exact mechanisms underlying AF are still largely unknown. Its complex electrical activity within the atria challenges understanding of the electro-pathophysiology of AF. Nowadays, catheter ablation of the pulmonary veins (PVs), believed to be the main source of ectopy triggering AF[1], is an established treatment for patients with symptomatic drug-refractory AF. However, relapses occur in up to 30% of paroxysmal AF (PAF) patients in the first year and 70% of patients with persistent AF (PsAF).[2] Since Konings et al. showed that areas of fractionated potentials during intraoperative mapping of human AF correspond with areas of inhomogeneous conduction and pivoting points[3], potentially reflecting the arrhythmogenic substrate of AF, ablative targeting of complex fractionated electrograms (CFEs) have gained interest.[4] As (randomized) studies failed to confirm clinical benefits of CFE ablation in addition to pulmonary vein isolation (PVI) for both PAF and PsAF patients[5-8], investigating the true mechanism of fractionated electrograms (EGMs) is of importance. Recent studies gained perspective on the electrophysiological origin of CFEs[9-12], its diverse definitions[12] and the potential role of atrial structure in inhomogeneous conduction[13,14]. To gain more insight in the role of atrial anatomy in fractionated EGMs, this review aims to investigate whether anatomical hotspots for fractionated EGMs exist. We therefore systematically reviewed the distribution of fractionated EGMs throughout the atria during AF.

Pathophysiology of fractionation

Extracellular cardiac EGMs display changes in electrical potential (in voltages) over a period of time, enabling visualization of (depolarizing) wave fronts.[9,15] In unipolar EGMs, a wavefront approaching the electrode causes a positive spike, whereas a wavefront moving away from the electrode causes a negative deflection.[15] Propagating in homogenous tissue, the unipolar EGM can thereby only have a biphasic (wavefront passing by) or a monophasic (wavefront originating or ending) morphology.[9] A bipolar EGM is made by subtracting two unipolar EGMs recorded at adjacent electrode sites, thereby reducing its "field of view" so that far-field signal disturbance is diminished.[15] The downside of bipolar EGMs is their dependence on interelectrode spacing and susceptibility to wavefront direction changes, both enabling non-physiological fractionated EGMs to occur.[9,15] Although exact definitions of fractionation greatly varies within literature, most studies agree that fractionation comprises a unipolar or bipolar EGM with multiple deflections and often a prolonged duration.[12] The underlying mechanism of EGM fractionation is generally restricted to three possibilities: (1) artifacts (e.g. movement or interference), (2) remote tissue activation (e.g. neighboring regions) and/or (3)

inhomogeneous tissue conduction within the recording area (e.g. through functional anisotropy or pathological tissue fibrosis).[9, 12] Fractionation can therefore occur in the presence of normal tissue functionality or due to pathological processes impeding homogeneous conduction, the latter believed to reflect the arrhythmogenic substrate of AF.[4, 9, 12] If so, identifying predilection sites for fractionation could not only greatly enhance knowledge regarding underlying electrophysiology of substrate-mediated AF, but also point out potential ablative targets.

Methods

A structured literature search was performed on PubMed using the following MeSH terms: *atrial fibrillation* or *heart atria*, and *electrophysiologic techniques*, *cardiac* or *electrophysiology* or *electrocardiography*, and *humans*. In addition to this, the titles and abstracts were screened for the following terms: *atrium* or *atria* or *atrial fibrillation* or *auricular fibrillation*, and *fractionation* or *fractionated* or *fragmentation* or *fragmented* or *CFAE* or *CFE* or *CEA* or *AF nest*, and *electrogram* or *ECG* or *electrophysiology* or *electrocardiography* or *electroanatomic*. Editorials, commentaries, reviews and case reports were excluded from the search. This search resulted in 565 articles, which were screened for inclusion and exclusion criteria. Only studies where the distribution of fractionated EGM occurrence within the left atrium (LA) and/or right atrium (RA) before ablation was described or could be derived were included. Based on these studies, nine separate regions for the LA were defined*: pulmonary veins (PVs), left atrial appendage (LAA), LA septum, LA posterior wall (LAPW), LA lateral wall (LALW), LA anterior wall (LAAW), LA floor, LA roof*, and the *mitral annulus (MA)* (*Figure 1*). For the RA also nine regions were defined: *caval veins (CVs), right atrial appendage (RAA), RA septum, RA posterior wall (RAPW), RA lateral wall (RALW), RA anterior wall (RAAW), RA roof, tricuspid annulus (TA)* and *crista terminalis (CT)* (*Figure 1*). The coronary sinus (CS) was considered a separate region. Articles which described the fractionation proportion within less than four LA and/or RA regions were excluded.

A total of 36 articles met all selection criteria (*Figure 2*). Proportions were transformed by the Freeman-Tukey double arcsine method to accomplish normally distributed data. For all studies the weighted average proportion and 95% CIs were derived and compared (if N>1) between patients with PAF and (longstanding) PsAF based on the DerSimonian-Laird random effects logistic regression model.

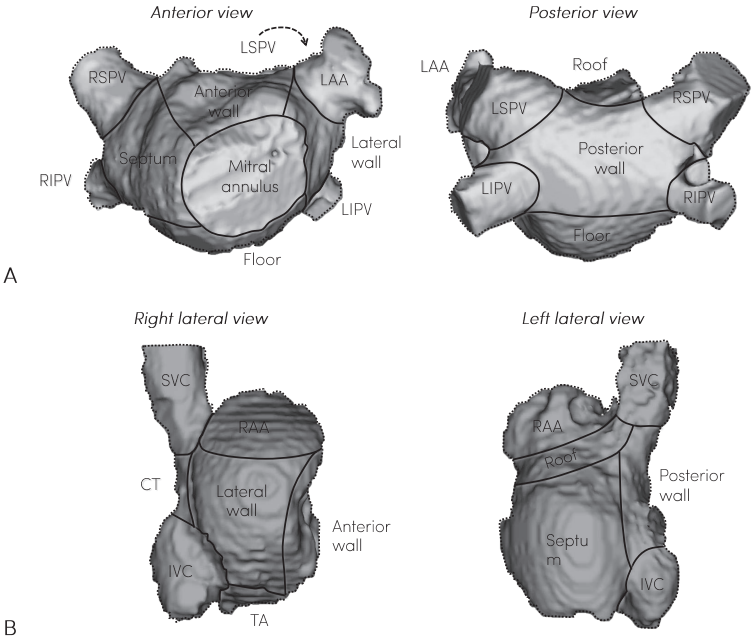

Figure 1 – Anatomic division of the left atrium (LA) and right atrium (RA). *A*: anterior and posterior views of the LA, showing its nine anatomic regions (the pulmonary veins together are one region). *B*: right lateral and left lateral views of the RA, showing its nine anatomic regions (both caval veins together are one region). CT, crista terminalis; IVC, inferior vena cava; LAA, LA appendage; LIPV, left inferior PV; LSPV, left superior PV; RAA, RA appendage; RIPV, right inferior PV; RSPV, right superior PV; SVC, superior vena cava; TA, tricuspid annulus.

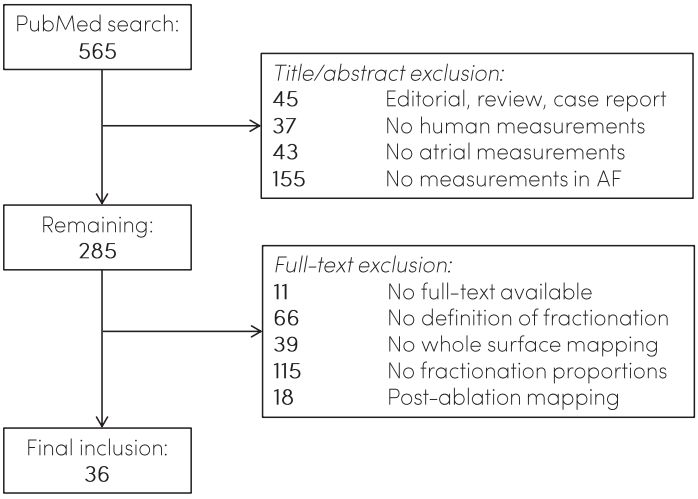

Figure 2 – Flowchart of article in- and exclusion and definitions. AF, atrial fibrillation.

Results

Baseline characteristics and recording techniques of all 36 included articles are listed in *Table 1*. All studies used endocardial mapping techniques and the majority (N=33) recorded bipolar EGMs. Four studies included patients with PAF, 18 studies with PsAF and the remainder (N=14) had both PAF and PsAF patients. Thirty-two studies described distal electrode size and 28 studies described interelectrode spacing. The minimal distal electrode size was 1 mm, interelectrode spacing mostly ranged between 2 and 5 mm.

Two units of fractionation proportions were used, preventing comparison of all articles together. The majority of the studies (N=21) determined the number of patients with fractionated EGMs at different anatomical regions and defined the fractionation proportion as the number of patients with fractionated EGMs at the region of interest divided by the total number of patients (% CFE: patients). Fifteen studies determined the number of fractionated EGMs at different anatomical regions within the atria, defining the fractionation proportion as the number of fractionated EGMs divided by the total number of obtained EGMs at the region of interest (% CFE: EGMs).

Table 1 – Baseline characteristics and recording techniques of all 36 included articles.

Author	Year	Type	PAF/ PsAF	No. of patients (PAF)	LA/ RA	CFE definition	Time window (s)	Uni/ bipolar	Catheter type	Distal electrode size (mm)	Inter-electrode spacing (mm)	Filter (Hz)
Nakahara [16]	2014	% CFE: patients	PsAF	44	LA	Mean CL ≤120 ms	5	Bipolar	20-pole 20mm Inquiry AFocusII, St Jude Medical	1	4	-
Teh [17]	2011	% CFE: EGMs	PsAF	12	LA	Mean CL ≤120 ms	5	Bipolar	20-pole 15-25mm Reflexion Spiral XX, St Jude Medical	2	1-4-1	30-500
Park [18]	2010	% CFE: EGMs	Mixed	100 (51)	LA	Mean CL ≤120 ms	6	Bipolar	-	-	-	32-300
Hwang [19]	2015	% CFE: patients	PsAF	43	LA	Mean CL ≤120 ms	>6	Bipolar	10-pole or 20-pole double-spiral Lasso, Biosense Webster	1	-	30-300
Yamabe [20]	2011	% CFE: patients	Mixed	19 (17)	LA	>2 deflections *or* mean CL ≤120 ms	10	Mixed	7-F quadripolar catheter, Japan Lifeline	8	-	50-600
Yamabe [21]	2009	% CFE: patients	PAF	16	LA	>2 deflections *or* mean CL ≤120 ms	10	Mixed	7-F quadripolar catheter, Japan Lifeline	8	-	50-600
Hunter [22]	2012	% CFE: patients	PsAF	19	LA	Mean CL ≤120 ms	5	Bipolar	14-pole 14.5-25 mm Orbiter PV catheter, Boston Scientific	1	5	-

Table 1 - Continued

Author	Year	Type	PAF/ PsAF	No. of patients (PAF)	LA/ RA	CFE definition	Time window (s)	Uni/ bipolar	Catheter type	Distal electrode size (mm)	Inter-electrode spacing (mm)	Filter (Hz)
Lo [23]	2010	% CFE: patients	Mixed	20 (13)	LA	Mean CL ≤120 ms with isoelectric interval of >50 ms	7.2	Mixed	Non-contact catheter Ensite, St. Jude Medical *and* EPT catheter, Boston Scientific	-, 4	-, 2.5	32-300
Saghy [24]	2012	% CFE: EGMs	PsAF	20	LA	Mean CL ≤70 ms	5	Bipolar	10-pole 15-25 mm Lasso, Biosense Webster	1	8	-
De Bortoli [25]	2015	% CFE: EGMs	PsAF	23	LA	Mean CL ≤120 ms	5	Bipolar	Cool Path *and* Cool Flex catheter, St Jude Medical	4, 4	1.5-5-2, 0.5-5-2	-
Knecht [26]	2010	% CFE: EGMs	Mixed	29 (13)	LA	Mean CL ≤120 ms	5	Bipolar	20-pole mapping catheter Pentaray, Biosense Webster	1	-	-
Nakahara [27]	2013	% CFE: patients	PsAF	62	LA	Mean CL ≤120 ms	5	Bipolar	20-pole 20mm Inquiry AFocusII, St Jude Medical	1	4	-
Bassiouny [28]	2016	% CFE: patients	PsAF	44	LA	Mean CL 50-120 ms	-	Bipolar	10-pole Lasso catheter, Biosense Webster	1	-	-

Table 1 - Continued

Author	Year	Type	PAF/ PsAF	No. of patients (PAF)	LA/ RA	CFE definition	Time window (s)	Uni/ bipolar	Catheter type	Distal electrode size (mm)	Inter-electrode spacing (mm)	Filter (Hz)
Matsuo [29]	2012	% CFE: EGMs	PsAF	40	LA	Mean CL ≤120 ms	5	Bipolar	20-pole double circular Inquiry AFocusII, St Jude Medical	1	4	-
Nakahara [30]	2014	% CFE: EGMs	PsAF	35	LA	Mean CL 50-120 ms	5	Bipolar	20-pole 20mm Inquiry AFocusII, St Jude Medical	1	4	-
Hunter [31]	2011	% CFE: EGMs	PsAF	20	LA	Continuous deflections of ≥70 ms width *and* occupying at least ≥70% of the time window	10	Bipolar	14-pole 14.5-25mm PV mapping catheter, Orbiter PV	1	5	30-250
Nagashima [32]	2012	% CFE: patients	Mixed	34 (16)	LA	Mean CL 50-120 ms	5	Bipolar	20-pole Livewire Spiral HP catheter, St Jude Medical	-	1.5	30-500
Lin [33]	2008	% CFE: patients	Mixed	27 (13)	LA	Mean CL ≤120 ms	1	Bipolar	EPT Blazer catheter, Boston Scientific	4	2.5	-
Verma [34]	2008	% CFE: EGMs	PsAF	24	LA	Mean CL ≤120 ms	6	Bipolar	Decapolar circular mapping catheter, Biosense Webster	1	2	30-500

Table 1 - Continued

Author	Year	Type	PAF/ PsAF	No. of patients (PAF)	LA/ RA	CFE definition	Time window (s)	Uni/ bipolar	Catheter type	Distal electrode size (mm)	Inter-electrode spacing (mm)	Filter (Hz)
Oral [35]	2008	% CFE: patients	PsAF	85	Both	Mean CL ≤120 ms *or* shorter than CL in the CS *or* CEA	-	Bipolar	ThermoCool quadripolar catheter, Biosense Webster	3.5	2-5-2	30-500
Miyamoto [36]	2010	% CFE: patients	Mixed	20 (16)	LA	Mean CL ≤120 ms	5	Bipolar	-	8	2	-
Kofune [37]	2013	% CFE: patients	Mixed	23 (14)	LA	Mean CL 50-120 ms	5	Bipolar	20-pole Livewire Spiral HP, St Jude Medical	-	1.5	30-500
Estner [38]	2008	% CFE: patients	PsAF	35	LA	>2 deflections *and/or* CEA *or* mean CL ≤120 ms	10	Bipolar	-	-	-	-
Chen [39]	2011	% CFE: patients	PAF	58	LA	Mean CL 50-120 ms	6	Bipolar	ThermoCool quadripolar catheter, Biosense Webster *or* quadripolar catheter IBI, St Jude Medical	3.5, -	2-5-2, -	30-500
Tada [40]	2008	% CFE: EGMs	Mixed	44 (25)	LA	Width ≥80 ms with isoelectric interval	>5	Bipolar	ThermoCool quadripolar catheter, Biosense Webster	3.5	2-5-2	30-500

Table 1 - Continued

Author	Year	Type	PAF/ PsAF	No. of patients (PAF)	LA/ RA	CFE definition	Time window (s)	Uni/ bipolar	Catheter type	Distal electrode size (mm)	Inter-electrode spacing (mm)	Filter (Hz)
El Haddad [41]	2011	% CFE: EGMs	PsAF	13	LA	Non-fractionated potentials separated by an isoelectric interval	2.5	Bipolar	14-pole circular Orbiter PV, Boston Scientific *and* ThermoCool quadripolar catheter, Biosense Webster	1, 3.5	5, 2-5-2	30-400
Verma [42]	2008	% CFE: patients	Mixed	35 (21)	LA	Mean CL ≤120 ms	5	Bipolar	Decapolar circular mapping catheter, Biosense Webster	1	2	30-500
Di Biase [43]	2009	% CFE: patients	PAF	34	Both	>2 deflections *or* CEA *or* mean CL ≤120 ms	10	Bipolar	ThermoCool quadripolar catheter, Biosense Webster	3.5	2-5-2	-
Verma [44]	2010	% CFE: patients	Mixed	34 (21)	Both	Mean CL ≤120 ms	5	Bipolar	Decapolar circular catheter, Biosense Webster *and/or* Therapy Cool Path catheter, St Jude Medical	1, 3.5	2, 2-5-2	30-500
Redfearn [45]	2009	% CFE: EGMs	PAF	10	LA	Mean CL 50-120 ms	4	Bipolar	Lasso catheter *and* ThermoCool quadripolar catheter, Biosense Webster	1, 3.5	-, 2-5-2	-

Table 1 - Continued

Author	Year	Type	PAF/ PsAF	No. of patients (PAF)	LA/ RA	CFE definition	Time window (s)	Uni/ bipolar	Catheter type	Distal electrode size (mm)	Inter-electrode spacing (mm)	Filter (Hz)
Calo [46]	2008	% CFE: EGMs	PsAF	25	Both	≥10 intervals of 70-120 ms between successive peaks (0.05-0.15mV)	2.5	Bipolar	ThermoCool quadripolar catheter, Biosense Webster	3.5	2-5-2	-
Estner [47]	2008	% CFE: patients	PsAF	23	LA	>2 deflections *and/or* CEA *or* mean CL ≤120 ms	2.5, 5	Bipolar	10 mm Lasso, Biosense Webster *or* 14.1 mm Orbiter PV, Boston Scientific	-, 1	-, 5	-
Porter [48]	2008	% CFE: patients	Mixed	67 (42)	LA	≥7 intervals of 60-120 ms between successive peaks (0.05-0.15mV)	2.5	Bipolar	ThermoCool quadripolar catheter *and* circular Lasso, Biosense Webster	3.5, -	2-5-2, -	30-400

Table 1 - Continued

Author	Year	Type	PAF/ PsAF	No. of patients (PAF)	LA/ RA	CFE definition	Time window (s)	Uni/ bipolar	Catheter type	Distal electrode size (mm)	Inter-electrode spacing (mm)	Filter (Hz)
Narayan [49]	2011	% CFE: EGMs	Mixed	18 (7)	Both	Magnitude <0.5 mV *and* width >50 ms with >3 deviations from baseline *and/or* CEA	8.2	Bipolar	7F MAP catheter, Biosense Webster	4	-	30-500
Roux [50]	2008	% CFE: patients	PsAF	15	LA	Mean CL ≤120 ms	2	Bipolar	10-pole 15-25 mm Lasso, Biosense Webster	1	8	-
Roux [51]	2009	% CFE: EGMs	PsAF	20	LA	Mean CL ≤120 ms	4	Bipolar	10-pole 15-25 mm Lasso, Biosense Webster	1	8	-

CEA, continuous electrical activity (without presence of an isoelectric line); CFE, complex fractionated electrogram; CL, cycle length (time interval between consecutive negative deflections); CS, coronary sinus; EGM, electrogram; LA, left atrium; PAF, paroxysmal atrial fibrillation; PsAF, persistent atrial fibrillation; RA, right atrium.

The distribution of fractionation within the LA

Figure 3 visualizes the observed fractionation distribution in the LA. The upper panel illustrates that patients had fractionated EGMs (% CFE: patients) regularly within all regions within the LA, with an overall average proportion of 60.8% (48.5-72.5%). The proportion of patients with fractionated EGMs was highest at the LA septum (70.7%, 62.9-78.0%) and the LA roof (68.9%, 58.7-78.2%). At the LALW and MA only 43.8% (28.6-59.7%) and 44.3% (32.6-56.2%) of the patients exhibited fractionated EGMs respectively.

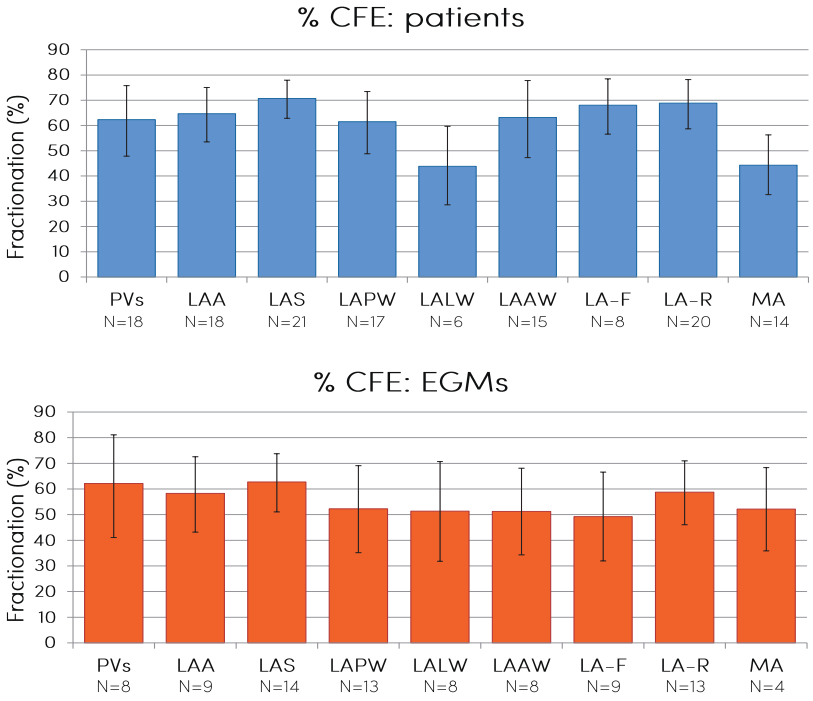

Figure 3 – Observed fractionation distribution of the left atrium (LA). Proportions are given in weighted averages with 95% CI. N = number of included studies. *Upper panel*: the number of patients with fractionated electrograms (EGMs) divided by the total number of patients at the regions of interest (% CFE: patients). *Lower panel*: the number of fractionated EGMs divided by the total number of obtained EGMs at the regions of interest (% CFE: EGMs). CFE, complex fractionated electrogram; LAA, LA appendage; LAAW, LA anterior wall; LA-F, LA floor; LALW, LA lateral wall; LAPW, LA posterior wall; LA-R = LA roof; LAS, LA septum; MA, mitral annulus; PVs, pulmonary veins.

The lower panel depicts the proportion of fractionated EGMs (% CFE: EGMs) within the LA, with an overall average proportion of 55.4% (38.9-71.2%). The proportion was highest in the LA septum (62.7%, 51.1-73.7%) and the PVs (62.2%, 41.1-81.1%), whereas the LA floor had the lowest proportion of fractionated EGMs (49.2%, 32.0-66.6%).

Comparing fractionation proportions between paroxysmal AF patients and persistent AF patients

Four articles with a PAF-only cohort, 18 articles with a PsAF-only cohort and six articles with a mixed cohort – describing the fractionation distribution separately for PAF and PsAF patients – could be used for comparisons. *Figure 4* shows the fractionation distribution within the LA for both PAF and PsAF patients.

The upper panel illustrates that the proportion of PAF patients that had fractionated EGMs (% CFE: patients) was highest at the LA floor (94%, N=1) and the LA roof (80.9%, 33.7-99.8%), whereas for PsAF patients it was highest at the LA septum (69.8%, 60.0-78.8%) and LA floor (67.6%, 52.9-80.7%). For both PAF and PsAF patients, the LALW had the least proportion of patients with fractionated EGMs (19%, N=1 and 55.1%, 46.4-63.7%). Average overall proportion was 62.5% (34.2-86.6%) for PAF and 63.3% (48.4-76.8%) for PsAF patients. None of the regions showed significant differences in fractionated EGM occurrence between PAF and PsAF patients (*Table 2*).

As seen in the lower panel, PAF patients exhibited most fractionated EGMs (% CFE: EGMs) at the LA septum (66.2%, 39.9-88.0%) and LA roof (63.6%, 45.9-79.6%), whereas for PsAF patients the LAA (72.5%, 60.9-82.7%) and LA septum (64.8%, 51.2-77.2%) showed most fractionated EGMs. The MA showed the lowest proportion (34%, N=1) of fractionated EGMs for PAF patients and the LA floor (50.5%, 32.4-68.6%) for PsAF patients. Average overall proportion was 55.8% (42.2-75.8%) for PAF and 60.5% (40.4-78.9%) for PsAF patients. None of the regions showed significant differences in fractionated EGM proportions between PAF and PsAF patients (*Table 2*).

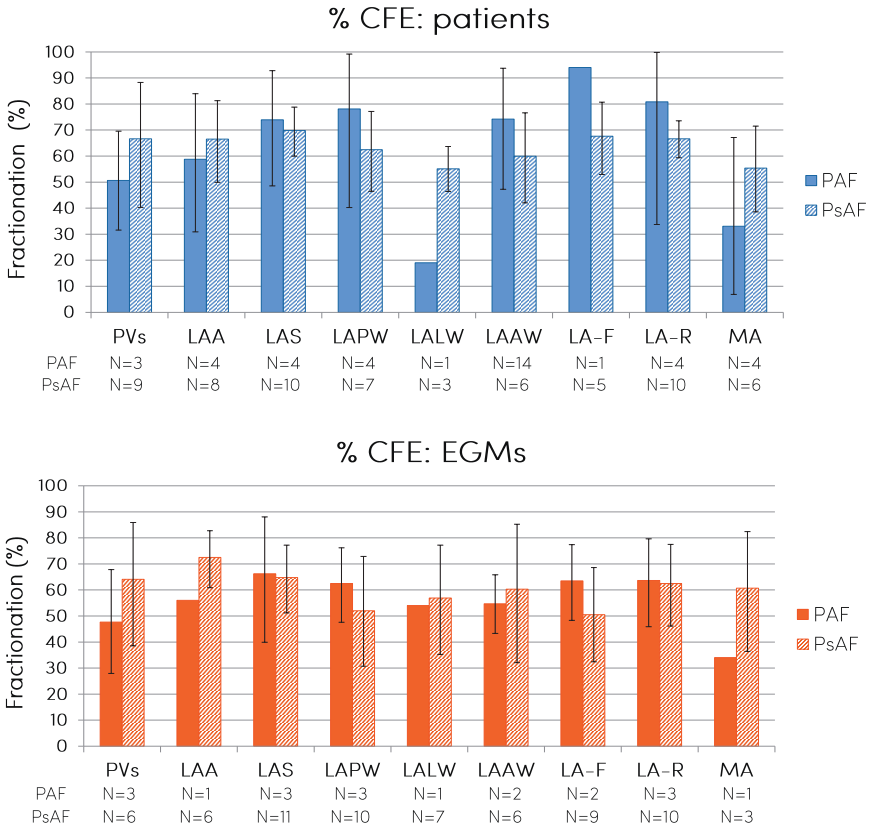

Figure 4 – Observed fractionation distribution of the left atrium (LA) for paroxysmal atrial fibrillation (PAF) and for persistent atrial fibrillation (PsAF) patients. Proportions are given in weighted averages with 95% CI. N = number of included studies. *Upper panel*: the number of patients with fractionated electrograms (EGMs) divided by the total number of patients at the regions of interest (% CFE: patients). *Lower panel*: the number of fractionated EGMs divided by the total number of obtained EGMs at the regions of interest (% CFE: EGMs). CFE, complex fractionated electrogram; LAA, LA appendage; LAAW, LA anterior wall; LA-F, LA floor; LALW, LA lateral wall; LAPW, LA posterior wall; LA-R, LA roof; LAS, LA septum; MA, mitral annulus; PVs, pulmonary veins.

Table 2 – P-values left atrium (LA) regions comparing fractionation proportions (if N>1) of patients with paroxysmal atrial fibrillation (AF) and (longstanding) persistent AF, based on the DerSimonian-Laird random effects logistic regression model.

Type	PVs	LAA	LAS	LAPW	LALW	LAAW	LA-F	LA-R	MA
% CFE: patients	0.33	0.63	0.75	0.43	-	0.37	-	0.53	0.25
% CFE: EGMs	0.32	-	0.92	0.43	-	0.72	0.28	0.93	-

CFE, complex fractionated electrogram; EGM, electrogram; LAA, LA appendage; LAAW, LA anterior wall; LA-F, LA floor; LALW, LA lateral wall; LAPW, LA posterior wall; LA-R, LA roof; LAS, LA septum; MA, mitral annulus; PVs, pulmonary veins

The distribution of fractionation within the CS

The distribution of fractionation within the CS was described in 11 articles. At the CS, the proportion of patients with either PAF or PsAF displaying fractionated EGMs was 58.2% (44.1-71.6%) (% CFE: patients, N=9), whereas the proportion of fractionated EGMs was 68.1% (16.2-99.8%) (% CFE: EGMs, N=2).

The distribution of fractionation within the RA

Only five articles described the distribution of fractionation within the RA (N=3 % CFE: patients, N=2 % CFE: EGMs). Noteworthy, the article of Oral et al. only mapped the RA in a subgroup of patients (33/85) in whom AF persisted after LA and CS CFE ablation.[35] *Figure 5* illustrates the reported fractionation distribution in the RA.

The upper panel illustrates that the proportion of patients that had fractionated EGMs (% CFE: patients) was highest at the CT (63.5%, 24.2-94.4%) and the RA septum (38.7%, 31.2-46.5%), whilst only 10.4% (6.1-15.7%) of patients had fractionation at the TA. The overall average proportion was 29.3% (17.2-40.7%). The proportions of the RAPW, RALW and RA roof were not provided in any of the three articles.

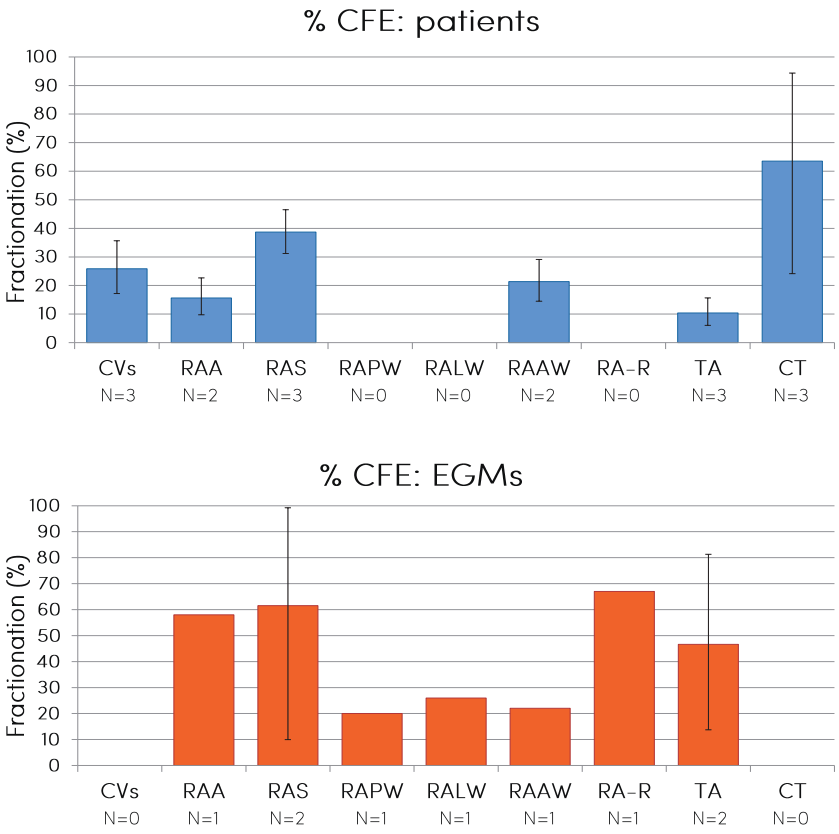

Figure 5 – Observed fractionation distribution of the right atrium (RA). Proportions are given in weighted averages with 95% CI. N = number of included studies. *Upper panel*: the number of patients with fractionated electrograms (EGMs) divided by the total number of patients at the regions of interest (% CFE: patients). *Lower panel*: the number of fractionated EGMs divided by the total number of obtained EGMs at the regions of interest (% CFE: EGMs). CFE, complex fractionated electrograms; CVs, caval veins; CT, crista terminalis; EGMs, electrograms; RAA, RA appendage; RAAW, RA anterior wall; RALW, RA lateral wall; RAPW, RA posterior wall; RA-R, RA roof; RAS, RA septum; TA, tricuspid annulus.

As seen in the lower panel, the RA roof showed the highest proportion of fractionated EGMs (67%, N=1) (% CFE: EGMs), whilst the RAPW exhibited the lowest number of fractionated EGMs (20%, N=1). Average overall proportion was 43.0% (11.9-90.3%). Fractionation numbers for the CVs and CT were not provided in the two articles.

Given the very low number of articles describing the distribution of fractionated EGMs within the RA, no sub-analysis was performed comparing the fractionation distribution between PAF and PsAF patients.

Discussion

Clinical perspective

Initially CFEs were considered promising targets for ablative therapy of PVI-resistant AF, until recent low success rates led to doubt regarding its utility in clinical practice. Nowadays, CFE ablation alone is favored less, whereas hybrid ablation, combining surgical intervention with catheter ablation, is an emerging therapy for PsAF. Hybrid ablation entails anatomic elimination of atrial activity in a wide area of LA – inclusive CFE areas – and has shown truly promising results in the treatment of PsAF patients.[52-55] No randomized controlled trials however have been performed yet to demonstrate effectiveness and safety relative to other ablative techniques (combined and alone).

Whilst atrial inhomogeneous conduction is widely believed to play a key role in initiation and maintenance of AF, identification of the responsible substrate tissue based on EGM morphology alone has been proven to be difficult. Both an intricate milieu of normal tissue response to differences in electrophysiological properties of the underlying myocardium (i.e. different refractoriness or different conduction velocities) and pathologic tissue critical for maintenance of AF is believed to impact EGM morphology.[9, 10, 12] Our review shows that high occurrence rates of CFEs are common in all regions of both atria. Simply targeting all CFEs would be very extensive, would unnecessarily increase scarring of healthy atrial tissue and increase the risk of post-ablative iatrogenic atrial tachyarrhythmias.

Relation between atrial anatomy and fractionation

Regional disparity of endocardial atrial activation during AF in humans was firstly observed in the study of Jais et al.[56] Several years later the fundamental study of Nademanee et al. concluded fractionated EGMs to be predominantly located in the interatrial septum (IAS), PVs, LA roof and proximal CS.[4] These anatomic regions harbor changes in muscle thickness, myocardial cell size, extracellular resistance, fiber orientation and cell-to-cell coupling, potentially enabling heterogeneous conduction rather than homogeneous conduction.[4, 9, 57, 58] Summarizing all studies performed on this topic however, our findings indicate that high occurrence rates of CFEs are not restricted to the IAS, PVs, LA roof and CS, but can be found abundantly within all areas of both atria. Aside from fractionation due to artifacts, the anatomic nature of atrial tissue itself seems an inherent hotspot for fractionation. Although still used in clinical practice, automated fractionation detection algorithms are unable to distinguish between "physiologic CFEs" and "pathologic CFEs" (illustrated in *Figure 6*), while only the latter reflects potential targets for ablative therapy of AF. As frequent causes of physiological fractionation are believed to be electrical activation of overlaying myocardial cells (due to embryologic development) and functional anisotropy, imaging (e.g. cardiac MRI) and histology techniques,

particularly if combined with high-resolution AF mapping studies, have high potential to characterize fractionation. Future studies in this field could aid in unraveling the role of pathological fractionation in substrate-mediated AF.

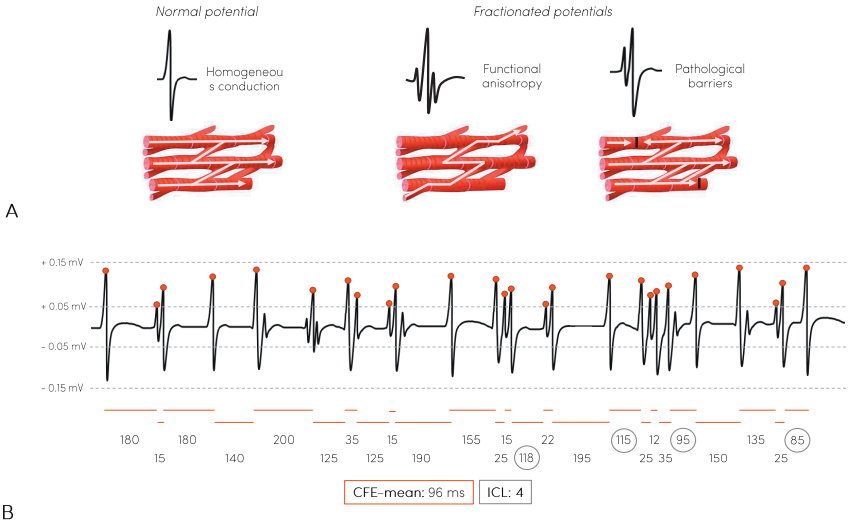

Figure 6 – Fractionation in bipolar electrograms. A, characteristics of normal and fractionated potentials. Homogeneous conduction results in a normal potential, whereas inhomogeneous conduction, either due to functional anisotropy or pathological barriers between myocardial fibers, results in fractionated potentials. **B**, schematic example illustrating two automated methods for fractionation detection: CFE-mean (mean cycle length between successive peaks >0.05 mV) and ICL (intervals of 70-120 ms between successive peaks 0.05-0.15mV). A complex fractionated electrogram (CFE) was defined as CFE-mean ≤ 120 ms or interval confidence level (ICL) ≥ 7 in this 2.5s AF electrogram. Example calculations: CFE-mean = (180+15+180+140+200+125+35+125+15+190+155+25+15+118+ 22+195+115+25+12+35+ 95+150+135+25+85)/25; ICL = number of intervals 70-120 ms = 4.

It is generally assumed that structural and electrophysiological remodeling is more pronounced in the LA than RA.[59] Specifically PsAF patients show more widespread CFE occurrence in both atria than PAF patients.[4, 48, 60-62] In our study fractionation was indeed found in a somewhat lesser extent in the RA, but due to the limited number of articles that analyzed fractionation distribution in the RA we could not confirm this hypothesis.

Only endocardial studies were included in this review. Proof of electrical dissociation between the endocardial and epicardial layer has been shown in animals[63] and humans[64] with (persistent) AF, and could potentially also play a major role in occurrence of CFEs. Simultaneous high-resolution mapping of the epicardial and endocardial wall could clarify this relation in the future.

Fractionation occurrence in paroxysmal AF and persistent AF patients

Only a few articles described the fractionation distribution throughout the LA in PAF patients, complicating the comparison between PAF and PsAF patients. In general, fractionation is believed to play a more pivotal role in PsAF patients than PAF patients. However, in our review no significant differences were found in fractionation proportions between PAF and PsAF patients in any of the LA regions. Highest fractionation proportions were found at varying LA regions in PAF and PsAF patients. Particularly in PAF patients, the PV ostia are considered important for initiation and perpetuation of AF[1, 65] and have been linked to a higher occurrence of fractionated EGMs[66, 67]. In our review however, PAF patients exhibited most fractionated EGMs at the LA floor, and not at the PV area. PAF patients showed (non-significantly) less fractionation at the PV area than PsAF patients.

Limitations of our study

A wide variety of mapping catheters are used within studies (*Table 1*). Importantly, many measurement properties of these catheters, e.g. unipolar/bipolar, interelectrode spacing, distal electrode size and even filter and amplification settings, are known to impact EGM morphology. Bipolar recordings, used in the majority of studies, are susceptive to fractionation when the direction of the propagating wavefront changes.[9, 15] Furthermore, recent studies showed that fractionation increased with increasing electrode spacing in bipolar recordings.[68] A narrow interelectrode spacing is therefore preferable for detection of true fractionation.[69] As the cardiac EGM displays the sum of activation potentials from all muscle fibers in close proximity to the electrode, electrode size also directly influences fractionation occurrence.[70] Within the included studies, electrode size ranged between 1 and 8 mm and interelectrode spacing between 0.5 and 8 mm. Distribution notations and boundaries of the 9 LA regions and 9 RA regions varied throughout the literature. Additionally, definition of CFEs varied between studies (*Table 1*). The majority of studies (N=25) used the NavX™ automated 'CFE-mean' algorithm, in which CFEs are generally considered to occur when the mean cycle length (CL) is ≤120 ms within the selected time window. Other studies included the number of deflections, span of activation and width in their definition. As illustrated in *Figure 6*, indices of bipolar CFEs correlate poorly with each other and with fractionation indices derived from unipolar electrograms.[68]

The obvious heterogeneity in used definitions and settings seriously complicates comparison of studies and could also partly be responsible for the lack of clinical success addressing CFE ablation studies, emphasizing the need for technological improvements and standardization of CFE mapping systems.

Conclusion

Fractionation was commonly found in high proportions within all regions of both atria and without a clear preference for specific sites. Furthermore, no differences were observed in fractionation proportions between PAF and PsAF patients within the LA and RA. Simply targeting all CFEs would be very extensive and short-sighted. Further research should therefore focus on how to distinguish "physiologic CFEs" from "pathologic CFEs", with only the latter reflecting potential targets for ablative therapy of AF.

References

1. Haissaguerre M, Jais P, Shah DC, Takahashi A, Hocini M, Quiniou G, Garrigue S, Le Mouroux A, Le Metayer P and Clementy J. Spontaneous initiation of atrial fibrillation by ectopic beats originating in the pulmonary veins. *N Engl J Med*. 1998;339:659-66.
2. Oral H, Knight BP, Tada H, Ozaydin M, Chugh A, Hassan S, Scharf C, Lai SW, Greenstein R, Pelosi F, Jr., Strickberger SA and Morady F. Pulmonary vein isolation for paroxysmal and persistent atrial fibrillation. *Circulation*. 2002;105:1077-81.
3. Konings KT, Smeets JL, Penn OC, Wellens HJ and Allessie MA. Configuration of unipolar atrial electrograms during electrically induced atrial fibrillation in humans. *Circulation*. 1997;95:1231-41.
4. Nademanee K, McKenzie J, Kosar E, Schwab M, Sunsaneewitayakul B, Vasavakul T, Khunnawat C and Ngarmukos T. A new approach for catheter ablation of atrial fibrillation: mapping of the electrophysiologic substrate. *J Am Coll Cardiol*. 2004;43:2044-53.
5. Verma A, Jiang CY, Betts TR, Chen J, Deisenhofer I, Mantovan R, Macle L, Morillo CA, Haverkamp W, Weerasooriya R, Albenque JP, Nardi S, Menardi E, Novak P, Sanders P and Investigators SAI. Approaches to catheter ablation for persistent atrial fibrillation. *N Engl J Med*. 2015;372:1812-22.
6. Providencia R, Lambiase PD, Srinivasan N, Ganesh Babu G, Bronis K, Ahsan S, Khan FZ, Chow AW, Rowland E, Lowe M and Segal OR. Is There Still a Role for Complex Fractionated Atrial Electrogram Ablation in Addition to Pulmonary Vein Isolation in Patients With Paroxysmal and Persistent Atrial Fibrillation? Meta-Analysis of 1415 Patients. *Circ Arrhythm Electrophysiol*. 2015;8:1017-29.
7. Vogler J, Willems S, Sultan A, Schreiber D, Luker J, Servatius H, Schaffer B, Moser J, Hoffmann BA and Steven D. Pulmonary Vein Isolation Versus Defragmentation: The CHASE-AF Clinical Trial. *J Am Coll Cardiol*. 2015;66:2743-52.
8. Dixit S, Marchlinski FE, Lin D, Callans DJ, Bala R, Riley MP, Garcia FC, Hutchinson MD, Ratcliffe SJ, Cooper JM, Verdino RJ, Patel VV, Zado ES, Cash NR, Killian T, Tomson TT and Gerstenfeld EP. Randomized ablation strategies for the treatment of persistent atrial fibrillation: RASTA study. *Circ Arrhythm Electrophysiol*. 2012;5:287-94.
9. de Bakker JM and Wittkampf FH. The pathophysiologic basis of fractionated and complex electrograms and the impact of recording techniques on their detection and interpretation. *Circ Arrhythm Electrophysiol*. 2010;3:204-13.
10. Caldwell J and Redfearn D. Ablation of complex fractionated atrial electrograms in catheter ablation for AF; where have we been and where are we going? *Curr Cardiol Rev*. 2012;8:347-53.
11. Makati KJ, Alsheikh-Ali AA, Garlitski AC, Link MS, Homoud M, Weinstock J and Estes Iii NA. Advances in mechanisms of atrial fibrillation: structural remodeling, high-frequency fractionated electrograms, and reentrant AF drivers. *J Interv Card Electrophysiol*. 2008;23:45-9.
12. van der Does LJ and de Groot NM. Inhomogeneity and complexity in defining fractionated electrograms. *Heart Rhythm*. 2017;14:616-624.
13. Sanchez-Quintana D, Lopez-Minguez JR, Pizarro G, Murillo M and Cabrera JA. Triggers and anatomical substrates in the genesis and perpetuation of atrial fibrillation. *Curr Cardiol Rev*. 2012;8:310-26.
14. Spach MS, Heidlage JF, Barr RC and Dolber PC. Cell size and communication: role in structural and electrical development and

remodeling of the heart. *Heart Rhythm*. 2004;1:500-15.
15. Stevenson WG and Soejima K. Recording techniques for clinical electrophysiology. *J Cardiovasc Electrophysiol*. 2005;16:1017-22.
16. Nakahara S, Hori Y, Hayashi A, Kobayashi S, Nakamura H, Okumura Y and Takayanagi K. Impact of left atrial appendage ridge ablation on the complex fractionated electrograms in persistent atrial fibrillation. *J Interv Card Electrophysiol*. 2014;41:55-64.
17. Teh AW, Kistler PM, Lee G, Medi C, Heck PM, Spence SJ, Sparks PB, Morton JB, Sanders P and Kalman JM. The relationship between complex fractionated electrograms and atrial low-voltage zones during atrial fibrillation and paced rhythm. *Europace*. 2011;13:1709-16.
18. Park JH, Park SW, Kim JY, Kim SK, Jeoung B, Lee MH, Hwang C, Kim YH, Kim SS and Pak HN. Characteristics of complex fractionated atrial electrogram in the electroanatomically remodeled left atrium of patients with atrial fibrillation. *Circ J*. 2010;74:1557-63.
19. Hwang SH, Oh YW, Lee DI, Shim J, Park SW and Kim YH. Relation between left atrial wall composition by late gadolinium enhancement and complex fractionated atrial electrograms in patients with persistent atrial fibrillation: influence of non-fibrotic substrate in the left atrium. *Int J Cardiovasc Imaging*. 2015;31:1191-9.
20. Yamabe H, Morihisa K, Koyama J, Enomoto K, Kanazawa H and Ogawa H. Analysis of the mechanisms initiating random wave propagation at the onset of atrial fibrillation using noncontact mapping: role of complex fractionated electrogram region. *Heart Rhythm*. 2011;8:1228-36.
21. Yamabe H, Morihisa K, Tanaka Y, Uemura T, Enomoto K, Kawano H and Ogawa H. Mechanisms of the maintenance of atrial fibrillation: role of the complex fractionated atrial electrogram assessed by noncontact mapping. *Heart Rhythm*. 2009;6:1120-8.
22. Hunter RJ, Liu Y, Lu Y, Wang W and Schilling RJ. Left atrial wall stress distribution and its relationship to electrophysiologic remodeling in persistent atrial fibrillation. *Circ Arrhythm Electrophysiol*. 2012;5:351-60.
23. Lo LW, Higa S, Lin YJ, Chang SL, Tuan TC, Hu YF, Tsai WC, Tsao HM, Tai CT, Ishigaki S, Oyakawa A, Maeda M, Suenari K and Chen SA. The novel electrophysiology of complex fractionated atrial electrograms: insight from noncontact unipolar electrograms. *J Cardiovasc Electrophysiol*. 2010;21:640-8.
24. Saghy L, Callans DJ, Garcia F, Lin D, Marchlinski FE, Riley M, Dixit S, Tzou WS, Haqqani HM, Pap R, Kim S and Gerstenfeld EP. Is there a relationship between complex fractionated atrial electrograms recorded during atrial fibrillation and sinus rhythm fractionation? *Heart Rhythm*. 2012;9:181-8.
25. De Bortoli A, Shi LB, Wang YC, Hoff PI, Solheim E, Ohm OJ and Chen J. Effect of flecainide on the extension and localization of complex fractionated electrogram during atrial fibrillation. *Scand Cardiovasc J*. 2015;49:168-75.
26. Knecht S, Wright M, Matsuo S, Nault I, Lellouche N, Sacher F, Kim SJ, Morgan D, Afonso V, Shinzuke M, Hocini M, Clementy J, Narayan SM, Ritter P, Jais P and Haissaguerre M. Impact of pharmacological autonomic blockade on complex fractionated atrial electrograms. *J Cardiovasc Electrophysiol*. 2010;21:766-72.
27. Nakahara S, Toratani N, Nakamura H, Higashi A and Takayanagi K. Spatial relationship between high-dominant-frequency sites and the linear ablation line in persistent atrial fibrillation: its impact on complex fractionated electrograms. *Europace*. 2013;15:189-97.
28. Bassiouny M, Saliba W, Hussein A, Rickard J, Diab M, Aman W, Dresing

T, Callahan Tt, Bhargava M, Martin DO, Shao M, Baranowski B, Tarakji K, Tchou PJ, Hakim A, Kanj M, Lindsay B and Wazni O. Randomized Study of Persistent Atrial Fibrillation Ablation: Ablate in Sinus Rhythm Versus Ablate Complex-Fractionated Atrial Electrograms in Atrial Fibrillation. *Circ Arrhythm Electrophysiol*. 2016;9:e003596.

29. Matsuo S, Yamane T, Date T, Tokutake K, Hioki M, Narui R, Ito K, Tanigawa S, Yamashita S, Tokuda M, Inada K, Arase S, Yagi H, Sugimoto K and Yoshimura M. Substrate modification by pulmonary vein isolation and left atrial linear ablation in patients with persistent atrial fibrillation: its impact on complex-fractionated atrial electrograms. *J Cardiovasc Electrophysiol*. 2012;23:962-70.
30. Nakahara S, Kamijima T, Hori Y, Tsukada N, Okano A and Takayanagi K. Substrate modification by adding ablation of localized complex fractionated electrograms after stepwise linear ablation in persistent atrial fibrillation. *J Interv Card Electrophysiol*. 2014;39:121-9.
31. Hunter RJ, Diab I, Tayebjee M, Richmond L, Sporton S, Earley MJ and Schilling RJ. Characterization of fractionated atrial electrograms critical for maintenance of atrial fibrillation: a randomized, controlled trial of ablation strategies (the CFAE AF trial). *Circ Arrhythm Electrophysiol*. 2011;4:622-9.
32. Nagashima K, Okumura Y, Watanabe I, Nakai T, Ohkubo K, Kofune M, Mano H, Sonoda K, Hiro T, Nikaido M and Hirayama A. Does location of epicardial adipose tissue correspond to endocardial high dominant frequency or complex fractionated atrial electrogram sites during atrial fibrillation? *Circ Arrhythm Electrophysiol*. 2012;5:676-83.
33. Lin YJ, Tai CT, Kao T, Chang SL, Wongcharoen W, Lo LW, Tuan TC, Udyavar AR, Chen YJ, Higa S, Ueng KC and Chen SA. Consistency of complex fractionated atrial electrograms during atrial fibrillation. *Heart Rhythm*. 2008;5:406-12.
34. Verma A, Wulffhart Z, Beardsall M, Whaley B, Hill C and Khaykin Y. Spatial and temporal stability of complex fractionated electrograms in patients with persistent atrial fibrillation over longer time periods: relationship to local electrogram cycle length. *Heart Rhythm*. 2008;5:1127-33.
35. Oral H, Chugh A, Good E, Crawford T, Sarrazin JF, Kuhne M, Chalfoun N, Wells D, Boonyapisit W, Gadeela N, Sankaran S, Kfahagi A, Jongnarangsin K, Pelosi F, Jr., Bogun F and Morady F. Randomized evaluation of right atrial ablation after left atrial ablation of complex fractionated atrial electrograms for long-lasting persistent atrial fibrillation. *Circ Arrhythm Electrophysiol*. 2008;1:6-13.
36. Miyamoto K, Tsuchiya T, Nagamoto Y, Yamaguchi T, Narita S, Ando S, Hayashida K, Tanioka Y and Takahashi N. Characterization of bipolar electrograms during sinus rhythm for complex fractionated atrial electrograms recorded in patients with paroxysmal and persistent atrial fibrillation. *Europace*. 2010;12:494-501.
37. Kofune M, Okumura Y, Watanabe I, Nagashima K, Sonoda K, Mano H, Kogawa R, Sasaki N, Ohkubo K, Nakai T, Nikaido M and Hirayama A. Comparative distribution of complex fractionated atrial electrograms, high dominant frequency (HDF) sites during atrial fibrillation and HDF sites during sinus rhythm. *J Interv Card Electrophysiol*. 2013;36:297-306.
38. Estner HL, Hessling G, Ndrepepa G, Luik A, Schmitt C, Konietzko A, Ucer E, Wu J, Kolb C, Pflaumer A, Zrenner B and Deisenhofer I. Acute effects and long-term outcome of pulmonary vein isolation in combination with electrogram-guided substrate ablation for persistent atrial fibrillation. *Am J Cardiol*. 2008;101:332-7.

39. Chen M, Yang B, Chen H, Ju W, Zhang F, Tse HF and Cao K. Randomized comparison between pulmonary vein antral isolation versus complex fractionated electrogram ablation for paroxysmal atrial fibrillation. *J Cardiovasc Electrophysiol*. 2011;22:973-81.
40. Tada H, Yoshida K, Chugh A, Boonyapisit W, Crawford T, Sarrazin JF, Kuhne M, Chalfoun N, Wells D, Dey S, Veerareddy S, Billakanty S, Wong WS, Kalra D, Kfahagi A, Good E, Jongnarangsin K, Pelosi F, Jr., Bogun F, Morady F and Oral H. Prevalence and characteristics of continuous electrical activity in patients with paroxysmal and persistent atrial fibrillation. *J Cardiovasc Electrophysiol*. 2008;19:606-12.
41. El Haddad M, Houben R, Claessens T, Tavernier R, Stroobandt R and Duytschaever M. Histogram analysis: a novel method to detect and differentiate fractionated electrograms during atrial fibrillation. *J Cardiovasc Electrophysiol*. 2011;22:781-90.
42. Verma A, Novak P, Macle L, Whaley B, Beardsall M, Wulffhart Z and Khaykin Y. A prospective, multicenter evaluation of ablating complex fractionated electrograms (CFEs) during atrial fibrillation (AF) identified by an automated mapping algorithm: acute effects on AF and efficacy as an adjuvant strategy. *Heart Rhythm*. 2008;5:198-205.
43. Di Biase L, Elayi CS, Fahmy TS, Martin DO, Ching CK, Barrett C, Bai R, Patel D, Khaykin Y, Hongo R, Hao S, Beheiry S, Pelargonio G, Dello Russo A, Casella M, Santarelli P, Potenza D, Fanelli R, Massaro R, Wang P, Al-Ahmad A, Arruda M, Themistoclakis S, Bonso A, Rossillo A, Raviele A, Schweikert RA, Burkhardt DJ and Natale A. Atrial fibrillation ablation strategies for paroxysmal patients: randomized comparison between different techniques. *Circ Arrhythm Electrophysiol*. 2009;2:113-9.
44. Verma A, Mantovan R, Macle L, De Martino G, Chen J, Morillo CA, Novak P, Calzolari V, Guerra PG, Nair G, Torrecilla EG and Khaykin Y. Substrate and Trigger Ablation for Reduction of Atrial Fibrillation (STAR AF): a randomized, multicentre, international trial. *Eur Heart J*. 2010;31:1344-56.
45. Redfearn DP, Simpson CS, Abdollah H and Baranchuk AM. Temporo-spatial stability of complex fractionated atrial electrograms in two distinct and separate episodes of paroxysmal atrial fibrillation. *Europace*. 2009;11:1440-4.
46. Calo L, De Ruvo E, Sciarra L, Gricia R, Navone G, De Luca L, Nuccio F, Sette A, Pristipino C, Dulio A, Gaita F and Lioy E. Diagnostic accuracy of a new software for complex fractionated electrograms identification in patients with persistent and permanent atrial fibrillation. *J Cardiovasc Electrophysiol*. 2008;19:1024-30.
47. Estner HL, Hessling G, Ndrepepa G, Wu J, Reents T, Fichtner S, Schmitt C, Bary CV, Kolb C, Karch M, Zrenner B and Deisenhofer I. Electrogram-guided substrate ablation with or without pulmonary vein isolation in patients with persistent atrial fibrillation. *Europace*. 2008;10:1281-7.
48. Porter M, Spear W, Akar JG, Helms R, Brysiewicz N, Santucci P and Wilber DJ. Prospective study of atrial fibrillation termination during ablation guided by automated detection of fractionated electrograms. *J Cardiovasc Electrophysiol*. 2008;19:613-20.
49. Narayan SM, Wright M, Derval N, Jadidi A, Forclaz A, Nault I, Miyazaki S, Sacher F, Bordachar P, Clementy J, Jais P, Haissaguerre M and Hocini M. Classifying fractionated electrograms in human atrial fibrillation using monophasic action potentials and activation mapping: evidence for localized drivers, rate acceleration, and nonlocal signal etiologies. *Heart Rhythm*. 2011;8:244-53.
50. Roux JF, Gojraty S, Bala R, Liu CF,

Hutchinson MD, Dixit S, Callans DJ, Marchlinski F and Gerstenfeld EP. Complex fractionated electrogram distribution and temporal stability in patients undergoing atrial fibrillation ablation. *J Cardiovasc Electrophysiol*. 2008;19:815-20.
51. Roux JF, Gojraty S, Bala R, Liu CF, Dixit S, Hutchinson MD, Garcia F, Lin D, Callans DJ, Riley M, Marchlinski F and Gerstenfeld EP. Effect of pulmonary vein isolation on the distribution of complex fractionated electrograms in humans. *Heart Rhythm*. 2009;6:156-60.
52. Mahapatra S, LaPar DJ, Kamath S, Payne J, Bilchick KC, Mangrum JM and Ailawadi G. Initial experience of sequential surgical epicardial-catheter endocardial ablation for persistent and long-standing persistent atrial fibrillation with long-term follow-up. *Ann Thorac Surg*. 2011;91:1890-8.
53. Bisleri G and Glover B. Hybrid ablation for atrial fibrillation: current approaches and future directions. *Curr Opin Cardiol*. 2017;32:17-21.
54. Bisleri G, Rosati F, Bontempi L, Curnis A and Muneretto C. Hybrid approach for the treatment of long-standing persistent atrial fibrillation: electrophysiological findings and clinical results. *Eur J Cardiothorac Surg*. 2013;44:919-23.
55. La Meir M, Gelsomino S, Luca F, Pison L, Parise O, Colella A, Gensini GF, Crijns H, Wellens F and Maessen JG. Minimally invasive surgical treatment of lone atrial fibrillation: early results of hybrid versus standard minimally invasive approach employing radiofrequency sources. *Int J Cardiol*. 2013;167:1469-75.
56. Jais P, Haissaguerre M, Shah DC, Chouairi S and Clementy J. Regional disparities of endocardial atrial activation in paroxysmal atrial fibrillation. *Pacing Clin Electrophysiol*. 1996;19:1998-2003.
57. Gardner PI, Ursell PC, Fenoglio JJ, Jr. and Wit AL. Electrophysiologic and anatomic basis for fractionated electrograms recorded from healed myocardial infarcts. *Circulation*. 1985;72:596-611.
58. Park J, Park CH, Lee HJ, Wi J, Uhm JS, Pak HN, Lee M, Kim YJ and Joung B. Left atrial wall thickness rather than epicardial fat thickness is related to complex fractionated atrial electrogram. *Int J Cardiol*. 2014;172:e411-3.
59. Rostock T, Rotter M, Sanders P, Takahashi Y, Jais P, Hocini M, Hsu LF, Sacher F, Clementy J and Haissaguerre M. High-density activation mapping of fractionated electrograms in the atria of patients with paroxysmal atrial fibrillation. *Heart Rhythm*. 2006;3:27-34.
60. Solheim E, Off MK, Hoff PI, Schuster P, Ohm OJ and Chen J. Characteristics and distribution of complex fractionated atrial electrograms in patients with paroxysmal and persistent atrial fibrillation. *J Interv Card Electrophysiol*. 2010;28:87-93.
61. Schmitt C, Estner H, Hecher B, Luik A, Kolb C, Karch M, Ndrepepa G, Zrenner B, Hessling G and Deisenhofer I. Radiofrequency ablation of complex fractionated atrial electrograms (CFAE): preferential sites of acute termination and regularization in paroxysmal and persistent atrial fibrillation. *J Cardiovasc Electrophysiol*. 2007;18:1039-46.
62. Oral H, Chugh A, Good E, Wimmer A, Dey S, Gadeela N, Sankaran S, Crawford T, Sarrazin JF, Kuhne M, Chalfoun N, Wells D, Frederick M, Fortino J, Benloucif-Moore S, Jongnarangsin K, Pelosi F, Jr., Bogun F and Morady F. Radiofrequency catheter ablation of chronic atrial fibrillation guided by complex electrograms. *Circulation*. 2007;115:2606-12.
63. Eckstein J, Zeemering S, Linz D, Maesen B, Verheule S, van Hunnik A, Crijns H, Allessie MA and Schotten U. Transmural Conduction Is the Predominant Mechanism of Breakthrough During Atrial Fibrillation Evidence From Simultaneous Endo-Epicardial High-

Density Activation Mapping. *Circ-Arrhythmia Elec*. 2013;6:334-341.
64. de Groot N, van der Does L, Yaksh A, Lanters E, Teuwen C, Knops P, van de Woestijne P, Bekkers J, Kik C, Bogers A and Allessie M. Direct Proof of Endo-Epicardial Asynchrony of the Atrial Wall During Atrial Fibrillation in Humans. *Circulation: Arrhythmia and Electrophysiology*. 2016;9(5).
65. Haissaguerre M, Sanders P, Hocini M, Jais P and Clementy J. Pulmonary veins in the substrate for atrial fibrillation: the "venous wave" hypothesis. *J Am Coll Cardiol*. 2004;43:2290-2.
66. Wu J, Estner H, Luik A, Ucer E, Reents T, Pflaumer A, Zrenner B, Hessling G and Deisenhofer I. Automatic 3D mapping of complex fractionated atrial electrograms (CFAE) in patients with paroxysmal and persistent atrial fibrillation. *J Cardiovasc Electrophysiol*. 2008;19:897-903.
67. Scherr D, Dalal D, Cheema A, Cheng A, Henrikson CA, Spragg D, Marine JE, Berger RD, Calkins H and Dong J. Automated detection and characterization of complex fractionated atrial electrograms in human left atrium during atrial fibrillation. *Heart Rhythm*. 2007;4:1013-20.
68. Lau DH, Maesen B, Zeemering S, Kuklik P, van Hunnik A, Lankveld TA, Bidar E, Verheule S, Nijs J, Maessen J, Crijns H, Sanders P and Schotten U. Indices of bipolar complex fractionated atrial electrograms correlate poorly with each other and atrial fibrillation substrate complexity. *Heart Rhythm*. 2015;12:1415-23.
69. Nagashima K, Okumura Y, Watanabe I, Nakai T, Ohkubo K, Kofune T, Kofune M, Mano H, Sonoda K and Hirayama A. Effects of inter-electrode spacing on complex fractionated atrial electrograms and dominant frequency detection. *J Interv Card Electrophysiol*. 2012;34:51-7.
70. Correa de Sa DD, Thompson N, Stinnett-Donnelly J, Znojkiewicz P, Habel N, Muller JG, Bates JH, Buzas JS and Spector PS. Electrogram fractionation: the relationship between spatiotemporal variation of tissue excitation and electrode spatial resolution. *Circ Arrhythm Electrophysiol*. 2011;4:909-16.

5

The impact of filter settings on morphology of unipolar fibrillation potentials

Roeliene Starreveld
Paul Knops
Maarten C. Roos-Serote
Charles Kik
Ad J.J.C. Bogers
Bianca J.J.M. Brundel
Natasja M.S. de Groot

Journal of Cardiovascular Translational Research. 2020 Dec;13(6):953-964

Abstract

Background

Using unipolar atrial electrogram morphology as guidance for ablative therapy is regaining interest. Although standardly used in clinical practice during ablative therapy, the impact of filter settings on morphology of unipolar AF potentials is unknown.

Methods

Thirty different filters were applied to 2,557,045 high-resolution epicardial AF potentials recorded from ten patients. Deflections with slope ≤-0.05mV/ms and amplitude ≥0.3mV were marked.

Results

High-pass filtering decreased the number of detected potentials, deflection amplitude, percentage of fractionated potentials (≥2 deflections) as well as fractionation delay time (FDT) and increased percentage of single potentials. Low-pass filtering decreased the number of potentials, percentage of fractionated potentials, whereas deflection amplitude, percentage of single potentials and FDT increased. Notch filtering (50Hz) decreased the number of potentials and deflection amplitude, whereas the percentage of complex fractionated potentials (≥3 deflections) increased.

Conclusion

Filtering significantly impacted morphology of unipolar fibrillation potentials, becoming a potential source of error in identification of ablative targets.

Introduction

Although insight into the pathophysiologic basis of fractionated atrial electrograms has increased in the past years, its "fact or artifact" remains a topic of debate. Extracellular electrograms – recorded directly from the heart – are generated by depolarization of cardiomyocytes, so signal morphology could provide information about the electrophysiological characteristics of the underlying myocardium.[1] Atrial potentials consisting of multiple components (i.e. fractionated) have been linked to abnormal conduction and arrhythmogenicity in patients with atrial fibrillation (AF)[1, 2], which led to targeted ablation of such fractioned potentials. However, the link between morphology of atrial potentials and pathology has proven to be anything but straightforward, considering that multiple physiological mechanisms and measurement properties, such as filtering, can cause fractionated potentials as well.[3, 4] In the 1980s Waxman and Sung discovered the phenomenon of frequency-dependent fractionation in human bipolar ventricular electrograms.[5] Klitzner and Stevenson showed that increasing the high-pass filter frequency above 10 Hz decreased potential duration and amplitude, whereas low-pass filtering altered potential amplitude slightly if decreased up to 100 Hz.[6] Such low- and high-pass filters are commonly used in clinical practice, as well as utilization of a 50 Hz (or 60 Hz) notch filter to suppress power-line interference.

Despite the clinical failure of targeting complex fractionated atrial electrograms (CFAEs) as stand-alone therapy[7-9], using atrial electrogram morphology as guidance for ablative therapy is regaining interest[10]. Up till recently, most clinically used ablative systems preferred bipolar above unipolar measurements, given its ability to reduce far-field potentials.[11] However, bipolar signals fail to represent incoherent waves during AF, which is why currently emerging innovative ablative systems, such as RhythmView™ and AcQMap®, prefer unipolar electrograms to identify local activation.[12, 13] As the study of van der Does et al. demonstrated electrogram morphology at the epi- and endocardium to be comparable[14], epicardial electrograms are suitable to investigate signal morphology, particularly as direct contact between the electrode and atrial tissue can be assured.

To our knowledge, the impact of filtering on unipolar fibrillation potentials has never been investigated in humans. This study therefore aims to elucidate the consequences of high-pass, low-pass and notch filtering on unipolar fibrillation potentials in AF patients.

Methods

Study population

The study population consisted of ten adult patients with a history of paroxysmal or persistent AF undergoing elective open heart mitral valve surgery in the Erasmus Medical Center Rotterdam. This study was approved by the institutional medical ethical committee (MEC 2010-054/MEC 2014-393).[15, 16] Written informed consent was obtained from all patients. Patient characteristics (e.g. age, medical history, date of AF diagnosis) were obtained from the patient's file.

Mapping procedure

Epicardial high-resolution mapping was performed prior to commencement to extra-corporal circulation, as previously described in detail.[17-19] A temporal bipolar epicardial pacemaker wire attached to the RA free wall served as a reference electrode. A steel wire fixed to the subcutaneous tissue of the thoracic cavity was used as an indifferent electrode. Epicardial mapping was performed with a 192-electrode array (electrode diameter 0.45mm, interelectrode distances 2.0 mm). The right pulmonary vein (PV) area was mapped from the sinus transversus fold along the borders of the right pulmonary vein down towards the atrioventricular groove (as illustrated in the left panel of *Figure 1*). Ten seconds of AF were recorded, including a surface ECG lead, a calibration signal of 2mV and 1000ms, a bipolar reference electrogram and all unipolar epicardial electrograms. Data was stored on a hard disk after amplification (gain 1000), filtering (band-pass 0.5-400 Hz), sampling (1 kHz) and analogue to digital conversion (16 bits).

Filter settings

The impact of additional high-pass, low-pass and notch filtering (i.e. narrow band-stop filter), as illustrated in the middle panel of *Figure 1*, was investigated by changing filter settings one at a time, while keeping the others at default:

- High-pass filter: 0.5 (default), 1, 2, 3, 5, 10, 20, 30, 40, 50, 60, 70, 75, 80, 90, 100 Hz
- Low-pass filter: 400 (default), 300, 250, 200, 150, 100, 75, 60, 50, 40, 30, 20, 10 Hz
- Notch filter at 50 Hz: off (default) and on

Settings were based on frequently used filter options within clinical mapping systems. Signals were zero-phase filtered with IIR Butterworth low- and high-pass filters (2nd-order: 12 dB/octave roll-off) and/or IIR notch filter with a quality factor of 30. Bode plots of the three filters are illustrated in *Supplemental figure 1*.

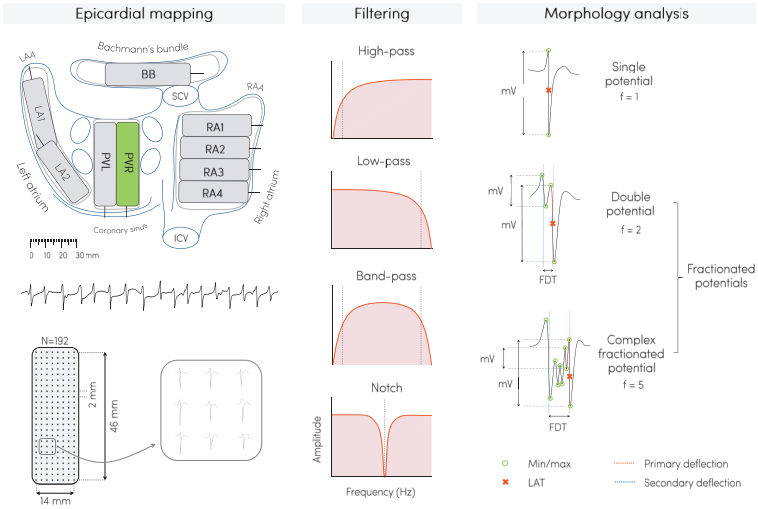

Figure 1 – Schematic representation of mapping analysis. *Left*: the right pulmonary vein (PVR) area is mapped from the sinus transversus fold along the borders of the PVR down towards the atrioventricular groove. Using a 192-electrode array ten seconds of AF is recorded. *Middle*: simplistic illustration of different filtering modes. *Right:* morphology analysis of all fibrillation potentials. The peak-to-peak amplitude of each deflection (mV), fractionation (f, number of deflections) and fractionation delay time (FDT) is derived. Fibrillation potentials were classified as either single potential (f = 1), double potential (f = 2) or complex fractionated potential (f ≥ 3). The steepest deflection of a potential is classified as the primary deflection (and marked as the local activation time), whereas additional deflections are classified as secondary deflections. BB, Bachmann's bundle; ICV, inferior caval vein; LA, left atrium; LAA, left atrial appendage; LAT, local activation time; PVL, left pulmonary vein; RA, right atrium; RAA, right atrial appendage; SCV, superior caval vein.

Data analysis

Electrogram morphology was semi-automatically analyzed in custom-made Python 3.6 software. Deflections of atrial potentials were automatically marked if the slope was ≤-0.05 mV/ms and the amplitude ≥0.3 mV; the refractory period was set to 40 ms[20]. The steepest negative deflection of a potential was classified as the 'primary deflection' and marked as the local activation time (LAT), whereas – in case of a fractionated potential – additional deflections were classified as 'secondary deflections'. Electrograms with injury potentials and artifacts were excluded from analysis by manual assessment and consensus of two independent investigators.

For each different filter setting, peak-to-peak amplitude (voltage), fractionation (f, number of deflections) and fractionation delay time (FDT, time interval between first and last deflection) of atrial potentials were analyzed. Peak-to-peak amplitude was analyzed for all deflections, as well as for primary and secondary deflections separately. FDT was only derived for fractionated potentials (f ≥ 2). For each

morphology parameter median values of all atrial potentials within the 192-array were derived and compared between filter settings. In addition, each fibrillation potential was classified as either single potential (SP, f = 1), double potential (DP, f = 2) or complex fractionated potential (CFP, f ≥ 3). *Figure 1* (right panel) illustrates derivation of morphology parameters and classification of fibrillation potentials.

Statistical analysis

The impact of filtering on characteristics of unipolar fibrillation potentials, including amplitude, fractionation and FDT, was analyzed using linear mixed effect models, while accounting for clustered data within a patient. Analyses were done for the three different types of filtering separately: low-pass, high-pass and notch filtering. The basic model only included a random intercept and presumed no relation between filtering and morphology characteristics. Based on the Akaike Information Criterion it was checked whether addition of a random slope improved the model. To model any non-linearity two splines were used. Residual plots were reviewed and log or square root transformed data was used if deviations from normality were observed. Statistical significance was tested using the Likelihood Ratio test. A p-value <0.05 was considered statistically significant. All statistical analyses were performed using R Statistical Software (RStudio, Inc., Boston, MA; version 1.0.153).

Results

Patient characteristics (n = 10) are shown in *Table 1*. All patients had a history of AF (paroxysmal n = 4, persistent n = 6) and age ranged from 56 to 77 years. In total, 3000 seconds of AF recordings were analyzed, consisting of 2,557,045 fibrillation potentials.

Table 1 – Patient characteristics

Study ID	Underlying heart disease	Age (y)	Gender	BMI	Type of AF	Time since AF diagnosis (y)
1	MVD	70	M	25.3	Paroxysmal	5.61
2	MVD + IHD	75	M	32.3	Persistent	2.07
3	MVD + IHD	67	M	21.8	Persistent	0.25
4	MVD	65	M	25.6	Persistent	20.33
5	MVD	77	F	26.7	Persistent	0.72
6	MVD	66	M	23.2	Persistent	1.13
7	MVD	56	M	26.4	Persistent	0.61
8	MVD + IHD	70	M	24.2	Paroxysmal	0.06
9	MVD	64	F	34.6	Paroxysmal	0.59
10	MVD	74	M	22.1	Paroxysmal	0.28

AF, atrial fibrillation; BMI, body mass index; F, female; IHD, ischemic heart disease; M, male; MVD, mitral valve disease.

The impact of frequently used high-pass, low-pass and notch filter settings on morphology of one example of a fractionated fibrillation potential is illustrated in *Figure 2*. General consequences of all filter settings are discussed in the sections below.

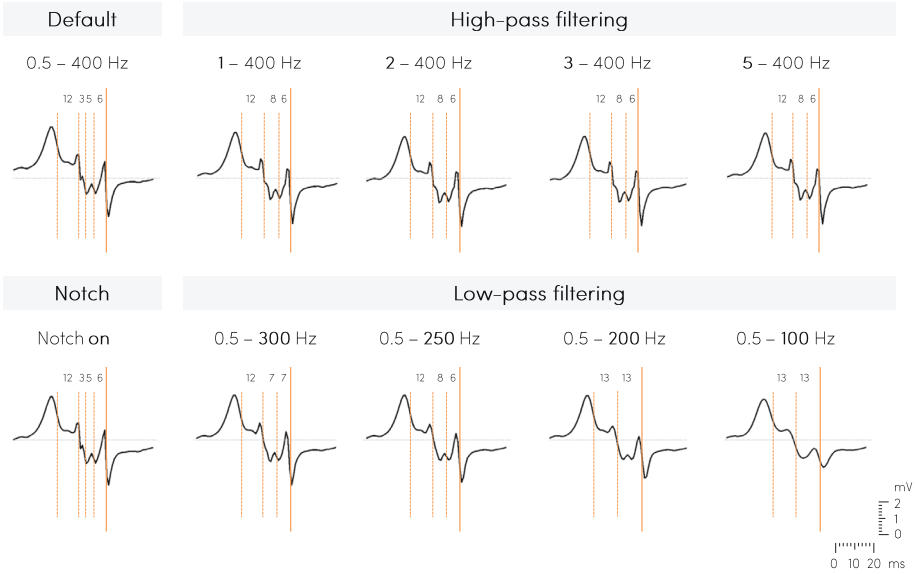

Figure 2 – Illustration of the impact of frequently used filter settings, i.e. high-pass, low-pass and notch filtering, on morphology of one fractionated unipolar fibrillation potential. Detected deflections are marked with orange vertical lines, a solid line representing the primary deflection and dashed lines the secondary deflections. The corresponding time interval between adjacent deflections is given (in ms).

Impact of high-pass filtering on morphology of fibrillation potentials

Increasing the high-pass filter frequency had a negative impact on the number of detected fibrillation potentials and deflection amplitudes, as illustrated in *Figure 3*. In the entire study population, the percentage of detected fibrillation potentials gradually decreased, with a loss ranging from 27.2% to 74.5% at the maximum high-pass frequency of 100 Hz ($p<0.01$, left upper panel). The overall median deflection amplitude decreased with increasing high-pass filtering for all patients (from 0.59-0.96 mV to 0.44-0.57 mV, $p<0.01$, right upper panel). This negative impact was also observed for median primary and secondary deflection amplitudes separately ($p<0.01$), and was primarily caused by loss of high amplitude deflections, as illustrated in the histograms in the lower panel of *Figure 3* (obtained from one representative patient).

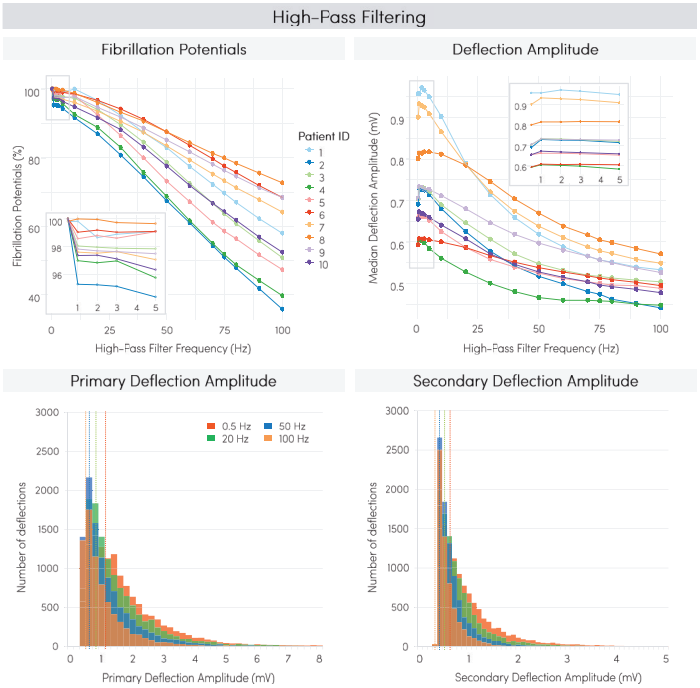

Figure 3 – The impact of high-pass filtering on detection of fibrillation potentials and deflection amplitude. *Upper left*: the number of detected fibrillation potentials, expressed as a percentage of maximal number of fibrillation potentials within the patient, of all patients. *Upper right*: overall median deflection amplitude of all patients. *Lower left*: stacked bar-plots of median primary deflection amplitude of one patient. *Lower right*: stacked bar-plots of median secondary deflection amplitude of one patient. For both lower figures, the data of patient 1 was taken as a representative case for all patients. The dotted vertical lines represent the median value of the corresponding stacked bar-plot, representing high-pass filtering at 0.5, 20, 50 or 100 Hz.

The impact of high-pass filtering on the degree of fractionation, i.e. FDT and distribution of the different fibrillation potential types, is illustrated in Figure 4. As observed in the left panel of *Figure 4*, increasing the high-pass filter frequency from 0.5 Hz to 100 Hz resulted in a slightly increasing percentage of SPs (from 36.1-57.6% to 31.6-70.2%) at the cost of (primarily) CFPs (from 15.9-36.0% to 7.3-37.8%), whereas only a minimal decline in the percentage of DPs was observed (from 25.8-32.9% to 22.5-31.6%) in all patients (all $p<0.01$). High-pass filtering decreased median FDT for all patients (from 16.0-25.0 ms to 11.0-15.0 ms, right upper panel), primarily due to a loss of fractionated potentials with a long FDT (right lower panel, histogram of one representative patient).

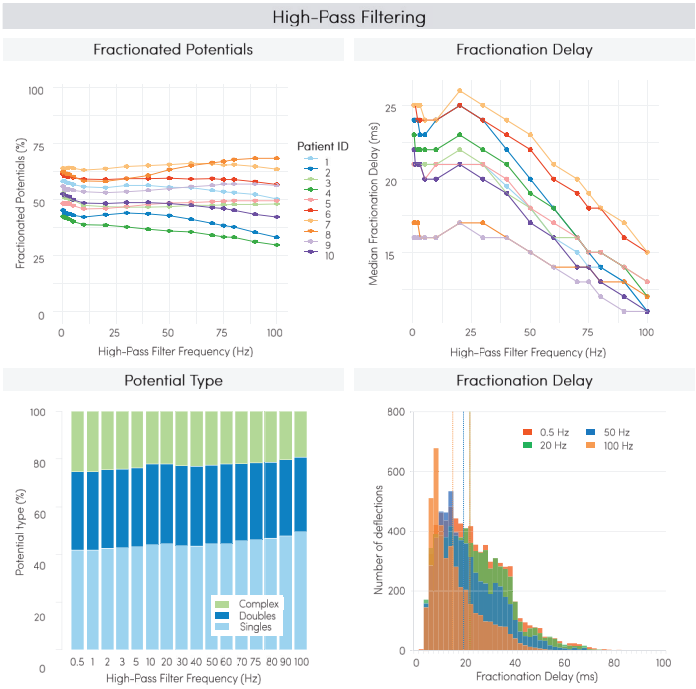

Figure 4 – The impact of high-pass filtering on fractionation. *Upper left*: the percentage fractionated potentials (two or more deflections per potential, expressed as a percentage of total detected fibrillation potentials) of all patients. *Upper right*: fractionation delay time (FDT, time interval between first and last deflection) of all patients. *Lower left*: stacked bar-plots of potential types obtained from one patient. Potential type is either single (one deflection), double (two deflections) or complex (three or more deflections) and expressed as a percentage of the total number of detected fibrillation potentials**.** *Lower right*: stacked bar-plots of median FDT obtained from one patient. The dotted vertical lines represent the median value of the corresponding stacked bar-plot representing high-pass filtering at 0.5, 20, 50 or 100 Hz. For both lower figures, the data of patient 1 was taken as a representative case for all patients.

Impact of low-pass filtering on morphology of fibrillation potentials

The impact of decreasing the low-pass filter frequency on morphology of unipolar fibrillation potentials is shown in *Figure 5* and *Figure 6*. The left upper panel of *Figure 5* indicates an exponentially decreasing percentage of detected fibrillation potentials with decreasing the low-pass filter frequency ($p<0.01$). As examples, low-pass filtering at 250 Hz induced a 2.5-11.6% loss of fibrillation potentials, which was 5.6-20.7% at 150 Hz and 20.3-58.4% at 75 Hz. Decreasing the low-pass filter frequency exponentially increased the median deflection amplitude for all patients (from 0.59-0.96 mV to 1.82-2.40 mV, right upper panel), a trend that was also observed within primary and secondary deflections separately. This increase in deflection amplitude is primarily caused by a loss of low amplitude deflections, as observed in the lower panel (histograms of one representative patient).

In *Figure 6* the impact of low-pass filtering on fractionation is visualized. The left upper panel illustrates a rapid decline of the percentage fractionated potentials ($p<0.01$). Decreasing the low-pass filter frequency increased the percentage of SPs (from 36.1-57.6% to 100%) at the cost of both DPs (from 25.8-32.9% to 0%) and CFPs (from 15.9-36.0% to 0%). For all patients, the impact of low-pass filtering on DPs was mainly when filtering at 150 Hz or lower, whereas presence of CFPs diminished almost linearly at frequencies below 400 Hz until none were left (left lower panel, stacked bar plot of one representative patient). Decreasing the low-pass filter frequency from 400 to 100 Hz did not substantially increase median FDT (from 16.0-25.0 ms to 19.0-24.0 ms respectively, right upper panel), since both fractionated potentials with a short and long FDT disappeared due to the filtering (right lower panel). Low-pass filtering below 100 Hz however resulted in a steep rise of FDT (up to 38.0 ms at 30 Hz), due to the exponential loss of fractionated potentials (right lower panel). The relation between FDT and low-pass filtering was significant ($p<0.01$).

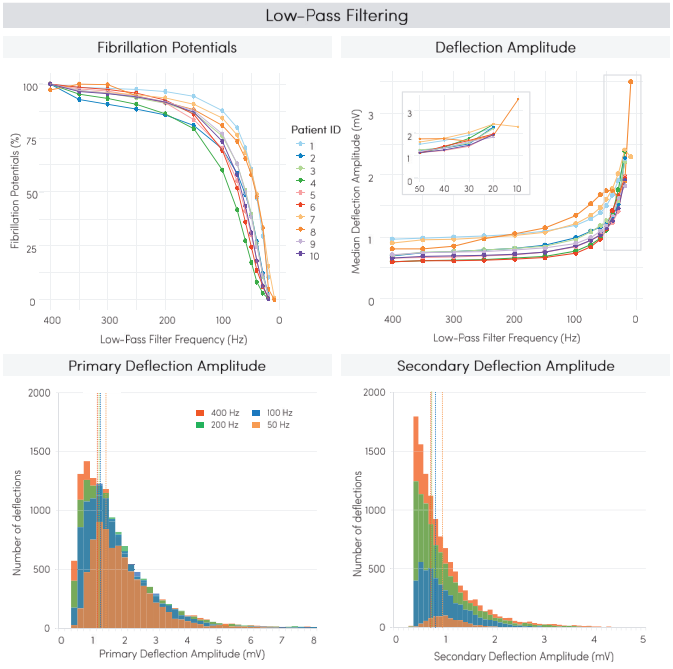

Figure 5 – The impact of low-pass filtering on detection of fibrillation potentials and deflection amplitude. *Upper left*: the number of detected fibrillation potentials (expressed as a percentage of maximal number of fibrillation potentials within the patient) of all patients. *Upper right*: overall median deflection amplitude of all patients. *Lower left*: stacked bar-plots of median primary deflection amplitude of one patient. *Lower right*: stacked bar-plots of median secondary deflection amplitude of one patient. For both lower figures, the data of patient 1 was taken as a representative case for all patients. The dotted vertical lines represent the median value of the corresponding stacked bar-plot, representing low-pass filtering at 400, 200, 100 or 50 Hz.

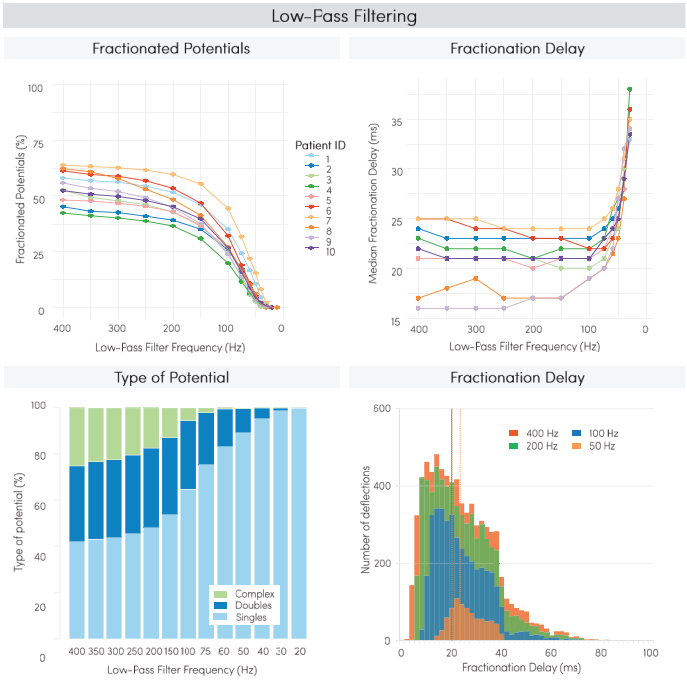

Figure 6 – The impact of low-pass filtering on fractionation. *Upper left*: the percentage fractionated potentials (two or more deflections per potential, expressed as a percentage of total detected fibrillation potentials) of all patients. *Upper right*: fractionation delay time (FDT, time interval between first and last deflection) of all patients. *Lower left*: stacked bar-plots with the distribution of potential types of one patient. Potential type is either single (one deflection), double (two deflections) or complex (three or more deflections). Distribution is expressed as a percentage of the total detected fibrillation potentials. *Lower right*: stacked bar-plots of median FDT of one patient. The dotted vertical lines represent the median value of the corresponding stacked bar-plot representing low-pass filtering at 400, 200, 100 or 50 Hz. For both lower figures, the data of patient 1 was taken as a representative case for all patients.

Impact of notch filtering on morphology of fibrillation potentials

As indicated in *Table 2*, notch filtering slightly decreased deflection amplitude and increased the percentage of CFPs, whereas no effect on FDT and the percentage of SPs and DPs was observed. Applying a notch filter at 50 Hz induced a loss of ~1% detected fibrillation potentials (from 9234-14545 to 9234-14405 potentials, p=0.01). This significant, yet minimal, effect was also observed in a decrease in median deflection amplitude (from 0.59-0.96 mV to 0.59-0.95 mV, p<0.01). Median FDT was not affected by notch filtering (from 16.0-25.0 ms to 16.0-25.0 ms, p=NS). Notch filtering also had no effect on the percentage of SPs and DPs (from 36.1-57.6% to 35.8-57.6% and from 25.8-32.9% to 25.8-32.3% respectively, p=NS), but did increase the percentage of CFPs significantly (from 15.9-36.0% to 16.2-37.0%, p=0.0157).

Table 2 – Impact of notch filtering on unipolar fibrillation potential morphology

Study ID	Δ Number of detected fibrillation potentials	Δ Median deflection amplitude (mV)	Δ Singles (%)	Δ Doubles (%)	Δ Complex (%)	Δ Median FDT (ms)
1	-42	-0.0125	0.2728	-0.5923	0.3196	0
2	-76	-0.0131	0.1949	-0.4636	0.2686	0
3	-132	-0.0094	0.2474	-0.1654	-0.0820	0
4	0	0.0000	0.0000	0.0000	0.0000	0
5	-213	-0.0081	-0.8585	0.4505	0.4080	0
6	-140	-0.0050	-0.3731	0.0758	0.2973	0
7	-61	-0.0119	-0.3039	-0.6978	1.0017	0
8	14	-0.0163	-0.4014	0.2530	0.1484	-1
9	-11	-0.0119	0.3255	-0.4528	0.1100	0
10	-190	-0.0081	-0.1262	0.0469	0.0875	0
min – max	-213 – 14	-0.0163 – 0.0000	-0.8585 – 0.3255	-0.6978 – 0.4505	-0.082 – 1.0017	-1 – 0
p-value	0.0043 *	<0.0001 *	0.3827	0.1973	0.0157 *	0.3047

Delta values (Δ = notch filter on – notch filter off) for all parameters and corresponding p-values based on the Likelihood Ratio test are given (* < 0.05). Potential type is either single (one deflection), double (two deflections) or complex (three or more deflections). FDT, fractionation delay time.

Filtering and detection of local activation time

As a subanalysis, the impact of filtering on detection of LAT was determined. Results are described in detail in the Supplemental material. All filter settings, i.e. all high-pass, low-pass and notch filter settings, evoked changes in LAT timing (*Supplemental figure 2*). Especially with more aggressive low-pass filtering, the percentage of fibrillation potentials that had a shift in LAT was high (e.g. 58.32 to 63.12% at 100 Hz). Filtering impacted LATs of all potential types (i.e. SPs, DPs and CFPs). Nevertheless, more complex and long fractionated potentials had a greater ΔLAT – and thus shifted more – than potentials with simpler morphology.

Discussion

All clinically used mapping systems – both unipolar and bipolar – standardly use signal filters while ablating. Although all mapping systems have different default filter settings, operators have the freedom and ability to change the filter settings according to their wishes. The results of our study clearly show that filtering choices have significant impact on unipolar signal morphology. Attempts to correct for noise or baseline drift can therefore easily result in erroneous (under)detection of fractionation and/or low-voltage areas and thus ablative targets during mapping.

Our study thereby complements and verifies previously reported findings by Schneider et al.[21] and Lin et al.[22], in which unipolar endocardial peak-to-peak voltage decreased with increasing high-pass filtering in patients with ectopic atrial tachyarrhythmias and atrial flutter, respectively.

Current clinical use of filtering in ablative techniques

Although initially developed as a stand-alone strategy, ablation of tissue exhibiting CFAEs is nowadays generally used as adjuvant therapy to PV isolation, particularly in persistent AF patients.[2, 23] Pathophysiological mechanisms of CFAE include pivoting points, inhomogeneous conduction, functional conduction block, reduced cell coupling and interstitial fibrosis.[2, 24] On signal level, fractionation is often considered high-frequency content with a low-amplitude.[25, 26] Accordingly, lowering particularly the low-pass filter frequency impacted presence of (complex) fractionated potentials in our study, since high-frequency content was eliminated. So whilst the decision to change the low-pass filter setting during CFAE ablation is probably made to reject high-frequency noise, detection of CFPs and thereby ablative targets is also strongly impeded. As an example, low-pass filtering at 100 Hz already eliminated up to 40% of fibrillation potentials and reduced presence of CFPs from 15.9-36.0% to 2.3-10.7% in all patients. Interestingly, increasing high-pass filtering did significantly decrease the percentage of fractionated potentials, primarily due to loss of complex fractionated potentials, as also observed in the decreasing FDT. In comparison to the impact of low-pass filtering however, this effect is clearly less substantial. In contrary, notch filtering increased presence of CFPs (max of 1.0017% increase) by adding artificial components to the unipolar fibrillation potential, just as in bipolar measurements.[3]

Our results also stress the significance of adequate (i.e. as minimal as possible) filtering for voltage mapping, as unipolar potential amplitude was impacted by high-pass, low-pass and notch filtering. Low-voltage areas (<0.5 mV) have been linked to fibrosis, poor cell-to-cell coupling, slowed and discontinuous electrical conduction and thus maintenance of AF, motivating targeted ablation of these areas as an isolated approach or in addition to CFAE ablation and/or PV isolation.[26, 27] As our results indicate, low-pass filtering decreased the number of low-amplitude deflections, thereby reducing the number of potential target sites for low-voltage ablation in clinical practice. In contrary, high-pass filtering attenuated the overall deflection amplitude and induced an increase in the number of low-amplitude signals, potentially leading to erroneous overdetection of low-voltage target sites. Notch filtering did significantly lower deflection amplitude, but its impact is rather small (-0.0163 – 0.0000 mV change in amplitude).

With increasing filtering (i.e. increasing high-pass or lowering low-pass cut-off frequencies), the number of detected fibrillation potentials declined. In addition, as

described in the *Supplemental material*, filtering impacted timing of LAT. Though not specifically analyzed in this study, the missing potentials as well as the shift in LATs could lead to changes in detected activation patterns during AF. As such, inadequate filtering could result in unintentional under- or overestimation of rotational activity and focal, or peripheral, waves during mapping. A future study on the precise impact of filtering on measured activation sequences during AF could be very insightful.

As implied in the word itself, filtering inherently results in loss of information. Nevertheless, filtering does not have to be inaccurate if the lost information is irrelevant to your case. The challenge always lies in balancing minimal filtering with maximal signal quality (e.g. without artifacts and noise). However, since the relevant frequency content of fractionated fibrillation potentials is unknown and physiological discrimination between true fractionation and noise contribution is (yet) unfeasible, this study validates the use of minimal filtering. A safer alternative to filtering could be implementation of a signal-to-noise ratio (SNR) within mapping systems, in which detection criteria for fractionated and/or low-voltage potentials become stricter in case of considerable noise, without affecting original signal morphology. Using such an approach also prevents artifacts induced by filtering, such as ringing artifacts, to manifest.

Due to its ability to reduce far-field potentials by subtracting two unipolar electrograms at adjacent sites, bipolar electrograms are clinically often preferred above unipolar measurements.[11] For purposes of fractionation analyses this favor is perhaps undeserved, since apart from filtering bipolar electrogram morphology is also susceptible to changes in interelectrode distance, electrode size and wavefront direction.[3, 11, 12, 28]

The pathophysiology of fractionation

The search for true – pathologic – fractionation remains an ongoing challenge. Differentiating between physiologic fractionation, due to e.g. overlaying myocardial fibers and functional anisotropy, and pathologic fractionation for now remains difficult. The fact that measurement settings, such as filtering, affect fractionation as well provides another challenge. Nevertheless, the potential of fractionation-guided ablation could be significant if one could find methods for discerning true fractionation identifying abnormal conduction and arrhythmogenicity in AF patients. Specifically high-resolution AF mapping studies, combined with imaging and/or histologic techniques, could aid in unraveling the "fact or artifact" of fractionation.

Limitations

In this observational study we included ten patients in whom we measured the impact of high-, low-pass and notch filtering. Even though sample size seems rather

small, a total of 3000 seconds of AF recordings, consisting of 2,557,045 fibrillation potentials were analyzed. Furthermore, our results indicate the impact of filtering to be very much alike between patients. Considering that filtering is a highly-reproducible technique, we hypothesize that the general conclusions of this study can be extrapolated to each individual patient. Nevertheless, in clinical practice there may be variations in filter properties. For example, to assure generalizability and reproducibility we used zero-phase filtering, but this might not be possible in daily clinical practice. For this study we used unipolar intra-operative high-resolution mapping data, which is different from (bipolar) endocardial mapping data during ablative therapy with typically lower resolution data. For establishing the impact of filtering on unipolar data however, not spatial resolution but temporal resolution – thus sampling rate – is an important and relevant property, since filtering is done in time-domain. Clinically used mapping systems have comparable sampling rates of ~1 or 1.2 kHz, so our results should be considered relevant for endocardial unipolar mapping as well. Increasing sampling rate, resolution of analogue to digital conversion and using wider band-pass filtering of origin could potentially further improve signal quality.

Conclusions

High-pass, low-pass and notch filtering impacted morphology of unipolar fibrillation potentials, including amplitude, fractionation and FDT, and decreased the number of detected fibrillation potentials, becoming a potential source of error in identification of low-voltage areas and (complex) fractionated potentials. Whilst searching for ablative targets during clinical mapping, operators should be well aware of the consequences of filtering. In case of considerable noise, application of a signal-to-noise ratio – not affecting original signal morphology – could be a safer alternative.

References

1. Konings KT, Smeets JL, Penn OC, Wellens HJ and Allessie MA. Configuration of unipolar atrial electrograms during electrically induced atrial fibrillation in humans. *Circulation*. 1997;95:1231-41.
2. Nademanee K, McKenzie J, Kosar E, Schwab M, Sunsaneewitayakul B, Vasavakul T, Khunnawat C and Ngarmukos T. A new approach for catheter ablation of atrial fibrillation: mapping of the electrophysiologic substrate. *J Am Coll Cardiol*. 2004;43:2044-53.
3. de Bakker JM and Wittkampf FH. The pathophysiologic basis of fractionated and complex electrograms and the impact of recording techniques on their detection and interpretation. *Circ Arrhythm Electrophysiol*. 2010;3:204-13.
4. van der Does LJ and de Groot NM. Inhomogeneity and complexity in defining fractionated electrograms. *Heart Rhythm*. 2017;14:616-624.
5. Waxman HL and Sung RJ. Significance of fragmented ventricular electrograms observed using intracardiac recording techniques in man. *Circulation*. 1980;62:1349-56.
6. Klitzner TS and Stevenson WG. Effects of filtering on right ventricular electrograms recorded from endocardial catheters in humans. *Pacing Clin Electrophysiol*. 1990;13:69-77.
7. Verma A, Jiang CY, Betts TR, Chen J, Deisenhofer I, Mantovan R, Macle L, Morillo CA, Haverkamp W, Weerasooriya R, Albenque JP, Nardi S, Menardi E, Novak P, Sanders P and Investigators SAI. Approaches to catheter ablation for persistent atrial fibrillation. *N Engl J Med*. 2015;372:1812-22.
8. Providencia R, Lambiase PD, Srinivasan N, Ganesh Babu G, Bronis K, Ahsan S, Khan FZ, Chow AW, Rowland E, Lowe M and Segal OR. Is There Still a Role for Complex Fractionated Atrial Electrogram Ablation in Addition to Pulmonary Vein Isolation in Patients With Paroxysmal and Persistent Atrial Fibrillation? Meta-Analysis of 1415 Patients. *Circ Arrhythm Electrophysiol*. 2015;8:1017-29.
9. Vogler J, Willems S, Sultan A, Schreiber D, Luker J, Servatius H, Schaffer B, Moser J, Hoffmann BA and Steven D. Pulmonary Vein Isolation Versus Defragmentation: The CHASE-AF Clinical Trial. *J Am Coll Cardiol*. 2015;66:2743-52.
10. Seitz J, Bars C, Theodore G, Beurtheret S, Lellouche N, Bremondy M, Ferracci A, Faure J, Penaranda G, Yamazaki M, Avula UM, Curel L, Siame S, Berenfeld O, Pisapia A and Kalifa J. AF Ablation Guided by Spatiotemporal Electrogram Dispersion Without Pulmonary Vein Isolation: A Wholly Patient-Tailored Approach. *J Am Coll Cardiol*. 2017;69:303-321.
11. Venkatachalam KL, Herbrandson JE and Asirvatham SJ. Signals and signal processing for the electrophysiologist: part II: signal processing and artifact. *Circ Arrhythm Electrophysiol*. 2011;4:974-81.
12. Zaman JAB, Schricker A, Lalani GG, Trikha R, Krummen DE and Narayan SM. Focal Impulse And Rotor Mapping (FIRM): Conceptualizing And Treating Atrial Fibrillation. *J Atr Fibrillation*. 2014;7:1103.
13. Grace A, Willems S, Meyer C, Verma A, Heck P, Zhu M, Shi X, Chou D, Dang L, Scharf C, Scharf G and Beatty G. High-resolution noncontact charge-density mapping of endocardial activation. *JCI Insight*. 2019;4:e126422.
14. van der Does LJME, Knops P, Teuwen CP, Serban C, Starreveld R, Lanters EAH, Mouws EMJP, Kik C, Bogers AJJC and de Groot NMS. Unipolar atrial electrogram morphology from an epicardial and endocardial perspective. *Heart Rhythm*. 2018;15:879-887.
15. Lanters EA, van Marion DM, Kik C, Steen H, Bogers AJ, Allessie MA, Brundel BJ and de Groot NM. HALT & REVERSE: Hsf1 activators lower cardiomyocyt damage; towards a novel approach to REVERSE atrial

fibrillation. *J Transl Med*. 2015;13:347.
16. van der Does LJ, Yaksh A, Kik C, Knops P, Lanters EA, Teuwen CP, Oei FB, van de Woestijne PC, Bekkers JA, Bogers AJ, Allessie MA and de Groot NM. QUest for the Arrhythmogenic Substrate of Atrial fibRillation in Patients Undergoing Cardiac Surgery (QUASAR Study): Rationale and Design. *J Cardiovasc Transl Res*. 2016;9:194-201.
17. Teuwen CP, Yaksh A, Lanters EA, Kik C, van der Does LJ, Knops P, Taverne YJ, van de Woestijne PC, Oei FB, Bekkers JA, Bogers AJ, Allessie MA and de Groot NM. Relevance of Conduction Disorders in Bachmann's Bundle During Sinus Rhythm in Humans. *Circ Arrhythm Electrophysiol*. 2016;9:e003972.
18. Mouws E, Lanters EAH, Teuwen CP, van der Does L, Kik C, Knops P, Bekkers JA, Bogers A and de Groot NMS. Epicardial Breakthrough Waves During Sinus Rhythm: Depiction of the Arrhythmogenic Substrate? *Circ Arrhythm Electrophysiol*. 2017;10:e005145.
19. Kik C, Mouws E, Bogers A and de Groot NMS. Intra-operative mapping of the atria: the first step towards individualization of atrial fibrillation therapy? *Expert Rev Cardiovasc Ther*. 2017;15:537-545.
20. de Groot NM, Houben RP, Smeets JL, Boersma E, Schotten U, Schalij MJ, Crijns H and Allessie MA. Electropathological substrate of longstanding persistent atrial fibrillation in patients with structural heart disease: epicardial breakthrough. *Circulation*. 2010;122:1674-82.
21. Schneider MA, Ndrepepa G, Weber S, Deisenhofer I, Schomig A and Schmitt C. Influence of high-pass filtering on noncontact mapping and ablation of atrial tachycardias. *Pacing Clin Electrophysiol*. 2004;27:38-46.22.
Lin YJ, Tai CT, Lo LW, Udyavar AR, Chang SL, Wongcharoen W, Tuan TC, Hu YF, Chiang SJ, Chen YJ and Chen SA. Optimal electrogram voltage recording technique for detecting the acute ablative tissue injury in the human right atrium. *J Cardiovasc Electrophysiol*. 2007;18:617-22.
23. Wu SH, Jiang WF, Gu J, Zhao L, Wang YL, Liu YG, Zhou L, Gu JN, Xu K and Liu X. Benefits and risks of additional ablation of complex fractionated atrial electrograms for patients with atrial fibrillation: a systematic review and meta-analysis. *Int J Cardiol*. 2013;169:35-43.
24. Konings KT, Kirchhof CJ, Smeets JR, Wellens HJ, Penn OC and Allessie MA. High-density mapping of electrically induced atrial fibrillation in humans. *Circulation*. 1994;89:1665-80.
25. Stiles MK, Brooks AG, Kuklik P, John B, Dimitri H, Lau DH, Wilson L, Dhar S, Roberts-Thomson RL, Mackenzie L, Young GD and Sanders P. High-density mapping of atrial fibrillation in humans: relationship between high-frequency activation and electrogram fractionation. *J Cardiovasc Electrophysiol*. 2008;19:1245-53.
26. Jadidi AS, Lehrmann H, Keyl C, Sorrel J, Markstein V, Minners J, Park CI, Denis A, Jais P, Hocini M, Potocnik C, Allgeier J, Hochholzer W, Herrera-Sidloky C, Kim S, Omri YE, Neumann FJ, Weber R, Haissaguerre M and Arentz T. Ablation of Persistent Atrial Fibrillation Targeting Low-Voltage Areas With Selective Activation Characteristics. *Circ Arrhythm Electrophysiol*. 2016;9.
27. Blandino A, Bianchi F, Grossi S, Biondi-Zoccai G, Conte MR, Gaido L, Gaita F, Scaglione M and Rametta F. Left Atrial Substrate Modification Targeting Low-Voltage Areas for Catheter Ablation of Atrial Fibrillation: A Systematic Review and Meta-Analysis. *Pacing Clin Electrophysiol*. 2017;40:199-212.
28. Stevenson WG and Soejima K. Recording techniques for clinical electrophysiology. *J Cardiovasc Electrophysiol*. 2005;16:1017-22.

Supplemental material

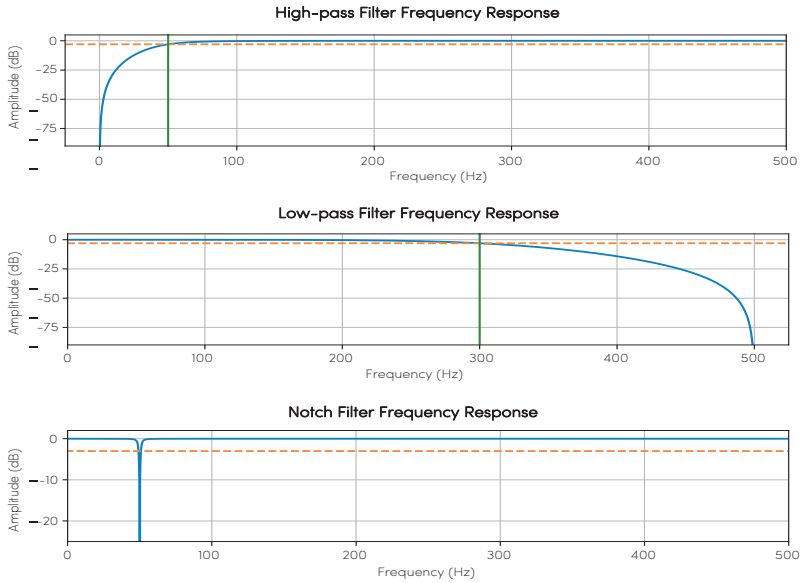

Supplemental figure 1 – Bode plots of the used filters. *Upper panel*: filter frequency response of IIR Butterworth high-pass filter, 2nd-order with 12 dB/octave roll-off with an exemplary half amplitude (-3 dB) cut-off frequency of 50 Hz. *Middle panel*: filter frequency response of IIR Butterworth low-pass filter, 2nd -order with 12 dB/octave roll-off with an exemplary half amplitude (-3 dB) cut-off frequency of 300 Hz. *Lower panel*: filter frequency response of IIR notch filter at 50 Hz, with a quality factor of 30.

Impact of filtering on detection of local activation time

As illustrated in *Figure 1*, the steepest negative deflection of a potential was marked as the local activation time (LAT). As a subanalysis, we investigated the impact of additional high-pass, low-pass and notch filtering on timing of LAT. For this purpose, the difference in LAT (ΔLAT) between each filter setting (see paragraph Filter settings) and the default setting (i.e. 0.5-400 Hz without notch) for all potentials in the 192-electrode array was determined. A median ΔLAT value of all atrial potentials within the 192-array was derived and compared between filter settings.

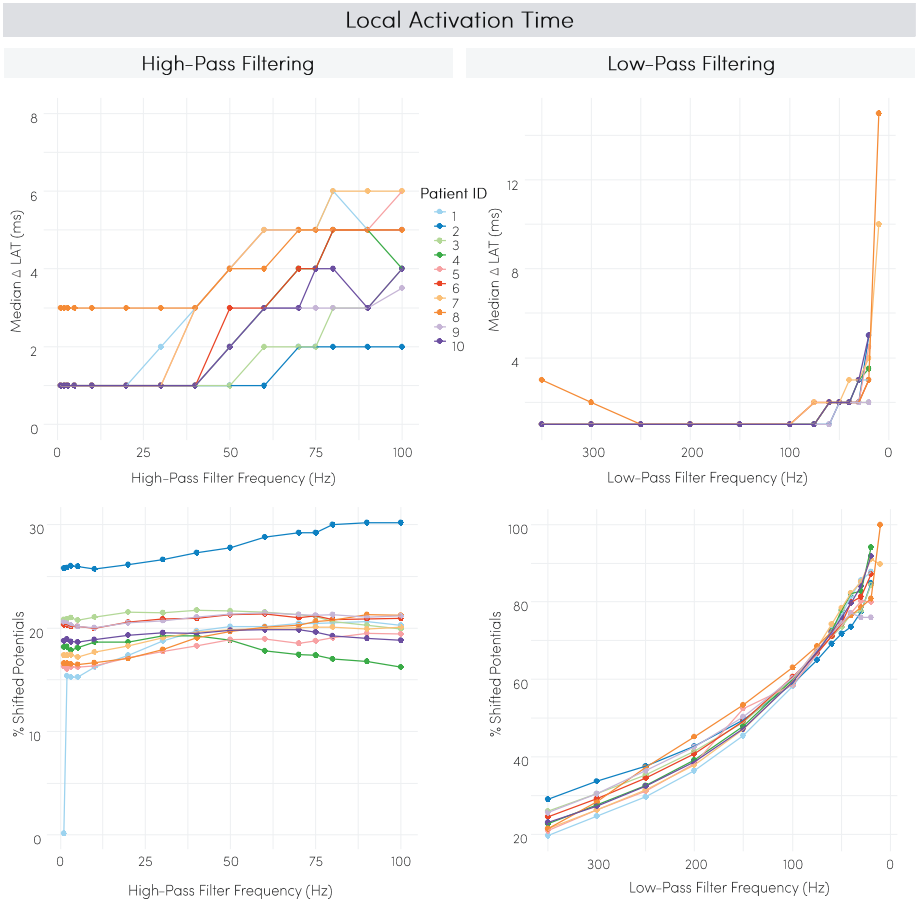

Supplemental figure 2 – Impact of high-pass (left panel) and low-pass (right panel) filtering on detection of local activation time (LAT). *Upper left*: effect of high-pass filtering on median ΔLAT (difference in LAT between each filter setting and the default setting) of all patients. *Upper right*: effect of low-pass filtering on median ΔLAT of all patients. *Lower left*: effect of high-pass filtering on number of shifted potentials (i.e. potentials in whom LAT changed, so ΔLAT ≥ 1; expressed as a percentage of number of detected fibrillation potentials at default setting). *Lower right*: effect of low-pass filtering on number of shifted potentials. In the left upper panel, one outlier is not visualized (patient 1: median ΔLAT 17.5ms at 1Hz).

High-pass filtering

Increasing the high-pass filter frequency increased ΔLAT, as illustrated in *Supplemental figure 2* ($p<0.01$, upper left panel). At the maximum high-pass frequency of 100 Hz, the median ΔLAT ranged from 2 to 6 ms. With increasing high-pass filtering, the percentage of potentials with a shift in LAT (i.e. ΔLAT ≥ 1) slightly increased (from 0.14-25.75% to 16.24-30.12%, $p<0.01$, lower left panel). In total,

286664 potentials shifted due to high-pass filtering, of which 33.21% were single potentials (one deflection, SP), 32.31% double potentials (two deflections, DP) and 34.48% complex fractionated potentials (more than two deflections, CFP). Overall, median ΔLAT (p5-p95) was 1 ms (1-21 ms) for SPs, 3 ms (1-30 ms) for DPs and 6 ms (1-31 ms) for CFPs.

Low-pass filtering
The impact of decreasing the low-pass filter frequency on timing of LAT is shown in the right panel of Supplemental figure 2. The right upper panel indicates an exponentially increasing ΔLAT with decreasing the low-pass filter frequency ($p<0.01$, from 1-3 ms to 2-15 ms). For all patients, decreasing the low-pass filter frequency increased the percentage of potentials with a shift in LAT (from 19.62-28.96% to 76.05-94.12%, $p<0.01$, right left panel). In total, 417119 potentials shifted due to low-pass filtering, of which 33.69% were SPs, 32.29% DPs and 34.02% CFPs. Overall, median ΔLAT (p5-p95) was 1 ms (1-8 ms) for SPs, 1 ms (1-27 ms) for DPs and 4 ms (1-31 ms) for CFPs.

Notch filtering
In nine out of ten patients, notch filtering lead to a shift in LAT of fibrillation potentials. In these patients, median ΔLAT ranged from 8 to 10 ms and 3.61 to 6.99% of potentials had a shift in LAT. A total of 5188 potentials shifted due to notch filtering, of which 32.79% were SPs, 37.95% DPs and 29.26% CFPs. Overall, median ΔLAT (p5-p95) was 3 ms (1-30 ms) for SPs, 10 ms (1-33 ms) for DPs and 11 ms (1-33 ms) for CFPs.

Morphological changes evoked by filtering as described in the manuscript, thereby induce the LAT of fibrillation potentials to shift, especially with more aggressive low-pass filtering. Although filtering impacted LATs of all potential types (i.e. SPs, DPs and CFPs), more complex and long fractionated potentials had a greater ΔLAT – and thus shifted more – than potentials with simpler morphology.

6

Classification of sinus rhythm single potential morphology in patients with mitral valve disease

Mathijs S. van Schie
Roeliene Starreveld
Maarten C. Roos-Serote
Yannick J.H.J. Taverne
Frank R.N. van Schaagen
Ad J.J.C. Bogers
Natasja M.S. de Groot

Europace. 2020 Oct;22(10):1509-1519

Abstract

Aims

The morphology of unipolar single potentials (SPs) contains information on intra-atrial conduction disorders and possibly the substrate underlying atrial fibrillation (AF). This study examined the impact of AF episodes on features of SP morphology during sinus rhythm (SR) in patients with mitral valve disease.

Methods

Intra-operative epicardial mapping (interelectrode distance 2mm) of the right and left atrium (RA, LA), Bachmann's Bundle (BB) and pulmonary vein area (PVA) was performed in 67 patients (27 male, 67±11 years) with or without a history of paroxysmal AF (PAF). Unipolar SPs were classified according to their differences in relative R- and S-wave amplitude ratios.

Results

A clear predominance of S-waves was observed at BB and the RA in both the no AF and PAF groups (BB 88.8% vs. 85.9%, RA: 92.1% vs. 85.1%, respectively). Potential voltages at the RA, BB and PVA were significantly lower in the PAF group ($P<0.001$ for each) and were mainly determined by the size of the S-waves amplitudes. The largest difference in S-wave amplitudes was found at BB; the S-wave amplitude was lower in the PAF group (4.08 [2.45–6.13] mV vs. 2.94 [1.40–4.75] mV; $P<0.001$). In addition, conduction velocity (CV) at BB was lower as well (0.97 [0.70–1.21] m/s vs. 0.89 [0.62–1.16] m/s, $P<0.001$).

Conclusions

Though excitation of the atria during SR is heterogeneously disrupted, a history of AF is characterized by decreased SP amplitudes at BB due to loss of S-wave amplitudes and decreased CV. This suggests that SP morphology could provide additional information on wavefront propagation.

Introduction

Analysis of atrial electrical activity plays an important role in revealing the underlying electrophysiological mechanisms responsible for the initiation and perpetuation of atrial fibrillation (AF). In daily clinical practice, electro-anatomical mapping is performed via endovascular catheters at the endocardial side, presenting a bipolar electrogram (EGM).[1, 2] The bipolar EGM is commonly used as it contains local information from the area of myocardium at the catheter tip between two electrodes. However, unipolar EGMs have the benefit over bipolar EGMs that their morphology carries additional information about the progression of the wavefront and remote activations, which are independent of the electrode orientation and wavefront direction.[2] Cardiac electrophysiologists often rely on low-voltage areas which are suggestive of the presence of atrial substrate.[3] However, low-voltage potentials are highly determined by their morphology, but these are currently not fully classified in clinical practice. Therefore, unipolar EGMs can provide additional helpful information in electrophysiological studies and ablation procedures, and are therefore increasingly used in newly developed mapping systems.

The morphology of atrial EGMs, represented by the relative positive (R-wave) and negative (S-wave) components of a unipolar EGM, contains information on intra-atrial conduction and hence conduction disorders giving rise to development of AF.[2, 4, 5] Prior studies have indeed demonstrated that areas of abnormal EGM morphologies of single potentials (SPs) are indicators of conduction abnormalities underlying AF.[6-8] Therefore, creation of an electrical signal profile obtained from high-resolution mapping data of the entire atria during AF -a so-called AF Fingerprint- may be used to determine the severity and extensiveness of local conduction disorders. The first step towards development of such an 'AF Fingerprint', is understanding variation in EGM morphologies of SPs during sinus rhythm (SR). The goal of this study is therefore to examine the impact of AF episodes on features of SP morphology at a high resolution scale during SR in patients with mitral valve disease (MVD).

Methods

Study population

The study population consisted of 67 adult patients undergoing mitral valve surgery or a combination of mitral valve and coronary bypass surgery in the Erasmus Medical Centre Rotterdam. This study was approved by the institutional medical ethical committee (MEC2010-054/MEC2014-393).[9, 10] Written informed consent was obtained from all patients. Patient characteristics (e.g. age, medical history, cardiovascular risk factors, time in AF) were obtained from the patient's medical

record. The study population was classified into patients without a history of AF (no AF group) and with a history of paroxysmal AF (PAF group).

Mapping procedure

Epicardial high-resolution mapping was performed prior to commencement of extra-corporal circulation, as previously described in detail.[11-13] A temporal bipolar epicardial pacemaker wire attached to the RA free wall served as a reference electrode. A steel wire fixed to subcutaneous tissue of the thoracic cavity was used as an indifferent electrode. Epicardial mapping was performed with a 128-electrode array or 192-electrode array (electrode diameter respectively 0.65mm or 0.45mm, interelectrode distances 2.0 mm). Mapping was conducted by shifting the electrode array along imaginary lines with a fixed anatomic orientation, following a predefined mapping scheme. The procedure covers the entire epicardial surface of the right atrium (RA), Bachmann's Bundle (BB), pulmonary vein area (PVA) and left atrium (LA), as illustrated in the upper panel of left panel of *Figure 1*. Omission of areas was avoided at the expense of possible small overlap between adjacent mapping sites. The RA was mapped from the cavotricuspid isthmus, shifting perpendicular to the caval veins towards the RA appendage. The PVA was mapped from the sinus transversus fold along the borders of the right and left pulmonary veins (PVR and PVL) down towards the atrioventricular groove. The left atrioventricular groove (LAVG) was mapped from the lower border of the left inferior pulmonary vein towards the LA appendage. BB was mapped from the tip of the LA appendage across the roof of the LA, behind the aorta towards the superior cavo-atrial junction.

Five seconds of SR were recorded from every mapping site, including a surface ECG lead, a calibration signal of 2 mV and 1000ms, a bipolar reference EGM and all unipolar epicardial EGMs. In patients who presented in AF, SR mapping was performed after electrical cardioversion. Data was stored on a hard disk after amplification (gain 1000), filtering (bandwidth 0.5-400 Hz), sampling (1 kHz) and analogue to digital conversion (16 bits).

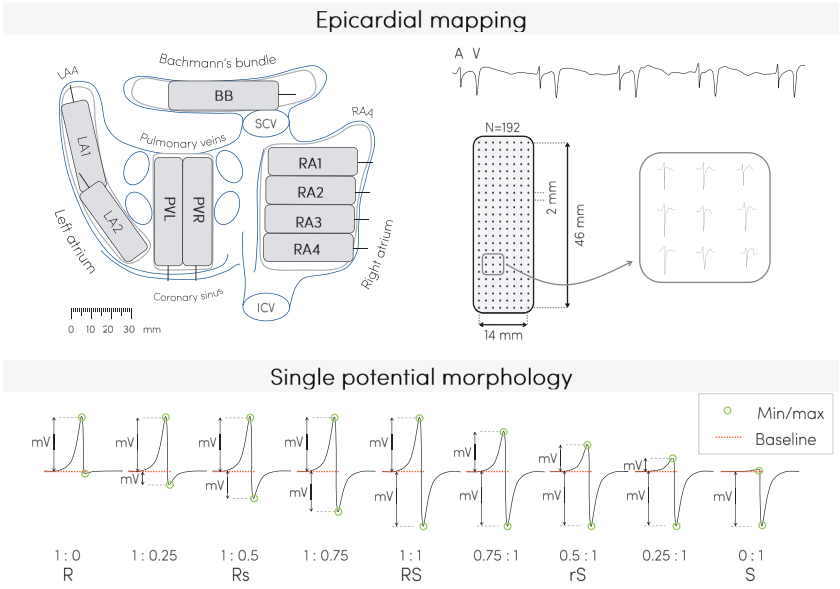

Figure 1 – Epicardial high-resolution mapping. *Upper left panel*: projection of the 192-unipolar electrode array on a schematic posterior view of the atria. *Upper right panel*: epicardial, unipolar potentials recorded during 5 seconds of SR containing atrial deflections (A) and far-field ventricular signals (V). Typical examples of 9 EGMs obtained from the RA are shown outside the mapping. *Lower panel*: EGMs with variable R/S ratios calculated by dividing the R-wave amplitude by the S-wave amplitude. ICV, inferior caval vein; SCV, superior caval vein; LAA, left atrial appendage; RAA, right atrial appendage; RA, right atrium; BB, Bachmann's Bundle; PV, pulmonary veins; LA, left atrium.

Data analysis

Unipolar EGM morphology was semi-automatically analyzed in custom-made software using Python 3. EGMs with injury potentials, recording sites with ≥25% excluded or missing EGMs and premature atrial complexes or aberrant beats were excluded from analysis. Atrial deflections were marked when the negative slope of a deflection was ≥10% of the steepest slope in the EGM and the amplitude of the deflection was at least two times the signal-to-noise ratio of the EGM. The steepest negative deflection of a potential was marked as the Local Activation Time (LAT). The minimal time between two successive deflections ('latency') was set to 2 ms. All EGM markings were manually checked and corrected in case of markings on electrical artefacts evaluated by a consensus of two investigators. Potentials were classified as single potential (SP, one deflection) or fractionated potential (FP, ≥2 deflections). SPs are characterized by a rapid negative deflection preceded by a positive R-wave and returning to the baseline (S-wave). As demonstrated in the lower panel of *Figure 1*, SPs were classified according to their differences in relative R- and S-wave amplitude and scaled from -1 (R-wave) to 1 (S-wave).

$$RS = \begin{cases} 1 - RS\,(n) & for\ RS\,(n) \leq 1 \\ \dfrac{1}{RS\,(n)} - 1 & for\ RS\,(n) > 1 \end{cases}$$

Furthermore, SPs were analyzed for peak-to-peak voltage (amplitude), relative R- and S-wave amplitudes and local wavefront conduction velocity (CV). Local CV was computed as an average of velocity estimations between neighboring electrodes (longitudinal, transversal and diagonal) based on a techniques derived from a finite differences method developed and described by Salama et al.[14]

Statistical analysis

All data were tested for normality. Normally distributed data are expressed as mean ± standard deviation and analyzed with a paired T-test or one-way ANOVA. Skewed data are expressed as median (25th-75th percentile) and analyzed with a Kruskal-Wallis test or Mann-Whitney U test. Categorical data are expressed as numbers and percentages and analyzed with a $\chi 2$ or Fisher exact test when appropriate. Distribution data was analyzed with a two-sample Kolmogorov-Smirnov test. A p-value <0.05 was considered statistically significant. A Bonferroni correction was applied for comparison of the four atrial regions; a p-value of <0.0083 (0.05/6) was considered statistically significant.

Results

Study population

Clinical characteristics of the study population, including 44 patients in the 'no AF' group and 23 patients in the 'PAF' group are described in *Table 1*. These groups differed in age (no AF: 65±13 years, PAF: 73±6 years, P=0.003). Patients had either ischemic and MVD (no AF: 20 [45%], PAF: 6 [26%]) or only MVD. LA dilation was present in 28 patients without AF (64%) and in 16 patients with PAF (70%). Most patients in both groups had normal left ventricular function (no AF: 29 [66%], PAF: 17 [74%]). 30% of the patients with PAF used class III antiarrhythmic drugs (no AF: 0 vs. PAF: 7 (30%), P<0.001).

Mapping data

As demonstrated in *Table 2*, a total of 523,019 SPs were analyzed out of 852 SR recordings of 5-seconds duration (no AF: RA: 179,700, BB: 34,069, PVA: 77,651, LA: 64,254; PAF: RA: 77,060; BB: 16,260; PVA: 38,720; LA: 35,305). Median unipolar SP amplitude in the PAF group was lower than in the no AF group (4.78 [2.14–7.21] mV vs. 5.05 [2.48–7.64] mV respectively (P<0.001)).

Table 1 – Patient characteristics (N=67)

	No AF	PAF	p-value
Patients	44 (66)	23 (34)	-
Male	17 (39)	10 (43)	0.903
Age (y)	65±12	73 ± 6	0.003
Cardiovascular risk factors			
- BMI (kg/m^2)	24.5 [22.1–26.8]	25.3 [22.2–31.9]	0.281
Underweight (<18.5)	2 (5)	0 (0)	0.778
Normal weight (18.5-25)	22 (50)	11 (48)	0.866
Overweight (25-30)	15 (34)	5 (22)	0.443
Obese (≥30)	5 (11)	7 (30)	0.110
- Hypertension	15 (34)	12 (52)	0.242
- Dyslipidaemia	14 (32)	2 (9)	0.071
- Diabetes mellitus	7 (16)	3 (13)	0.755
Left atrial dilatation >45 mm	28 (64)	16 (70)	0.830
Left ventricular dysfunction	15 (34)	6 (26)	0.694
Mitral stenosis	3 (7)	1 (4)	0.685
Severe mitral insufficiency	31 (70)	16 (70)	0.940
Coronary artery disease	20 (45)	6 (26)	0.200
Antiarrhythmic agents			
- Class I	1 (2)	0 (0)	0.466
- Class II	23 (52)	11 (48)	0.930
- Class III	0 (0)	7 (30)	<0.001
- Class IV	1 (2)	2 (9)	0.559

Values are presented as mean ± standard deviation, median [interquartile ranges] or as n (%). (P)AF, (paroxysmal) atrial fibrillation; BMI, body mass index.

In both the no AF and PAF group, SP amplitudes differed between the atrial regions (no AF: RA: 5.21 [3.03–7.67] mV, BB: 5.71 [3.40–8.87] mV, PVA: 4.48 [2.03–8.19] mV, LA: 4.72 [2.19–8.24] mV (P<0.001 for all comparisons); PAF group: RA: 5.10 [2.89–7.55] mV, BB: 4.09 [2.18–6.70] mV, PVA: 4.36 [1.95–8.38] mV, LA: 4.74 [2.47–7.63] mV (P<0.001 for all comparisons)). Furthermore, SP amplitudes of the RA, BB and PVA were lower in the PAF group compared to the no AF group (RA: 5.21 [3.03–7.67] mV vs. 5.10 [2.89–7.55] mV (P<0.001), BB: 5.71 [3.40–8.87] mV vs. 4.09 [2.18–6.70] mV (P<0.001), PVA: 4.48 [2.03–8.19] mV vs. 4.36 [1.95–8.38] mV (P<0.001)).

Table 2 – Mapping data characteristics (N=523,019)

		No AF	PAF	p-value
Right atrium				
-	Single potentials	179,700 (85)	77,060 (85)	
-	Amplitude (mV)	5.21 [3.03–7.67]	5.10 [2.89–7.55]	< 0.001
-	R-wave (mV)	1.65 [0.74–2.79]	1.69 [0.79–2.81]	< 0.001
-	S-wave (mV)	3.48 [2.07–5.08]	3.30 [1.86–4.97]	< 0.001
-	R/S ratio	0.52 [0.28–0.71]	0.46 [0.22–0.67]	< 0.001
-	Conduction velocity (m/s)	0.93 [0.71–1.15]	0.94 [0.72–1.17]	< 0.001
Bachmann's bundle				
-	Single potentials	34,069 (76)	16,260 (73)	
-	Amplitude (mV)	5.71 [3.40–8.87]	4.09 [2.18–6.70]	< 0.001
-	R-wave (mV)	1.57 [0.74–3.00]	1.11 [0.49–2.21]	< 0.001
-	S-wave (mV)	4.08 [2.45–6.13]	2.94 [1.40–4.75]	< 0.001
-	R/S ratio	0.57 [0.35–0.76]	0.58 [0.29–0.77]	< 0.001
-	Conduction velocity (m/s)	0.97 [0.70–1.21]	0.89 [0.62–1.16]	< 0.001
Left atrium				
-	Single potentials	64,254 (84)	35,305 (83)	
-	Amplitude (mV)	4.72 [2.19–8.24]	4.74 [2.47–7.63]	0.067
-	R-wave (mV)	2.44 [1.13–4.39]	2.24 [1.21–3.94]	< 0.001
-	S-wave (mV)	1.91 [0.83–3.89]	2.12 [0.93–3.86]	< 0.001
-	R/S ratio	-0.16 [-0.52–0.30]	-0.03 [-0.46–0.38]	< 0.001
-	Conduction velocity (m/s)	0.91 [0.54–1.23]	0.94 [0.60–1.23]	< 0.001
Pulmonary vein area				
-	Single potentials	77,651 (87)	38,720 (77)	
-	Amplitude (mV)	4.48 [2.03–8.19]	4.36 [1.95–8.38]	< 0.001
-	R-wave (mV)	1.94 [0.94–3.72]	1.98 [0.84–4.10]	0.177
-	S-wave (mV)	2.28 [0.92–4.12]	2.13 [0.94–4.22]	< 0.001
-	R/S ratio	0.14 [-0.33–0.45]	0.12 [-0.29–0.44]	0.156
-	Conduction velocity (m/s)	0.98 [0.66–1.25]	1.00 [0.70–1.25]	< 0.001

Values are presented as median (interquartile range) or as n (%). (P)AF, (paroxysmal) atrial fibrillation.

Focusing only on the magnitude of the R- and S-wave, the largest R-wave amplitude was found in the LA in both the no AF group (2.44 [1.13–4.39] mV) and PAF group (2.24 [1.21–3.94] mV), whereas the largest S-wave amplitude was found in BB in the no AF group (4.08 [2.45–6.13] mV) and in the RA in the PAF group (3.30 [1.86–4.97] mV). In general, the amplitude of the atrial potential was mainly determined by the S-wave amplitude.

The largest difference in S-wave amplitudes between both groups was found at BB; the S-wave median amplitude was higher in the no AF group (4.08 [2.45–6.13] mV) than in the PAF group (2.94 [1.40–4.75] mV; P<0.001).

The CV differed between atrial regions in both the no AF and PAF group (no AF: RA: 0.93 [0.71–1.15] m/s, BB: 0.97 [0.70–1.21] m/s, PVA: 0.98 [0.66–1.25] m/s, LA: 0.91

[0.54–1.23] m/s (P<0.001 for all comparisons); PAF group: RA: 0.94 [0.72–1.17] m/s, BB: 0.89 [0.62–1.16] m/s, PVA: 1.00 [0.70–1.25] m/s, LA: 0.94 [0.60–1.24] m/s (P<0.001 for all comparisons)). In the PAF group, CVs at BB were lower compared to the no AF group (0.97 [0.70–1.21] m/s vs. 0.89 [0.62–1.16] m/s, P<0.001).

Regional differences in R/S ratio

Figure 2 shows a typical example of the color-coded spatial distribution of the R/S ratios during one SR beat in a patient without AF. This map shows a wide variation of R/S ratios throughout the atria. The majority of the SPs recorded in the superior part of RA consisted of monophasic S-waves, compared to rS-waves and biphasic RS-waves in the mid and inferior part of the RA. A clear R-wave predominance was found in between the pulmonary veins, whereas biphasic RS-waves and rS-waves were recorded from the superior and inferior sites of the PVA. The LA appendage revealed a R-wave predominance as well, whereas S-wave predominance was mainly found in the RA and BB.

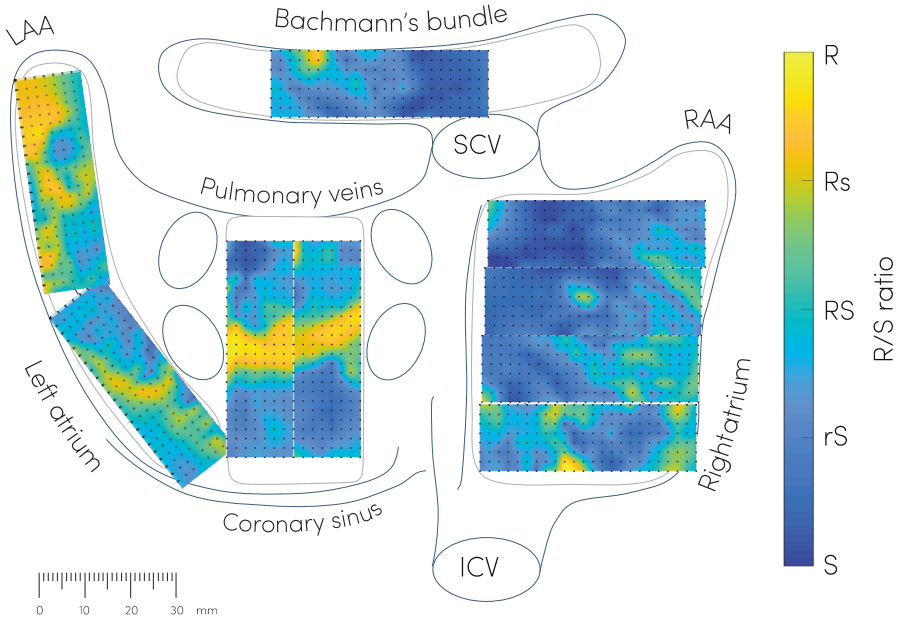

Figure 2 – Typical example of the color-coded spatial distribution of the R/S ratios during one sinus beat in a patient without AF. The color scale of the R/S ratios ranges from S-waves (blue), via biphasic RS-waves (green) to R-waves (yellow). ICV, inferior caval vein; SCV, superior caval vein; LAA, left atrial appendage; RAA, right atrial appendage.

Figure 3 shows the regional differences in the distribution of the R/S ratios in the RA, BB, PVA and LA in the no AF group (upper panels) and PAF group (lower panels). The relative frequency of the R/S ratios are ranked from -1 (R-waves) to 1 (S-waves)

and divided into four equal quartiles. For each quartile the relative number of potentials is given on top of the plots. The SPs revealed a wide variation of R- and S-wave amplitude ratios. However, a clear predominance of S-waves was observed in the BB and RA in both the no AF group (88.8% and 92.1% respectively) as PAF group (85.9% and 85.1% respectively). Differences between the no AF and PAF groups were found at the RA, BB and LA (P=0.021, P=0.003 and P=0.013). In the PAF group, there was a larger number of dominant R-waves in both the RA and BB and a higher number of rS-waves in the LA.

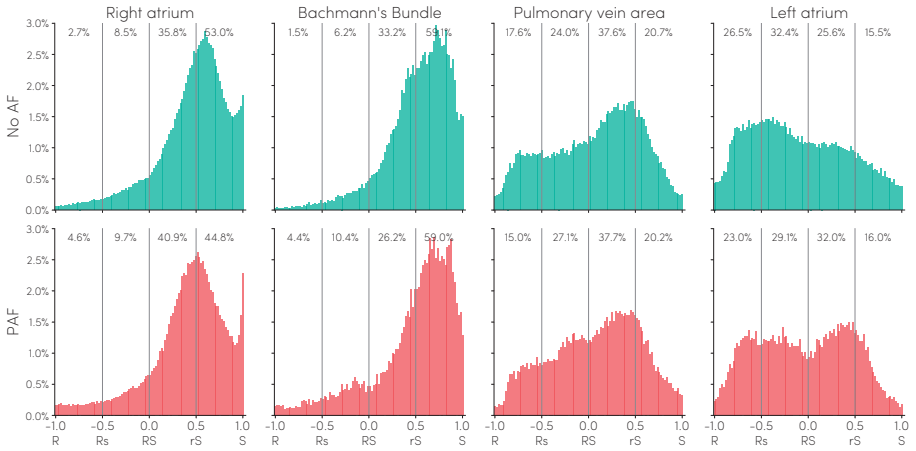

Figure 3 – Relative frequency histograms of all R/S ratios. The R/S ratios of unipolar SPs during SR in patients without AF (turquoise) and patients with PAF (red), recorded from BB (n = 34,069 vs. n = 16,260), LA (n = 64,254 vs. n = 35,305), PVA (n = 77,651 vs. n = 38,720) and RA (n = 179,700 vs. n = 77,060). The histograms are divided into four equal quartiles; for each quartile the relative number of potentials is given on top of the plots. (P)AF, (paroxysmal) atrial fibrillation.

Individual differences in R/S ratios

Figure 4 demonstrates interindividual differences in R/S ratios. In all patients there was a clear S-wave predominance in the RA and BB. In contrast, in the PVA and LA there was less S-wave predominance and a wider variation in SP morphology.

Figure 5 demonstrates all R/S ratios (subdivided into nine categories) with their corresponding amplitudes. In both the no AF and PAF group, the largest SP amplitudes were observed in the range of biphasic RS- to rS-waves (no AF: RA: 6.39 [4.25–8.89] mV, BB: 7.61 [4.51–12.55] mV, PVA: 5.96 [3.30–9.86] mV, LA: 6.77 [3.78–10.95] mV; PAF: RA: 5.96 [3.83–8.34] mV, BB: 5.45 [2.78–9.28] mV, PVA: 6.10 [3.21–10.44] mV, LA: 6.02 [3.53–8.90] mV). In the PAF group, SP amplitudes of all different R/S ratios were smaller in BB compared to the no AF group (P<0.001). At the other atrial regions, there were no consistent significant differences in amplitudes of the

various R/S ratios. The majority of the monophasic S-wave potentials were found in the RA in both groups (4.2% and 4.3% respectively). A high number of S-wave potentials (3.7% for both groups) were found in BB as well, whereas these potentials were rarely present in the PVA and LA.

Figure 4 – Stacked bar plots of the R/S distributions depicted for each patient separately in the RA, BB, PVA and LA. (P)AF, (paroxysmal) atrial fibrillation.

R/S ratio in low voltage areas

The p5 of all measured SPs was 1.0 mV, which was used as a cut-off value for low voltages. *Figure 6* illustrates the regional distribution of the R/S ratios of low voltage potentials. Although a wide variation of R/S ratios was observed, an S-wave predominance was found in the RA and BB in both groups. Compared to the no AF group, the relative number of dominant R-waves in low voltage areas in the PAF group was larger in the RA and BB, whereas a larger number of dominant S-waves was observed in the PVA.

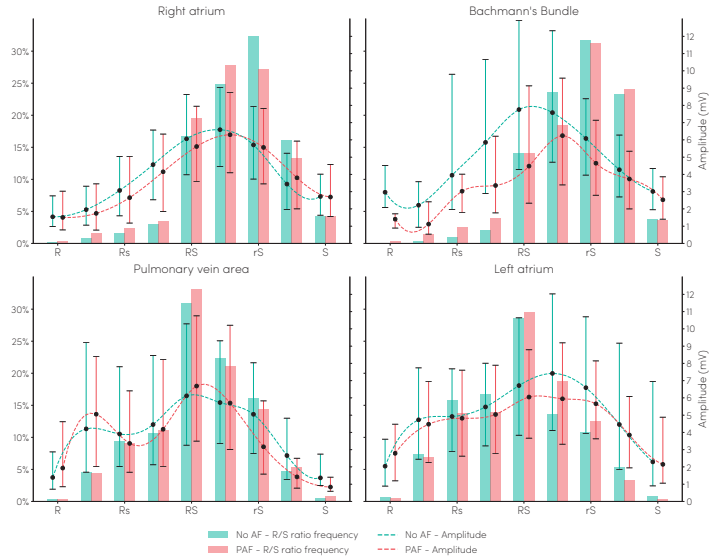

Figure 5 – Relative frequency histograms of the R/S ratios and amplitudes of unipolar SPs during SR in patients without AF (turquoise) and with PAF (red). The bars represent the relative frequency of the R/S ratios and the dotted line the median amplitudes with interquartile ranges. The asterisk indicates a significant difference in median amplitudes between the patients without AF and patients with PAF (P<0.001). (P)AF, (paroxysmal) atrial fibrillation.

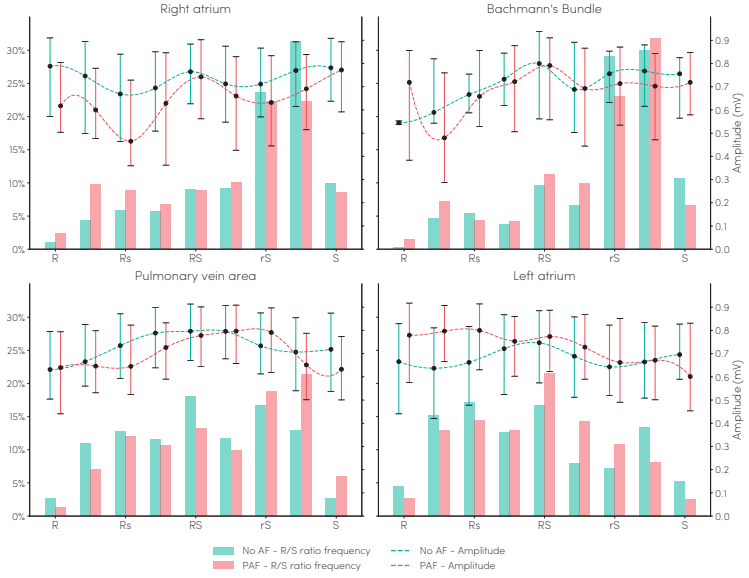

Figure 6 – Relative frequency histograms of the RS ratios and amplitudes of unipolar SPs in low voltage areas during SR in patients without AF (turquoise) and with PAF (red). The bars represent the relative frequency of the R/S ratios and the dotted line the median amplitudes with interquartile ranges. (P)AF, (paroxysmal) atrial fibrillation.

Discussion

High-resolution mapping of the atria in patients with MVD demonstrated a wide variation of unipolar SP morphology throughout the atria, resulting in specific regional differences in SP amplitude and R/S ratios. Amplitudes were mainly determined by the S-wave amplitude, which resulted in a high number of predominant S-wave potentials with large amplitudes in the RA and BB, whereas a larger range of SP amplitudes was found in the LA and PVA together with a high variation in R/S ratios. Compared to the no AF group, lower SP amplitudes and S-wave amplitudes were found in patients with PAF, along with more R-wave predominance in the RA, BB and PVA.

Genesis of unipolar potential morphologies

EGM morphology is often used for the identification of structural or electrical remodeled areas with arrhythmogenic properties. In most settings, electro-anatomical mapping is performed via endovascular catheters at the endocardial side, recording EGMs which are the product of a voltage difference between recording electrodes (bipolar recordings).[1, 15] In case of unipolar EGMs, the signal reflects the cardiac electrical activity of the tissue surrounding the recording electrode which decreases with distance. It is obtained by an exploring electrode positioned in the heart and an indifferent electrode located at an infinite distance.[2, 16] It is for these reasons that there is an increase in mapping systems using unipolar EGMs.

The morphology of unipolar potentials can be regarded as the sum of instantaneous current dipoles of a wavefront, generating a positive deflection when the activation wavefront propagates towards the electrode and a steeply negative deflection as the wavefront reaches the electrode and propagates away, thereby generating a biphasic RS-wave.[2, 5, 17] When the electrode is located at a site of initial activation, depolarization produces a wavefront that propagates radially away from the electrode, thus generating a monophasic S-wave. In contrast, positive R-waves are characteristic of termination of the activation wavefront. Areas of fast conduction with conduction along the longitudinal axis of the fibers are characterized by large amplitude RS-waves, whereas in slow areas the potentials are of lower amplitude.[5] Abnormal myocardial substrate can be defined by substrate mapping by identifying areas of low voltage, as amplitude also depends on the volume of simultaneously activated cardiac tissue.[5, 6] In addition, asymmetry of unipolar potentials has been proposed as a morphology parameter, determined by wavefront curvature, wavefront collisions, anisotropy and conduction heterogeneity.[18, 19]

Regional differences in single potential morphology

In our study population, there were clear regional differences in potential morphology. During SR, the initial excitation site is located in the RA in which wavefronts are

generated by cells in the sinoatrial (SA) node area. From there, a wavefront is propagated by the prominent muscle bundles contiguous with the SA node; i.e. the crista terminalis, Bachmann's Bundle and the septo-pulmonary bundle, which contributes to fast electrical propagation and enables efficient electromechanical coupling of both atria during each normal sinus beat.[4, 20] At sites of wavefront activation, monophasic S-waves were expected and were - indeed - mainly recorded in the RA in our study population. In addition, fast propagating wavefronts are characterized by EGMs with large amplitude, predominant S-waves, which evolve towards biphasic RS-waves when the wavefront propagates away from the excitation site. These types of potentials were indeed mainly found in the RA and BB.

Using diffusion tensor imaging of human hearts, Pashakhanloo et al.[21] have demonstrated that in some areas of the atrial wall, e.g. the crista terminalis and the antrum of the PVs, the uniform distribution of myocardial fibers is disrupted by multiple complex crossings of multiple fibers, which underlies non-uniform anisotropic propagation. Previous studies have demonstrated that there are changes in patients with MVD in the myocardial structure of the atria due to altered hemodynamic effects.[22-24] Structural remodelling affects intra-atrial conduction and thereby predisposes to development of atrial tachyarrhythmias. The higher incidence of AF in patients with MVD suggests the presence of a higher degree of atrial remodelling in these patients, characterized by LA enlargement, loss of myocardium and scarring.[25-27] The resulting anisotropic propagation causes local wavefront termination or collision, resulting in more R-wave predominance and monophasic R-waves, which were - indeed - mainly found in the LA and PVA.

In our study, we demonstrated inter-individual differences in R/S ratios in - especially - the LA and PVA areas. Anatomic studies of the fiber orientation using dissection, visual tracing or MR techniques demonstrated variations in the location and orientation of bundles between human hearts, in which mixed and oblique patterns of fibers were present in the roof of the atria encircling the pulmonary veins.[21, 28] In addition, intraoperative epicardial mapping also demonstrated that atrial excitation during SR is affected by the underlying heart disease and AF, resulting in alternative routes for BB and PVA with high inter-individual variability.[29, 30] Together with the patient specific impact of the presence of MVD, these differences might have resulted in the more prominent inter-individual R/S differences in these areas.

Several computer models of electrical propagation in the atria have been developed and showed mostly single biphasic potentials in the uniform atria, whereas dominant S-waves were more common in anisotropic tissue and dominant R-waves were found due to the multiple collisions.[19] Using such computer models it has been demonstrated that anisotropy has a greater impact on amplitude variation and asymmetry than the shape and curvature of the conducting wavefront.

However, the models differ in the level of electrophysiological and anatomical details, such as fiber orientation, presence of the main muscle bundles, structural modifications and anisotropy, and mainly focus on arrhythmia simulations.[19, 31-34] S-wave predominance has also been reported in the RA in patients during AF, but could not be strongly correlated to wavefront curvature or anisotropy.[35] A tilted transmural stance of the wavefront resulting in an epicardial lead with constant epicardial to endocardial activation was proposed as a theoretical explanation for S-wave predominance during AF, which would present with more R-wave predominance at the endocardium.[35] However, Van der Does et al.[36] reported that both epicardial and endocardial EGMs showed an S-wave predominance, and endocardial EGMs did not have higher R/S ratios than epicardial EGMs. Though these mapping studies were performed during SR, data clearly showed absence of an oblique transmurally propagating wave. In our study, we indeed demonstrated an S-wave predominance in the RA but not in the LA and PVA.

Influence of paroxysmal atrial fibrillation

In our study, SP morphology differences between patients without AF and with PAF were most prominent in the BB. Patients with PAF had lower amplitudes, more R-wave predominance and slower wavefront propagation. The lower amplitude was mainly determined by a decrease in S-wave amplitude, which is observed with reversible tissue injury and is associated with conduction block during ablative therapy.[18, 37] Recent studies indeed found more conduction abnormalities in the BB during SR in patients with AF or patients who developed post-operative AF.[11, 38] BB is by far the largest of the anatomic interatrial connections and probably accounts for the largest part of interatrial conduction. It is a highly organized bundle of muscular fibers arranged in parallel fashion, but due to its anisotropic features BB is more vulnerable to structural remodelling that can even be identified during SR. In addition, the muscular fibers of the BB are not enclosed by fibrous tissue and may therefore also be vulnerable to disruption by stretch due to the hemodynamic changes in the atria caused by MVD.[20, 22, 39] This could lead to slower wavefront propagation and slower CVs which were - indeed – found in patients with PAF. Structural changes of the atrial myocardium are more extensive in patients with PAF than in patients without AF, especially involving the BB.[40]

Clinical implications

Despite most of atrial mapping procedures are performed endocardially using bipolar EGMs, there is an increase in mapping systems using unipolar EGMs. Therefore, detailed knowledge of unipolar EGM morphology becomes more important. In a prior study of Van der Does et al.[36], no differences were found between unipolar endo- and epicardial EGMs. This indicates that the observed change in R/S ratios and decrease of S-wave amplitudes will also be found at the endocardium.

In clinical practice, low voltage areas are regarded as part of the arrhythmogenic substrate underlying AF. However, our data shows that the EGM voltage is mainly determined by the R/S ratio which differs per region. In addition, low peak-to-peak voltages do not automatically indicate 'diseased' tissue, but can also be explained by the potential morphology as R- and S-waves have a smaller amplitude compared to RS-waves. Therefore, using voltage mapping alone to guide ablative therapy might be misleading.

Study limitations

Whether general anesthesia and intraoperative drugs influence conduction is unknown; however, a standard anesthetic protocol was used for all patients and SR was confirmed during all mapping procedures. Therefore, possible effects of anesthesia would be equally dispersed among the patient population. High-resolution mapping of the interatrial septum could not be performed with our closed beating heart approach. Several patients with history of AF used antiarrhythmic drugs class III. Amiodarone has class I antiarrhythmic properties via inhibition of sodium channels during phase 0 of the cardiac action potential which can slow intra-atrial conduction. Therefore, the use of amiodarone could have affected our results. In addition, there was a difference in age between the no AF and PAF group. The differences between both groups could be related to the impact of age. However, no correlation was found between any of signal profiles and age. Still, the possible effect could not be completely excluded, just as the effects of hypertension or obesity, although not significantly different between the groups.

Conclusions

A specific regional distribution of EGM morphology, involving R/S ratios, EGM voltage and R- and S-wave amplitudes exist during SR in patients with MVD. Though excitation of the atria during SR is heterogeneously disrupted in patients with MVD, the occurrence of AF in this patient group is characterized by decreased SP amplitudes at BB due to loss of S-wave amplitudes together with a decreased CV. Therefore, BB is an area that could especially be interesting for AF Fingerprinting. Our findings that variation in EGM morphologies in our population is considerable –particularly at the LA and PVA- and specific EGM morphologies at regions such as BB are related to AF suggests that the potential morphology could provide additional information on CV and wavefront propagation, and emphasizes the need for a diagnostic tool enabling identification of arrhythmogenic substrate in the individual patient.

References

1. Koutalas E, Rolf S, Dinov B, Richter S, Arya A, Bollmann A, Hindricks G and Sommer P. Contemporary Mapping Techniques of Complex Cardiac Arrhythmias - Identifying and Modifying the Arrhythmogenic Substrate. *Arrhythm Electrophysiol Rev*. 2015;4:19-27.
2. Stevenson WG and Soejima K. Recording techniques for clinical electrophysiology. *J Cardiovasc Electrophysiol*. 2005;16:1017-22.
3. Wong GR, Nalliah CJ, Lee G, Voskoboinik A, Prabhu S, Parameswaran R, Sugumar H, Anderson RD, McLellan A, Ling LH, Morton JB, Sanders P, Kistler PM and Kalman JM. Dynamic Atrial Substrate During High-Density Mapping of Paroxysmal and Persistent AF: Implications for Substrate Ablation. *JACC Clin Electrophysiol*. 2019;5:1265-1277.
4. Spach MS, King TD, Barr RC, Boaz DE, Morrow MN and Herman-Giddens S. Electrical potential distribution surrounding the atria during depolarization and repolarization in the dog. *Circ Res*. 1969;24:857-73.
5. Spach MS, Miller WT, 3rd, Miller-Jones E, Warren RB and Barr RC. Extracellular potentials related to intracellular action potentials during impulse conduction in anisotropic canine cardiac muscle. *Circ Res*. 1979;45:188-204.
6. de Groot NM, Schalij MJ, Zeppenfeld K, Blom NA, Van der Velde ET and Van der Wall EE. Voltage and activation mapping: how the recording technique affects the outcome of catheter ablation procedures in patients with congenital heart disease. *Circulation*. 2003;108:2099-106.
7. Otomo K, Uno K, Fujiwara H, Isobe M and Iesaka Y. Local unipolar and bipolar electrogram criteria for evaluating the transmurality of atrial ablation lesions at different catheter orientations relative to the endocardial surface. *Heart Rhythm*. 2010;7:1291-300.
8. Bortone A, Appetiti A, Bouzeman A, Maupas E, Ciobotaru V, Boulenc JM, Pujadas-Berthault P and Rioux P. Unipolar signal modification as a guide for lesion creation during radiofrequency application in the left atrium: prospective study in humans in the setting of paroxysmal atrial fibrillation catheter ablation. *Circ Arrhythm Electrophysiol*. 2013;6:1095-102.
9. Lanters EA, van Marion DM, Kik C, Steen H, Bogers AJ, Allessie MA, Brundel BJ and de Groot NM. HALT & REVERSE: Hsf1 activators lower cardiomyocyt damage; towards a novel approach to REVERSE atrial fibrillation. *J Transl Med*. 2015;13:347.
10. van der Does LJ, Yaksh A, Kik C, Knops P, Lanters EA, Teuwen CP, Oei FB, van de Woestijne PC, Bekkers JA, Bogers AJ, Allessie MA and de Groot NM. QUest for the Arrhythmogenic Substrate of Atrial fibRillation in Patients Undergoing Cardiac Surgery (QUASAR Study): Rationale and Design. *J Cardiovasc Transl Res*. 2016;9:194-201.
11. Teuwen CP, Yaksh A, Lanters EA, Kik C, van der Does LJ, Knops P, Taverne YJ, van de Woestijne PC, Oei FB, Bekkers JA, Bogers AJ, Allessie MA and de Groot NM. Relevance of Conduction Disorders in Bachmann's Bundle During Sinus Rhythm in Humans. *Circ Arrhythm Electrophysiol*. 2016;9:e003972.
12. Mouws E, Lanters EAH, Teuwen CP, van der Does L, Kik C, Knops P, Bekkers JA, Bogers A and de Groot NMS. Epicardial Breakthrough Waves During Sinus Rhythm: Depiction of the Arrhythmogenic Substrate? *Circ Arrhythm Electrophysiol*. 2017;10:e005145.
13. Kik C, Mouws E, Bogers A and de Groot NMS. Intra-operative mapping of the atria: the first step towards individualization of atrial fibrillation

therapy? *Expert Rev Cardiovasc Ther*. 2017;15:537-545.
14. Salama G, Kanai A and Efimov IR. Subthreshold stimulation of Purkinje fibers interrupts ventricular tachycardia in intact hearts. Experimental study with voltage-sensitive dyes and imaging techniques. *Circ Res*. 1994;74:604-19.
15. Friedman PA. Novel mapping techniques for cardiac electrophysiology. *Heart*. 2002;87:575-82.
16. Blanchard SM, Damiano RJ, Jr., Asano T, Smith WM, Ideker RE and Lowe JE. The effects of distant cardiac electrical events on local activation in unipolar epicardial electrograms. *IEEE Trans Biomed Eng*. 1987;34:539-46.
17. Cantwell CD, Roney CH, Ng FS, Siggers JH, Sherwin SJ and Peters NS. Techniques for automated local activation time annotation and conduction velocity estimation in cardiac mapping. *Comput Biol Med*. 2015;65:229-42.
18. Villacastin J, Almendral J, Arenal A, Castellano NP, Gonzalez S, Ortiz M, Garcia J, Vallbona B, Moreno J, Portales JF and Torrecilla EG. Usefulness of unipolar electrograms to detect isthmus block after radiofrequency ablation of typical atrial flutter. *Circulation*. 2000;102:3080-5.
19. Jacquemet V, Virag N, Ihara Z, Dang L, Blanc O, Zozor S, Vesin JM, Kappenberger L and Henriquez C. Study of unipolar electrogram morphology in a computer model of atrial fibrillation. *J Cardiovasc Electrophysiol*. 2003;14:S172-9.
20. Ho SY, Anderson RH and Sanchez-Quintana D. Atrial structure and fibres: morphologic bases of atrial conduction. *Cardiovasc Res*. 2002; 54:325-36.
21. Pashakhanloo F, Herzka DA, Ashikaga H, Mori S, Gai N, Bluemke DA, Trayanova NA and McVeigh ER. Myofiber Architecture of the Human Atria as Revealed by Submillimeter Diffusion Tensor Imaging. *Circ Arrhythm Electrophysiol*. 2016;9:e004133.
22. Anne W, Willems R, Roskams T, Sergeant P, Herijgers P, Holemans P, Ector H and Heidbuchel H. Matrix metalloproteinases and atrial remodeling in patients with mitral valve disease and atrial fibrillation. *Cardiovasc Res*. 2005;67:655-66.
23. Castonguay MC, Wang Y, Gerhart JL, Miller DV, Stulak JM, Edwards WD and Maleszewski JJ. Surgical pathology of atrial appendages removed during the cox-maze procedure: a review of 86 cases (2004 to 2005) with implications for prognosis. *Am J Surg Pathol*. 2013;37:890-7.
24. Kim SJ, Choisy SC, Barman P, Zhang H, Hancox JC, Jones SA and James AF. Atrial remodeling and the substrate for atrial fibrillation in rat hearts with elevated afterload. *Circ Arrhythm Electrophysiol*. 2011;4:761-9.
25. Nowicki ER, Birkmeyer NJ, Weintraub RW, Leavitt BJ, Sanders JH, Dacey LJ, Clough RA, Quinn RD, Charlesworth DC, Sisto DA, Uhlig PN, Olmstead EM, O'Connor GT, Northern New England Cardiovascular Disease Study G and the Center for Evaluative Clinical Sciences DMS. Multivariable prediction of in-hospital mortality associated with aortic and mitral valve surgery in Northern New England. *Ann Thorac Surg*. 2004;77:1966-77.
26. Messika-Zeitoun D, Bellamy M, Avierinos JF, Breen J, Eusemann C, Rossi A, Behrenbeck T, Scott C, Tajik JA and Enriquez-Sarano M. Left atrial remodelling in mitral regurgitation--methodologic approach, physiological determinants, and outcome implications: a prospective quantitative Doppler-echocardiographic and electron beam-computed tomographic study. *Eur Heart J*. 2007;28:1773-81.
27. John B, Stiles MK, Kuklik P, Chandy ST, Young GD, Mackenzie L, Szumowski L, Joseph G, Jose J, Worthley SG,

Kalman JM and Sanders P. Electrical remodelling of the left and right atria due to rheumatic mitral stenosis. *Eur Heart J*. 2008;29:2234-43.
28. Nathan H and Eliakim M. The junction between the left atrium and the pulmonary veins. An anatomic study of human hearts. *Circulation*. 1966;34:412-22.
29. Mouws E, Lanters EAH, Teuwen CP, van der Does L, Kik C, Knops P, Yaksh A, Bekkers JA, Bogers A and de Groot NMS. Impact of Ischemic and Valvular Heart Disease on Atrial Excitation:A High-Resolution Epicardial Mapping Study. *J Am Heart Assoc*. 2018;7.
30. Mouws E, Kik C, van der Does L, Lanters EAH, Teuwen CP, Knops P, Bogers A and de Groot NMS. Novel Insights in the Activation Patterns at the Pulmonary Vein Area. *Circ Arrhythm Electrophysiol*. 2018;11:e006720.
31. Seemann G, Hoper C, Sachse FB, Dossel O, Holden AV and Zhang H. Heterogeneous three-dimensional anatomical and electrophysiological model of human atria. *Philos Trans A Math Phys Eng Sci*. 2006;364:1465-81.
32. Aslanidi OV, Colman MA, Stott J, Dobrzynski H, Boyett MR, Holden AV and Zhang H. 3D virtual human atria: A computational platform for studying clinical atrial fibrillation. *Prog Biophys Mol Biol*. 2011;107:156-68.
33. Krogh-Madsen T, Abbott GW and Christini DJ. Effects of electrical and structural remodeling on atrial fibrillation maintenance: a simulation study. *PLoS Comput Biol*. 2012;8:e1002390.
34. Tobon C, Ruiz-Villa CA, Heidenreich E, Romero L, Hornero F and Saiz J. A three-dimensional human atrial model with fiber orientation. Electrograms and arrhythmic activation patterns relationship. *PLoS One*. 2013;8:e50883.
35. Houben RP, de Groot NM, Smeets JL, Becker AE, Lindemans FW and Allessie MA. S-wave predominance of epicardial electrograms during atrial fibrillation in humans: indirect evidence for a role of the thin subepicardial layer. *Heart Rhythm*. 2004;1:639-47.
36. van der Does L, Knops P, Teuwen CP, Serban C, Starreveld R, Lanters EAH, Mouws E, Kik C, Bogers A and de Groot NMS. Unipolar atrial electrogram morphology from an epicardial and endocardial perspective. *Heart Rhythm*. 2018;15:879-887.
37. Kumar S and Michaud GF. Unipolar electrogram morphology to assess lesion formation during catheter ablation of atrial fibrillation: successful translation into clinical practice. *Circ Arrhythm Electrophysiol*. 2013;6:1050-2.
38. Roberts-Thomson KC, Stevenson I, Kistler PM, Haqqani HM, Spence SJ, Goldblatt JC, Sanders P and Kalman JM. The role of chronic atrial stretch and atrial fibrillation on posterior left atrial wall conduction. *Heart Rhythm*. 2009;6:1109-17.
39. Ho SY, Anderson RH and Sanchez-Quintana D. Gross structure of the atriums: more than an anatomic curiosity? *Pacing Clin Electrophysiol*. 2002;25:342-50.
40. Becker AE. How structurally normal are human atria in patients with atrial fibrillation? *Heart Rhythm*. 2004;1:627-31.

7

Sinus rhythm voltage fingerprinting in patients with mitral valve disease using a high-density epicardial mapping approach

Mathijs S. van Schie
Roeliene Starreveld
Ad J.J.C. Bogers
Natasja M.S. de Groot

Europace. 2021 Jan:euaa336

Abstract

Aims

Unipolar voltage (UV) mapping is increasingly used for guiding ablative therapy of atrial fibrillation (AF) as unipolar electrograms (U-EGMs) are independent of electrode orientation and atrial wavefront direction. This study was aimed at constructing individual, high-resolution sinus rhythm (SR) UV fingerprints in order to identify low voltage areas and study the effect of AF episodes in patients with mitral valve disease (MVD).

Methods

Intra-operative epicardial mapping (interelectrode distance 2mm) of the right and left atrium (RA, LA), Bachmann's Bundle (BB) and pulmonary vein area (PVA) was performed in 67 patients (27 male, 67±11 years) with or without a history of paroxysmal AF (PAF).

Results

In all patients, there were considerable regional variations in voltages. UVs at BB were lower in patients with PAF compared to those without (no AF: 4.94 [3.56–5.98] mV, PAF: 3.30 [2.25–4.57] mV, P=0.006). A larger number of low voltage potentials were recorded at BB in the PAF group (no AF: 2.13 [0.52–7.68] %, PAF: 12.86 [3.18–23.59] %, P=0.001). In addition, areas with low voltage potentials were present in all patients, yet we did not find any predilection sites for low voltage potentials to occur.

Conclusions

Even in SR, advanced atrial remodeling in MVD patients shows marked interindividual and regional variation. Low UVs are even present during SR in patients without a history of AF indicating that low UVs should carefully be used as target sites for ablative therapy.

Introduction

Unipolar voltage (UV) mapping is increasingly used to define the substrate of cardiac arrhythmias like atrial fibrillation (AF).[1] In recent studies, low bipolar voltage areas are regarded sites of structurally remodeled tissue and have therefore become targets for e.g. AF ablation.[2-4] However, there are many discrepancies between studies in for example mapping and ablation strategies, rhythm during mapping and patient selection, resulting in mixed outcomes.[5] In daily clinical practice, electro-anatomical mapping is performed via endovascular catheters at the endocardial side, using bipolar electrograms (EGMs). However, non-substrate related factors such as activation direction also influences voltages of bipolar EGMs.[5] Unipolar electrograms (U-EGMs), on the other hand, are independent of the electrode orientation and atrial wavefront direction, and have the benefit over bipolar EGMs that their morphology contains additional information on the progression of the wavefront and remote activations. It is for these reasons that U-EGMs are increasingly used in recent electrophysiological studies and newly developed mapping systems guiding (ventricular) ablation procedures.[6,7] However, the use of unipolar voltage mapping remains less established in mapping of the atrial substrate.

Nevertheless, multiple methods and thresholds have been defined to identify low voltage areas and abnormal tissue in both bipolar- as U-EGMs. In addition, several studies have shown local variation in endocardial bipolar EGM voltages during sinus rhythm (SR) between atrial regions and that specific regional differences exist between patients with and without AF, especially within the left atrium (LA).[8,9]

As no significant differences were found between endocardial and epicardial U-EGM voltages by Van der Does et al.[10], high-resolution epicardial mapping data of the entire atria can be used to create a representative UV profile, reflecting characteristics of unipolar potentials. These voltage fingerprints can be used to identify low voltage areas and to examine the effect of AF episodes on SR potential voltages. Therefore, this study was aimed at constructing individual, high-resolution unipolar SR voltage profiles in order to identify low UV areas and study the effect of AF episodes on UV potentials in patients with mitral valve disease (MVD).

Methods

Study population

The study population consisted of 67 successive adult patients undergoing mitral valve surgery or a combination of mitral valve and coronary bypass surgery in the Erasmus Medical Center Rotterdam. This study was approved by the institutional

medical ethical committee (MEC2010-054/MEC2014-393).[11, 12] Written informed consent was obtained from all patients and patient characteristics (e.g. age, medical history, cardiovascular risk factors, time in AF) were obtained from the patient's medical record. The study population was classified into two groups: those without a history of AF (no AF group) and those with a history of paroxysmal AF (PAF group).

Mapping procedure

Epicardial high-resolution mapping was performed prior to commencement of extra-corporal circulation, as previously described in detail.[11, 12] A temporal bipolar epicardial pacemaker wire attached to the RA free wall served as a reference electrode and a steel wire fixed to subcutaneous tissue of the thoracic cavity was used as an indifferent electrode. Epicardial mapping was performed with a 128-electrode array or 192-electrode array (electrode diameter respectively 0.65mm or 0.45mm, interelectrode distances 2.0 mm). Mapping was conducted by shifting the electrode array along imaginary lines with a fixed anatomic orientation, covering the entire epicardial surface of the right atrium (RA), Bachmann's bundle (BB), pulmonary vein area (PVA) and left atrium (LA), following a predefined mapping scheme as illustrated in the upper left panel of *Figure 1*. Omission of areas was avoided at the expense of possible small overlap between adjacent mapping sites. The RA was mapped from the cavo-tricuspid isthmus, shifting perpendicular to the caval veins towards the RA appendage. The PVA was mapped from the sinus transversus fold along the borders of the right and left pulmonary veins (PVR and PVL) down towards the atrioventricular groove. The left atrio-ventricular groove (LAVG) was mapped from the lower border of the left inferior pulmonary vein towards the LA appendage. BB was mapped from the tip of the LA appendage across the roof of the LA, behind the aorta towards the superior cavo-atrial junction.

Five seconds of SR were recorded from every mapping site, including a surface ECG lead, a calibration signal of 2 mV and 1000 ms, a bipolar reference electrogram and all unipolar epicardial EGMs. In patients who presented in AF, SR mapping was performed after electrical cardioversion. Patients who could not be converted to SR were excluded from analysis. Data was stored on a hard disk after amplification (gain 1000), filtering (bandwidth 0.5-400 Hz), sampling (1 kHz) and analogue to digital conversion (16 bits).

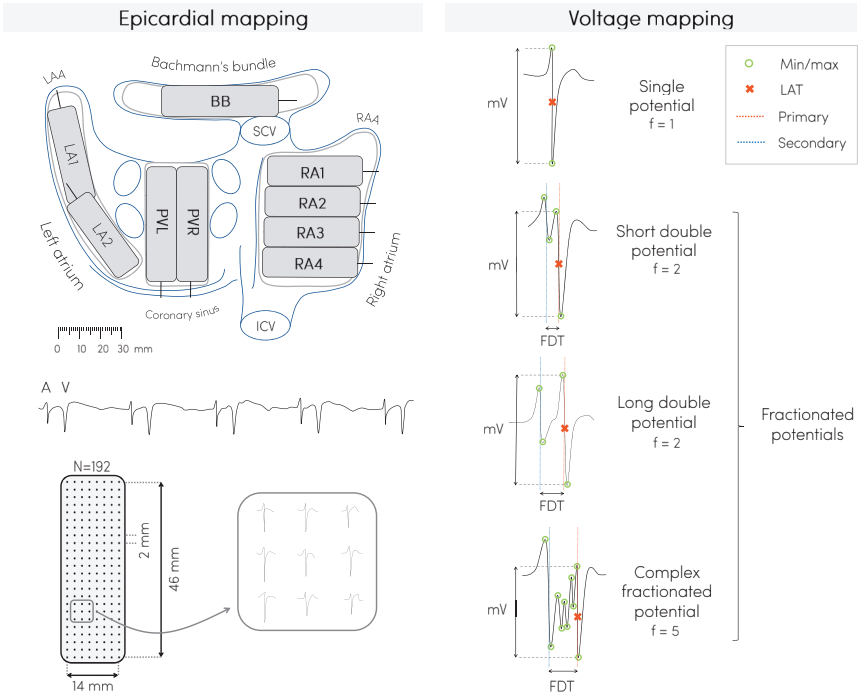

Figure 1 – Epicardial high-resolution mapping. *Upper left panel*: projection of the 192-unipolar electrode array on a schematic posterior view of the atria. *Lower left panel*: epicardial, unipolar potentials recorded during 5 seconds of SR containing atrial deflections (A) and far-field ventricular signals (V). Typical examples of 9 unipolar potentials obtained from the RA are shown outside the mapping. *Right panel*: classification of potential type according to the number of deflections (f). EGM voltage is determined as the peak-to-peak amplitude of the steepest (primary) deflection. FDT, fractionation delay time; ICV, inferior caval vein; SCV, superior caval vein; LAA, left atrial appendage; RAA, right atrial appendage, RA, right atrium, BB, Bachmann's bundle, PV, pulmonary veins, LA, left atrium.

Data analysis

U-EGM morphology was semi-automatically analyzed using custom-made software. EGMs with injury potentials, recording sites with ≥25% excluded or missing EGMs and atrial extrasystoles were excluded from analysis. The steepest negative slope of an atrial deflection was marked as the local activation time (LAT), provided that the amplitude of the deflection was at least two times the signal-to-noise ratio of the EGM. The minimal time between two successive deflections ('latency') was set to 2 ms. All signal markings were manually checked and corrected in case of markings on electrical artifacts evaluated by a consensus of two investigators.

The potential amplitude is defined as the peak-to-peak voltage of the steepest deflection. Low voltage is defined as the fraction of potentials with an amplitude

below the 5th percentile of all potentials obtained from all MVD patients without AF. Fractionated potentials are defined as potentials with ≥2 deflections. Conduction velocity (CV) is computed using discrete velocity vectors as previously described. Slowing of conduction was defined as a local CV of <28 cm/s and conduction block as a local conduction delay of <18 cm/s. Simultaneous activated areas without CV were excluded to avoid inclusion of far field potentials.

Statistical analysis

All data were tested for normality. Normally distributed data are expressed as mean±SD and analyzed with a paired T-test or one-way ANOVA. Skewed data are expressed as median [25th–75th percentile] and analyzed with a Kruskal-Wallis test, Mann-Whitney U test or Wilcoxon signed-rank test, whichever appropriate. Categorical data are expressed as numbers and percentages and analyzed with a $\chi 2$ or Fisher exact test. Correlation was determined by an ordinary least squares regression model. Distribution data was analyzed with a two-sample Kolmogorov-Smirnov test. A p-value <0.05 was considered statistically significant. Bonferroni correction was applied for comparison of the four atrial regions; a p-value of <0.0083 (0.05/6) was considered statistically significant.

Results

Study population

Clinical characteristics of the study population, including 44 patients without ('no AF group') and 23 patients with PAF, are described in detail in *Table 1*. These groups differed in age (no AF: 65±12 vs. PAF: 73±6 years, P=0.003) and the use of class III antiarrhythmic drugs (no AF: 0 vs. PAF: 7 (30%), P<0.001). Patients had either ischemic and mitral valve disease (no AF: 20 [45%], PAF: 6 [26%]) or only solely mitral valve disease. The gradient of both mitral insufficiency and stenosis did not differ between both groups; the majority of the patients had severe mitral insufficiency (no AF: 31 (70%), PAF: 13 (70%), P=0.940). LA dilation was present in 28 patients without AF (64%) and in 16 patients with PAF (70%). Most patients in both groups had normal left ventricular function (no AF: 29 [66%], PAF: 17 [74%]).

Table 1 – Patient characteristics (N=67)

	No AF	PAF	p-value
Patients	44 (66)	23 (34)	-
Male	17 (39)	10 (43)	0.903
Age (y)	65±12	73±6	0.003
Cardiovascular risk factors			
- BMI (kg/m^2)	24.5 [22.1–26.8]	25.3 [22.2–31.9]	0.281
Underweight (<18.5)	2 (5)	0 (0)	0.778
Normal weight (18.5-25)	22 (50)	11 (48)	0.866
Overweight (25-30)	15 (34)	5 (22)	0.443
Obese (≥30)	5 (11)	7 (30)	0.110
- Hypertension	15 (34)	12 (52)	0.242
- Dyslipidemia	14 (32)	2 (9)	0.071
- Diabetes mellitus	7 (16)	3 (13)	0.755
Left atrial dilatation >45 mm	28 (64)	16 (70)	0.830
Left ventricular dysfunction	15 (34)	6 (26)	0.694
Mitral stenosis			
- No	41 (93)	22 (96)	0.685
- Severe	3 (7)	1 (4)	0.685
Mitral insufficiency			
- Mild	1 (2)	0 (0)	0.466
- Moderate	8 (18)	3 (13)	0.848
- Moderate-to-severe	4 (9)	4 (17)	0.550
- Severe	31 (70)	16 (70)	0.940
Coronary artery disease	20 (45)	6 (26)	0.200
Antiarrhythmic agents			
- Class I	1 (2)	0 (0)	0.466
- Class II	23 (52)	11 (48)	0.930
- Class III	0 (0)	7 (30)	<0.001
- Class IV	1 (2)	2 (9)	0.559

Values are presented as mean ± standard deviation, median [interquartile ranges] or as N (%).
(P)AF, (paroxysmal) atrial fibrillation; BMI, body mass index.

Data characteristics

As demonstrated in *Table 2*, a total of 600,722 potentials were analyzed out of 829 SR recordings of 5-seconds duration. There was no difference between the median number of potentials between the no AF and PAF group and the median amplitude of all potentials recorded from the entire epicardial surface did also not differ between these two groups (no AF: 4.70 [4.05–5.43] mV vs. PAF: 4.52 [3.73–5.25] mV, p=0.138).

Correlation between unipolar voltage and interatrial conduction

There was no clear correlation between UV and CV, though smaller voltages were recorded in areas of conduction slowing (1.74 [0.88 – 3.53] mV vs. 4.72 [2.46 – 7.61] mV, P<0.001) and conduction block (1.22 [0.69 – 2.26] mV vs. 4.79 [2.55 – 7.65] mV,

P<0.001). There was a clear difference in UV between fractionated potentials and single potentials in which the former type results in smaller voltages compared to the latter (2.05 [1.04 – 3.75] mV vs. 5.16 [2.85 – 8.01] mV, P<0.001). In addition, as demonstrated in *Figure 2*, there was a clear inversely proportional relationship between UV and the number of additional deflections (1: 5.16 [2.85 – 8.01] mV; 2: 2.20 [1.14 – 3.95] mV; 3: 1.21 [0.68 – 2.26] mV; ≥4: 0.94 [0.52 – 1.71] mV, P<0.001 for all). Furthermore, UV was inversely correlated with age and BMI (R2=0.21; age: -0.04 mV/year, P=0.005; BMI: -0.07 mV/kg/m2, P=0.043). There was no difference in UV between patients with different gradients of mitral insufficiency or stenosis.

Table 2 – Analysis of electrophysiological parameters per patient (N=67)

	MVD without AF (N=44)	MVD with AF (N=23)	p-value
Right atrium			
Number of potentials	4,067 [3,346–5,797]	4,229 [2,881–4,936]	0.086
Amplitude (mV)	4.86 [3.97–5.71]	4.75 [3.84–6.15]	0.492
Fractionated potentials (%)	14.79 [9.76–19.60]	16.55 [8.70–23.83]	0.197
Low voltage (%)	6.49 [2.34–9.15]	8.37 [2.94–14.06]	0.150
Fractionated low voltage (%)	50.0 [37.5–64.4]	54.4 [37.2–65.0]	0.433
Bachmann's bundle			
Number of potentials	984 [783–1,206]	940 [779–1,126]	0.295
Amplitude (mV)	4.92 [3.45–6.09]	2.95 [2.24–4.57]	0.007
Fractionated potentials (%)	19.58 [12.40–31.72]	28.68 [17.70–39.55]	0.064
Low voltage (%)	1.79 [0.37–8.02]	11.98 [2.95–21.50]	0.001
Fractionated low voltage (%)	85.0 [77.5–98.3]	74.6 [50.2–96.2]	0.080
Pulmonary vein area			
Number of potentials	1,979 [1,441–2,608]	2,136 [1,592–2,596]	0.497
Amplitude (mV)	3.84 [2.45–7.15]	3.95 [2.62–5.02]	0.268
Fractionated potentials (%)	11.89 [9.08–17.01]	21.70 [13.48–28.63]	< 0.001
Low voltage (%)	6.49 [0.20–13.31]	10.19 [3.89–14.28]	0.061
Fractionated low voltage (%)	36.7 [18.5–61.7]	51.3 [23.6–65.4]	0.342
Left atrium			
Number of potentials	1,626 [1,132–2,302]	1,777 [1,062–2,077]	0.439
Amplitude (mV)	4.42 [2.99–5.87]	4.64 [3.65–5.72]	0.363
Fractionated potentials (%)	10.92 [6.43–17.74]	17.47 [11.30–20.54]	0.062
Low voltage (%)	3.63 [1.57–11.35]	4.04 [0.72–8.98]	0.358
Fractionated low voltage (%)	25.9 [10.7–48.8]	29.6 [17.5–73.4]	0.144

Values are presented as median [interquartile ranges] or as N (%). (P)AF, (paroxysmal) atrial fibrillation.

Unipolar voltage mapping

In *Figure 3*, 12 representative examples of color-coded spatial distributions of potential voltages during SR in 6 patients without and 6 with PAF are shown. In all patients, there is a wide variation in potential voltages throughout the entire atrial surface without a clear predilection site for low voltages.

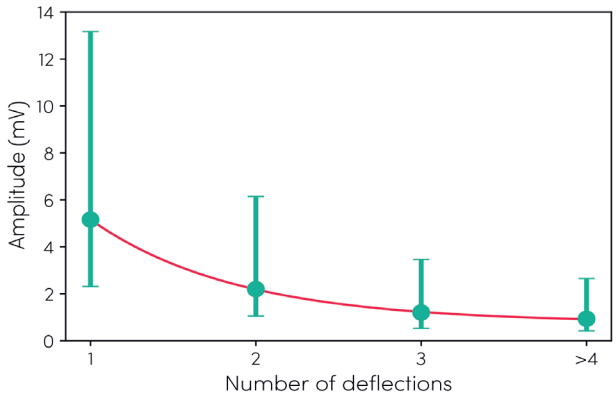

Figure 2 – Relation between potential amplitude and number of deflections. Potential amplitude is given as median with interquartile ranges.

Regional differences in unipolar voltages

In the following step, U-EGMs were subdivided according to the corresponding atrial recording regions (RA, BB, PVA and LA); their characteristics are listed in *Table 2*. In the no AF group, there were no significant differences in median potential voltages between the various atrial regions (P=0.750). However, in the PAF group, UVs of potentials recorded at BB (2.95 [2.24–4.57] mV) were significantly lower compared to RA potentials (4.75 [3.84–6.15] mV, P=0.004) and LA potentials (4.64 [3.65–5.72] mV, P=0.003). Comparing the no AF and PAF group, UVs at BB were significantly lower in the latter group (no AF: 4.92 [3.45–6.09] mV, PAF: 2.95 [2.24–4.57] mV, P=0.007).

In the no AF group, there was a significantly higher number of fractionated potentials at BB (19.58 [12.40–31.72] %) compared to the RA (14.79 [9.76–19.60] %, P<0.001), PVA (11.89 [9.08–17.01] %, P<0.001) and LA (10.92 [6.43–17.74] %, P<0.001). In the PAF group, a significantly higher number of fractionated potentials was observed in BB (28.68 [17.70–39.55] %) compared to the RA (16.55 [8.70–23.83] %, P<0.001) and LA (17.47 [11.30–20.54] %, P=0.001), but not at the PVA (21.70 [13.48–28.63] %, P=0.114). Compared to the no AF group, more fractionated potentials at the PVA were found in the PAF group (no AF: 11.89 [9.08–17.01] %; PAF: 21.70 [13.48–28.63] %; P<0.001).

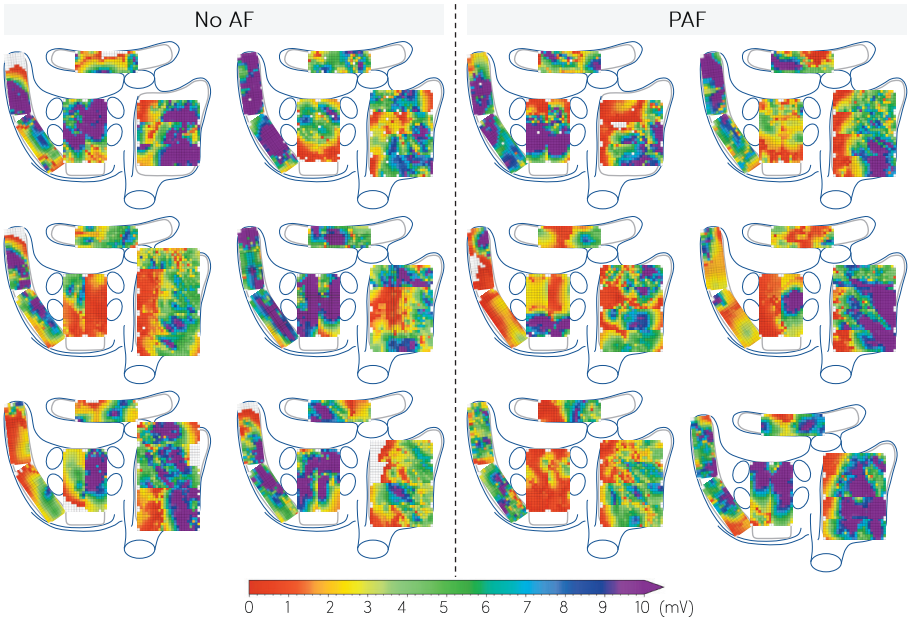

Figure 3 – Representative examples of unipolar epicardial voltage maps. Maps during one sinus beat in six patients without history of AF (left) and six patients with PAF (right). (P)AF, (paroxysmal) atrial fibrillation are shown.

Determination of low voltage areas

The p5 of all potentials obtained from all MVD patients without AF was 1.0 mV, which was therefore used as cut-off value in identification of low voltage areas. As demonstrated in *Table 2*, a larger number of low voltage potentials were recorded at BB in the PAF group compared to the no AF group (no AF: 1.79 [0.37–8.02] %, PAF: 11.98 [2.95–21.50] %, P=0.001).

Regional differences in low voltage areas

Within the areas of low voltage, 46.2 [31.0–59.8] % of the potentials were fractionated in the no AF group and 47.1 [38.9–56.4] % in the PAF group (P=0.450). Specifically, in the no AF group, most fractionated low voltage potentials were found at BB (BB: 85.0 [77.5–98.3] % vs. RA: 50.0 [37.5–64.4] %, P<0.001; PVA: 36.7 [18.5–61.7] %, P<0.001; LA: 25.9 [10.7–48.8] %, P<0.001). In addition, the amount of fractionated low voltage potentials was higher at the RA compared to the LA (P<0.001). In the PAF group, however, BB was only higher compared to the PVA and LA (BB: 74.6 [50.2–96.2] % vs. PVA: 51.3 [23.6–65.4] % and LA: 29.6 [17.5–73.4] %, P=0.003 & P=0.006 respectively).

Individual voltage fingerprints

The voltage distribution is depicted for each individual patient in a so-called voltage fingerprint, as demonstrated in *Figure 4*. In all patients, there was a considerable

variation in voltage distribution between all atrial regions and clear inter-individual differences were found. In the no AF group, considerable inter-individual variations in the dispersion of median voltages were found between the atrial regions ranging from 0.78 to 9.90 mV (median: 4.11 mV), while in the PAF group the variations ranged from 0.51 to 7.23 mV (median: 3.45 mV) (P=0.070). The p5 of the voltages differed between the individual patients, and between the patients without AF and with PAF (no AF: 0.84 [0.71–1.12] mV; PAF: 0.65 [0.57–1.01] mV; P=0.041). In all patients, fractionation was found in one or more atrial regions, ranging in the no AF group from 0.54 % to 31.89 % (median: 15.60 %) and from 8.86 % to 29.77 % (median: 18.61 %) in the PAF group (P=0.037).

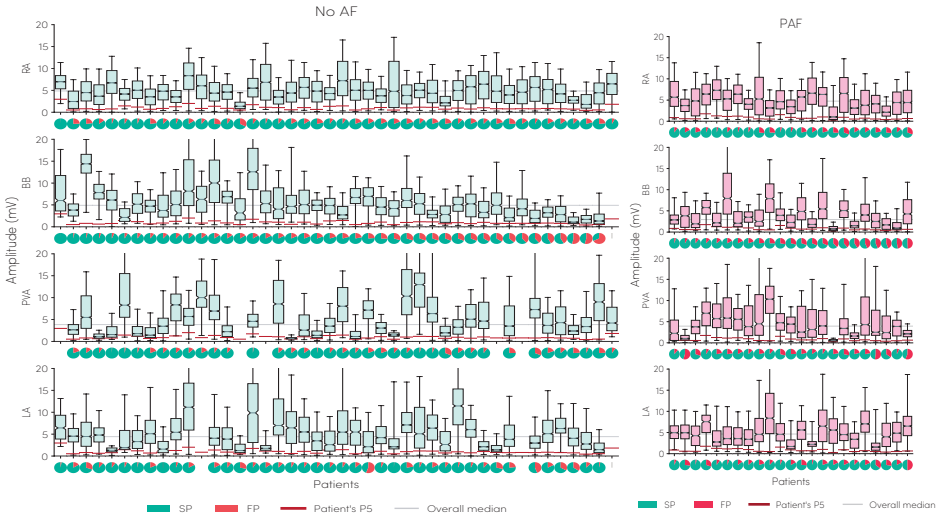

Figure 4 – Boxplots of the voltage distributions during SR for patients without AF (left) and PAF (right). Plots are depicted for each patient separately, recorded at the right atrium (RA), Bachmann's bundle (BB), pulmonary vein area (PVA) and left atrium (LA). For each patient a pie plot of the potential type distribution is given, indicating the number of single potentials (green) and fractionated potentials (red). The red line indicates a patient's voltage p5 and the grey line represents the overall voltage median per atrial region. Patients are ranked in descending order according to the amount of single potentials at BB.

Predilection sites for low voltage areas

For each individual patient, the location with the highest amount of low voltage was determined, as demonstrated in *Figure 5*. In the no AF group, there was no clear predilection site for low voltage areas. However, the amount of low voltage areas at the RA (7.8 [3.1–11.4] %) was lower compared to BB and PVA (22.3 [11.6–26.2] % and 19.8 [12.5–32.5] %; p=0.007 & p<0.001 respectively). In the PAF group, low voltage areas occurred more frequently at BB (48%), yet, comparable to the no AF group, there were no significant regional differences in the amount of low voltage areas.

Comparing the no AF and PAF group, low voltage areas occurred more frequently at BB (21% vs. 48%; p=0.020) in the PAF group. However, the amount of low voltage sites did not differ at any region between both groups.

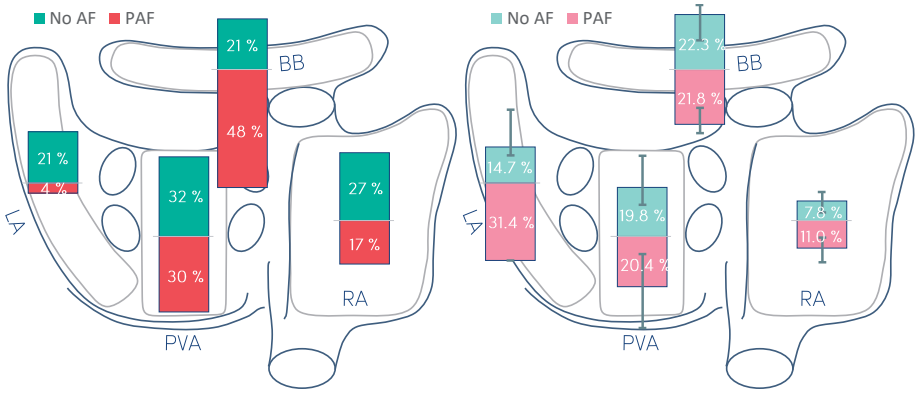

Figure 5 – Areas of low voltage and amount of low voltage. Bars plotted on a schematic posterior view of the atria demonstrating the most prominent site of low voltage areas (left panel) and amount of low voltage (right panel), depicted for patients without atrial fibrillation (AF, blue) and with paroxysmal AF (red) in the right atrium (RA), Bachmann's bundle (BB), pulmonary vein area (PVA) and left atrium (LA).

Discussion

In this study, we measured UVs at a high resolution scale in MVD patients with and without history of PAF and demonstrated extensive intraregional and inter-individual differences in voltage distribution in both patients without and with a history of AF. Even in SR, patients with PAF have lower UVs at BB and a higher number of low voltage potentials. In addition, areas with low voltage potentials were present in all patients, yet we did not find any predilection sites for low voltage potentials to occur.

Unipolar voltage mapping

Structural properties of atrial tissue can be estimated from the spatial distribution of EGM amplitudes, commonly known as voltage mapping. These EGMs are recorded in either the unipolar or bipolar configuration. In daily clinical practice, the bipolar EGM is more commonly used as it contains more local information from the area of myocardium between two electrodes. However, in bipolar recordings, several non-substrate related factors can theoretically influence the EGM voltage, like activation orientation, electrode spacing, electrode size, tissue contact and filtering, and may therefore provide less accurate information on the arrhythmogenicity of the underlying myocardial tissue.[5, 13, 14] U-EGMs, on the other hand, can be

regarded as the sum of instantaneous current dipoles of a wavefront, reflecting cardiac electrical activity of the tissue surrounding the recording electrode. As the amplitude depends on the volume of simultaneously activated cardiac tissue, synchronous activation of myocardium results in relative large amplitude U-EGMs, whereas areas of asynchronously activated myocardium cause a decrease in U-EGM amplitudes.[15] It is for these reasons that U-EGMs are more and more used in newly developed mapping systems.[6, 7]

Determination of low voltage areas

Low-UV EGMs are commonly associated with areas of fibrosis, which produce reduced electric fields and consequently lower potential differences.[16] The relationship between clinical outcomes, AF substrate factors, AF triggers and low voltage areas depend critically on the voltage threshold chosen to define low voltage. A value of 0.5 mV is commonly used to define low voltage in atrial bipolar EGMs which is not based on the presence of defined underlying abnormalities in atrial structure or function.[17] In our study, we used a value of 1.0 mV, which was based on the 5th percentile of all measured potential amplitudes in the MVD patients without AF. Other studies define abnormal voltage as the voltage at the 5th percentile of all mapping points within one patient, resulting in a wide range of threshold values and various thresholds for different atrial segments depending on the locations of the mapping points. In both groups, there was a large inter-individual variability in the 5th percentile. We only used data of the patients without AF to determine a 'threshold' for identification of low voltage areas, though structural remodeling is most likely also present in this population. The extent of remodeling is more pronounced in patients with AF, which is reflected by the lower 5th percentiles observed in the PAF group. However, the absolute voltage threshold for structural remodeling remains arbitrary, as we have no true healthy population undergoing cardiac surgery available.

Determinants of atrial voltage

UV is primarily determined by cardiac electrical activity of the tissue surrounding the recording electrode which decreases with distance. Areas of synchronous activation in the longitudinal axis of myocardial fibers result in fast wavefront propagation and large UV potentials.[15] In addition, thicker cardiac muscle bundles will result in larger UV potentials as compared to small bundles. In case of areas with non-uniform anisotropy, activation becomes asynchronous. This will result in smaller UV potentials as smaller volumes of cardiac tissue are simultaneously activated. In particular, low-voltage fractionated potentials with multiple additional deflections are regarded as part of the arrhythmogenic substrate underlying AF.[16] We demonstrated that UV decreases when the number of additional deflections increases. It is generally assumed that low amplitude, fractionated potentials reflect critical regions of slow conduction or conduction block.[18] Moreover, we demonstrated that UV is lower in

areas of slowed conduction or conduction block, which might indicate areas of fibrotic tissue. However, even in the areas of conduction block, not all recorded potentials were fractionated, low amplitude potentials and there was therefore no generally clear relation between UV and CV. In a previous study, we demonstrated that UV of single potentials are mainly determined by their relative R- and S-wave morphology, which could provide additional information on CV and wavefront propagation.[19] Consequently, low voltage potentials could also be explained by asymmetry of the relative R- and S-wave amplitudes. It is for these reasons that (low) UV alone does not automatically indicate 'diseased' atrial tissue and therefore an absolute voltage threshold for structural remodeling remains arbitrary.

Regional differences in epicardial voltage

Several studies have described differences in voltages between various atrial regions as well as regional differences between paroxysmal and persistent AF patients.[8, 9, 20] We did not find regional differences in median voltages in patients without AF. However, as demonstrated by our voltage fingerprints, there were considerable differences in voltage distributions throughout the atria in all patients.

Given that voltage is affected by atrial wall thickness and that wall thickness varies throughout the atria, it is likely that some of these differences are explained by variations in wall thickness. Nevertheless, other factors such as external pressing with the electrode array and atrial walls stress may also influence the recorded voltages.

Structural remodeling

MVD patients undergoing cardiac surgery, – even without a history of AF – usually have advanced structurally remodeled atria due to altered hemodynamics and therefore MVD is a well-known risk factor for developing AF.[21-23] Extensive areas of low voltage potentials are therefore also present in MVD patients without history of AF. In addition, AF itself also causes electrical remodeling, thereby increasing the arrhythmogenic substrate. While these changes may be a consequence of AF, it could also be a result of primary structural abnormalities caused by MVD. In addition, in patients with MVD it has been demonstrated that there are electrophysiological differences between and within both the LA and RA. Based on these observations, it was suggested that the structural changes responsible for initiating and maintaining AF could be diffusely located and different to patients with lone AF.[23]

A prior study in MVD patients with AF suggested that the posterior wall may be especially rich in fibrotic tissue compared to the LA appendage.[24] In addition, patients with MVD with enlarged LA dimensions – resulting in elevated atrial wall

stress – have an increased risk of developing AF.[25] Interestingly, in our population, there were no differences in voltages obtained from the LA and PVA between the no AF and PAF group. However, more fractionated potentials were found in these areas in patients with PAF. As fractionation represents asynchronous activation caused by e.g. fibrotic tissue, this could also be indicative of an increased deposition of fibrotic tissue in these areas.[16] This is supported by a study of Boldt et al. who found an increased expression of fibrosis in the left atrial tissue of patients with MVD.[26]

Multiple earlier mapping studies found clear correlations between the presence of low voltage areas and the development of AF.[2-4] In our study, low voltage areas were found in all patients, though lower UVs and more low voltage areas were found in the PAF group at BB. In addition, we could not find any predilection site for low voltage areas in both of our groups, though significant inter-individual differences were found in UV and low voltage areas. Besides, earlier studies found more conduction disorders at BB in patients with valvular heart disease, possibly relating to the increased amount of low voltage areas and lower epicardial voltage at this region.[27, 28] These observations further support the concept that structural remodeling associated with AF development is diffusely located in the atria in this patient population.

Clinical implications

MVD patients frequently undergo cardiac surgery and concomitant arrhythmia surgery is performed when AF is present. In these patients, next to PV isolation, epicardial mapping during surgery could provide additional information on the arrhythmogenic substrate as potential target sites for ablation. However, though the extend of remodeling is more pronounced in patients with AF, the absolute voltage threshold applied in this study for structurally remodeled atria does not permit to clearly separate patients for whom those areas may be suitable target sites for ablation. Therefore, low voltage areas during SR should carefully be used as target sites for (surgical) ablative therapy in this patient population.

In addition, large intra- and inter-individual variation in potential voltages found in our study population highlights the requirement of an individualized, patient tailored diagnosis and therapy of the arrhythmogenic substrate in patients with MVD and AF. It is likely, that due to increased nonuniform anisotropic properties of atrial myocardium in MVD patients, UVs alter when the direction of the activation wavefront, during e.g. atrial extrasystolic beats and tachyarrhythmias, changes. Therefore, the next step is to examine voltage maps during tachyarrhythmias such as AF and to compare them with SR voltage maps in order to decode electrical conduction properties and possible additional frequency- and direction dependent conduction disorders.

Study limitations

Most patients with AF in our study had PAF instead of (longstanding) persistent AF. Electrical and structural remodeling in these patients is considered to be less extensive, therefore more differences in SP morphology are expected with increasing AF persistence. In addition, as MVD patients undergoing cardiac surgery, -even without a history of AF- usually have advanced structurally remodeled atria, this population is not representative of all patients undergoing AF ablation.

The recorded UV might also be influenced by variable contact of the electrode array with the cardiac tissue, which could have introduced a bias in the data. However, this bias is considered to be minimal as confirmation of good contact of the electrode array with cardiac tissue was an important step in the mapping procedure. Besides, loss of contact could be easily recognized during post processing of the data. In addition, the presence of epicardial fat could have influenced our results as earlier studies showed that the presence of thick fat is associated with attenuated EGM voltages.[29] Though these observations are based on bipolar EGMs and we did not experience any large effects of visually present epicardial fat, we cannot ascertain that the presence of epicardial fat has influenced our results.

Whether general anesthesia and intraoperative drugs influence conduction is yet to be investigated; however, a standard anesthetic protocol was used for all patients and SR was confirmed during all mapping procedures. Possible effects of anesthesia would therefore be equally dispersed among the patient population. In addition, high-resolution mapping of the interatrial septum could not be performed with our closed beating heart approach.

Conclusions

Unipolar voltage mapping at high resolution scale in patients with MVD, demonstrated dissimilarities in voltage distribution between the various atrial regions and individual patients. Even in SR, potential voltages at BB were lower in MVD patients with PAF compared to those without AF. Though there were no predilection sites for low voltages to occur, low voltage areas were even present in MVD patients without a history of AF. In addition, an increased number of low voltage potentials was found at BB in MVD patients with PAF. Both considerable intra- and inter-individual variation in potential voltages were found in our study population, which underlines the importance of an individualized electrical signal profile which can be used to characterize complex conduction disorders and to develop patient tailored diagnoses and therapy.

References

1. Bazan V, Frankel DS, Santangeli P, Garcia FC, Tschabrunn CM and Marchlinski FE. Three-dimensional myocardial scar characterization from the endocardium: Usefulness of endocardial unipolar electroanatomic mapping. *J Cardiovasc Electrophysiol*. 2019;30:427-437.
2. Yagishita A, Gimbel JR, S DEO, Manyam H, Sparano D, Cakulev I, Mackall J and Arruda M. Long-Term Outcome of Left Atrial Voltage-Guided Substrate Ablation During Atrial Fibrillation: A Novel Adjunctive Ablation Strategy. *J Cardiovasc Electrophysiol*. 2017;28:147-155.
3. Rolf S, Kircher S, Arya A, Eitel C, Sommer P, Richter S, Gaspar T, Bollmann A, Altmann D, Piedra C, Hindricks G and Piorkowski C. Tailored atrial substrate modification based on low-voltage areas in catheter ablation of atrial fibrillation. *Circ Arrhythm Electrophysiol*. 2014;7:825-33.
4. Kottkamp H, Bender R and Berg J. Catheter ablation of atrial fibrillation: how to modify the substrate? *J Am Coll Cardiol*. 2015;65:196-206.
5. Sim I, Bishop M, O'Neill M and Williams SE. Left atrial voltage mapping: defining and targeting the atrial fibrillation substrate. *J Interv Card Electrophysiol*. 2019.
6. Venlet J, Piers SRD, Kapel GFL, de Riva M, Pauli PFG, van der Geest RJ and Zeppenfeld K. Unipolar Endocardial Voltage Mapping in the Right Ventricle: Optimal Cutoff Values Correcting for Computed Tomography-Derived Epicardial Fat Thickness and Their Clinical Value for Substrate Delineation. *Circ Arrhythm Electrophysiol*. 2017;10.
7. Chinyere IR, Hutchinson M, Moukabary T, Lancaster J, Goldman S and Juneman E. Monophasic action potential amplitude for substrate mapping. *Am J Physiol Heart Circ Physiol*. 2019;317:H667-H673.
8. Kogawa R, Okumura Y, Watanabe I, Nagashima K, Takahashi K, Iso K, Watanabe R, Arai M, Kurokawa S, Ohkubo K, Nakai T, Hirayama A, Sonoda K and Tosaka T. Left atrial remodeling: Regional differences between paroxysmal and persistent atrial fibrillation. *J Arrhythm*. 2017;33:483-487.
9. Marcus GM, Yang Y, Varosy PD, Ordovas K, Tseng ZH, Badhwar N, Lee BK, Lee RJ, Scheinman MM and Olgin JE. Regional left atrial voltage in patients with atrial fibrillation. *Heart Rhythm*. 2007;4:138-44.
10. van der Does L, Knops P, Teuwen CP, Serban C, Starreveld R, Lanters EAH, Mouws E, Kik C, Bogers A and de Groot NMS. Unipolar atrial electrogram morphology from an epicardial and endocardial perspective. *Heart Rhythm*. 2018;15:879-887.
11. Lanters EA, van Marion DM, Kik C, Steen H, Bogers AJ, Allessie MA, Brundel BJ and de Groot NM. HALT & REVERSE: Hsf1 activators lower cardiomyocyt damage; towards a novel approach to REVERSE atrial fibrillation. *J Transl Med*. 2015;13:347.
12. van der Does LJ, Yaksh A, Kik C, Knops P, Lanters EA, Teuwen CP, Oei FB, van de Woestijne PC, Bekkers JA, Bogers AJ, Allessie MA and de Groot NM. QUest for the Arrhythmogenic Substrate of Atrial fibRillation in Patients Undergoing Cardiac Surgery (QUASAR Study): Rationale and Design. *J Cardiovasc Transl Res*. 2016;9:194-201.
13. Blauer JJ, Swenson D, Higuchi K, Plank G, Ranjan R, Marrouche N and Macleod RS. Sensitivity and specificity of substrate mapping: an in silico framework for the evaluation of electroanatomical substrate mapping strategies. *J Cardiovasc Electrophysiol*. 2014;25:774-80.
14. Kovoor P, Daly M, Pouliopoulos J, Dewsnap MB, Eipper V and Ross DL. Effect of inter-electrode distance on bipolar intramural radiofrequency ablation. *Pacing Clin Electrophysiol*. 2005;28:514-20.
15. Spach MS, Miller WT, 3rd, Miller-Jones E, Warren RB and Barr RC. Extracellular potentials related to intracellular action potentials during impulse conduction

in anisotropic canine cardiac muscle. *Circ Res*. 1979;45:188-204.
16. Nademanee K, McKenzie J, Kosar E, Schwab M, Sunsaneewitayakul B, Vasavakul T, Khunnawat C and Ngarmukos T. A new approach for catheter ablation of atrial fibrillation: mapping of the electrophysiologic substrate. *J Am Coll Cardiol*. 2004;43:2044-53.
17. Josephson ME and Anter E. Substrate Mapping for Ventricular Tachycardia: Assumptions and Misconceptions. *JACC Clin Electrophysiol*. 2015;1:341-352.
18. Konings KT, Smeets JL, Penn OC, Wellens HJ and Allessie MA. Configuration of unipolar atrial electrograms during electrically induced atrial fibrillation in humans. *Circulation*. 1997;95:1231-41.
19. van Schie MS, Starreveld R, Roos-Serote MC, Taverne YJHJ, van Schaagen FRN, Bogers AJJC and de Groot NMS. Classification of sinus rhythm single potential morphology in patients with mitral valve disease. *EP Europace*. 2020.
20. Prabhu S, Voskoboinik A, McLellan AJA, Peck KY, Pathik B, Nalliah CJ, Wong GR, Azzopardi SM, Lee G, Mariani J, Ling LH, Taylor AJ, Kalman JM and Kistler PM. A comparison of the electrophysiologic and electroanatomic characteristics between the right and left atrium in persistent atrial fibrillation: Is the right atrium a window into the left? *J Cardiovasc Electrophysiol*. 2017;28:1109-1116.
21. Anne W, Willems R, Roskams T, Sergeant P, Herijgers P, Holemans P, Ector H and Heidbuchel H. Matrix metalloproteinases and atrial remodeling in patients with mitral valve disease and atrial fibrillation. *Cardiovasc Res*. 2005;67:655-66.
22. Castonguay MC, Wang Y, Gerhart JL, Miller DV, Stulak JM, Edwards WD and Maleszewski JJ. Surgical pathology of atrial appendages removed during the cox-maze procedure: a review of 86 cases (2004 to 2005) with implications for prognosis. *Am J Surg Pathol*. 2013;37:890-7.
23. John B, Stiles MK, Kuklik P, Chandy ST, Young GD, Mackenzie L, Szumowski L, Joseph G, Jose J, Worthley SG, Kalman JM and Sanders P. Electrical remodelling of the left and right atria due to rheumatic mitral stenosis. *Eur Heart J*. 2008;29:2234-43.
24. Corradi D, Callegari S, Benussi S, Maestri R, Pastori P, Nascimbene S, Bosio S, Dorigo E, Grassani C, Rusconi R, Vettori MV, Alinovi R, Astorri E, Pappone C and Alfieri O. Myocyte changes and their left atrial distribution in patients with chronic atrial fibrillation related to mitral valve disease. *Hum Pathol*. 2005;36:1080-9.
25. Kim HJ, Cho GY, Kim YJ, Kim HK, Lee SP, Kim HL, Park JJ, Yoon YE, Zo JH and Sohn DW. Development of atrial fibrillation in patients with rheumatic mitral valve disease in sinus rhythm. *Int J Cardiovasc Imaging*. 2015;31:735-42.
26. Boldt A, Wetzel U, Lauschke J, Weigl J, Gummert J, Hindricks G, Kottkamp H and Dhein S. Fibrosis in left atrial tissue of patients with atrial fibrillation with and without underlying mitral valve disease. *Heart*. 2004;90:400-5.
27. van der Does L, Lanters EAH, Teuwen CP, Mouws E, Yaksh A, Knops P, Kik C, Bogers A and de Groot NMS. The Effects of Valvular Heart Disease on Atrial Conduction During Sinus Rhythm. *J Cardiovasc Transl Res*. 2020;13:632-639.
28. Mouws E, Lanters EAH, Teuwen CP, van der Does L, Kik C, Knops P, Yaksh A, Bekkers JA, Bogers A and de Groot NMS. Impact of Ischemic and Valvular Heart Disease on Atrial Excitation:A High-Resolution Epicardial Mapping Study. *J Am Heart Assoc*. 2018;7.
29. Saba MM, Akella J, Gammie J, Poston R, Johnson A, Hood RE, Dickfeld TM and Shorofsky SR. The influence of fat thickness on the human epicardial bipolar electrogram characteristics: measurements on patients undergoing open-heart surgery. *Europace*. 2009;11:949-53.

8

Unipolar atrial electrogram morphology from an epicardial and endocardial perspective

Lisette J.M.E. van der Does
Paul Knops
Christophe P. Teuwen
Corina Serban
Roeliene Starreveld
Eva A.H. Lanters
Elisabeth M.J.P. Mouws
Charles Kik
Ad J.J.C. Bogers
Natasja M.S. de Groot

Heart Rhythm. 2018 Jun;15(6):879-887

Abstract

Background
Endo-epicardial asynchrony (EEA) and the interplay between these layers could be important in the pathophysiology of atrial arrhythmias. The morphological differences between epicardial and endocardial atrial electrograms have not been described so far and electrogram morphology may hold information about the presence of EEA.

Objective
This study directly compared epicardial to endocardial unipolar electrogram morphology during sinus rhythm (SR) and evaluated whether EEA contributes to electrogram fractionation by correlating fractionation to spatial activation patterns.

Methods
In 26 patients undergoing cardiac surgery, unipolar electrograms were simultaneously recorded from the epicardium and endocardium at the inferior, middle and superior right atrial (RA) free wall during SR. Potentials were analyzed for epi-endocardial differences in local activation time, voltage, RS-ratio and fractionation. The surrounding and opposite electrograms of fractionated deflections were evaluated for corresponding local activation times in order to determine if fractionation originated from EEA.

Results
The superior-RA was predisposed for delayed activation, EEA and fractionation. Both epicardial and endocardial electrograms demonstrated an S-predominance. Fractionation was for the majority similar between both sides, however, incidentally deflections up to 4mV on one side could be absent on the other side. Remote activation was responsible for most fractionated deflections (95%) in SR of which 4% could be attributed to EEA.

Conclusions
Local epi-endocardial differences in electrogram fractionation occur occasionally during SR, but will likely increase during arrhythmias due to increasing EEA and (functional) conduction disorders. Electrogram fractionation can originate from EEA and we demonstrated that unipolar electrogram fractionation can potentially identify EEA.

Introduction

Differences in electrophysiological properties of the ventricular epicardial and endocardial wall have been long recognized and linked to arrhythmogenesis.[1] Although wavefronts travelling out of sync at the epi- and endocardium of the thin atrial wall were already demonstrated more than two decades ago[2], unravelling of the link between endo-epicardial asynchrony (EEA) and atrial arrhythmias has only started recently[3]. Asynchrony in epi- versus endocardial propagating waves and the complex fiber arrangement of the atria may also give rise to epi-endocardial differences in the morphology of electrograms. Houben et al. have proposed that the ratio between the R-peak and S-peak of unipolar atrial electrograms may differ between the epicardium and endocardium and could identify the leading layer.[4] Other features of electrogram morphology such as amplitude and fractionation have been used to identify areas with scar tissue and arrhythmogenic areas.[5] Electrogram fractionation occurs when there is inhomogeneity in conduction within or remotely from the recording site and can have structural or functional causes.[6] The intricate structure of the atria might be a substrate for epi-endocardial differences in fractionation and occurrence of EEA. Asynchronous activation within the wall could in turn be responsible for additional deflections in electrograms.

In a clinical setting, epi- and endocardial mapping is never performed simultaneously and therefore, the differences and relationships between epi- and endocardial atrial electrogram morphology are so far unknown. This study is the first to directly compare unipolar epicardial electrograms to endocardial electrograms that have been recorded simultaneously at the right atrial wall during sinus rhythm (SR) in order to evaluate 1) if (local) morphologic features differ between epi- and endocardial electrograms and 2) if a fractionated electrogram morphology can arise from local EEA in activation. To this end, we developed a method to classify fractionation to its electrophysiological origin by correlating fractionated potentials to spatial patterns of activation.

Methods

Study population

Twenty-six adult patients undergoing first-time cardiac surgery with use of cardiopulmonary bypass were included (21 male; 67±10 years). Nineteen(73%) patients were operated for coronary artery disease, 12(46%) for (concomitant) valvular heart disease, 11(42%) patients had a history of atrial fibrillation (AF) and 6(23%) had impaired left ventricular function. Clinical characteristics are further described in *Supplemental table 1*. The study protocol was approved by the local ethics committee (MEC2015-373) and all patients gave informed consent for inclusion prior to surgery.

Intraoperative epi-endocardial mapping

Two multi-electrode arrays, each containing 128 electrodes with 2 mm inter electrode spacing, were fixed on spatulas and positioned directly opposite to each other (*Figure 1*, left panel). After arterial cannulation for cardiopulmonary bypass, an incision was made in the right atrial appendage for venous cannulation. Before venous cannulation, one spatula was introduced in the right atrium through the incision and the opening around the spatula was closed with a purse string suture.[7] Atrial epi- and endocardial unipolar electrograms were simultaneously recorded for 5-10 seconds during SR at three different locations of the RA free wall: 1) inferior-RA, 2) mid-RA, 3) superior-RA. Unipolar electrograms were sampled at 1kHz and stored on hard disk after amplification, filtering (0.5-500Hz) and analogue-to-digital conversion. Detailed methods are provided in the *Supplemental material*.

Data analysis

Electrogram morphology was analyzed semi-automatically in MATLAB R2016a (The MathWorks Inc., Natick, MA, USA). Electrograms with injury potentials were excluded from analysis and recording sites with ≥25% excluded or missing electrograms were excluded in total (*Supplemental figure 1*). SR potentials were analyzed for fractionation (number of deflections), peak-to-peak amplitude (voltage) and RS-ratios; atrial extrasystoles were excluded. The potentials in each electrogram were averaged for voltage and RS-ratio comparison. The steepest negative deflection of a potential was marked as local activation time (AT) if the slope was ≥0.05mV/ms and the deflection had a signal-to-noise ratio >2. Additional deflections with a slope ≥10% of the local AT (and ≥0.05mV/ms), a peak-to-noise ratio >2 and, either an amplitude of >1/6 of the amplitude of the local activation deflection, or a signal-to-noise ratio >5 were marked as fractionation (*Supplemental figure 2*). Only non-fractionated potentials (single deflections) were analyzed for the ratio between the R-peak and S-peak (RS-ratio).4 All signal markings were manually checked and corrected in case of markings on electrical artifacts evaluated by a consensus of two investigators. *Figure 1* demonstrates the analysis of signal amplitudes and RS-ratios. Delayed activation is defined as interelectrode differences in AT >11ms (<17cm/s) of electrodes in the same plane. The amount of delayed activation is expressed in mm: the number of interelectrode differences >11ms × the interelectrode distance (2mm).

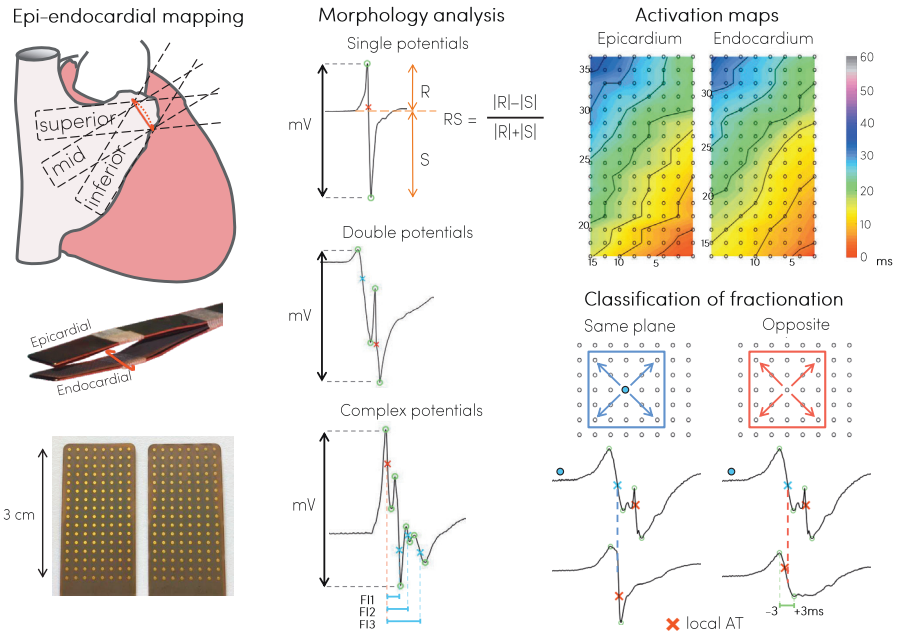

Figure 1 – Epi-endocardial mapping and signal analyses. *Left*: two spatulas with 128-electrode arrays are fixed together and one spatula is introduced in the right atrium through the incision for venous cannulation. Unipolar electrogram recordings are made on 3 locations: towards the inferior vena cava (inferior-RA), the superior vena cava (superior-RA) and in between, towards the terminal crest (mid-RA). *Middle*: the steepest deflection is marked as local activation time (AT, red cross) and additional deflections (blue crosses) are marked as fractionated deflections if the criteria for fractionation are met (see text). Signal morphology is analyzed for number of deflections, the RS-ratio (only single potentials) and peak-to-peak amplitude (potentials with multiple deflections: amplitude between the maximal and minimal peak). Fractionation interval (FI) is the time between the fractionated deflection and local AT within the potential. *Right*: an example of epi-endocardial activation time maps with isochrones is shown on the top. For classification, two rings of electrograms around a fractionated deflection (blue dot) in the same and opposite plane are searched for coinciding (peak-to-peak time distance ±3ms error margin) deflections of local ATs.

Analysis of local epi-endocardial differences

Local differences in AT, RS-ratio and fractionation between the epi- and endocardium were determined by comparing each electrogram with the electrograms in the opposite square; the exact opposite electrogram and its 8 surrounding electrograms. The local difference was the minimal difference of the potentials in the opposite square, as previously described.3 Border electrodes were excluded from analysis of local differences. For local differences in RS-ratio only recordings with <25% fractionated potentials were included. Fractionated potentials with ≥15ms between the first and last deflection were analyzed for detection of all (separate) deflections on both sides at the same time (epi-endocardial comparison

of coinciding deflections). Each deflection was tested whether its steepest point fell within peak-to-peak time limits (±3ms error margin) of deflections at the opposite square. The deflections that were not detected on the other side, as no coinciding deflection meeting the annotation criteria was present, were also manually examined for visual absence.

Classification of fractionation

Each fractionated deflection was evaluated if it could be attributed to remote activation: to delayed (discontinuous) activation in the surrounding tissue in the same layer or to EEA. The adjacent and opposite, first and second electrode-ring around the fractionated potential were searched for deflections of local ATs coinciding with the fractionated deflection. If the fractionated deflection fell within peak-to-peak time limits (±3ms) of the deflections of local ATs, it was classified based on the plane(s) where the corresponding local AT(s) was located in (*Figure 1*, right panel).

Corresponding ATs were either present in: 1) same plane, 2) opposite plane, 3) both planes or 4) none (absence of corresponding local AT). Border electrodes were excluded from analysis. Fractionation interval for fractionated deflections was defined as the time interval between the fractionated deflection and the deflection of the local AT (*Figure 1*, middle panel).

Statistical analysis

Normally distributed data are presented as the mean±SD and skewed data are presented as the median (p10-p90). Electrophysiological parameters were in square root or log transformed in case of a non-normal distribution. Linear mixed models were used to investigate the associations between location (independent variable) and electrophysiological parameters (dependent variable). Random intercepts were used for location. When normal distributions could not be obtained using transformations, the Friedman test was used to investigate the associations. Comparison of epi- and endocardial amounts of delayed activation was done with the Wilcoxon signed rank test. Spearman rho coefficient was used to determine the correlation between cycle length and amount of delayed activation. The associations of location and side with morphological parameters of electrograms were evaluated using Generalized Estimated Equations. The skewed distribution of RS-ratios could not be transformed to a normal distribution and RS-ratios were therefore converted to a binomial distribution by setting the lowest-quartile (<-0.51) of RS values as "highly" S-dominant. Correlation structure was chosen based on the Goodness of Fit in the Quasi Likelihood function and the inferior-RA served as the reference in the models evaluating locations. Statistical analyses were performed with IBM SPSS Statistics version 21 (IBM corp.,Armonk, NY).

Results

Electrophysiological data and parameters

Recordings at the inferior, mid and superior-RA were included of respectively, 26, 25 and 21 patients. SR cycle lengths did not change between the RA locations; inferior: 902±202, mid: 908±193 (p=0.72) and superior: 827±162 (p=0.17). The amount of delayed activation increased from the inferior to the superior-RA: 12(0-80), 32(0-99)(p=0.095), 74(18-178)mm (p<0.001). At the superior-RA, the endocardium demonstrated more delayed activation than the epicardium; 26(0-61) vs. 44(7-124) mm (p=0.010). No correlation was present between SR cycle length and amount of delayed activation (r=0.05, p=0.81). A total of 102,129 potentials were analyzed in 16,954 electrograms, including 50,714 potentials of 8,423 electrograms recorded at the epicardium and 51,415 potentials of 8,531 electrograms recorded at the endocardium. An overview of the individual patient results has been provided in *Supplemental table 2*.

Unipolar voltages

From the inferior to the middle and superior-RA electrogram voltage decreased gradually from 8.0(3.1-16.3), to 6.4(2.4-13.3)(p=0.001) and to 4.9(1.7-11.7)mV (p<0.001). Opposite epi- and endocardial electrogram amplitudes demonstrated a positive linear relationship (*Figure 2*, lower left panel). As it was expected that voltage is dependent on fractionation, potentials were categorized into singles, doubles and complex fractionated (>2 deflections) potentials. Figure 2 demonstrates that unipolar voltage indeed decreased with more fractionated potentials at both the epi- and endocardium. The largest epi-endocardial difference in amplitude was observed for unipolar potentials with single deflections which had an epi- versus endocardial amplitude of respectively 8.3(3.8-14.7) vs. 6.7(2.8-16.1)mV (p=0.08). Double potentials had epi-endocardial amplitudes of 4.1(1.6-8.3) vs. 3.8(1.3-8.5)mV (p=0.45) and complex fractionated potentials had amplitudes of 2.5(1.1-4.7) vs. 2.7(1.2-5.1)mV (p=0.08). The percentile-ranges of endocardial potentials were wider than of epicardial potentials.

RS-ratio of epi-endocardial single deflections

The RS-ratios of potentials with single deflections recorded at the epi- and endocardium are demonstrated in *Figure 3* for each RA-location. Both sides demonstrated a clear S-predominance, which increased at the mid-RA (p=0.001) and superior-RA (p<0.001). Epi- vs endocardial median RS-ratios at the inferior-RA were -0.23(-0.53- +0.26) vs. -0.25(-0.53-+0.26), at the mid-RA, -0.32(-0.78-+0.06) vs. -0.34(-0.72-+0.07) and at the superior-RA, -0.43(-0.96-+0.09) vs. -0.46(-0.97-+0.11). Many potentials at the superior-RA, the area of the sinus node, had an S-morphology (RS-ratio of -1) at both sides (11 vs 13%). Local differences in RS-ratios were between 0-0.22 for 95% of the data, without either side having more S-predominance than the other side (*Figure 3*).

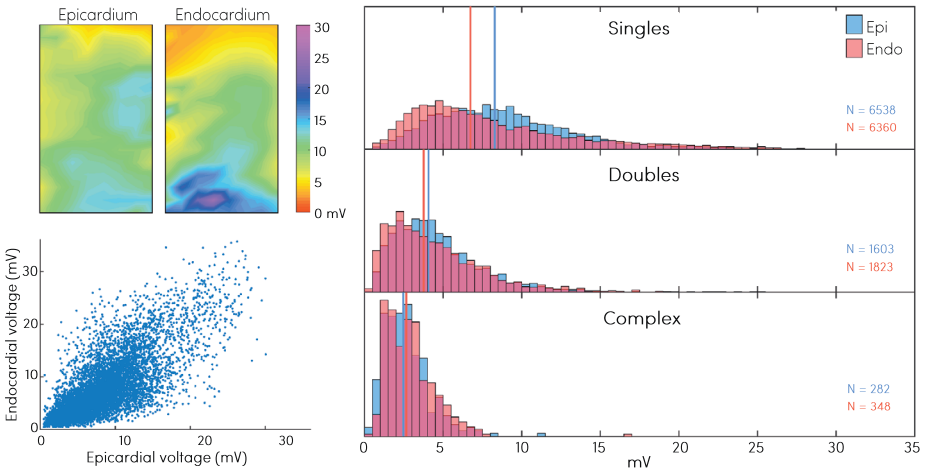

Figure 2 – Epi-endocardial unipolar voltage. *Top left*: example of epi- and endocardial voltage maps. *Bottom left*: scatter plot of epi-endocardial unipolar voltages. *Right*: relative frequency histograms of unipolar epicardial and endocardial electrogram voltage for singles, doubles and complex fractionated potentials. Vertical lines indicate the median.

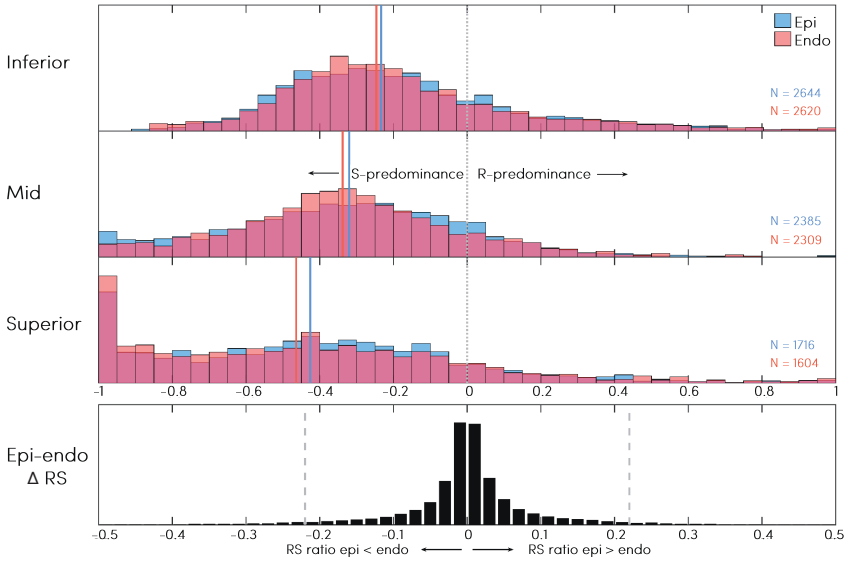

Figure 3 – Relative frequency histograms of epicardial and endocardial RS-ratios and local epi-endocardial RS differences. *Top three panels*: RS-ratios per location, negative values represent increasing S-predominance, positive values represent increasing R-predominance. Medians are indicated by vertical colored lines. *Bottom panel*: local differences in RS-ratio between epi- and endocardium. Negative values represent smaller RS-ratio values at the epicardium, positive values represent smaller RS-ratio values at the endocardium. Between the dashed grey lines 95% of the data is represented.

Epi-endocardial differences in fractionation

Relative incidence of singles, doubles, triples and potentials with more than 3 deflections was respectively, 76, 20, 3 and <1%. Incidence of fractionated potentials (>1 deflection) demonstrated an increasing trend from the inferior-RA (16%) towards the mid-RA (22%, p=0.136) and was highest at the superior-RA (36%, p<0.001). Epi- versus endocardial incidence of fractionation was at the inferior-RA 15 vs. 17%(p=0.29), at the mid-RA 21 vs. 22%(p=0.45), and the superior-RA demonstrated a trend towards more fractionated potentials at the endocardium: 33 vs. 38%(p=0.09). Local epi-endocardial differences in the number of detected deflections occurred in 6.6% (*Table 1*).

Table 1 – Epicardial vs. endocardial fractionation

	Total fractionation (%)								**Local differences in fractionation**			
	Singles		**Doubles**		**Triples**		**Complex (>3)**		**Δ Epi-endo no. of deflections (%)**			
	Epi	Endo	Epi	Endo	Epi	Endo	Epi	Endo	0	1	2	≥3
Inferior	84.7	82.9	12.8	14.5	2.3	2.4	0.2	0.2	95.7	4.1	0.2	<0.1
Mid	79.4	77.7	17.5	19.2	2.6	2.8	0.4	0.3	93.2	6.5	0.2	<0.1
Superior	67.3	62.0	27.1	30.6	4.4	6.4	1.2	1.1	90.8	8.7	0.5	<0.1
Total	77.8	75.0	18.6	20.8	3.0	3.7	0.6	0.5	93.4	6.3	0.3	<0.1

A total of 1580 electrograms contained potentials with fractionated deflections with a fractionation interval ≥15ms. In 271 of those 1580 cases, deflections remained undetected on the other side, based on the annotation criteria, and 53 of those 271 deflections were also visually completely absent. In 41 of 271 cases, the same number of deflections were present on both sides but with epi-endocardial time-differences between the corresponding deflections of 4-85ms (median 13ms). In the remaining 177 of 271 cases, a (small) deflection was visually observed, not meeting the criteria for a deflection. Examples of epi-endocardial differences in fractionation are provided in *Figure 4* and demonstrate that deflections up to a maximum of 4mV on one side could be absent on that location on the other side.

EEA during SR

Right atrial EEA >14ms, as previously defined for AF[3], occurred at the inferior-RA in 12% of the patients, the mid-RA in 19% and the superior-RA in 57%. EEA increased from the inferior to the superior-RA (p=0.001). One patient had by far the most EEA of the study group (44.4% at the mid-RA) with an endocardial delay of >50ms. EEA during SR is mainly determined by one side being delayed. The degree and incidence of EEA is demonstrated in *Supplemental figure 3*.

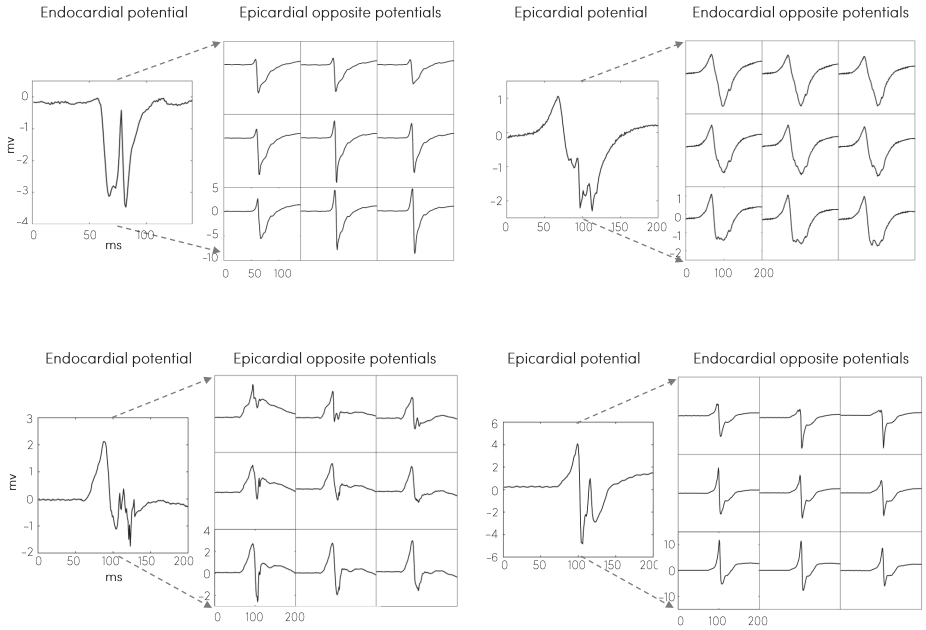

Figure 4 – Examples of local differences in fractionation between epi- and endocardium. Four fractionated potentials are shown recorded at the epicardium or endocardium with the nine electrograms on the direct opposite side (direct opposite and its 8 surrounding electrograms). In the lower right example the second deflection of 4mV at the epicardium is totally absent at the endocardium.

Fractionation attributable to delayed activation or EEA

For the far majority (95%) of fractionated deflections a corresponding local AT was present in the surrounding tissue of the same or opposite layer (*Table 2*). In 4% a local AT was only observed in the opposite plane which corresponds to sites with EEA (*Figure 5A*). In 9% a corresponding local AT was only observed in the same plane, which corresponded to a site with delayed activation that was asymmetrical between the epicardium and endocardium (local delayed activation in one plane) (blue outlined potential, *Figure 5B*). In 83% of fractionated deflections a matching local AT was present in both planes. This group contains 3 underlying causes: 1) symmetrical epi-endocardial delayed activation (*Figure 5C*), 2) asymmetrical epi-endocardial delayed activation; after the site with a delay in activation (*Figure 5B*), 3) short fractionation intervals (Figure 5C). Most can be attributed to short fractionation intervals as the median fractionated interval for these deflections was only 12ms (*Table 2*). For the remaining 5% of fractionated deflections no matching local AT was found. Some of those had corresponding local ATs distanced >4mm of the fractionated site (*Figure 5B*) and more than half (61%) were deflections on electrodes that did not have a complete second ring to search for corresponding

ATs (relative border electrodes). *Figure 5D* illustrates an example of a fractionated deflection likely reflecting intramural inhomogeneity in conduction; it only appears in center electrodes without any corresponding local AT. Potentials with more than 3 deflections most often had deflections without any corresponding local AT compared to doubles and singles (17% vs. 3% and 5%).

Table 2 – Classification of fractionated deflections corresponding with local activation times

	Doubles			**Triples**			**Complex (>3)**			**Total**
	N	**%**	**FI (ms)**	**N**	**%**	**FI (ms)**	**N**	**%**	**FI (ms)**	**N (%)**
Same plane	144	7	28 (14-58)	73	11	22 (10-27)	24	15	13 (11-47)	241 (9)
Opposite plane	69	3	27 (11-60)	26	4	26 (16-37)	8	5	38 (22-38)	103 (4)
Both planes	1682	85	12 (8-24)	553	82	12 (8-23)	99	63	14 (9-39)	2334 (83)
None	91	5	32 (17-60)	22	3	30 (18-56)	27	17	35 (21-35)	140 (5)

FI, fractionation interval

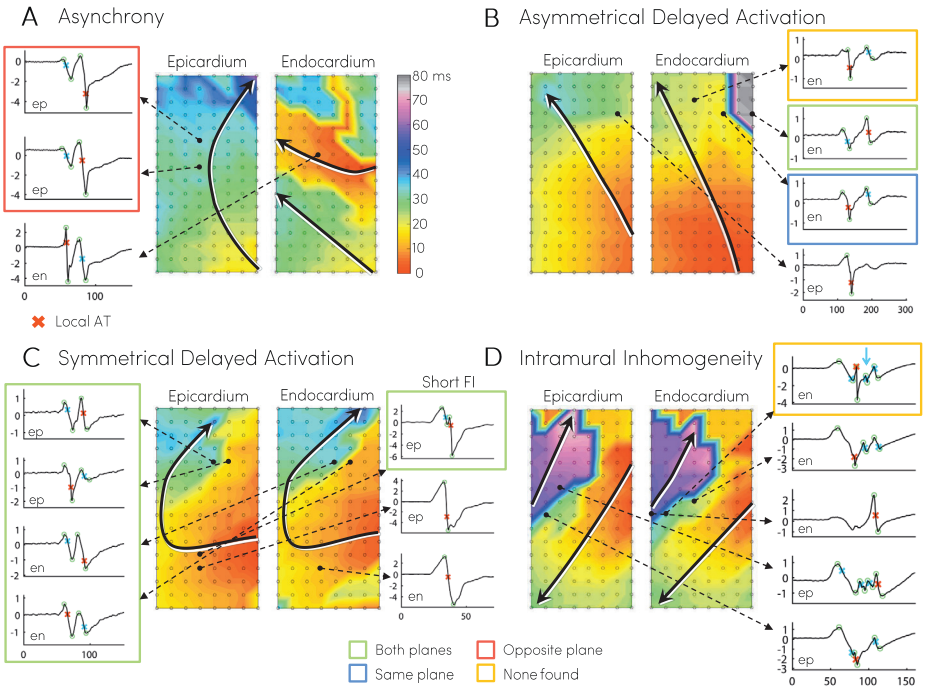

Figure 5 – Fractionated potentials attributable to various patterns of conduction disorders. Panels A-D demonstrate examples where fractionated potentials correspond to remote myocardial activation in the same plane (outlined in blue), in the opposite plane (outlined in red) or in both planes (outlined in green) or do not correspond with any remote activation (outlined in orange). *A*: epi-endocardial asynchrony causes fractionated deflections (blue marked deflections) at the epicardium, matching local activation times (AT, red marked deflections) are only present in the opposite plane. *B*: at sites with asymmetrical delayed activation (DA), fractionated deflections in front of an area of DA correspond to local ATs in the same plane, however at the delayed site, fractionated deflections correspond to ATs in both planes. In some cases, even sites >4mm of the DA site show corresponding fractionated potentials. *C*: fractionated deflections at sites with symmetrical DA at both sides, local ATs are present in both planes. Deflections with short fractionation intervals (FI) similar to normal conduction velocity will also mostly have matching local ATs at both sides. *D*: the third deflection of the upper complex fractionated potential does not correspond to any local AT in the same or opposite plane, demonstrating intramural inhomogeneity in conduction.

Discussion

Electrogram morphology is often used for the identification of structural or electrical remodeled areas with arrhythmogenic properties. Electroanatomical mapping is in most settings performed via endovascular catheters at the endocardial side. In recent perspective, it has become clear that asynchrony within the atrial wall can have an important role in the mechanism of atrial arrhythmias.[3, 8] Our study has shown that EEA over 50ms can already be present during SR and that unipolar electrogram fractionation can represent the presence of EEA. However, electrical activity within or on the opposite side of the atrial wall can also occasionally be missed when only recording electrograms from one side of the wall. At the superior-RA the highest amount of delayed activation and EEA was observed and resulted, due to their interdependence, in the highest amount of fractionated electrograms and lowest voltages.

Right atrial anatomy

Variations between epi- and endocardial unipolar voltage can be explained from the anatomical structure of the RA wall. The surface of the endocardial right atrial appendage, unlike the smooth epicardial side, is very irregular due to the pectinate muscles of varying diameters and the thick terminal crest. The mass of cardiac bundles is positively correlated to unipolar electrogram voltage and anatomical studies have shown that pectinate muscles can vary from <1-7mm.[9, 10] The different sizes and arrangement of the bundles also cause a variation in the level of contact with the electrodes on the flat array. Our high-resolution epicardial mapping study demonstrated recently that epicardial breakthrough waves during SR were most frequently observed at the superior-RA.[11] EEA indeed occurred most often in this area which also correlated to the highest amount of delayed activation and fractionation. The superior-RA contains the sinus node within its fibrous case and the thickest part of the anisotropic terminal crest which may underlie the proneness of this area to delays in activation, EEA and breakthrough waves.[9, 12] The structural variability of the RA therefore influences epi-endocardial synchronicity and electrogram morphology. Electrical activity that remains undetected on one side may relate to thicker or more irregular parts of the RA.

The value of unipolar electrograms

Unipolar electrograms have the benefit over bipolar electrograms that their morphology carries additional information about the progression of the wavefront and remote activations; the ratio between the positive and negative component of a unipolar electrogram characterizes the start or end of a wavefront and possibly the curvature of the wavefront and conduction velocity.[13] Epicardial electrograms recorded during AF demonstrated an S-predominance which could not be strongly correlated to wavefront curvature or anisotropy.[4] A tilted transmural stance of the

wavefront resulting in an epicardial lead with constant epicardial to endocardial activation was proposed as theoretical explanation for S-predominance during AF which would present with more R-predominance at the endocardium. In this study both epicardial and endocardial electrograms showed an S-predominance and endocardial electrograms did not have higher RS-ratios than epicardial electrograms. S-predominance during SR can therefore not be explained by epicardial to endocardial activation or vice versa. Previous studies demonstrated that endocardial unipolar electrogram voltage is more useful for detecting areas of scar at the epicardium than bipolar electrogram voltage due to their range of view.[14] We established that the view of unipolar electrograms can signify presence of EEA and can reveal areas with intramural inhomogeneous conduction. Detecting EEA from the endocardium alone requires the atrial "farfield" potentials on unipolar electrograms that will be filtered out with standardly used bipolar recordings. Furthermore, the limitations of registering all atrial activity from throughout the atrial wall demonstrated by our high-density contact mapping approach, will only increase with non-contact mapping systems. Current mapping approaches may therefore be insufficient to detect transmural atrial activity.

Epi-endocardial electrograms during atrial arrhythmias

The incidence of local differences in epi- and endocardial electrogram morphology and of electrogram fractionation due to EEA is relatively low during SR. In the observations of Schuessler et al. epi-endocardial differences in activation were least prominent during SR and high-rate pacing, but significantly increased with premature stimulation.[2] In a goat model of AF the amount of EEA increased with AF persistence which was also associated with more inhomogeneous conduction patterns and a shortening of fibrillation cycle length.[15] Our previous study in humans also demonstrated more EEA at the right atrial wall during AF with incidences between 0.9-55.9%.3 EEA occurs more frequently in atrial arrhythmias due to the increase of inhomogeneous conduction and (functional) conduction disorders. Fractionation due to EEA and local differences in epi-endocardial electrogram fractionation are therefore expected to increase during atrial arrhythmias. Especially the right atrial appendage, which has the thickest wall of the whole atria, is susceptible to local differences in electrogram morphology and EEA. Nevertheless, also at the left atrium breakthrough waves occur frequently indicating presence of EEA and with wavefronts decreasing in size during AF, electrogram amplitude will decrease causing local differences in fractionation more likely to occur in any area.[11, 16] When fractionated electrograms are only ablated from the endocardial side, epicardial fractionated sites could be overlooked, but more importantly, these fractionated sites have different pathophysiological origins including EEA and ablating all fractionated electrograms would only increase needless atrial scarring.

Study limitations

Intraoperative simultaneous epi-endocardial mapping in living humans can only be safely performed at the right atrium, therefore we could not evaluate the relation of epi- and endocardial electrograms at the structurally less complicated left atrium. However, epicardial breakthroughs also often present at the left atrium, indicating the occurrence of EEA at the left atrium during SR as well.[11] The finite area of the mapping array and relatively low incidence of (complex) fractionation during SR limited the classification of fractionated deflections to those situated in the center of the array. The relatively small number of fractionated deflections classified to no corresponding local AT is probably still an overestimation.

Conclusions

In SR, EEA of the right atrial free wall occurs to over 50ms difference between epicardium and endocardium, which has never been described before. Electrograms on both sides demonstrate an S-predominance and the RS-ratio cannot be used to identify the leading layer during SR. Fractionated potentials are not always identical on a high resolution scale and can have local mismatches, however, these mismatches occur in a minority of cases. If a potential is fractionated during SR, most additional deflections can be explained by conduction disorders in the same plane and in a small percentage they represent EEA. The incidence of EEA and EEA based fractionation is relatively low during SR as was expected. However, during atrial arrhythmias the presence of (functional) conduction disorders and EEA will increase and therefore epi-endocardial differences in electrogram morphology and EEA based fractionation will likely increase as well. Particularly interesting, especially for clinical practice, is the observation that the morphology of unipolar electrograms can potentially be a tool to identify areas of EEA when recording electrograms only on one side of the wall.

References

1. Lukas A and Antzelevitch C. Differences in the electrophysiological response of canine ventricular epicardium and endocardium to ischemia. Role of the transient outward current. *Circulation*. 1993;88:2903-15.
2. Schuessler RB, Kawamoto T, Hand DE, Mitsuno M, Bromberg BI, Cox JL and Boineau JP. Simultaneous epicardial and endocardial activation sequence mapping in the isolated canine right atrium. *Circulation*. 1993;88:250-63.
3. de Groot N, van der Does L, Yaksh A, Lanters E, Teuwen C, Knops P, van de Woestijne P, Bekkers J, Kik C, Bogers A and Allessie M. Direct Proof of Endo-Epicardial Asynchrony of the Atrial Wall During Atrial Fibrillation in Humans. *Circulation: Arrhythmia and Electrophysiology*. 2016;9(5).
4. Houben RP, de Groot NM, Smeets JL, Becker AE, Lindemans FW and Allessie MA. S-wave predominance of epicardial electrograms during atrial fibrillation in humans: indirect evidence for a role of the thin subepicardial layer. *Heart Rhythm*. 2004;1:639-47.
5. Nademanee K, McKenzie J, Kosar E, Schwab M, Sunsaneewitayakul B, Vasavakul T, Khunnawat C and Ngarmukos T. A new approach for catheter ablation of atrial fibrillation: mapping of the electrophysiologic substrate. *J Am Coll Cardiol*. 2004;43:2044-53.
6. van der Does LJ and de Groot NM. Inhomogeneity and complexity in defining fractionated electrograms. *Heart Rhythm*. 2017;14:616-624.
7. Knops P, Kik C, Bogers AJ and de Groot NM. Simultaneous endocardial and epicardial high-resolution mapping of the human right atrial wall. *J Thorac Cardiovasc Surg*. 2016;152:929-31.
8. Pathik B, Lee G, Sacher F, Haissaguerre M, Jais P, Massoullie G, Derval N, Sanders P, Kistler P and Kalman JM. Epicardial-endocardial breakthrough during stable atrial macroreentry: Evidence from ultra-high-resolution 3-dimensional mapping. *Heart Rhythm*. 2017;14:1200-1207.
9. Sanchez-Quintana D, Anderson RH, Cabrera JA, Climent V, Martin R, Farre J and Ho SY. The terminal crest: morphological features relevant to electrophysiology. *Heart*. 2002;88:406-11.
10. Spach MS and Dolber PC. Relating extracellular potentials and their derivatives to anisotropic propagation at a microscopic level in human cardiac muscle. Evidence for electrical uncoupling of side-to-side fiber connections with increasing age. *Circ Res*. 1986;58:356-71.
11. Mouws E, Lanters EAH, Teuwen CP, van der Does L, Kik C, Knops P, Bekkers JA, Bogers A and de Groot NMS. Epicardial Breakthrough Waves During Sinus Rhythm: Depiction of the Arrhythmogenic Substrate? *Circ Arrhythm Electrophysiol*. 2017;10:e005145.
12. Fedorov VV, Glukhov AV, Chang R, Kostecki G, Aferol H, Hucker WJ, Wuskell JP, Loew LM, Schuessler RB, Moazami N and Efimov IR. Optical mapping of the isolated coronary-perfused human sinus node. *J Am Coll Cardiol*. 2010;56:1386-94.
13. Spach MS, Miller WT, 3rd, Miller-Jones E, Warren RB and Barr RC. Extracellular potentials related to intracellular action potentials during impulse conduction in anisotropic canine cardiac muscle. *Circ Res*. 1979;45:188-204.
14. Tokuda M, Tedrow UB, Inada K, Reichlin T, Michaud GF, John RM, Epstein LM and Stevenson WG. Direct comparison of adjacent endocardial and epicardial electrograms: implications for substrate mapping. *J Am Heart Assoc*. 2013;2:e000215.
15. Eckstein J, Zeemering S, Linz D, Maesen

B, Verheule S, van Hunnik A, Crijns H, Allessie MA and Schotten U. Transmural Conduction Is the Predominant Mechanism of Breakthrough During Atrial Fibrillation Evidence From Simultaneous Endo-Epicardial High-Density Activation Mapping. *Circ-Arrhythmia Elec*. 2013;6:334-341.

16. de Groot NM, Houben RP, Smeets JL, Boersma E, Schotten U, Schalij MJ, Crijns H and Allessie MA. Electropathological substrate of longstanding persistent atrial fibrillation in patients with structural heart disease: epicardial breakthrough. *Circulation*. 2010;122:1674-82.

Supplemental material

Mapping procedure

Mapping arrangement

Two 16-by-8 multi-electrode arrays (GS Swiss PCB AG, Küssnacht, Swiss) were sterilized by the local sterilization unit and fixed on sterilized steel spatulas by the operation staff with Steri-Strip™ adhesives. The spatulas are then bound together in the middle and end to secure an exact opposite position of the two arrays during the mapping. The spatula for the epicardial recording was marked for easy recognition by the surgeon. The connecter side of the array was wrapped in a sterile sack and both arrays are connected via 3m long shielded cables wrapped in the sterile sack. Correct connection was ensured by labeling the cables destined for the epicardial and endocardial side.

Operative and mapping procedure

All patients were anesthetized during cardiothoracic surgery with propofol and remifentanil or sufentanil and received continuous infusion of norepinephrine or phenylephrine. Standard monitoring during cardiac surgery included monitoring of arterial blood pressure, central venous pressure, electrocardiography and pulse-oximetry. The mapping procedure was performed right before the start of cardiopulmonary bypass if the hemodynamic status of the patient was stable. Arterial cannulation was performed first, followed by the preparation for mapping by stitching a bipolar pacing wire to the terminal crest as a reference signal and placing a steel wire in subcutaneous tissue as the indifferent electrode. Venous cannulation was initiated by an incision in the right atrial appendage, but before introducing the cannula, the endocardial spatula with the array was placed in the right atrium on the endocardial side and the epicardial spatula on the epicardial side. A purse-string suture closed the opening around the endocardially positioned spatula. Simultaneous epi-endocardial unipolar electrogram recordings were performed at three positions for 5-10 seconds during sinus rhythm. In case of patients with persistent atrial fibrillation, internal electrical cardioversion with 5-10J was performed for mapping of sinus rhythm. After the mapping procedure, the operation procedure continued with venous cannulation, cardiopulmonary bypass and cardioplegia for repair of structural heart disease.

Data analysis

Patient data inclusion

First activation was required to occur at the top or right atrial side of the mapping area of the superior or middle right atrial recording site, otherwise the rhythm was labelled as an ectopic atrial rhythm and the patient was not included for analysis.

Patients required two included recording sites (see below) in order to qualify for study inclusion.

Electrogram exclusion criteria

Electrograms with injury potentials (that can appear due to firm contact with local tissue) were excluded for RS-ratio analysis only or excluded for all analyses based on the following criteria:

RS ratio exclusion criteria:	elevation of the baseline after the local potential ≥1/3 and < total amplitude of local potential + concordant shift of potential
Total exclusion criteria:	elevation of the baseline after the local potential ≥1 mV and ≥ total amplitude of local potential

Examples are provided in *Supplemental figure 1*. Recording sites with 25% of missing or total excluded electrograms were excluded from further data analysis which included either a total number of missing/excluded electrograms ≥64 or a total of 32 electrodes from which the exact opposite electrode was missing/excluded. Excluded recording sites of patients are shown in *Supplemental table 2*.

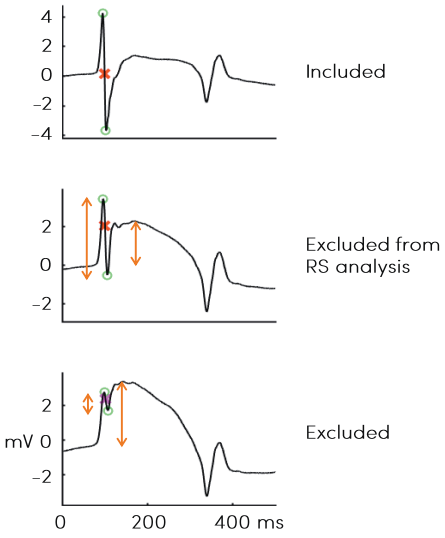

Supplemental figure 1 – Examples of potentials excluded from analysis. The baseline after the potential in the middle is elevated > 1/3 of the total potential amplitude with a concordant shift of the potential to a positive dominance, this potential is excluded from RS analysis. The bottom potential is excluded from all analyses as the elevation of the baseline after the potential is larger than the total potential amplitude.

Signal marking

Deflections and peaks were marked by the criteria stated in the manuscript using MATLAB R2016a (The MathWorks Inc., Natick, MA, USA). The signal-to-noise ratio was determined by the amplitude of the deflection in relation to the amplitude of the noise (*Supplemental figure 2*, top). The peak-prominence of a new peak was used to evaluate the peak-to-noise ratio which defined a new deflection (*Supplemental figure 2*, bottom). Noise levels were determined for each electrode separately. All signal markings were checked manually and markings of artifacts were corrected based on a consensus of two investigators.

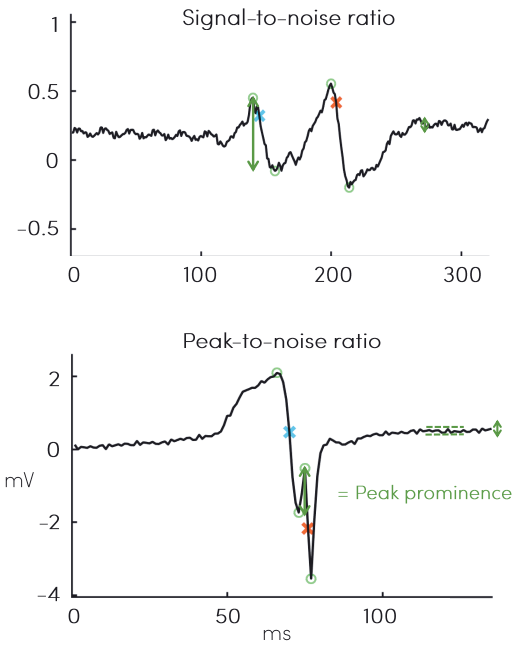

Supplemental figure 2 – signal-to noise and peak-to-noise ratio. *Top*: the ratio between the amplitude of the deflection and amplitude of the noise defined the signal-to-noise ratio. *Bottom*: the ratio between the peak prominence and the amplitude of the noise determined the detection of a new peak and the presence of a new deflection.

Analysis of local epi-endocardial differences

Local epi-endocardial differences are analyzed by comparing each potential to the exact opposite potential and its 8 surrounding potentials; 9 potentials in total (=opposite square) and determined by the minimal difference of these 9 comparisons. If the opposite square consisted of 6 or less potentials the electrode was considered a border electrode and was excluded from analysis of local differences.

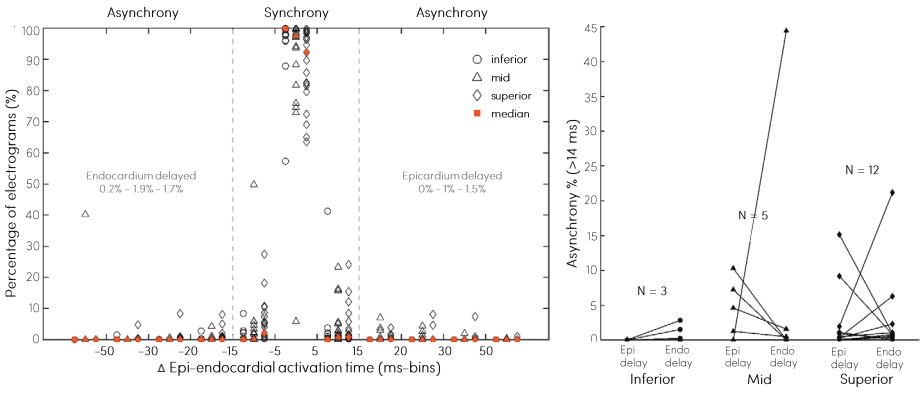

Supplemental figure 3 – Asynchrony in epi-endocardial activation. *Left*: relative frequency histogram demonstrating the distribution of epi-endocardial time-differences in activation per patient. The time-differences are divided into bins (0-5, 5-15ms, etc.) and shown as the percentage of epi-endocardial electrograms per location for each patient. The median patient values are depicted in red. For example, the most left triangle at 40% represent a patient with 40% of electrograms at the mid-RA having an endocardial delay >50ms. Incidence of epi-endocardial activation differences of only 0-5ms decreased from the inferior to superior-RA and, consequentially, incidence of intermediate (5-14ms) and large (>15ms) differences increased. The average percentages of >14ms asynchrony with endo- or epicardial delay are displayed next to the dashed lines for, respectively, the inferior, mid and superior right atrium. *Right*: percentage of asynchrony (>14ms) with epicardial vs. endocardial delay per location for all patients with asynchrony. Asynchrony percentages are connected for each patient.

Supplemental table 1 – Clinical characteristics

Patient no.	Age (yr)	Gender	Structural heart disease	History of AF	RCA S1 stenosis	Dilated RA	LV function	Hypertension	Diabetes mellitus	Dyslipidemia	AAD
1	80	Male	IHD; MVD	Paroxysmal	No	No	Normal	Yes	No	Yes	Class 3
2	71	Male	IHD	None	No	No	Normal	Yes	No	No	Class 2
3	67	Male	IHD	None	Yes	Unknown	Normal	Yes	Yes	No	Class 2
4	70	Male	IHD	None	Yes	Unknown	Normal	Yes	Yes	Yes	Class 2
5	54	Female	IHD	None	No	Unknown	Normal	Yes	Yes	No	-
6	49	Female	IHD; MVD	None	No	Unknown	Mild impairment	No	No	No	-
7	79	Male	IHD; MVD	Persistent	No	Yes	Mild impairment	No	No	No	Class 2, digoxin
8	61	Male	IHD; MVD; PFO	None	No	No	Normal	No	No	No	Class 2
9	73	Male	AVD	None	No	No	Normal	No	No	No	-
10	59	Male	AVD	None	No	Unknown	Normal	Yes	No	No	Class 2
11	68	Male	IHD	Paroxysmal	No	No	Mild impairment	No	No	No	Class 2
12	53	Male	IHD	Paroxysmal	No	Unknown	Normal	No	No	No	Class 2
13	72	Male	IHD	None	No	No	Normal	Yes	Yes	Yes	Class 3
14	64	Female	AVD; MVD	None	No	No	Normal	No	Yes	No	Class 2
15	67	Male	AVD	None	No	Unknown	Normal	Yes	Yes	Yes	-
16	47	Male	IHD	None	No	Unknown	Normal	No	Yes	No	Class 2
17	85	Male	IHD	Paroxysmal	No	Unknown	Normal	Yes	No	No	Class 2, digoxin
18	65	Male	IHD	None	No	Unknown	Normal	Yes	No	No	Class 2
19	53	Male	IHD	Persistent	Yes	Yes	Severe impairment	No	No	No	Class 2, digoxin
20	71	Male	-	Paroxysmal	No	Unknown	Normal	Yes	No	No	Class 2+3
21	71	Male	IHD; MVD	Paroxysmal	Yes	No	Moderate impairment	Yes	No	Yes	Class 1+2
22	64	Male	IHD; AVD	Paroxysmal	No	No	Normal	Yes	No	Yes	Class 2
23	76	Female	MVD	Longstanding Persistent	No	Yes	Normal	Yes	Yes	No	Class 2, digoxin
24	64	Female	MVD; TVD	Longstanding Persistent	No	Unknown	Mild impairment	No	No	No	Class 4, digoxin
25	67	Male	IHD	None	No	No	Normal	No	Yes	Yes	Class 2
26	82	Male	IHD	None	No	Unknown	Normal	Yes	Yes	No	Class 2
Total/ mean	*67±10*	*Male 21 (81%)*	*IHD 19 (73%) VHD 12 (46%)*	*11 (42%)*	*4 (15%)*	*3*	*Normal 20 (77%)*	*15 (58%)*	*10 (39%)*	*7 (27%)*	-

AAD = antiarrhythmic drug; AF, atrial fibrillation; AVD, aortic valve disease; IHD, ischemic heart disease; LV, left ventricular; MVD, mitral valve disease; PFO, persistent foramen ovale; RCA S1 = right coronary artery segment 1 (proximal); TVD, triscuspid valve disease; VHD, valvular heart disease

Supplemental table 2 – Individual results of electrophysiological parameters and epi-endocardial electrogram morphology

Patient no.	Location	SRCL (ms)	DA (mm)		Voltage (mV)		RS ratio		Fractionation (%)		EEA (%)	Epi delay (%)	Endo delay (%)
			Epi	Endo	Epi	Endo	Epi	Endo	Epi	Endo			
1	inferior	1047	32	20	9.9	12.5	-0.24	-0.19	17	25	0	0	0
	mid	1171	8	12	7.5	9.5	-0.22	-0.32	16	25	0	0	0
	superior	563	24	36	7.6	7.4	0.19	0.07	35	37	0	0	0
2	inferior	1024	8	12	10.7	12.1	-0.41	-0.43	10	11	0	0	0
	mid	1008	72	36	6.3	6.6	-0.60	-0.61	56	55	6.2	4.6	1.6
	superior	excluded											
3	inferior	998	58	46	5.9	6.6	-0.20	-0.30	49	44	0.2	0	0.2
	mid	excluded											
	superior	1002	50	58	3.3	3.1	0.10	0.14	55	57	0	0	0
4	inferior	1088	2	8	9.5	11.3	-0.28	-0.24	19	12	0	0	0
	mid	1043	34	66	3.9	3.1	-0.80	-0.67	27	49	1.7	1.3	0.5
	superior	840	54	130	4.6	2.8	-0.68	-0.74	34	62	0.5	0.1	0.4
5	inferior	669	0	0	9.1	5.2	-0.47	-0.39	1	0	0	0	0
	mid	672	0	0	8.4	7.1	-0.31	-0.28	12	7	0	0	0
	superior	707	38	50	4.1	1.9	-0.65	-0.97	24	45	10.0	9.2	0.8
6	inferior	717	0	0	10.4	11.4	-0.21	-0.23	0	2	0	0	0
	mid	696	0	4	8.5	7.9	-0.32	-0.41	3	7	0	0	0
	superior	682	0	24	6.1	5.5	-0.76	-0.96	26	29	0.4	0	0.4
7	inferior	1577	8	2	8.9	7.8	-0.18	-0.20	14	11	0	0	0
	mid	1472	2	6	9.1	7.9	-0.17	-0.28	12	12	0	0	0
	superior	excluded											
8	inferior	729	0	0	9.1	7.5	-0.23	-0.17	5	4	0	0	0
	mid	718	8	24	8.9	6.3	-0.26	-0.34	14	19	0	0	0
	superior	705	18	44	7.1	5.9	-0.39	-0.41	23	24	0	0	0
9	inferior	793	22	44	5.9	3.6	-0.14	-0.28	39	49	0	0	0
	mid	793	12	38	6.0	3.9	-0.23	-0.33	39	43	0	0	0

Supplemental table 2 – Continued

Patient no.	Location	SRCL (ms)	DA (mm)		Voltage (mV)		RS ratio		Fractionation (%)		EEA (%)	Epi delay (%)	Endo delay (%)
			Epi	Endo	Epi	Endo	Epi	Endo	Epi	Endo			
	superior	895	66	68	4.0	3.4	-0.65	-0.87	51	49	2.6	0.3	2.3
10	inferior	895	4	6	11.5	7.6	-0.46	-0.43	12	4	0	0	0
	mid	1004	8	28	7.5	4.4	-0.73	-0.56	19	21	0	0	0
	superior	1005	22	60	4.3	4.1	-0.99	-0.83	36	72	1.5	0.5	1.1
11	inferior	954	0	0	9.7	9.6	-0.24	-0.20	4	5	0	0	0
	mid	1005	6	6	8.7	6.5	-0.26	-0.24	15	12	0	0	0
	superior	970	26	18	6.1	4.8	-0.26	-0.19	33	34	0.8	0	0.8
12	inferior	983	0	0	9.4	14.3	-0.49	-0.44	6	3	0	0	0
	mid	990	38	60	5.1	4.6	-0.63	-0.69	49	49	10.3	10.3	0
	superior	975	54	146	3.0	1.9	-0.77	-0.90	49	89	23.1	2.0	21.2
13	inferior	1014	0	22	5.1	6.0	-0.22	-0.18	22	28	0	0	0
	mid	962	14	24	5.7	5.8	0.05	-0.05	17	19	0	0	0
	superior	1005	16	12	4.6	4.6	-0.11	-0.09	32	23	0	0	0
14	inferior	677	36	34	5.7	3.3	0.44	0.44	30	25	2.8	0.0	2.8
	mid	820	24	16	3.7	3.2	-0.52	-0.57	26	11	0	0	0
	superior	689	62	72	1.9	1.9	-0.68	-0.84	35	16	6.6	0.4	6.3
15	inferior	849	0	0	16.9	16.9	0.19	0.25	2	5	0	0	0
	mid	720	0	0	17.8	14.5	-0.16	-0.22	3	9	0	0	0
	superior	571	0	0	16.3	13.4	-0.06	-0.17	3	9	0	0	0
16	inferior	1155	0	6	9.7	9.1	-0.25	-0.25	4	17	0	0	0
	mid	1135	0	0	11.2	6.0	-0.21	-0.18	4	4	0	0	0
	superior	1130	0	16	9.0	4.5	-0.41	-0.51	4	17	0	0	0
17	inferior	966	6	14	8.0	3.7	-0.39	-0.43	9	9	0	0	0
	mid	1053	50	34	3.6	2.3	-0.51	-0.49	29	31	0	0	0
	superior	excluded											
18	inferior	732	0	4	7.2	4.9	-0.36	-0.31	7	2	0	0	0
	mid	869	0	2	9.1	5.5	-0.32	-0.36	0	2	0	0	0

Supplemental table 2 – Continued

Patient no.	Location	SRCL (ms)	DA (mm)		Voltage (mV)		RS ratio		Fractionation (%)		EEA (%)	Epi delay (%)	Endo delay (%)
			Epi	Endo	Epi	Endo	Epi	Endo	Epi	Endo			
	superior	excluded											
19	inferior	1088	48	20	3.5	3.2	0.36	0.42	42	45	0	0	0
	mid	1067	14	12	8.1	6.8	0.10	0.23	12	10	0	0	0
	superior	974	24	50	8.0	6.9	-0.05	0.08	31	29	0	0	0
20	inferior	702	4	4	6.1	5.5	-0.11	-0.19	6	13	0	0	0
	mid	703	6	6	5.9	6.3	-0.44	-0.44	12	24	0	0	0
	superior	704	14	30	4.7	6.0	-0.66	-0.60	25	33	1.1	1.1	0
21	inferior	834	2	14	5.7	4.1	-0.24	-0.40	11	36	1.5	0	1.5
	mid	784	8	48	2.8	0.9	-0.65	-0.46	26	60	44.4	0	44.4
	superior	776	48	34	4.7	5.3	-0.32	-0.44	58	36	0	0	0
22	inferior	678	0	0	9.2	7.0	-0.12	-0.20	4	4	0	0	0
	mid	698	4	20	8.1	5.5	-0.47	-0.54	22	19	0	0	0
	superior	675	56	100	7.3	4.4	-0.69	-0.96	38	43	1.1	0.9	0.2
23	inferior	954	12	2	18.0	18.0	-0.07	-0.12	9	13	0	0	0
	mid	972	22	3	14.9	12.8	-0.26	-0.31	20	10	0	0	0
	superior	952	30	6	9.8	8.4	-0.35	-0.42	28	17	0	0	0
24	inferior	787	2	14	11.2	8.4	-0.22	-0.21	12	24	0	0	0
	mid	773	38	38	8.3	7.8	-0.11	-0.29	30	25	0	0	0
	superior	excluded											
25	inferior	728	72	32	3.7	2.8	-0.53	-0.60	45	37	0	0	0
	mid	770	60	22	4.7	4.4	-0.43	-0.25	23	5	7.2	7.2	0.0
	superior	750	50	34	5.2	3.8	-0.77	-0.56	39	40	16.1	15.1	1.0
26	inferior	802	20	24	11.5	10.7	-0.11	-0.16	19	18	0	0	0
	mid	800	26	32	9.5	6.8	-0.23	-0.22	28	31	0	0	0
	superior	794	14	48	7.7	6.2	-0.29	-0.40	28	38	0.6	0	0.6

DA, delayed activation; EEA, endo-epicardial asynchrony; SRCL, sinus rhythm cycle length

9

Detection of endo-epicardial asynchrony in the atrial wall using one-sided unipolar and bipolar electrograms

Lisette J.M.E. van der Does
Roeliene Starreveld
Rohit K. Kharbanda
Paul Knops
Charles Kik
Ad J.J.C. Bogers
Natasja M.S. de Groot

Submitted

Abstract

Objectives

We aimed to determine the sensitivity and best recording modus to detect atrial endo-epicardial asynchronous activation (EEA) with use of electrogram fractionation.

Background

EEA is a new mechanism possibly maintaining atrial fibrillation. However, clinical electrophysiology studies can mostly record electrical activity at only one side of the atrial wall. EEA could be detected from one-sided electrograms by identifying farfield electrical activity (fractionation) reflecting EEA.

Methods

Simultaneously obtained right atrial endo- and epicardial multi-electrogram maps from 22 patients during cardiac surgery demonstrating EEA were selected. Unipolar electrograms were converted to bipolar electrograms in the horizontal (bi-x) and vertical (bi-y) direction. Unipolar electrograms and bipolar electrograms were analyzed by two investigators for presence and characteristics of unipolar and bipolar fractionation corresponding to EEA.

Results

Sensitivity of presence of fractionation corresponding to asynchronous activation was high in patients (86-96%) and moderately-high for the asynchronous surface area for both unipolar and bipolar electrograms equally (epi: 75% vs 65% (bi-x) and 69% (bi-y), endo: 72% vs 78% (bi-x) and 72% (bi-y)). Using the bipolar recording mode, signal-to-noise ratio of EEA corresponding fractionation decreased (from 11 (6-25) to 4 (2-7) in bi-y, $p<0.001$) and additional fractionation increased for electrograms recorded at the endocardium (53% (10-86) to 82% (52-100) in bi-x, $p=0.019$).

Conclusions

Sensitivity of fractionation corresponding to EEA is high for both unipolar and bipolar electrograms. However, unipolar electrograms are more suited for detection of EEA due to a larger signal-to-noise ratio and less disturbance of additional fractionation.

Introduction

The electrical pathophysiological mechanisms of persistent atrial fibrillation remain to this day largely unknown. Recent evidence suggests that dissociated electrical conduction between the layers of the atrial wall presenting as endo-epicardial asynchrony (EEA) in excitation is a potential significant mechanism for persistence of atrial fibrillation.[1, 2] The asynchronous activation of epicardial and endocardial layers provide opportunity for waves of excitation to travel transmurally and cause new breakthrough waves on the opposite side of the wall. After canine and goat models, a new simultaneous endo-epicardial mapping approach finally allowed for documentation of EEA of the right atrial wall in patients as well.[1, 3, 4] However, this technique can only be applied in patients undergoing cardiac surgery and is limited to the right atrial appendage/free wall and occasionally the left atrial appendage.[5] A method to detect EEA during endovascular electrophysiological studies would greatly benefit research into the mechanisms of atrial fibrillation. Recently, we investigated simultaneously recorded unipolar endocardial and epicardial electrograms during sinus rhythm and discovered that EEA causes unipolar electrogram fractionation (additional deflections on the electrogram). By relating unipolar electrogram fractionation to spatial patterns of activation, fractionation could be attributed to EEA.[6] However, most electrophysiological studies use a bipolar recording mode for mapping to reduce farfield effects recorded by unipolar electrograms.[7] In case of EEA, remote activation on unipolar electrograms could be an important feature to detect EEA while recording on only one side of the atrial wall. We therefore hypothesized that unipolar electrograms are more sensitive in detection of atrial EEA than bipolar electrograms. Electrogram features of sites with EEA were analyzed in 22 patients and we compared the sensitivity of unipolar and bipolar electrograms for detection of EEA from only one side of the atrial wall.

Methods

Study population

Twenty-two patients from the ongoing Epic End study in the Erasmus Medical Center were selected. The Epic End study is approved by the local medical ethics committee (MEC-2015-373) and includes patients over 18 years of age undergoing cardiac surgery for coronary artery disease, heart valve disease and/or congenital heart disease. This study complies with the Declaration of Helsinki and prior to participation all patients gave informed consent. Mean age of selected patients was 65±9 years and 15 of 22 were male. Cardiac surgery was performed for coronary artery disease (N=15) and/or valvular heart disease (N=12), ten patients had a history of atrial fibrillation of whom one had persistent atrial fibrillation.

Endo-epicardial mapping

Mapping during cardiac surgery was performed just prior to commencement of cardiopulmonary bypass and after arterial cannulation. Simultaneous endo-epicardial mapping was conducted by introducing one of two 128-electrode (8x16) arrays in the right atrium via the incision for venous cannulation for endocardial mapping. The other array was placed on top of the epicardium for epicardial mapping. Both electrode arrays (0.45mm electrodes, 2mm interelectrode spacing) were fixed on a steel spatula and bound together to ensure good contact and precise alignment of the two arrays. Unipolar electrograms of the right atrial wall were recorded for 5-10 seconds during sinus rhythm and pacing at the superior, middle and inferior right atrial free wall (see *Figure 1A-C*). In one patient, endo-epicardial electrograms were recorded from the left atrial appendage before excision. Electrograms were sampled at 1000Hz, filtered (0.5-400 Hz) and digitized (16-bits conversion) and, with a calibration signal of 2 mV, stored on hard disk for offline analysis. Details of the endo-epicardial mapping procedure were previously described.[5]

Data analysis: electrogram selection, conversion and marking

Recorded data during sinus rhythm and pacing of all patients included in our study were analyzed for the presence of EEA (see *Figure 1D*). Only patients demonstrating EEA were included and if multiple recording sites of a patient demonstrated EEA, only the recording site with the largest area of EEA was included. Local activation time (LAT) in unipolar electrograms was marked at the steepest negative slope (dV/dt) with a minimum of 0.05mV/ms. Activation maps were constructed for both epicardium and endocardium. EEA was determined from these maps by calculating the differences between the local activation time at each electrode and the nine opposite electrodes in the other plane; direct opposite and its eight surrounding electrodes. Minimal time difference with these nine opposite electrode sites determined the time difference for the electrode. EEA was defined as a difference between epicardial and endocardial local activation time of ≥15ms. If unipolar asynchrony maps demonstrated EEA at ≥4 adjacent electrode sites that did not include border electrodes, the recording site was included for analysis. Border electrodes, defined as electrodes with <7 opposite local activation times, and electrodes missing the exact opposite electrogram were excluded from analysis. One electrode site corresponds to an area of 4mm2.

Unipolar electrograms were converted to bipolar electrograms by subtracting the unipolar electrogram from one electrode from the unipolar electrogram at the adjacent electrode of the array. Bipolar conversion was performed two times: in the horizontal (x) direction and in the vertical (y) direction. Local AT in bipolar electrograms was marked at the largest (maximal or minimal) peak. EEA and electrode inclusion was then determined as described above with the exception

that bipolar electrograms at the right or left border in case of x-direction conversion and top or bottom border in case of y-direction conversion were included for analysis (see *Figure 2*). In addition, for the bipolar activation maps, only electrodes with EEA on similar sites of EEA on the unipolar activation maps were included. This assured only electrograms from the same EEA site were analyzed so there was no disagreement between the unipolar and bipolar EEA sites.

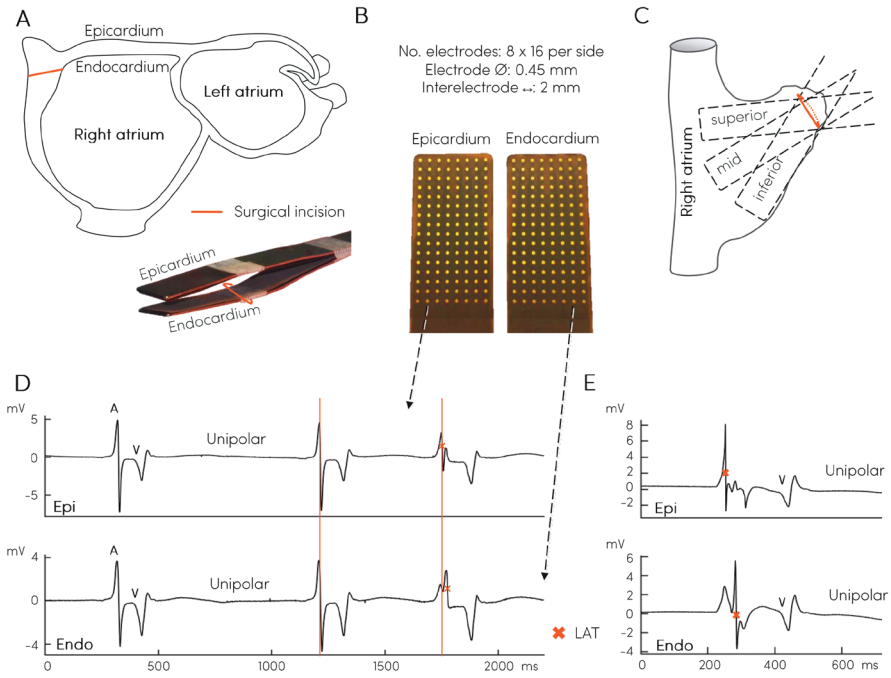

Figure 1 – Simultaneous endo-epicardial mapping in patients during cardiac surgery. *A*: the mapping tool consists of two identical electrode arrays fixed to each other. One leg (electrode array) of the mapping tool is introduced in the right atrium via a standard surgical incision for cardio-pulmonary bypass. This allows to record electrograms from the epicardium (outside wall) and endocardium (inside wall) simultaneously. *B*: the properties of the electrode array. *C*: mapping locations at the right atrium. *D*: examples of directly opposite epicardial (epi) and endocardial (endo) unipolar electrograms. Endo-epicardial atrial activation (A) is in synchrony in the first two beats, the following atrial extrasystole demonstrates asynchronous endo-epicardial atrial activation. V, ventricular activation; LAT, local activation time. *E*: example of atrial asynchrony and additional deflections next to the LAT-deflection on unipolar electrograms (=fractionation). One fractionation-deflection on each electrogram corresponds to the asynchronous activation on the opposite side.

Included unipolar electrograms with EEA were then inspected for visual presence of additional (fractionated/farfield) deflections (see *Figure 1E*), or additional peaks in case of bipolar electrograms. All markings were evaluated by two investigators

independently. Bipolar fractionation peaks were marked by the investigators based on previous studies marking bipolar fractionated electrograms using the change in polarity of the depolarization slope to tag bipolar peaks.[8, 9] Each additional marked peak on bipolar electrograms within baseline noise, defined as up to 120% of the noise, was excluded. Of each primary (=LAT) and fractionated unipolar deflection the following parameters were derived: amplitude (peak-to-peak voltage), the time of steepest slope (FT, fractionation time) and signal-to-noise ratio (SNR). Primary and fractionation peaks of bipolar electrograms were analyzed for voltage (peak-to-baseline), time of the peaks (LAT or FT) and SNR.

Corresponding fractionation analysis

At each EEA site, the primary epicardial deflection or peak and the endocardial primary deflection or peak were compared to the direct opposite electrogram for the presence of fractionation corresponding to the primary deflection/ peak. If the FT of a fractionation peak or deflection on the opposite side was ≤7ms of the LAT, it was labelled as corresponding fractionation (to the primary deflection/ peak) (see *Figure 2*). This cut-off was chosen based on our previous definitions of conduction delay and block.[10] In case of multiple deflections or peaks meeting this criterion, first the closest deflection/ peak, otherwise the largest deflection/ peak, was selected as fractionation corresponding to EEA. Parameters of the corresponding unipolar deflection or bipolar peak included voltage, SNR and voltage compared to the primary deflection/ peak on the same electrogram (in %). In addition, the time difference between the LAT and corresponding FT was analyzed to determine level of time accuracy.

Additional fractionation analysis

Besides analysis of fractionation corresponding to EEA, each opposite electrogram was analyzed for the presence of fractionation in addition to the EEA corresponding fractionation with a FT ≥15ms separated from the LAT. This fractionation can be confused for EEA and does not correspond to the primary deflection on the other side and could complicate determining presence of EEA.

Statistical analysis

Data with a normal distribution are presented as the mean ±SD and skewed data are presented as the median (p25-p75). To assess differences between unipolar and bipolar electrograms, Friedman's test was used in case of skewed data and ANOVA repeated measures was used in case of normally distributed data. Post hoc tests between 1) unipolar and bipolar-x and 2) unipolar and bipolar-y were performed with Wilcoxon signed rank test. Statistical significance was set at $p \leq 0.05$, post hoc test significance levels were adjusted according to Bonferroni at $p \leq 0.025$. Data of which outcomes of statistical significance were similar between observers is presented in the text as the mean of the two medians and percentiles and the highest p-value is presented.

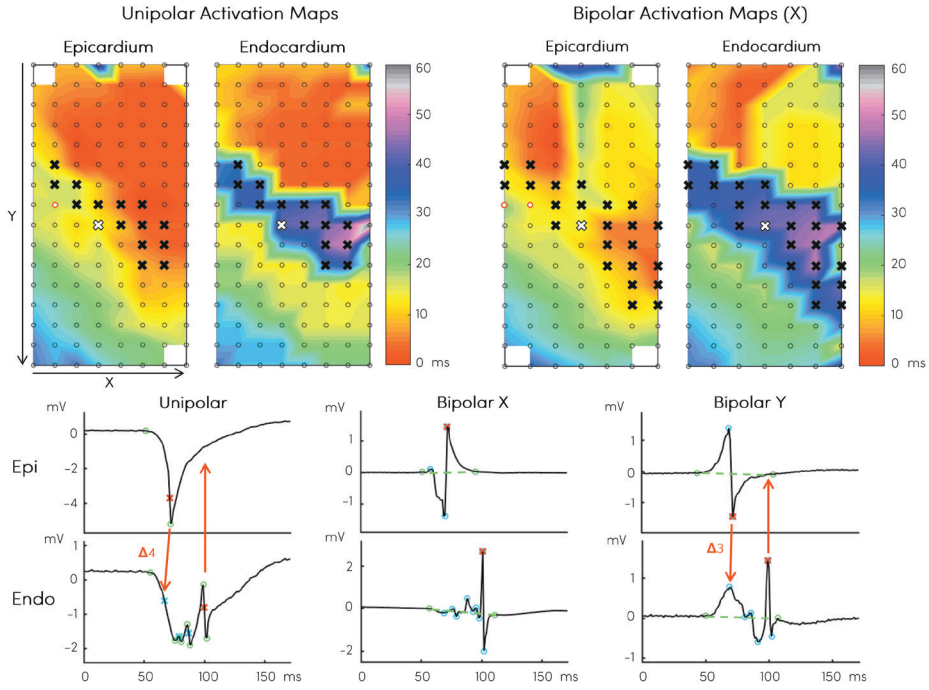

Figure 2 – Data selection and analysis. *Top left*: epi- and endocardial activation maps constructed from unipolar electrograms acquired from simultaneous endo-epicardial mapping. *Top right*: endo-epicardial activation maps constructed after subtracting unipolar electrograms in the horizontal (X) direction creating bipolar electrograms. Crosses indicate electrogram sites with endo-epicardial asynchrony (EEA) that are included for the study. Red circles represent a broken electrode site and endo-epicardial electrograms at this site are excluded from the study. *Bottom*: unipolar and bipolar epi- and endocardial electrograms from the site marked with the white cross. Local activation time is marked at the steepest slope for unipolar electrograms and at the largest peak for bipolar electrograms (red crosses). Fractionation time (FT) is determined by marking the steepest slope of additional deflections for unipolar electrograms and by marking additional peaks for bipolar electrograms (blue markers). If the difference between a FT and the local activation time of the opposite electrogram is ≤7ms, 4ms in the unipolar electrogram example and 3ms in the bipolar (Y) electrogram example, this fractionation is defined as fractionation corresponding to EEA. In this example, no fractionation corresponding to EEA (the endocardial local activation time) is present on the epicardial electrogram. Unipolar voltage of corresponding fractionation is measured as the difference between peaks (between green circles). Bipolar voltage of corresponding fractionation is measured as the difference between peak and baseline; baseline is virtually constructed as a straight line (green line) between the two green markers placed by the observers in bipolar electrograms (green circles) thereby correcting for baseline drift. Bipolar fractionation (blue circled peaks) within noise level of this virtual baseline are excluded from analysis, in this example the second blue circled peak on the y-bipolar endocardial electrogram is excluded. Fractionation (blue crosses or peaks) that does not correspond to EEA with a difference ≥15ms of the local activation time in the same electrogram is counted to determine presence of additional fractionation.

Results

EEA area and electrogram characteristics

Included EEA areas occurred during sinus rhythm in 14 patients, during an atrial extrasystole in 7 patients and during pacing at 240 bpm in one patient. EEA was present on a median surface of 52 (31-94) mm2 in unipolar maps and no difference was observed between unipolar and bipolar maps (bipolar-x: 42 (22-87) mm2, bipolar-y: 52 (32-94) mm2, p=0.78, see *Table 1*). Activation time differences between epicardium and endocardium in unipolar maps ranged from 16 to 96 ms per patient with a median delay of 26 (21-33) ms. Bipolar endo-epicardial delays were similar to unipolar endo-epicardial delays (p=0.37). Amplitudes of bipolar electrograms were lower compared to unipolar electrograms for both epicardial and endocardial electrograms (p<0.001). In addition, SNR of bipolar electrograms in the y-direction was lower compared to unipolar electrograms: 32 (16-62) vs 62 (32-114) for epicardial electrograms and 13 (5-35) vs 28 (18-52) for endocardial electrograms (p≤0.001).

Table 1 – Endo-epicardial asynchrony and electrogram characteristics

	Unipolar	Bipolar-x	Bipolar-y	p-value
EEA area (mm^2)	52 (31-94)	42 (22-87)	52 (32-94)	0.78
EEA delay (ms)	26 (21-33)	25 (22-32)	24 (21-30)	0.37
Epicardium				
Voltage* (mV)	3.4 (2.1-5.9)	1.1 (0.7-3.0)	1.4 (0.9-2.9)	<0.001
SNR	62 (32-114)	73 (25-115)	32 (16-62)	<0.001
Endocardium				
Voltage* (mV)	1.8 (1.1-2.8)	0.5 (0.3-1.3)	0.8 (0.2-1.8)	<0.001
SNR	28 (18-52)	29 (7-52)	13 (5-35)	<0.001

* Maximal peak-to-peak voltage of uni- and bipolar electrograms. EEA, endo-epicardial asynchrony; SNR, signal-to-noise ratio.

EEA corresponding fractionation

Both unipolar and bipolar electrograms demonstrated EEA related fractionation in equal amounts (see *Figure 3*). Fractionation corresponding to EEA was present at 75% (34-96%) of the electrode sites per patient for epicardial unipolar electrograms and at 72% (41-96%) for endocardial unipolar electrograms. Bipolar epicardial electrograms showed fractionation corresponding to EEA at 64% (30-89%) of electrode sites per patient in the x-direction and 69% (24-92%) in the y-direction. Bipolar endocardial electrograms showed EEA corresponding fractionation in the x- and y-direction at respectively 78% (49-97%) and 72% (33-92%) of electrode sites. Complete absence of EEA fractionation occurred in one patient (<5%) for unipolar epicardial electrograms and in maximal two patients (<10%) for bipolar epicardial electrograms and in maximal three patients (<14%) for unipolar and bipolar endocardial electrograms (see *Supplemental table 1*).

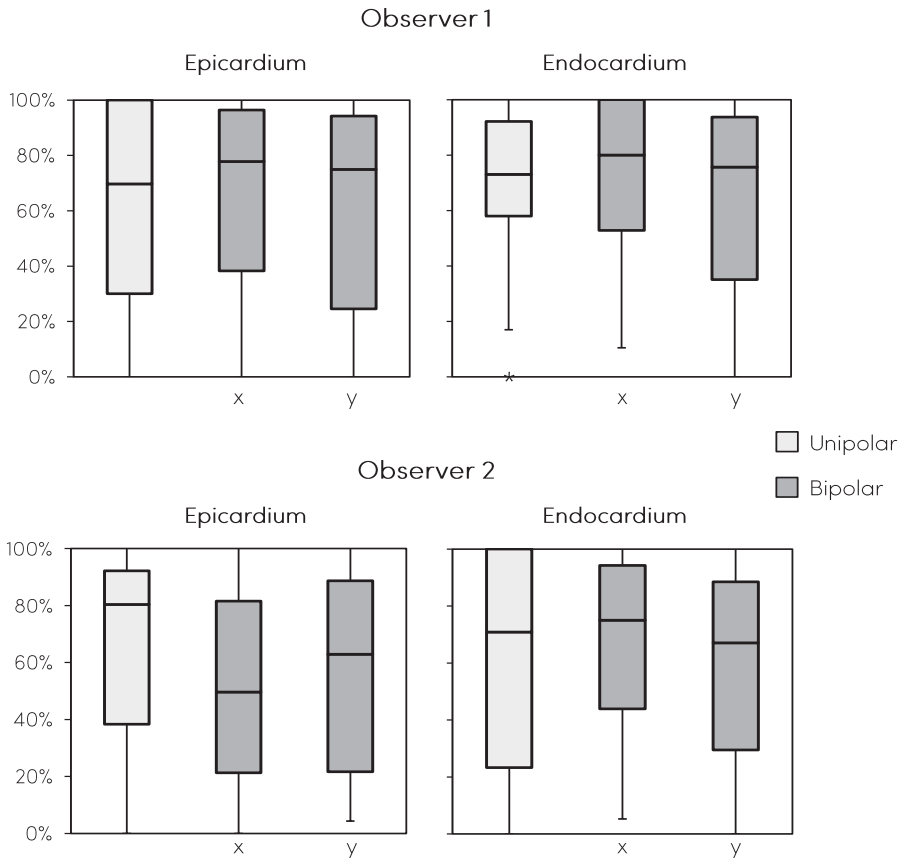

Figure 3 – Presence of EEA corresponding fractionation on unipolar and bipolar electrograms. Boxplots of the percentage of electrode-sites with EEA where the electrogram shows fractionation corresponding to EEA for observer 1 (top) and observer 2 (bottom). Outliers (>1.5 interquartile range) are presented as asterisks.

Absolute voltage of EEA corresponding fractionation was higher on unipolar electrograms than on bipolar electrograms (see *Table 2*). However, relative size of EEA corresponding fractionation to the primary deflection or peak, representing the LAT, did not differ between unipolar and bipolar electrograms. The SNR of corresponding fractionation, or the ease in which the signal can be separated from the noise, was significantly decreased in bipolar electrograms created in the y-direction at the endocardium (unipolar SNR: 11 (6-25) vs bipolar-y SNR: 4 (2-7), $p<0.001$). Examples of SNR decrease in bipolar electrograms are shown in *Figure 4A*. Time accuracy of corresponding FT compared to the LAT was similar for unipolar and bipolar electrograms at an average of 2 to 3 ms.

Table 2 – Characteristics of corresponding fractionation

	Observer 1							Observer 2						
	Unipolar		**Bipolar-x**		**Bipolar-y**		**p-value**	**Unipolar**		**Bipolar-x**		**Bipolar-y**		**p-value**
Epicardium														
Voltage (mV)	0.61	(0.27-1.38)	0.19	(0.08-0.31)	0.28	(0.14-0.48)	<0.001	0.57	(0.21-1.35)	0.22	(0.12-0.31)	0.31	(0.17-0.48)	<0.001
Relative to primary (%)	24	(13-37)	17	(9-31)	21	(16-32)	0.51	20	(12-43)	20	(11-39)	26	(17-42)	0.49
SNR	13	(4-22)	10	(4-13)	5	(3-12)	0.04	11	(4-23)	12	(5-16)	5	(4-11)	0.12
Time accuracy (ms)	2	±1.8	3	±1.3	3	±1.3	0.56	3	±1.6	3	±1.5	3	±1.6	0.60
Endocardium														
Voltage (mV)	0.56	(0.29-1.6)	0.17	(0.07-0.36)	0.18	(0.12-0.48)	<0.001	0.66	(0.27-1.74)	0.20	(0.09-0.37)	0.20	(0.11-0.45)	<0.001
Relative to primary (%)	49	(31-78)	34	(29-49)	34	(19-48)	0.14	50	(35-78)	39	(30-58)	35	(25-59)	0.37
SNR	11	(6-23)	9	(4-15)	4	(2-7)	<0.001	10	(6-26)	11	(3-18)	4	(2-7)	<0.001
Time accuracy (ms)	3	±1.6	2	±1.4	3	±1.1	0.53	3	±1.5	2	±1.6	3	±1.3	0.67

SNR, signal-to-noise ratio.

Additional fractionation

The presence of other fractionation that does not correspond to EEA, will complicate determining presence of EEA based on fractionation. *Table 3* presents the percentage of electrograms that showed fractionation other than the EEA corresponding fractionation and the average number of additional deflections/ peaks per electrogram. At the endocardium, bipolar electrograms in the x-direction demonstrated more additional fractionation than unipolar electrograms: 82% (52-100) vs 53% (10-86) (p=0.019) of electrograms and 2 peaks (1-3) vs 1 (0-1) deflection per electrogram (p=0.004). *Figure 4B* shows examples of increase of additional fractionation on bipolar endocardial electrograms.

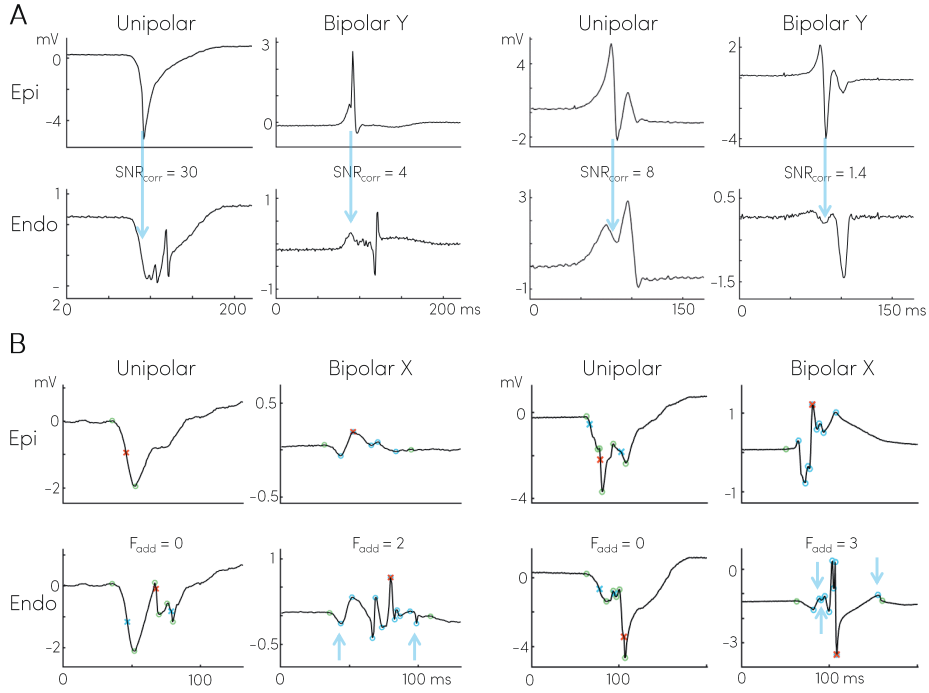

Figure 4 – Unipolar versus bipolar electrograms. *A*: two electrogram examples demonstrating decrease of signal-to noise ratio of fractionation corresponding to EEA (SNR_{corr}) in bipolar endocardial electrograms in the y-direction. Blue arrow points to fractionation on the endocardial electrogram corresponding to the primary deflection/ peak of the local activation time on the epicardial electrogram. *B*: two electrogram examples demonstrating increase of additional fractionation (F_{add}) on the bipolar endocardial electrogram in the x-direction. Red cross indicates local activation time. Blue crosses or circles indicate fractionation. Blue arrows indicate fractionation which 1) does not correspond to EEA, 2) not within noise level of the baseline and 3) is ≥15ms removed from the local activation time (= F_{add}).

Table 3 – Presence of additional fractionation

	Unipolar	Bipolar-x	Bipolar-y	p-value
Epicardium				
Electrogram %				
obs. 1	39 (0-79)	63 (24-100)	65 (29-87)	0.011
obs. 2	48 (2-66)	49 (19-100)	60 (23-77)	0.098
No. per electrogram				
obs. 1	0 (0-1)	1 (0-2)	1 (0-1)	0.002
obs. 2	1 (0-1)	1 (0-2)	1 (1-1)	0.056
Endocardium				
Electrogram %				
obs. 1	59 (11-90)	85 (55-100)	68 (37-87)	0.006
obs. 2	46 (8-81)	79 (49-100)	63 (45-83)	0.002
No. per electrogram				
obs. 1	1 (0-1)	2 (1-2)	1 (0-2)	0.002
obs. 2	1 (0-1)	2 (1-3)	1 (1-1)	0.001

Interobserver differences

Results of each observer are shown in *Supplemental tables 1-5*. Differences between observers in the significant statistical outcomes of the presented results above included SNR of corresponding fractionation at the epicardium (p=0.04 vs p=0.12) and percentage and number of additional fractionation at the epicardium (p=0.011 vs p=0.098 and p=0.002 vs p=0.056). At the endocardium, the higher number of additional fractionation per electrogram reached significance in only one observer (p=0.023 vs p=0.027).

Discussion

Previously, it was shown that most fractionation occurs due to inhomogeneous conduction patterns.[6,11] Almost all fractionated deflections in unipolar electrograms can be traced to neighboring electrical activation sites including the opposite side of the atrial wall.[6] Most clinical studies that have investigated electrogram fractionation use bipolar electrograms as this is the preferred recording method in clinical practice.[7] This study has demonstrated that EEA is reflected equally on unipolar and bipolar electrograms. However, fractionation reflecting EEA is less easy to distinguish from noise on endocardial electrograms using the bipolar recording mode. Furthermore, bipolar electrograms from the endocardium demonstrate more additional fractionation compared to unipolar electrograms that could complicate detection of EEA. This study has also shown that EEA reflects well on electrograms, over 86% of patients have at least one site showing fractionation corresponding to EEA.

Factors influencing bipolar electrograms

Because a bipolar electrogram is the product of two unipolar electrograms, several factors influence the morphology of a bipolar electrogram. For one, the distance between the two poles of a bipolar electrogram effects degree of fractionation. A computer model, which was also validated in a clinical population of atrial fibrillation patients, demonstrated that a larger interelectrode distance increases electrogram fractionation in bipolar electrograms in case of inhomogeneous activation patterns.[12] Also, increasing electrode size increases fractionation on both bipolar and unipolar electrograms.[12] Recordings of bipolar electrograms at scarred ventricular tissue representing a potential arrhythmogenic substrate in a study of Takigawa et al. confirmed the effect of orientation of the two poles on bipolar electrogram voltage and presence of abnormal electrograms of low voltage or with fractionation.[13] A parallel or transversal orientation of bipolar poles to the direction of activation resulted in differences in bipolar voltage of 50%. Sites with abnormal (fractionated) electrograms only matched in 57% between the different bipolar pole orientations and 30% of sites with abnormal (fractionated) electrograms were missed in the other pole orientation.[13] Therefore, the diverse morphology of bipolar electrograms based on electrode size, interelectrode spacing and catheter orientation, especially under conditions of complex activation patterns, complicates the use of bipolar electrogram morphology.

What do components of fractionated bipolar electrograms depict?

Components (deflections) of a unipolar fractionated electrogram relate to remote parts of dissociatively activated myocardium e.g. after a line of conduction block or to dissociation in activation of myocardial bundles underneath the electrode.[11, 14] A bipolar electrogram is meant to present (an approximation to) the derivate of the unipolar electrograms and the maximal peak in the derivate (or bipolar electrogram) coincides with the negative steepest slope(s) of the unipolar electrogram. The timing of the two unipolar signals (signal at the negative pole is earlier vs later than the signal at the positive pole) determines if the peak on the bipolar electrogram is a maximum or a minimum (see top of *Figure 5*). However, as seen in *Figure 5*, the bipolar electrogram also demonstrates peaks for the (steepest) positive slopes of the unipolar electrograms. Converting fractionated unipolar electrograms to bipolar electrograms makes distinguishing between bipolar peaks due to positive or negative components of the unipolar electrograms impossible. The electrograms at the bottom of *Figure 5* demonstrate that peaks in bipolar electrograms can represent negative deflections as well as positive deflections in unipolar electrograms. This concept could explain why additional fractionation presented more frequently in bipolar electrograms in this study.

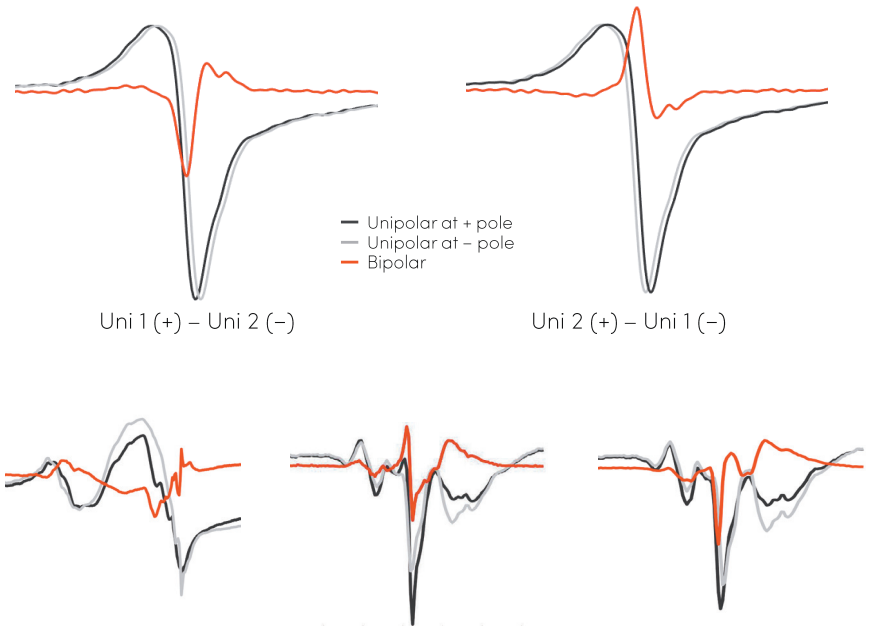

Figure 5 – Peaks in bipolar electrograms. *Top left*: a bipolar electrogram from two similar shaped signals with only one moved 1 sample on the time (x-)axis is the same as the derivative (Δ) of the signal. The minimum of the derivative is the steepest negative slope of the original signal. *Top right*: if the positive and negative poles are switched, the bipolar electrogram is the negative derivate (-Δ). The maximum of the bipolar electrogram is in this case the steepest negative slope of the signal. *Bottom:* three examples of fractionated unipolar electrograms where the two unipolar electrograms switch in which is de leading electrogram between the different fractionated components. For example, for the electrograms on the left, the light grey unipolar electrogram deflects negatively before the dark unipolar electrogram. The bipolar electrogram shows a positive peak at this point. However, with the following deflection, the dark unipolar electrogram deflects before the lighter unipolar electrogram deflects. Here the bipolar electrogram shows a negative peak. Therefore, it is not possible in these bipolar electrograms to determine if a peak is a unipolar negative deflection (voltage decrease) or a rise (voltage increase) in the unipolar electrogram.

EEA detection with use of unipolar fractionation

EEA has been suggested as a pathophysiological mechanism for persistence of atrial fibrillation.[1] Unfortunately, simultaneous mapping of epi- and endocardium is mostly limited to the right atrial free wall and only possible during cardiac surgery. Therefore, new techniques to identify EEA need to be developed in order to diversify research into the role of endo-epicardial asynchrony in arrhythmogenesis. Previously, we discovered that at least 95% of unipolar fractionation corresponds to remote activation by using automated detection of fractionation. In this study, fractionation was identified visually by two investigators to maximize detection of EEA based fractionation and because automated signal detection in clinical

practice is often evaluated by visual standards of the electrophysiologist. Outcome differences between the investigators were mainly limited to the epicardium. This may be explained by the larger SNR at the epicardium, making small peaks or deflections harder to detect visually. A positive finding is that a great majority (86%) of patients with EEA demonstrates fractionation corresponding to EEA on the other side of the atrial wall. This study did show that unipolar electrograms are better suited than bipolar electrograms for fractionation based EEA detection due to less interference of additional fractionation and because EEA corresponding signals are better distinguishable from the noise. During atrial fibrillation, activation waves are often much smaller and with more complex activation patterns with frequent wave break, wave collision and conduction block.[15] Unipolar voltage and SNR of fractionated components will be even smaller during atrial fibrillation than in this study emphasizing the use of unipolar over bipolar electrograms. The next steps in order to develop an EEA-detection tool would be to 1) label unipolar fractionated deflections corresponding to remote activation in the longitudinal plane and 2) find the most sensitive and specific signal parameters to diagnose fractionated deflections corresponding to asynchronous activation within the atrial wall.

Study limitations

Endo-epicardial mapping was mainly performed at the right atrial free wall as left atrial simultaneous endo-epicardial mapping can only be performed in very select cases. The differences between unipolar and bipolar electrograms may not apply to the thinner wall of the left atrium.

Conclusions

In SR, EEA of the right atrial free wall occurs to over 50ms difference between epicardium and endocardium, which has never been described before. Electrograms on both sides demonstrate an S-predominance and the RS-ratio cannot be used to identify the leading layer during SR. Fractionated potentials are not always identical on a high resolution scale and can have local mismatches, however, these mismatches occur in a minority of cases. If a potential is fractionated during SR, most additional deflections can be explained by conduction disorders in the same plane and in a small percentage they represent EEA. The incidence of EEA and EEA based fractionation is relatively low during SR as was expected. However, during atrial arrhythmias the presence of (functional) conduction disorders and EEA will increase and therefore epi-endocardial differences in electrogram morphology and EEA based fractionation will likely increase as well. Particularly interesting, especially for clinical practice, is the observation that the morphology of unipolar electrograms can potentially be a tool to identify areas of EEA when recording electrograms only on one side of the wall.

References

1. de Groot N, van der Does L, Yaksh A, Lanters E, Teuwen C, Knops P, van de Woestijne P, Bekkers J, Kik C, Bogers A and Allessie M. Direct Proof of Endo-Epicardial Asynchrony of the Atrial Wall During Atrial Fibrillation in Humans. *Circulation: Arrhythmia and Electrophysiology*. 2016;9(5).
2. de Groot NM, Houben RP, Smeets JL, Boersma E, Schotten U, Schalij MJ, Crijns H and Allessie MA. Electropathological substrate of longstanding persistent atrial fibrillation in patients with structural heart disease: epicardial breakthrough. *Circulation*. 2010;122:1674-82.
3. Schuessler RB, Kawamoto T, Hand DE, Mitsuno M, Bromberg BI, Cox JL and Boineau JP. Simultaneous epicardial and endocardial activation sequence mapping in the isolated canine right atrium. *Circulation*. 1993;88:250-63.
4. Eckstein J, Maesen B, Linz D, Zeemering S, van Hunnik A, Verheule S, Allessie M and Schotten U. Time course and mechanisms of endo-epicardial electrical dissociation during atrial fibrillation in the goat. *Cardiovascular Research*. 2011;89:816-824.
5. Knops P, Kik C, Bogers AJ and de Groot NM. Simultaneous endocardial and epicardial high-resolution mapping of the human right atrial wall. *J Thorac Cardiovasc Surg*. 2016;152:929-31.
6. van der Does L, Knops P, Teuwen CP, Serban C, Starreveld R, Lanters EAH, Mouws E, Kik C, Bogers A and de Groot NMS. Unipolar atrial electrogram morphology from an epicardial and endocardial perspective. *Heart Rhythm*. 2018;15:879-887.
7. van der Does LJ and de Groot NM. Inhomogeneity and complexity in defining fractionated electrograms. *Heart Rhythm*. 2017;14:616-624.
8. Yoshida K, Ulfarsson M, Tada H, Chugh A, Good E, Kuhne M, Crawford T, Sarrazin JF, Chalfoun N, Wells D, Jongnarangsin K, Pelosi F, Jr., Bogun F, Morady F and Oral H. Complex electrograms within the coronary sinus: time- and frequency-domain characteristics, effects of antral pulmonary vein isolation, and relationship to clinical outcome in patients with paroxysmal and persistent atrial fibrillation. *J Cardiovasc Electrophysiol*. 2008;19:1017-23.
9. Scherr D, Dalal D, Cheema A, Cheng A, Henrikson CA, Spragg D, Marine JE, Berger RD, Calkins H and Dong J. Automated detection and characterization of complex fractionated atrial electrograms in human left atrium during atrial fibrillation. *Heart Rhythm*. 2007;4:1013-20.
10. Teuwen CP, Yaksh A, Lanters EA, Kik C, van der Does LJ, Knops P, Taverne YJ, van de Woestijne PC, Oei FB, Bekkers JA, Bogers AJ, Allessie MA and de Groot NM. Relevance of Conduction Disorders in Bachmann's Bundle During Sinus Rhythm in Humans. *Circ Arrhythm Electrophysiol*. 2016;9:e003972.
11. Spach MS and Dolber PC. Relating extracellular potentials and their derivatives to anisotropic propagation at a microscopic level in human cardiac muscle. Evidence for electrical uncoupling of side-to-side fiber connections with increasing age. *Circ Res*. 1986;58:356-71.
12. Correa de Sa DD, Thompson N, Stinnett-Donnelly J, Znojkiewicz P, Habel N, Muller JG, Bates JH, Buzas JS and Spector PS. Electrogram fractionation: the relationship between spatiotemporal variation of tissue excitation and electrode spatial resolution. *Circ Arrhythm Electrophysiol*. 2011;4:909-16.

13. Takigawa M, Relan J, Martin R, Kim S, Kitamura T, Frontera A, Cheniti G, Vlachos K, Massoullie G, Martin CA, Thompson N, Wolf M, Bourier F, Lam A, Duchateau J, Klotz N, Pambrun T, Denis A, Derval N, Magat J, Naulin J, Merle M, Collot F, Quesson B, Cochet H, Hocini M, Haissaguerre M, Sacher F and Jais P. Effect of bipolar electrode orientation on local electrogram properties. *Heart Rhythm*. 2018;15:1853-1861.
14. Konings KT, Smeets JL, Penn OC, Wellens HJ and Allessie MA. Configuration of unipolar atrial electrograms during electrically induced atrial fibrillation in humans. *Circulation*. 1997;95:1231-41.
15. Allessie MA, de Groot NM, Houben RP, Schotten U, Boersma E, Smeets JL and Crijns HJ. Electropathological substrate of long-standing persistent atrial fibrillation in patients with structural heart disease: longitudinal dissociation. *Circ Arrhythm Electrophysiol*. 2010;3:606-15.

Supplemental material

Supplemental table 1 – Percentage of electrograms with EEA corresponding fractionation per patient

	Observer 1						Observer 2					
	Epicardium			Endocardium			Epicardium			Endocardium		
no.	uni	bi-x	bi-y	uni	bi-x	bi-y	uni	bi-x	bi-y	uni	bi-x	bi-y
1	75	78	92	50	89	77	75	67	92	25	89	77
2	100	100	75	88	100	38	88	100	25	100	100	38
3	56	95	67	70	71	87	56	81	63	70	62	77
4	67	85	100	89	100	100	100	54	88	100	92	50
5	73	22	43	34	33	74	32	13	15	18	22	66
6	11	85	23	100	100	100	44	69	38	100	100	100
7	20	86	14	100	100	100	40	71	14	100	86	100
8	100	100	50	86	73	60	100	45	60	71	73	50
9	40	83	75	100	100	100	60	83	63	100	100	100
10	33	100	100	17	80	0	33	90	100	0	80	0
11	3	44	25	73	54	68	3	38	20	70	26	30
12	100	50	88	100	100	88	86	25	88	100	100	88
13	100	100	100	89	13	92	100	100	100	89	25	92
14	16	16	22	60	11	4	16	16	22	0	5	4
15	100	78	100	0	89	0	86	22	100	0	100	0
16	67	50	86	100	75	100	89	25	64	100	75	93
17	0	4	0	67	75	87	0	8	4	67	67	87
18	65	0	80	88	50	87	65	0	27	82	50	87
19	100	100	100	0	100	0	100	100	100	17	50	0
20	91	48	86	70	97	73	91	30	82	70	82	68
21	97	20	20	72	14	28	95	18	12	74	22	28
22	86	60	71	71	80	57	86	55	79	64	75	36
median	70	78	75	73	80	76	80	50	63	71	75	67

Supplemental table 2 – Voltage and relative voltage of corresponding fractionation per patient

	Observer 1												Observer 2											
	Voltage (mV)						Relative Voltage (%)						Voltage (mV)						Relative Voltage (%)					
	Epicardium			Endocardium			Epicardium			Endocardium			Epicardium			Endocardium			Epicardium			Endocardium		
no.	uni	bi-x	bi-y	uni	bi-x	bi-y	uni	bi-x	bi-y	uni	bi-x	bi-y	uni	bi-x	bi-y	uni	bi-x	bi-y	uni	bi-x	bi-y	uni	bi-x	bi-y
1	1.27	0.29	0.96	1.60	0.33	0.60	23	4	26	30	7	8	1.24	0.31	1.04	2.15	0.32	0.63	23	5	30	54	9	10
2	0.95	0.23	0.20	0.29	0.09	0.09	25	22	13	31	69	50	1.15	0.22	0.30	0.27	0.09	0.10	29	21	27	27	65	71
3	0.69	0.31	0.25	1.64	0.36	0.30	35	40	20	44	32	19	0.57	0.30	0.25	1.74	0.37	0.37	29	39	20	45	35	22
4	0.63	0.18	0.30	0.56	0.17	0.18	21	10	21	35	49	16	0.56	0.19	0.32	0.57	0.20	0.18	13	9	21	35	58	18
5	0.41	0.15	0.10	0.46	0.11	0.13	28	26	12	77	42	19	0.45	0.10	0.06	1.24	0.17	0.13	58	39	17	70	48	35
6	0.23	0.07	0.15	1.57	0.32	0.48	25	41	40	172	38	64	0.15	0.11	0.18	1.57	0.30	0.52	12	47	28	172	38	65
7	0.33	0.48	1.15	1.99	0.52	0.48	2	12	62	107	29	27	0.17	0.57	1.14	1.99	0.40	0.58	2	10	61	107	26	25
8	1.42	0.06	0.61	0.12	0.07	0.14	44	14	41	10	23	35	1.38	0.09	0.41	0.17	0.08	0.17	44	19	43	14	21	70
9	0.19	0.39	0.50	1.77	0.48	0.49	6	50	31	78	38	34	0.16	0.37	0.68	1.77	0.51	0.45	3	58	37	78	40	29
10	2.28	0.76	0.77	0.23	0.17	-	107	25	28	21	41	-	2.28	0.79	0.71	-	0.20	-	107	24	21	-	71	-
11	0.25	0.17	0.23	0.51	0.09	0.12	9	9	11	19	7	9	0.25	0.19	0.33	0.46	0.09	0.14	9	14	15	18	7	26
12	0.94	0.09	0.16	0.66	0.28	0.17	27	8	19	36	63	24	0.92	0.06	0.17	0.66	0.25	0.27	31	6	15	36	58	31
13	1.55	0.30	0.42	1.12	0.40	0.25	16	6	15	40	90	23	1.55	0.29	0.49	1.12	0.61	0.21	16	6	17	40	87	25
14	0.21	0.12	0.09	0.18	0.03	0.07	13	60	32	50	56	74	0.20	0.14	0.10	-	0.04	0.07	12	73	43	-	80	59
15	0.59	0.08	0.33	-	0.05	-	37	10	34	-	69	-	0.67	0.29	0.41	-	0.05	-	39	18	50	-	73	-
16	0.07	0.04	0.08	0.27	0.04	0.06	13	32	32	66	40	41	0.06	0.04	0.12	0.27	0.04	0.07	13	44	49	66	39	50
17	-	0.19	-	2.27	0.23	0.31	-	59	-	163	27	40	-	0.15	0.11	2.29	0.34	0.29	-	45	30	163	35	38
18	0.73	-	0.16	0.44	0.10	0.16	16	-	5	49	33	63	0.62	-	0.18	0.45	0.12	0.11	14	-	7	48	44	50
19	5.91	0.85	0.14	-	0.51	-	84	19	2	-	34	-	5.91	0.84	0.17	0.07	0.62	-	84	18	3	1	39	-
20	0.43	0.26	0.36	1.55	0.05	0.24	7	10	20	168	27	42	0.43	0.19	0.29	1.55	0.13	0.20	7	24	25	168	30	46
21	0.39	0.04	0.09	0.32	0.05	0.06	18	7	20	54	34	48	0.38	0.04	0.12	0.30	0.05	0.10	17	17	26	53	46	66
22	2.12	0.20	0.43	0.21	0.61	0.64	68	21	19	8	34	27	2.12	0.22	0.44	0.22	0.58	0.67	68	20	15	9	34	33
median	0.63	0.19	0.25	0.54	0.17	0.18	23	19	20	47	36	34	0.57	0.19	0.29	0.66	0.20	0.20	17	20	25	48	40	35

Supplemental table 3 - Signal-to-noise ratio (SNR) and time accuracy of corresponding fractionation per patient

	Observer 1												Observer 2											
	SNR						Time accuracy (ms)						SNR						Time accuracy (ms)					
	Epicardium			Endocardium			Epicardium			Endocardium			Epicardium			Endocardium			Epicardium			Endocardium		
no.	uni	bi-x	bi-y	uni	bi-x	bi-y	uni	bi-x	bi-y	uni	bi-x	bi-y	uni	bi-x	bi-y	uni	bi-x	bi-y	uni	bi-x	bi-y	uni	bi-x	bi-y
1	31	13	20	28	17	11	2	3	1	5	4	3	31	16	23	45	15	12	2	3	1	4	3	3
2	22	8	4	8	4	2	0	1	2	1	0	4	24	8	6	7	3	3	0	1	1	1	0	4
3	13	19	4	25	15	4	1	2	4	3	2	3	10	19	4	26	19	4	1	1	3	3	1	3
4	5	8	4	6	9	3	4	2	3	4	3	3	5	8	4	6	11	3	3	3	3	3	3	4
5	17	12	6	20	10	7	1	5	2	2	5	3	20	9	3	60	13	7	0	5	1	3	5	3
6	3	3	3	16	14	9	4	3	2	0	1	0	2	5	4	16	13	9	3	2	5	0	1	0
7	3	12	17	15	15	10	0	4	4	0	1	1	1	15	16	15	11	10	3	4	4	0	2	1
8	20	2	10	2	2	2	1	3	2	1	1	2	20	3	7	2	2	2	1	3	2	1	1	2
9	3	13	14	34	17	11	5	2	3	4	2	1	3	14	17	34	18	10	4	2	2	4	2	1
10	12	21	4	2	4	-	5	3	3	2	4	-	12	20	4	-	5	-	5	3	3	-	3	-
11	8	10	7	17	4	3	6	5	3	5	5	3	8	11	9	15	4	4	6	6	5	5	5	5
12	13	2	3	10	6	3	2	2	3	2	2	2	13	1	3	10	6	5	3	3	3	2	2	2
13	16	12	6	10	12	2	3	1	2	2	1	3	16	12	7	10	18	2	3	1	2	2	4	3
14	3	4	2	3	1	1	1	6	4	2	4	2	3	5	2	-	2	1	1	6	4	-	6	2
15	30	9	18	-	4	-	4	2	3	-	2	-	32	27	23	-	4	-	4	2	4	-	2	-
16	2	4	2	7	3	2	2	3	0	4	1	3	1	4	4	7	3	2	3	3	0	4	1	4
17	-	7	-	47	14	5	-	1	-	5	2	3	-	7	2	47	27	5	-	2	2	5	2	3
18	28	-	5	11	5	5	0	-	3	3	2	2	22	-	7	10	6	3	0	-	4	3	2	2
19	202	71	4	-	47	-	3	3	3	-	1	-	202	69	7	5	86	-	3	3	2	0	1	-
20	9	21	13	23	4	6	3	3	2	3	3	4	9	16	11	23	10	4	3	2	2	3	3	4
21	5	1	2	4	1	1	1	4	6	4	3	4	5	1	2	4	1	2	1	5	6	4	3	5
22	33	10	5	3	23	7	1	2	1	1	2	2	33	9	4	3	24	7	1	2	2	1	1	3
median	13	10	5	11	8	4	2	3	3	3	2	3	12	9	5	10	10	4	3	3	3	3	2	3

Supplemental table 4 – Percentage of electrograms with additional fractionation per patient

	Observer 1						Observer 2					
	Epicardium			Endocardium			Epicardium			Endocardium		
no.	uni	bi-x	bi-y	uni	bi-x	bi-y	uni	bi-x	bi-y	uni	bi-x	bi-y
1	100	100	100	75	100	77	100	100	100	75	89	77
2	0	100	25	0	100	50	6	100	25	0	100	100
3	33	71	73	56	71	87	30	48	70	52	76	67
4	0	8	63	0	69	38	0	8	38	0	46	25
5	84	72	91	93	94	98	45	76	77	84	94	98
6	0	62	31	11	92	92	0	62	77	11	100	77
7	60	43	71	80	57	100	60	14	14	80	57	86
8	100	100	100	95	100	60	95	100	90	95	100	50
9	60	100	75	0	100	88	80	100	75	0	100	88
10	50	50	56	92	80	0	50	50	67	33	80	22
11	3	23	8	63	77	78	3	21	3	57	77	63
12	100	0	38	100	25	50	100	0	50	100	25	63
13	0	25	8	11	38	83	0	25	17	11	0	83
14	40	32	63	92	5	0	52	32	52	88	26	4
15	86	22	100	0	67	50	57	11	50	0	67	50
16	78	100	71	89	100	21	78	100	79	78	100	29
17	0	25	4	47	96	83	0	29	9	40	92	83
18	35	0	20	88	100	87	12	0	0	88	100	60
19	0	100	100	33	50	50	0	100	100	0	50	0
20	9	67	50	22	91	36	9	36	45	22	58	55
21	38	80	68	28	33	20	62	61	68	26	35	56
22	57	65	86	71	90	93	50	55	71	71	85	64
median	39	63	65	59	85	68	48	49	59	46	78	63

Supplemental table 5 – Average number of additional fractionation per electrogram per patient

	Observer 1						Observer 2					
	Epicardium			Endocardium			Epicardium			Endocardium		
no.	uni	bi-x	bi-y	uni	bi-x	bi-y	uni	bi-x	bi-y	uni	bi-x	bi-y
1	1	3	4	1	2	2	1	3	4	1	2	1
2	0	2	1	0	1	1	0	2	1	0	3	1
3	0	2	1	1	2	2	0	2	1	1	2	1
4	0	0	1	0	1	0	0	0	1	0	1	0
5	1	3	3	2	5	5	1	2	2	1	4	4
6	0	1	0	0	2	1	0	1	1	0	3	2
7	1	1	1	1	1	3	1	0	0	1	1	2
8	1	2	1	2	3	1	1	1	1	1	3	1
9	1	3	1	0	2	3	1	3	2	0	3	2
10	1	1	1	1	1	0	1	1	1	0	1	0
11	0	0	0	1	2	2	0	0	0	1	2	1
12	2	0	0	2	0	1	2	0	1	2	0	1
13	0	0	0	0	0	1	0	0	0	0	0	1
14	0	0	1	1	0	0	1	0	1	1	0	0
15	1	0	2	0	1	1	1	0	1	0	1	1
16	1	3	1	1	2	0	1	3	1	1	2	0
17	0	1	0	1	4	2	0	1	0	1	3	3
18	0	0	0	1	2	2	0	0	0	1	3	1
19	0	2	3	0	1	1	0	2	3	0	1	0
20	0	1	1	0	1	0	0	0	1	0	1	1
21	0	1	1	0	0	0	1	1	1	0	0	1
22	1	2	2	1	3	2	1	2	2	1	3	1
median	0	1	1	1	2	1	1	1	1	1	2	1

10

The impact of obesity on early postoperative atrial fibrillation burden

Corina Serban
Johnmary T. Arinze
Roeliene Starreveld
Eva A.H. Lanters
Ameeta Yaksh
Charles Kik
Yalin Acardag
Paul Knops
Ad J.J.C. Bogers
Natasja M.S. de Groot

Journal of Thoracic and Cardiovascular Surgery. 2020 Mar;159(3):930-938

Abstract

Background

Obesity has been linked to development of postoperative atrial fibrillation (PoAF). This study is aimed at investigating the role of BMI in the evolution of de-novo, early PoAF by assessing differences between obese and non-obese patients undergoing cardiac surgery.

Methods

Patients with early de-novo PoAF were included. Continuous cardiac rhythms were recorded during the first 5 postoperative days in obese (N=67, 66 ± 9 years; 51 (76%) male) and non-obese (N=89, 69 ± 9; 75 (84%) male) patients without an AF history undergoing cardiac surgery. PoAF burden was defined as the ratio between total duration of all AF episodes and total recording time (AFB(%)).

Results

A total of 1191 (median: 5/patient) PoAF episodes were identified in the obese group compared to 1218 (median: 4/patient) in the non-obese group. The median duration and number of prolonged (>60 minutes) PoAF episodes was higher in obese patients (250 versus 145 minutes, p=0.003 and median of 2 versus 1 episode, p=0.031). Obesity was associated with a larger early PoAF burden (obese patients: median 7%; IQR: 2.5-19.7% versus non-obese patients: median 3.2%; IQR: 0.5-8.8%, p=0.001) mainly on the third postoperative day (p=0.021).

Conclusions

Obesity predisposes to a larger number of prolonged AF episodes in the early, postoperative period after cardiac surgery for coronary artery disease and/or valvular heart disease. The higher AF burden in the early postoperative period occurred particularly on the third day. Future studies will determine whether obesity prevention may play a key role in reducing the incidence of PoAF in patients undergoing cardiac surgery.

Introduction

Obesity is a worldwide epidemic affecting people of all ages. There is strong evidence that obesity is a predictor for development of atrial fibrillation (AF).[1-4] The association between obesity and evolution of AF is multifactorial and still incompletely elucidated. Prior studies have demonstrated that metabolic syndrome, ischemic heart disease, local and systemic inflammatory processes, epicardial fat distribution, cardiac remodelling and genetic factors play an important role in AF development.[3, 5] In mice, obesity is associated with reversible ionic remodelling of the left atrial appendage (LAA) resulting in higher incidence of AF inducibility and burden.[6, 7]

Obesity is becoming more prevalent in patients undergoing cardiac surgery, particularly in those referred for coronary artery bypass grafting (CABG) and is associated with an increase in the short and long-term postoperative morbidity and mortality.[4, 8-12] De-novo postoperative atrial fibrillation (PoAF) is a common complication that occurs more frequently in obese patients.[13-16] However, characteristics of de-novo early PoAF (EPoAF) episodes including the number and duration of PoAF episodes in obese patients have so far not been investigated.

Therefore, the purpose of our study is to investigate the role of BMI in the characteristics of de-novo PoAF by assessing differences between obese and non-obese patients undergoing cardiac surgery with regards to EPoAF episodes.

Methods

This study was conducted as part of two prospective observational projects including Quest for Arrhythmogenic Substrate of Atrial fibrRillation (QUASAR, MEC 2010-054) and Hsf1 Activators Lower cardiomyocyte damage Towards a novel approach to REVERSE atrial fibrillation (HALT & REVERSE, MEC 2014-393). Both projects were approved by the local ethics committee of the Erasmus Medical Centre and adhere to the Declaration of Helsinki principles. Accordingly, written consent was obtained from participating patients before surgical intervention.

Study population

The study population consisted of adult patients scheduled for elective cardiac surgery for coronary artery disease (CAD), either isolated or in combination with aortic (CAD+AVD) or mitral (CAD+MVD) valve disease, isolated aortic (AVD) or mitral (MVD) valve disease. Patients presenting early PoAF were included. Exclusion criteria were history of AF, prior ablation of atrial tachyarrhythmias, severe renal failure, patients with an atrial pacing device and requiring mechanical or inotropic

support. Patients scheduled for elective cardiac surgery for congenital heart defects (CHD) were also excluded. The sample was divided into two categories: 1) obese (BMI ≥ 30) and 2) non-obese (BMI < 30) patients.

Automatic detection of early postoperative atrial fibrillation

Cardiac rhythms of every patient were continuously recorded during the first 5 postoperative days using bedside monitors (Draeger Infinity™). All postoperative continuous rhythm registrations (.CPZ) were converted into a MATLAB compatible format (.ECG) prior to analysis. Algorithms were used to detect the start and ending of each AF episode from the moment of arrival on the surgical ward to the end of the 5th postoperative day. All PoAF episodes detected by the software were cross-checked in Synescope by two blinded operators in order to eliminate potential false positive registrations induced by artefacts. Additionally, ECGs and patients records were manually evaluated for the presence of AF during the first 5 days of postoperative hospitalization.

Characterization of PoAF

PoAF was defined as a series of supraventricular beats with irregularly irregular R-R intervals, in the absence of P-waves, persisting for ≥ 30 seconds. For every patient, the number and duration of AF episodes in the continuous rhythm registrations were quantified manually and used to calculate the PoAF burden during the first 5 post-surgical days. The PoAF burden was defined as the ratio between the total duration of all AF episodes and the total recording time (AFB (%) = total time spent in AF (minutes) / recording time (minutes) * 100).

Antiarrhythmic treatment for early de-novo PoAF

On the first postoperative day, all patients received oral β-blocker, starting with a dose of 25 mg twice daily. Patients with PoAF were cardioverted to sinus rhythm (SR) within 48 hours using intravenous bolus of amiodarone 300 mg. Amiodarone was discontinued when AF converted to SR. If conversion was not achieved within less than 48 hours from PoAF onset, electrical cardioversion was performed and anticoagulant therapy was started combined with oral amiodarone 200 mg three times daily for another 4 days. Patients who were hemodynamically unstable at PoAF onset were electrically cardioverted to SR followed by 4 days of oral amiodarone 200 mg three times daily. If AF was accepted, the β-blocker dosage was increased if HR>110 bpm.

Statistical analysis

Statistical analysis was performed using the IBM SPSS Statistics 24 software (Corp., Armonk, NY software). Data were tested using Shapiro Wilk test of normality. Continuous, normally distributed data is expressed as mean ± SD and skewed data as median and interquartile range (IQR) (P25/P75). Student's T-test was used to

compare normally distributed continuous variables, while skewed parameters were compared using Mann-Whitney-U-test. Comparisons between related skewed variables were performed using Wilcoxon test. Variability between and within groups was assessed using ANOVA. Categorical variables were compared using Chi-Square test and are presented as percentages. Bonferroni correction was used to adjust p value for multiple comparisons. Possible factors associated with early PoAF burden were introduced in a linear regression analysis. PoAF burden was transformed using the logarithm function. The variables manually introduced in the linear regression model included all the baseline clinical characteristics presented in *Table 1*, provided that the model maintained significance. Pearson correlation test was used to evaluate the linear relationship between continuous variables. A two-sided P-value of <0.05 was considered statistically significant.

Results

Study population

Baseline characteristics of both the obese (N=67, 66 ± 9 years; 51 (76%) male) and non-obese group (N=89, 69 ± 9; 75 (84%) male) are presented in *Table 1*. Clinical characteristics between the obese and non-obese group only differed in age (66 ± 9.7 years versus 69 ± 9.2 years; P=0.024), BMI (32.4 ± 2.3 versus 25.2 ± 4.3; P<0.001) and incidence of diabetes mellitus (DM) (N=21 (31.3%) versus N=12 (13.4%); P=0.01). Coronary artery bypass grafting (CABG) was the main surgical procedure performed in both groups (42 (63%) obese patients and 50 (56%) non-obese patients).

Table 1 – Patient characteristics

	Obese patients (BMI ≥ 30) (N=67)	**Non-obese patients (BMI < 30) (N=89)**	**P-value**
Age (y)	66.1 ± 9.7	69.1 ± 9.2	0.027
Male	51 (76)	75 (84)	0.223
BMI	32.4 ± 2.3	25.2 ± 4.3	<0.001
Risk factors			
- Hypertension	34 (50)	42 (47)	0.747
- Diabetes mellitus	21 (31.3)	12 (13.4)	0.018
- Dyslipidemia	19 (28.3)	36 (40.4)	0.130
Left ventricular function			0.361
- Normal (EF>55%)	42 (62.6)	62 (63.2)	
- Mild impairment (EF 46-55%)	15 (22.3)	21 (23.5)	
- Moderate impairment (EF 36-45%)	5 (7.5)	4(4.5)	
- Severe impairment (EF<35%)	5 (7.5)	2(2.24)	
Left atrial dilatation (diameter ≥45 mm)	14 (21)	16 (18)	0.205
CHA_2DS_2-VASc score			0.229
- Low (0)	5 (7.4)	10 (11.2)	
- Low-moderate (1)	13 (19.4)	27 (30.3)	
- Moderate-high (≥2)	49 (73.1)	52 (58.4)	
Preoperative medication			
- Anti-arrhythmic drugs			
Class II	46 (68.6)	59 (66.2)	0.863
Class IV	2 (3)	4 (4.4)	0.467
- ACE inhibitors/AG-II	42 (62.6)	49 (55)	0.412
Surgical procedure			0.307
- CABG	42 (62.6)	50 (56)	
- AVD	11 (16.4)	10 (11.2)	
- MVD	4 (6)	5 (5.6)	
- CABG+AVD	8 (11.9)	14 (15.7)	
- CABG+MVD	2 (3)	10 (11.2	

Values are presented as mean ± standard deviation or as N (%). BMI, body mass index; EF, ejection fraction; CABG, coronary artery bypass grafting; AVD, aortic valve disease; MVD, mitral valve disease.

Duration of postoperative atrial fibrillation episodes

In the postoperative rhythm registrations, 1191 PoAF episodes were identified in the obese group and 1218 in the non-obese group. Characteristics of PoAF episodes for obese and non-obese patients are depicted in *Table 2*. In the obese and non-obese groups, the median number of PoAF episodes per patient was respectively 5 (IQR:2-16) and 4 (IQR:2-15). *Figure 1* shows that the median duration of PoAF episodes was higher in obese (median 294.5 ; IQR 105.5-1036.5; minutes) compared to non-obese patients (median 182.5; IQR 22.5-498.3 minutes, p=0.008).

Table 2 – Characteristics of PoAF episodes

	Obese patients		Non-obese patients	
Time (minutes)	**Number of PoAF episode(s)**	**Duration of PoAF episode(s) (minutes)**	**Number of PoAF episode(s)**	**Duration of PoAF episode(s) (minutes)**
0-5	746; 3.5 (1-14)	89.25; 1.5 (1-2.5)	834; 7 (2-14)	94; 1.5 (1-2)
5.5-10	128; 2 (1-5)	190.25; 7 (6-7.25)	116; 2 (1-5)	238.5; 7(6-8.5)
10.5-15	55; 1 (1-4)	265; 12.75 (12-13.5)	62; 2 (1-4)	275.75; 12.75 (11.43-13.5)
15.5-20	36; 1(1-2.75)	284.5; 17.6 (17-18.5)	20; 1 (1-2)	351; 19 (17.75-19.75)
20.5-25	20; 1 (1-2.5)	198.5; 22 (21.25-22.75)	19; 1 (1-2)	245; 21.5 (20.5-23.75)
25.5-30	12; 1	299.75; 27 (26-28)	13; 1	303; 27 (26-28.5)
30.5-35	20; 1 (1-2)	390.2; 33 (31-33.5)	8; 1	229.5; 32.5 (32-33.5)
35.5-40	14; 1 (1-2)	407.25; 36.5 (36.5-38.5)	10; 1	378; 38.25 (36.25-39.5)
40.5-45	11; 1	425.25; 42.3 (41.87-43.25)	9; 1 (1-2)	300.5; 42.75 (42-44)
45.5-50	6; 1 (1-5)	240.5; 49 (46.25-49.5)	5; 1	338.5; 49 (47-50)
50.5-55	9; 1	422; 52.5 (51.5-54)	10; 1	311.75; 51.37 (50.5-53.5)
55.5-60	7; 1 (1-2)	266; 56.5 (56.1-56.8)	14; 1 (1-1.5)	518.75; 58 (56.5-58.6)

The number and duration of postoperative atrial fibrillation (PoAF) episodes are categorized according to their duration. Values are presented as total, median (IQR).

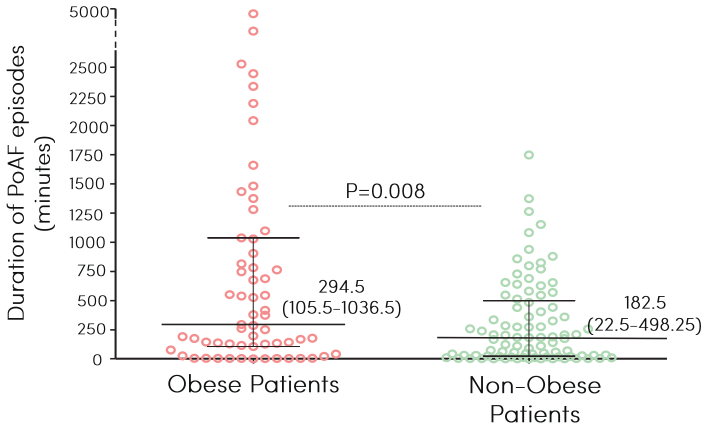

Figure 1 – Scatter plot demonstrating the relative frequency distribution of the duration of all PoAF episodes. There is a significantly higher duration of early PoAF episodes in obese patients (median 294.5; IQR 105.5-1036.5) compared to non-obese patients (median 182.5; IQR 22.5-498.25) (p=0.008). The thick black lines indicate the median and the thin lines the IQR (P25/P75). PoAF, postoperative atrial fibrillation;

The median duration of PoAF episodes lasting longer than 60 minutes is depicted in *Figure 2*. There was a significant increase in the median duration of prolonged (>60 minutes) PoAF episodes in obese (250; IQR 135-421 minutes) compared to non-obese patients (145.4; IQR 97.4-252.4 minutes) (p=0.003). For episodes lasting between 30 seconds and one hour, no significant change in median duration of PoAF episodes was found between obese and non-obese patients.

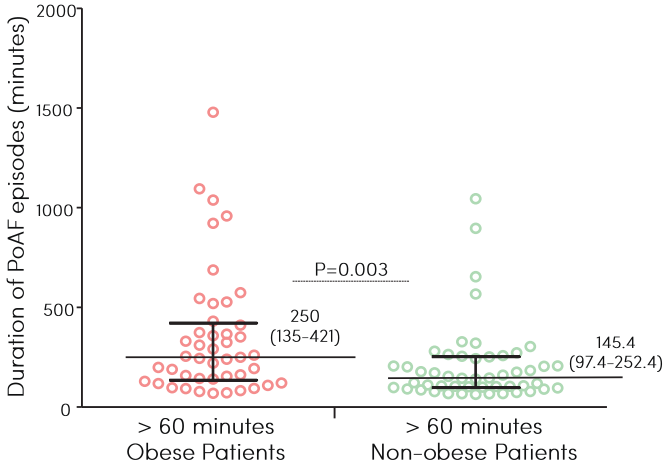

Figure 2 – Relative frequency distribution of the duration of PoAF episodes lasting longer than 60 minutes. In the obese group, there is a significant higher median time of prolonged PoAF episodes (p=0.003). The thick black lines indicate the median and the thin lines the IQR (P25/P75). PoAF: postoperative atrial fibrillation

Figure 3 depicts the median number of PoAF episodes for the obese and non-obese patients separately. As demonstrated in the upper panel of Figure 3, obese patients had significantly more prolonged PoAF episodes (episodes lasting >60 minutes) compared to non-obese patients (p=0.031). The lower panel of Figure 3 shows no significant difference in the median number of PoAF episodes lasting less than one hour between obese and non-obese patients.

In obese patients, the majority of PoAF episodes (746 (62.6%), median 3.5; IQR 1-14) terminated within 5 minutes; 318 episodes (27%, median 1; IQR 1.0-3.7) lasted between five and 60 minutes and one hundred and twenty PoAF episodes (10%, median 2; IQR 1-4%) had a duration longer than one hour. In non-obese patients, most of PoAF episodes (834, 68.4%, median 7; IQR 2-14) also terminated within 5 minutes and two hundred and eighty-six episodes (23%, median 1; IQR 1.0-3.7%) lasted between five minutes and one hour. However, only ninety-six PoAF episodes (8%, median 1; IQR 1-2) had a duration longer than 60 minutes.

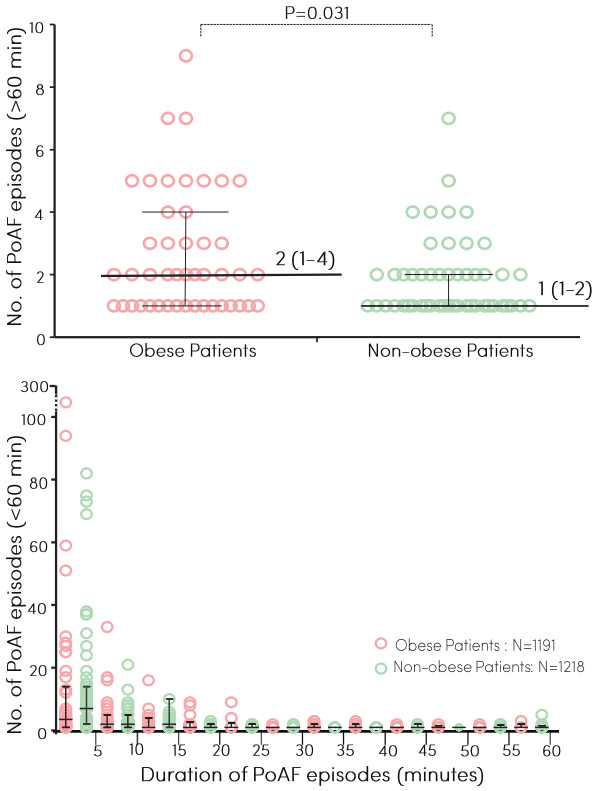

Figure 3 – Characteristics of PoAF episodes. *Upper panel*: the median number of PoAF episodes lasting longer than 60 minutes for obese and non-obese patients separately. There was a significantly higher number of prolonged PoAF episodes in obese patients (1191; median 2; IQR 1-4) compared to non-obese patients (1218; median 1; IQR 1-2) (p=0.031). *Lower panel*: the median number of PoAF episodes categorized individually between 30 seconds and 60 minutes. There was no significant difference in the number of episodes lasting less than one hour between obese and non-obese patients. Thick black lines indicate the median and thin lines the IQR (P25/P75). PoAF, postoperative atrial fibrillation; N, number of episodes

Burden of PoAF episodes

The PoAF burden for each patient individually is plotted in *Figure 4* and shows that the PoAF burden is larger in the obese patients (median 7%; IQR: 2.5-19.7%) compared to the non-obese patients (median 3.2%; IQR: 0.5-8.8%) (p=0.001).

Variables introduced in the linear regression model of early PoAF burden are shown in *Table 3*. The relationship between PoAF burden and possible associated factors is plotted in *Supplemental figure 1*. BMI was the only variable (β1=0.13, p=0.002) significantly correlated with early PoAF burden whereas age, gender and surgical procedure had no relationship.

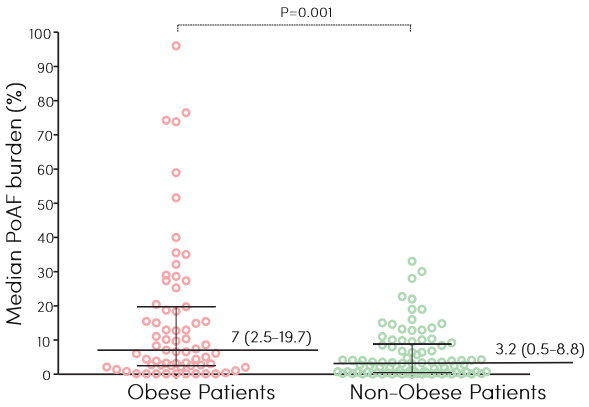

Figure 4 – Scatter plots demonstrating the relative frequency distribution of the PoAF burden (%) in obese and non-obese patients separately. There is a significantly higher early PoAF burden in obese patients (median 7 (IQR: 2.5-19.7)) compared to non-obese patients (median 3.2 (IQR: 0.5-8.8) (p=0.001). Thick black lines indicate the median and thin lines the IQR (P25/P75). PoAF, postoperative atrial fibrillation;

Table 3 – Multivariate analysis of predictors for early PoAF burden.

Variables	Beta (β)	95% CI for β	p-value
Body mass index	0.13	0.05 - 0.21	0.002
Age	0.02	-0.02 – 0.06	0.330
Gender	0.43	-0.44 – 1.29	0.328
Surgical procedure	0.09	-0.24 – 0.42	0.585

Supplemental figure 2 shows the PoAF burden and duration of PoAF episodes during the first five postoperative days separately. The upper panel shows that in the obese group the highest PoAF burden was observed on the third postoperative day (median 6.1%; IQR 1.3-13.7%). In non-obese patients, the highest PoAF burden occurred on the second postoperative day (median 3.5%; IQR 0.2-6.1%). The lower panel of *Supplemental figure 2* shows that obese patients spent the longest time in PoAF during the third postoperative day (median 316 minutes; IQR 93.4-779.3). In non-obese patients however, the longest time spent in PoAF was on the second postoperative day (median 194.5 minutes; IQR 11.8-355.8). At the third postoperative day, obese patients had longer PoAF episodes and higher PoAF burden compared to non-obese patients (median 135.8 minutes; IQR 18.4-443.9; p=0.035; median 2%; IQR 0.4-6.6%; p=0.021).

The relative frequency distribution of prolonged PoAF episodes for each of the first 5 postoperative days is depicted in *Table 4*. In both obese and non-obese groups, PoAF episodes lasting longer than 60 minutes occurred mainly on the second and third postoperative days. However, there was no significant difference in the incidence of prolonged PoAF episodes on either of the first five postoperative days.

Table 4 – Characteristics of PoAF burden, duration and number of prolonged (>60 minutes) PoAF episodes for each postoperative day

	Obese patients					**Non-obese patients**				
	Day 1	**Day 2**	**Day 3**	**Day 4**	**Day 5**	**Day 1**	**Day 2**	**Day 3**	**Day 4**	**Day 5**
PoAF burden (%) *median (IQR)*	0.24 (0.01-7.37)	3 (0.36-11.5)	6.1 (1.34-13.6)	3.83 (0.12-5.72)	0.42 (0.04-15.9)	0.15 (0.03-0.43)	3.5 (0.21-6.14)	2 (0.35-6.6)	0.7 (0.09-2.4)	1.4 (0.6-2.8)
PoAF duration (min) *median (IQR)*	12.5 (1-430.87)	175.5 (24.2 (658.2)	316 (93.3-779.2)	103 (5.25-273)	11 (1.5-1375)	6 (1-28.1)	194.7 (11.8-355.8)	135.7 (18.3-443.8)	49 (5.62-132.2)	69 (33-150.6)
Prolonged PoAF episodes %	6.25 (6/96)	14.05 (26/185)	8.92 (57/639)	12 (24/201)	10 (7/70)	10 (7/68)	15.4 (33/213)	9 (33/363)	6.6 (19/286)	3.8 (11/288)

PoAF, postoperative atrial fibrillation.

Clinical outcome

In the obese group, rate control therapy of PoAF was achieved with antiarrhythmic drugs including β1-blockers (N=43 patients, 64% [43/67]), Digoxin (N=10 patients, 15% [10/67]) or rhythm control with Amiodarone (N=15 patients, 22.3% [15/67]). In the non-obese group, therapy was aimed at either rate control in 79 patients (β1-blockers: N=63 patients, (70.7% [63/89]) and/or digoxin: N=16 patients, (18% [16/89])) or rhythm control in 20 patients (22.4% [20/89]). The efficacy of amiodarone in reducing or converting PoAF to sinus rhythm was similar in the obese and non-obese group (p=1.000).The effect of amiodarone was determined by calculating the difference in median duration of PoAF episodes and PoAF burden between the fifth postoperative day and the day prior to initiation of treatment.

There was no significant difference in both PoAF burden (obese patients: median (-11%); IQR (-14.9)-3.1%; non-obese patients: median (-4%); IQR (-9.2)-1.5%; p=0.059) and duration (obese patients: median -545; IQR (-817)-76 minutes; non-obese patients: (median (-319.2); IQR (-562.2)-103.0 minutes; p=0.298) of PoAF episodes before and after amiodarone administration. Additional electrical cardioversion rhythm was performed in 8 obese patients (12% [8/67]) and 6 non-obese patients (6.7% [6/89]) (p=0.274), resulting in SR in 3 obese patients (4.4% [3/67]) and all non-obese patients (6.7% [6/89]) (p=0.733).

Discussion

Key findings

The present study demonstrated that for patients presenting early PoAF, the burden is significantly higher in obese patients compared to non-obese patients. Overall, long PoAF episodes, lasting between 60 minutes and 24 hours occurred more frequently in the obese population. These long PoAF episodes occurred mainly on the third postoperative day. There was a significant relationship between BMI and PoAF burden.

Clinical relevance of de novo postoperative AF

De-novo early PoAF following cardiac surgery has been associated with increased rates of mortality, morbidity (e.g., stroke) and subsequently increased hospitalization time and readmissions. Several risk factors contribute to development of longer duration of PoAF including older age, male gender[4] and obesity[17]. Intra-operative factors (e.g., duration of cardioplegic arrest, postoperative inflammation) may affect atrial electrical properties, thus increasing the likelihood for AF development.[4, 18] Previous studies have demonstrated that de-novo onset PoAF predicts development of late PoAF, associated with an increased rate of hospital readmissions, cardiovascular events and even mortality.[19] The duration of PoAF episodes after cardiac surgery is also associated with decreased long-term

survival.[20] Sigurdsson et al. have demonstrated that survival was significantly worse in patients who experienced PoAF episodes lasting longer than two days. In our study, we found that the majority of PoAF episodes lasted less than five minutes in both obese (62.6%) and non-obese (68.4%) patients. Episodes lasting longer than one hour were significantly more likely to occur in obese patients (10%) compared to non-obese patients (8%). Thus, the combination between prolonged PoAF episodes and increased associated postoperative morbidity due to obesity[21], may also severely affect the survival and postoperative quality of life in obese patients.

De-novo early PoAF burden

The term AF burden is applied to describe the temporal dynamic pattern of AF, in terms of presence and duration of AF episodes, as detected by various devices (e.g., bedside monitors, Holter monitors, implantable devices). Accurate assessment of the AF burden is important as it is related to development of stroke.

Previous studies have demonstrated that BMI, a measure of overall adiposity, is a strong independent associated factor with not only AF but also PoAF.[22-24] In a meta-analysis of the association between obesity and PoAF in patients without previous history of AF, Phan et. al found that obesity was associated with a significant risk of PoAF. The assessment of de-novo early PoAF burden in obese patients however, has not been examined. In our study, we found that obese patients had a significantly higher PoAF burden during the first five postoperative days, when compared to the non-obese patients. Moreover, obese patients experienced more prolonged PoAF episodes, particularly on the third postoperative day. This is an important finding since prior studies have shown that prolonged episodes are associated with a high risk of stroke.[25]

In a pooled analysis performed by Boriani et al., the Cox regression analysis adjusted for CHADS2 and anticoagulants at baseline demonstrated that the AF burden was an independent predictor of stroke and a threshold of 1 hour was associated with the highest HR for stroke (i.e. 2.11 (95% CI 1.22-3.64, p=0.008).[26]

Our study showed that a 0.13 unit increase in BMI resulted in an increase in early PoAF burden (p=0.002). Even though our data showed no significant relationship between age, gender or surgical procedure and PoAF burden, they could still play an important role in the incidence of early de-novo PoAF in a larger population. Other clinical factors such as subcutaneous fat, visceral fat including epicardial adipose tissue (EAT) could contribute to the increase in PoAF burden in obese patients as well. EAT has not been assessed in our study, however it is positively correlated with BMI.[27] EAT also plays an important role in AF pathophysiology by modifying the atrial substrate through the release of inflammatory cytokines as well as adipokines into adjacent myocardium.[28] In addition, experimental studies have shown that weight loss can reduce AF burden and obesity related ionic remodelling.[7]

Age and incidence of DM at baseline were different in our population. Non-obese patients were older than obese patients and the incidence of DM was significantly lower in the non-obese group (*Table 1*). However, no relationship was found between either age or incidence of DM and early PoAF burden. The remainder of baseline characteristics were similar between the obese and non-obese group, yet this may depend on the sample size. Hypertension is associated with obesity and is more frequently encountered in patients with PoAF.[24, 29] The majority of our obese patients were hypertensive (50%), but the incidence did not differ from the non-obese group.

Therapy of early PoAF

In our study, we found that amiodarone did not affect the overall number or duration of PoAF episodes.. Previous studies have shown that intravenous amiodarone significantly decreases the incidence of PoAF if administered before[30] or immediately after completion of the surgical procedure[31]. Further research is needed in assessing whether amiodarone is beneficial in reducing the incidence of the PoAF burden.

Conclusions

Obesity predisposes to a larger number of prolonged AF episodes in the early, postoperative period after cardiac surgery for coronary artery disease and/or valvular heart disease. The higher AF burden in the early postoperative period occurred particularly on the third day. In order to determine the impact of the early PoAF burden on long-term clinical outcome, further larger prospective studies are mandatory. Since the effects of obesity on the AF substrate is reversible with weight control, preventive life style prior to cardiac surgery may play an invaluable role.

References

1. Go AS, Hylek EM, Phillips KA, Chang Y, Henault LE, Selby JV and Singer DE. Prevalence of diagnosed atrial fibrillation in adults: national implications for rhythm management and stroke prevention: the AnTicoagulation and Risk Factors in Atrial Fibrillation (ATRIA) Study. *JAMA*. 2001;285:2370-5.
2. Ahlsson A, Fengsrud E, Bodin L and Englund A. Postoperative atrial fibrillation in patients undergoing aortocoronary bypass surgery carries an eightfold risk of future atrial fibrillation and a doubled cardiovascular mortality. *Eur J Cardiothorac Surg*. 2010;37:1353-9.
3. Goudis CA, Korantzopoulos P, Ntalas IV, Kallergis EM and Ketikoglou DG. Obesity and atrial fibrillation: A comprehensive review of the pathophysiological mechanisms and links. *J Cardiol*. 2015;66:361-9.
4. Almassi GH, Schowalter T, Nicolosi AC, Aggarwal A, Moritz TE, Henderson WG, Tarazi R, Shroyer AL, Sethi GK, Grover FL and Hammermeister KE. Atrial fibrillation after cardiac surgery: a major morbid event? *Ann Surg*. 1997;226:501-11; discussion 511-3.
5. Lin YK, Chen YJ and Chen SA. Potential atrial arrhythmogenicity of adipocytes: implications for the genesis of atrial fibrillation. *Med Hypotheses*. 2010;74:1026-9.
6. Savio-Galimberti E. Weight loss reverses ionic remodeling responsible for increased atrial fibrillation inducibility and burden in high-fat diet induced obese mice [Abstract]. *American Heart Association's 2016 Scientific Sessions and Resuscitation Science Symposium*. 2016.
7. Savio-Galimberti E, Kannankeril P, Wasserman D and Darbar D. Weight loss reduces atrial fibrillation inducibility and burden in severe obesity induced by either high-fat diet or genetic hyperphagia in mice[Abstract]. *American Heart Association's 2015 Scientific Sessions and Resuscitation Science Symposium*. 2015.
8. Lauer MS, Eagle KA, Buckley MJ and Desanctis RW. Atrial-Fibrillation Following Coronary-Artery Bypass-Surgery. *Prog Cardiovasc Dis*. 1989;31:367-378.
9. Hravnak M, Hoffman LA, Saul MI, Zullo TG, Whitman GR and Griffith BP. Predictors and impact of atrial fibrillation after isolated coronary artery bypass grafting. *Crit Care Med*. 2002;30:330-337.
10. Zaman AG, Archbold RA, Helft G, Paul EA, Curzen NP and Mills PG. Atrial fibrillation after coronary artery bypass surgery: a model for preoperative risk stratification. *Circulation*. 2000;101:1403-8.
11. Mathew JP, Parks R, Savino JS, Friedman AS, Koch C, Mangano DT and Browner WS. Atrial fibrillation following coronary artery bypass graft surgery - Predictors, outcomes, and resource utilization. *Jama-J Am Med Assoc*. 1996;276:300-306.
12. Amar D, Shi W, Hogue CW, Zhang H, Passman RS, Thomas B, Bach PB, Damiano R and Thaler HT. Clinical prediction rule for atrial fibrillation after coronary artery bypass grafting. *Journal of the American College of Cardiology*. 2004;44:1248-1253.
13. Yaksh A, Kik C, Knops P, van Ettinger MJ, Bogers AJ and de Groot NM. Early, de novo atrial fibrillation after coronary artery bypass grafting: Facts and features. *Am Heart J*. 2017;184:62-70.
14. Zacharias A, Schwann TA, Riordan CJ, Durham SJ, Shah AS and Habib RH. Obesity and risk of new-onset atrial fibrillation after cardiac surgery. *Circulation*. 2005;112:3247-55.

15. Kuduvalli M, Grayson AD, Oo AY, Fabri BM and Rashid A. Risk of morbidity and in-hospital mortality in obese patients undergoing coronary artery bypass surgery. *Eur J Cardiothorac Surg*. 2002;22:787-93.
16. Gao M, Sun J, Young N, Boyd D, Atkins Z, Li Z, Ding Q, Diehl J and Liu H. Impact of Body Mass Index on Outcomes in Cardiac Surgery. *J Cardiothorac Vasc Anesth*. 2016;30:1308-16.
17. Sun X, Boyce SW, Hill PC, Bafi AS, Xue Z, Lindsay J and Corso PJ. Association of body mass index with new-onset atrial fibrillation after coronary artery bypass grafting operations. *Ann Thorac Surg*. 2011;91:1852-8.
18. Mathew JP, Fontes ML, Tudor IC, Ramsay J, Duke P, Mazer CD, Barash PG, Hsu PH, Mangano DT, Investigators of the Ischemia R, Education F and Multicenter Study of Perioperative Ischemia Research G. A multicenter risk index for atrial fibrillation after cardiac surgery. *JAMA*. 2004;291:1720-9.
19. Lee SH, Kang DR, Uhm JS, Shim J, Sung JH, Kim JY, Pak HN, Lee MH and Joung B. New-onset atrial fibrillation predicts long-term newly developed atrial fibrillation after coronary artery bypass graft. *Am Heart J*. 2014;167:593-600 e1.
20. Sigurdsson MI, Longford NT, Heydarpour M, Saddic L, Chang TW, Fox AA, Collard CD, Aranki S, Shekar P, Shernan SK, Muehlschlegel JD and Body SC. Duration of Postoperative Atrial Fibrillation After Cardiac Surgery Is Associated With Worsened Long-Term Survival. *Ann Thorac Surg*. 2016;102:2018-2026.
21. Jongnarangsin K, Chugh A, Good E, Mukerji S, Dey S, Crawford T, Sarrazin JF, Kuhne M, Chalfoun N, Wells D, Boonyapisit W, Pelosi F, Jr., Bogun F, Morady F and Oral H. Body mass index, obstructive sleep apnea, and outcomes of catheter ablation of atrial fibrillation. *J Cardiovasc Electrophysiol*. 2008;19:668-72.
22. Esato M, Shimizu A, Chun YH, Tatsuno H, Yamagata T and Matsuzaki M. Electrophysiologic effects of a class I antiarrhythmic agent, cibenzoline, on the refractoriness and conduction of the human atrium in vivo. *J Cardiovasc Pharmacol*. 1996;28:321-7.
23. Wang TJ, Parise H, Levy D, D'Agostino RB, Sr., Wolf PA, Vasan RS and Benjamin EJ. Obesity and the risk of new-onset atrial fibrillation. *Jama*. 2004;292:2471-7.
24. Phan K, Khuong JN, Xu J, Kanagaratnam A and Yan TD. Obesity and postoperative atrial fibrillation in patients undergoing cardiac surgery: Systematic review and meta-analysis. *Int J Cardiol*. 2016;217:49-57.
25. Boriani G, Diemberger I, Ziacchi M, Valzania C, Gardini B, Cimaglia P, Martignani C and Biffi M. AF burden is important - fact or fiction? *Int J Clin Pract*. 2014;68:444-52.
26. Boriani G, Glotzer TV, Santini M, West TM, De Melis M, Sepsi M, Gasparini M, Lewalter T, Camm JA and Singer DE. Device-detected atrial fibrillation and risk for stroke: an analysis of >10,000 patients from the SOS AF project (Stroke preventiOn Strategies based on Atrial Fibrillation information from implanted devices). *Eur Heart J*. 2014;35:508-16.
27. Rabkin SW. The relationship between epicardial fat and indices of obesity and the metabolic syndrome: a systematic review and meta-analysis. *Metab Syndr Relat Disord*. 2014;12:31-42.
28. Zghaib T, Ipek EG, Zahid S, Balouch MA, Misra S, Ashikaga H, Berger RD, Marine JE, Spragg DD, Zimmerman SL, Zipunnikov V, Trayanova N, Calkins H and Nazarian S. Association of left atrial epicardial adipose tissue with electrogram bipolar voltage and fractionation: Electrophysiologic substrates for atrial fibrillation. *Heart Rhythm*. 2016;13:2333-2339.
29. Stamou SC, Nussbaum M, Stiegel RM, Reames MK, Skipper ER, Robicsek F

and Lobdell KW. Effect of body mass index on outcomes after cardiac surgery: is there an obesity paradox? *Ann Thorac Surg*. 2011;91:42-7.
30. Guarnieri T, Nolan S, Gottlieb SO, Dudek A and Lowry DR. Intravenous amiodarone for the prevention of atrial fibrillation after open heart surgery: the Amiodarone Reduction in Coronary Heart (ARCH) trial. *J Am Coll Cardiol*. 1999;34:343-7.
31. Hohnloser SH, Meinertz T, Dammbacher T, Steiert K, Jahnchen E, Zehender M, Fraedrich G and Just H. Electrocardiographic and antiarrhythmic effects of intravenous amiodarone: results of a prospective, placebo-controlled study. *Am Heart J*. 1991;121:89-95.

Supplemental material

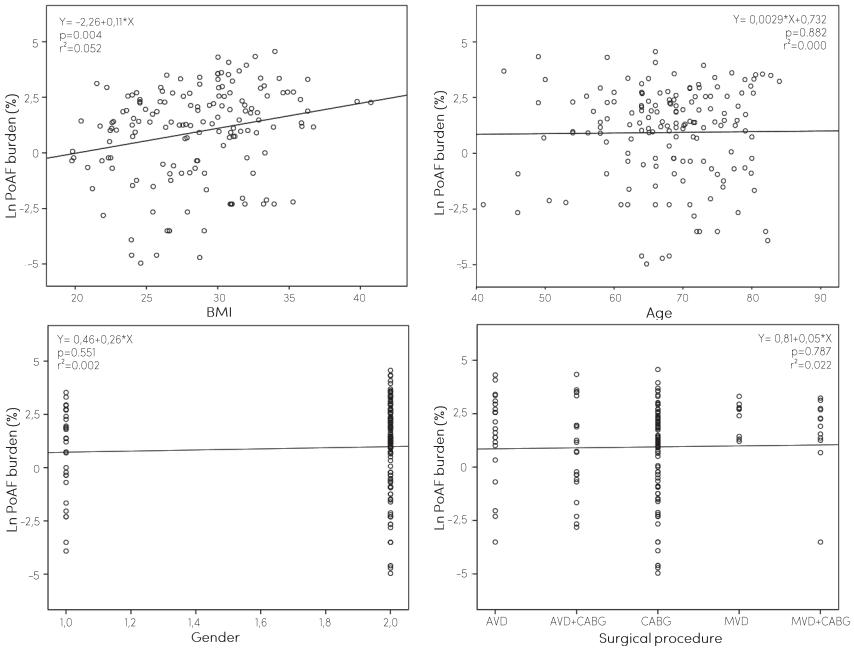

Supplemental figure 1 – Scatterplots of the linear correlations and their intercepts between the natural logarithm of PoAF and independent variables. The upper left panel shows the relationship between BMI and PoAF burden. There is a small (r^2=0.052) but significant linear association between BMI and PoAF(p=0.004). The upper right panel shows the relationship between age and PoAF burden. There is no significant association between the two variables (r^2=0.000, p=0.882). The lower left and right panels shows the association between PoAF burden and gender and surgical procedure respectively. No significant relationship was found between either gender (r^2=0.002; p=0.551) or surgical procedure (r^2=0.022; p=0.787) and PoAF burden. PoAF, postoperative atrial fibrillation; Ln PoAF, natural logarithm of postoperative atrial fibrillation; AVD, atrial valve disease; CABG, coronary artery bypass grafting; MVD, mitral valve disease; r^2, coefficient of determination.

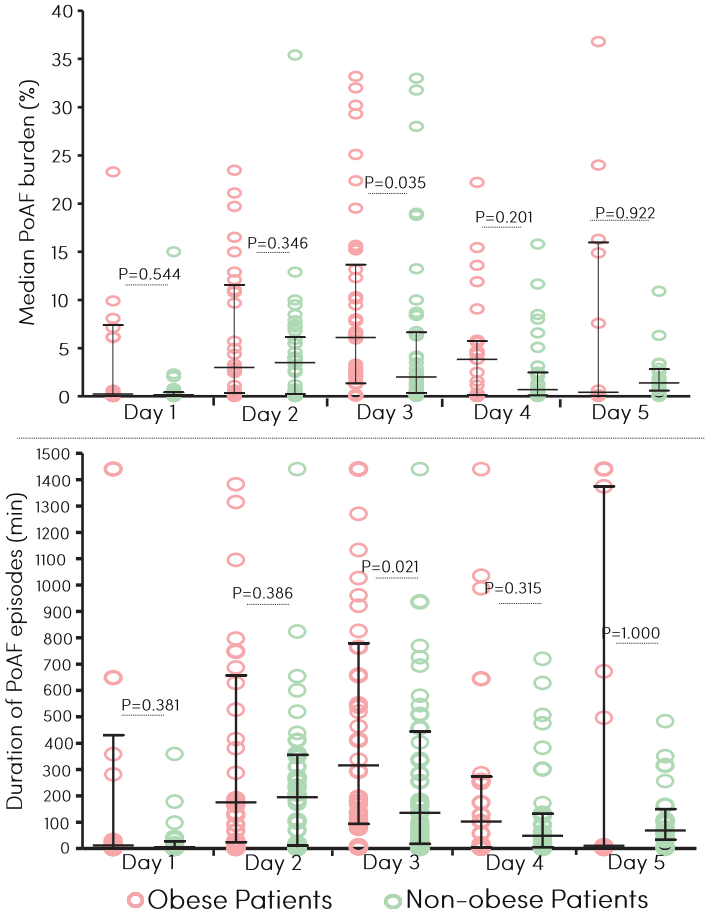

Supplemental figure 2 – Daily analysis of PoAF episodes lasting >60 minutes. *Upper panel*: the relative frequency distribution of PoAF burden for each of the five postoperative days individually. On the third postoperative day, there is an increase in the PoAF burden in the obese group (median 6.1%; IQR 1.3-13.6%) compared to the non-obese group (median 2; IQR 0.4-6.6) (p=0.031). *Lower panel*: the relative frequency distribution of the median time spent in AF on each of the 5 postoperative days individually. Obese patients (median 316 minutes; IQR 93.3-779.2) spent longer time in AF compared to non-obese patients (median 135.7 minutes; IQR 18.3-443.8) (p=0.021) during the third postoperative day. PoAF, postoperative atrial fibrillation; IQR, inter-quartile range.

12

Biomarkers to non-invasively determine the atrial fibrillation progression phenotype: a bridge to individualized ablative therapy?

Roeliene Starreveld
Natasja M.S. de Groot

Editorial to manuscript of Büttner et al. Heart Rhythm. 2018 Aug;15(8):1138-1139

Finding the adequate therapy for patients with atrial fibrillation (AF) can often feel like a never-ending challenge. Although AF represents the most common age-related, progressive cardiac arrhythmia worldwide, there still is no curative therapy. Ablative therapy seemed promising, but many patients have recurrences or require multiple ablation procedures. Pulmonary vein isolation (PVI) is like flipping a coin, as single-procedure freedom from atrial arrhythmia at long-term follow-up is only ~50% in the overall population.[1] Progression of the disease, i.e. from paroxysmal to persistent AF, entails even worse ablation success (54% vs. 42% at 5-years follow-up, respectively).[1] Especially for patients with persistent AF, multiple ablative strategies in addition to PVI have been proposed, including linear ablation and targeting of complex fractionated atrial electrograms (CFAE). The STAR AF 2 trial however showed that freedom from AF recurrence after 18 months did not increase when either linear ablation or ablation of CFAEs was added to PVI ablation (46% for linear ablation + PVI vs. 49% for CFAE + PVI vs. 59% for PVI alone, P=0.15).[2] Even though the mechanisms responsible for progression of AF are still of key debate, atrial electro-anatomical remodeling is a widely-recognized factor in the pathogenesis of AF. Known manifestations of advanced atrial remodeling include left atrial (LA) dilation and atrial interstitial fibrosis or scarring. The latter can serve as a substrate for slow-conduction and intra-atrial re-entry, which could predispose to (recurrent) AF.[3] Based on the conception that low voltage (≤0.5mV) implies presence of scar tissue, and thus arrhythmia substrate, multiple studies have found a significant correlation between presence of low-voltage areas (LVA) and progression of AF.[4] Furthermore, late recurrence of AF (beyond two-months) after PVI was found to be significantly higher in patients with pre-existence of LA scarring compared to patients without LA scarring (57% vs. 19% respectively, P=0.003).[3] Periprocedural evidence of LVA during sinus rhythm yielded a stronger predictor of AF recurrence after PVI than other known risk factors such as age, ejection fraction and LA size.[3] Nowadays, voltage-guided substrate modification by targeting LVA in addition to PVI is an emerging therapy with promising results. A recent systematic review concluded LVA-ablation in addition to PVI more effective (i.e. reduction of postablation atrial arrhythmia occurrence) and safer (e.g. reduced procedure time) than PVI alone, especially in nonparoxysmal patients.[5] There is, however, still more than enough room for improvement. With all the additional ablation options out there, especially the use of a more individualized ablation approach could increase effectiveness.

In this issue of Heart Rhythm, Büttner et al. propose using a blood-based biomarker to non-invasively characterize the stage of AF progression to refine therapy and follow-up strategies.[6] Although AF type and LA diameter are easy obtainable clinical parameters, detection of the more directional parameter LVA is only possible periprocedural. Büttner et al. therefore investigated whether brain natriuretic peptide (BNP) and atrial natriuretic peptide (ANP) levels were associated with AF progression phenotypes, defined as switch from paroxysmal to persistent

AF, presence of LVA and increased LA diameter.[6] For this study a discovery (n=51) and validation set (n=241) of consecutively selected AF patients undergoing first AF radiofrequency ablation were used. Presence of LVA was found in 22% of patients within the discovery set (of which 70% with persistent AF) and in 26% of patients within the validation set (of which 82% with persistent AF). Interestingly, levels of NT-proANP, but not NT-proBNP, were significantly associated with presence of LVA in both the discovery and validation cohort (28±12 vs. 17±12 ng/mL, P=0.009 and 25±20 vs. 18±13 ng/mL, P=0.016, respectively).[6] Higher NT-proANP levels were also significantly associated with larger LA diameter (in both cohorts) and with greater LA volume (in the validation cohort). For assessment of the relation between NT-proANP and NT-proBNP levels and AF progression phenotypes, four groups of phenotypes were defined: 1) paroxysmal AF without LVA (n=86); 2) persistent AF without LVA (n=90); 3) paroxysmal AF with LVA (n=12) and 4) persistent AF with LVA (n=53). Only levels of NT-proANP increased with disease progression and advanced electro-anatomical remodeling, as NT-proANP was significantly higher in patients in group 2 and 3 compared to group 1, and highest in patients in group 4 (means: 15, 20, 19 and 27 ng/mL, P=0.004).[6]

Büttner et al. should be complimented for their valuable work, indicating that natriuretic peptides show sensitivity in phenotyping AF progression and remodeling. Their findings can really be a first step towards an approach where the stage of electro-anatomic remodeling can be determined noninvasively, which could directly aid in selection of the appropriate ablation approach for the individual patient. Biomarkers in the blood have great potential to be included within the treatment chain of AF, since they are relatively easy accessible in every patient and can be of great diagnostic and predictive value. Increased pre-ablation level of NT-proANP has previously been associated with greater risk of post-interventional AF recurrence.[7] Biomarkers can also indicate a potential target of therapy. So did Brundel et al. recently show that heat shock proteins (HSPs) in the blood exhaust with AF progression in AF patients, and that pharmacological induction of these HSPs using geranylgeranylacetone protected against atrial remodeling in dogs.[8, 9]

The findings of Büttner and colleagues are promising, but there are some side notes that should be made. The association between NT-proANP and LA diameter and LVA was found only weak to moderate, indicating that more larger studies should be performed to validate the outcomes. Furthermore, although "low voltage" and "scar" are often used interchangeably, it can be questioned whether LVA always represents scar tissue, especially when bipolar recordings are used for construction of LA voltage maps. Bipolar voltage amplitude is known to be a nonspecific variable, since it is influenced by multiple factors, including: 1) conduction velocity; 2) fiber orientation and curvature; 3) wavefront of activation; 4) tissue contact; 5) presence of insulating tissue (i.e. edema or fat) and 6) characteristics of the

recording catheter and mapping system (i.e. electrode size, interelectrode spacing, angle of incidence, filtering, mapping density, mapping resolution).[10, 11] Therefore, interpretation of bipolar voltages is anything but straightforward and should be done with extreme caution. As stated earlier, mapping of low-voltage areas is based on the conception that low voltage (≤0.5mV) implies presence of scar tissue and thus arrhythmia substrate. Not only do the above mentioned confounders question the direct relationship between low voltage and scar tissue, they also give rise to considerable doubts regarding the direct link between low voltage and the arrhythmogenic substrate. Insight could and should be enhanced by using unipolar catheters or small bipolar catheters with very close interelectrode distance, a standard wavefront of activation such as during pacing and adequate tissue contact force.[11] Future studies should be performed to elucidate which parameter(s) can be used best to represent the arrhythmogenic substrate.

References

1. Ganesan AN, Shipp NJ, Brooks AG, Kuklik P, Lau DH, Lim HS, Sullivan T, Roberts-Thomson KC and Sanders P. Long-term outcomes of catheter ablation of atrial fibrillation: a systematic review and meta-analysis. *J Am Heart Assoc*. 2013;2:e004549.
2. Verma A, Jiang CY, Betts TR, Chen J, Deisenhofer I, Mantovan R, Macle L, Morillo CA, Haverkamp W, Weerasooriya R, Albenque JP, Nardi S, Menardi E, Novak P, Sanders P and Investigators SAI. Approaches to catheter ablation for persistent atrial fibrillation. *N Engl J Med*. 2015;372:1812-22.
3. Verma A, Wazni OM, Marrouche NF, Martin DO, Kilicaslan F, Minor S, Schweikert RA, Saliba W, Cummings J, Burkhardt JD, Bhargava M, Belden WA, Abdul-Karim A and Natale A. Pre-existent left atrial scarring in patients undergoing pulmonary vein antrum isolation: an independent predictor of procedural failure. *J Am Coll Cardiol*. 2005;45:285-92.
4. Kogawa R, Okumura Y, Watanabe I, Nagashima K, Takahashi K, Iso K, Watanabe R, Arai M, Kurokawa S, Ohkubo K, Nakai T, Hirayama A, Sonoda K and Tosaka T. Left atrial remodeling: Regional differences between paroxysmal and persistent atrial fibrillation. *J Arrhythm*. 2017; 33:483-487.
5. Blandino A, Bianchi F, Grossi S, Biondi-Zoccai G, Conte MR, Gaido L, Gaita F, Scaglione M and Rametta F. Left Atrial Substrate Modification Targeting Low-Voltage Areas for Catheter Ablation of Atrial Fibrillation: A Systematic Review and Meta-Analysis. *Pacing Clin Electrophysiol*. 2017;40:199-212.
6. Buttner P, Schumacher K, Dinov B, Zeynalova S, Sommer P, Bollmann A, Husser D, Hindricks G and Kornej J. Role of NT-proANP and NT-proBNP in patients with atrial fibrillation: Association with atrial fibrillation progression phenotypes. *Heart Rhythm*. 2018;15:1132-1137.
7. Jiang H, Wang W, Wang C, Xie X and Hou Y. Association of pre-ablation level of potential blood markers with atrial fibrillation recurrence after catheter ablation: a meta-analysis. *Europace*. 2017;19:392-400.
8. Brundel BJ, Henning RH, Ke L, van Gelder IC, Crijns HJ and Kampinga HH. Heat shock protein upregulation protects against pacing-induced myolysis in HL-1 atrial myocytes and in human atrial fibrillation. *J Mol Cell Cardiol*. 2006;41:555-62.
9. Brundel BJ, Shiroshita-Takeshita A, Qi X, Yeh YH, Chartier D, van Gelder IC, Henning RH, Kampinga HH and Nattel S. Induction of heat shock response protects the heart against atrial fibrillation. *Circ Res*. 2006;99:1394-402.
10. Anter E and Josephson ME. Bipolar voltage amplitude: What does it really mean? *Heart Rhythm*. 2016;13:326-7.
11. Josephson ME and Anter E. Substrate Mapping for Ventricular Tachycardia: Assumptions and Misconceptions. *JACC Clin Electrophysiol*. 2015;1:341-352.

13

Daily supplementation of L-glutamine in atrial fibrillation patients: the effect on heat shock proteins and metabolites

Roeliene Starreveld
Kennedy S. Ramos
Agnes J.Q.M. Muskens
Bianca J.J.M. Brundel
Natasja M.S. de Groot

Cells. 2020 Jul;9(7):1729

Abstract

Pharmaco-therapeutic strategies of atrial fibrillation (AF) are moderately effective and do not prevent AF onset and progression. Therefore, there is an urgent need to develop novel therapies. Previous studies revealed heat shock protein (HSP)-inducing compounds to mitigate AF onset and progression. Such an HSP inducing compound is L-glutamine. In the current study we investigate the effect of L-glutamine supplementation on serum HSP27 and HSP70 levels and metabolite levels in patients with AF patients (n = 21). Hereto, HSP27 and HSP70 levels were determined by ELISAs and metabolites with LC-mass spectrometry. HSP27 levels significantly decreased after 3-months of L-glutamine supplementation [540.39 (250.97–1315.63) to 380.69 (185.68–915.03), p = 0.004] and normalized to baseline levels after 6-months of L-glutamine supplementation [634.96 (139.57–3103.61), p < 0.001]. For HSP70, levels decreased after 3-months of L-glutamine supplementation [548.86 (31.50–1564.51) to 353.65 (110.58–752.50), p = 0.045] and remained low after 6-months of L-glutamine supplementation [309.30 (118.29–1744.19), p = 0.517]. Patients with high HSP27 levels at baseline showed normalization of several metabolites related to the carbohydrates, nucleotides, amino acids, vitamins and cofactors metabolic pathways after 3-months L-glutamine supplementation. In conclusion, L-glutamine supplementation reduces the serum levels of HSP27 and HSP70 within 3-months and normalizes metabolite levels. This knowledge may fuel future clinical studies on L-glutamine to improve cardioprotective effects that may attenuate AF episodes.

Introduction

Atrial fibrillation (AF) is a progressive, age-related disease affecting worldwide approximately 33.5 million individuals and is therefore regarded as one of the cardiovascular epidemics of the 21th century.[1] AF is associated with severe complications such as thrombo-embolic events, impaired cognitive function and even increased mortality.[2]

At present, treatment modalities for AF are only moderately effective and do not prevent AF onset and progression from recurrent intermittent episodes to finally permanent AF. Though invasive ablation therapy initially seemed promising in early stage AF, up to 50% of the AF patients with more persistent types of AF have recurrences within 1 year and require multiple procedures.[3] Pharmacological therapy of AF is even less effective, and its usage is limited by severe and potentially life-threatening side-effects. Main reason for AF therapy failure is that pharmaco-therapeutic strategies are not directed at mechanistic root causes of AF, which drive structural cardiomyocyte damage, mitochondrial dysfunction and consequently electrical and contractile dysfunction of atrial cardiomyocytes.[4, 5]

Emerging research findings indicate that heat shock proteins (HSP) mitigate AF onset and progression in experimental model systems for AF.[6-9] Especially HSP27 (small HSP) has shown promising protective effects against AF in-vitro.[10] Importantly, patients with persistent AF reveal exhaustion of HSP27 and HSP70, and not HSP40 and HSP90, atrial tissue levels when compared to control patients in sinus rhythm. In line, pharmacological induction of HSP levels with HSP-inducing compounds attenuated AF promotion in dog models for atrial tachypacing and ischemia-induced AF.[10, 11] Evidence reveals that L-glutamine, a semi-essential amino acid, represents a potent inducer of intracellular HSP levels, which has been progressively investigated in cardiovascular research. Clinical and experimental studies have consistently presented increased intracellular expression of HSPs, especially HSP27 and HSP70, after L-glutamine administration.[12-14] Given the fact that human body levels of L-glutamine are rapidly metabolized and in deficit under catabolic conditions[15], L-glutamine supplementation resulted in attenuation of experimental cellular injury and in prognostic amelioration of critically ill patients diagnosed with sepsis, heart failure and patients undergoing cardiopulmonary bypass surgery[14, 16-19]. In prior studies, it was shown that L-glutamine enhances translocation of trimerized phosphorylated HSF1 from cytosol to the nucleus, followed by increased DNA binding to heat shock elements in the promotor sequence of hsp genes, thereby resulting in increased HSP expression.[20] Increased HSP expression promotes enhancement of contractile function and prevents loss of cellular integrity during AF.[9] In addition to a role in HSP expression, L-glutamine and its metabolites are important in ATP, DNA and nucleotide formation, suppression

of inflammation, attenuation of oxidative stress and apoptosis, and increased blood fluidity and flow.[21-25] Although the role of L-glutamine as an inducer of HSP expression and protector against various diseases including ischemic heart disease and heart failure has been recognized[17, 18], its potential protective role in AF progression has not been investigated.

Based on experimental and clinical pilot studies, we hypothesize that L-glutamine suppletion alters blood-based HSP levels and improves the metabolic stage of AF patients. In this pilot study, we therefore measured the effect of L-glutamine on serum HSP levels, and studied the influence on serum metabolite levels in AF patients. This knowledge may fuel future clinical studies on L-glutamine to attenuate AF episodes.

Materials and methods

This prospective interventional trial was part of the Glutamine Suppletion Minimizes the Atrial Fibrillation Burden (Glutaminimize AF) project, which was approved by the local ethics committee in the Erasmus University Medical Center Rotterdam (MEC-2017-524). Written informed consent was obtained from all patients.

Study population

Patients with diagnosed AF and frequent symptoms of AF episodes (≥ 1/week) were recruited at the outpatient clinic of the Cardiology department. Patients with diabetes mellitus or a soya, gluten or shellfish allergy were excluded. Patients were instructed to maintain their regular diet during the whole study. Patient characteristics (e.g., age, medical history, cardiovascular risk factors, type of AF) were obtained from the patient's medical records.

Study design

Patients started with oral intake of the KABI® Glutamine sachets containing 10 g of L-glutamine, twice daily (once in the morning, once in the evening) for a period of six months. Patients were evaluated at a dedicated outpatient clinic at baseline and at three and six months after start of L-glutamine intake (*Figure 1*). During those visits, blood was drawn for testing of HSP levels and metabolomics.

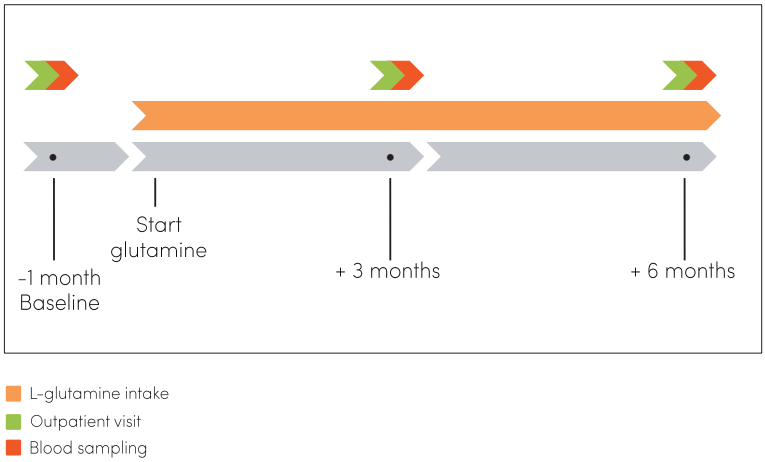

Figure 1 – Time course of the Glutaminimize AF project. At baseline, 3-month and 6-month follow-up all patients visited the outpatient clinic (green bar) for electrocardiography and blood sampling (red bar). After one month, patients started with oral intake of the KABI® Glutamine sachets containing 10 g of L-glutamine (orange bar), twice daily for a period of six months.

Data analysis: HSP measurements

Immediately after blood sample collection, serum was harvested from blood in BD Vacutainer™ SST™ II Advance Tubes (Fisher Scientific) by centrifugation at 2000× g for 10 min at 4 °C and frozen in –80 °C until analysis of HSP27 and HSP70. For measurement of serum HSP27 levels, samples were diluted six times and for HSP70 levels samples were diluted twice in 1% BSA in PBS. The amount of HSP27 and HSP70 protein was detected in triplicates using human HSP27 or HSP70 DuoSet® ELISA kits from R&D Systems (Cat. no. DY1580 and DY1663, respectively) according to the manufacturer's instructions with minor adjustments (serum was incubated at 4 °C overnight, instead of 2 h at room temperature). The HSP levels, as well as the difference in HSP27 or HSP70 levels between follow-up moments, were the primary study parameters.

Data analysis: metabolomics

For a subanalysis, mass spectrometry was used to derive metabolite levels from four pooled patients with the highest HSP27 levels and five pooled patients with the lowest HSP27 levels at baseline. The metabolite levels of the same pooled patients at 3-month follow-up were also obtained. Metabolite measurements from the four mentioned pooled samples were used to determine the effect of L-glutamine supplementation on various metabolites levels. Ratios were derived between the pooled metabolites of high HSP27 at baseline and 3-months of L-glutamine supplementation (high HSP: 3M/baseline), low HSP27 at baseline and 3-months of L-glutamine supplementation (low HSP: 3M/baseline) and high HSP27 and low HSP27 at baseline (baseline: low HSP/high HSP).

Determination of metabolites was performed as previously described, with minor adjustments.[26] A 75 µL mixture of internal standards in water, as listed in the *Supplemental material*, was added to each sample. Subsequently, 425 µL water, 500 µL methanol and 1 mL chloroform were added to the same 2 mL tube before thorough mixing and centrifugation for 10 min at 14,000 rpm. The top layer, containing the polar phase, was transferred to a new 1.5 mL tube and dried using a vacuum concentrator at 60 °C. Dried samples were reconstituted in 100 µL methanol/water (6/4; v/v). Metabolites were analyzed using a Waters Acquity ultra-high-performance liquid chromatography system coupled to a Bruker Impact II™ Ultra-High Resolution Qq-Time-Of-Flight mass spectrometer. Samples were kept at 12 °C during analysis and 5 µL of each sample was injected. Chromatographic separation was achieved using a Merck Millipore SeQuant ZIC-cHILIC column (PEEK 100 × 2.1 mm, 3 µm particle size). Column temperature was held at 30 °C. Mobile phase consisted of (A) 1:9 acetonitrile:water and (B) 9:1 acetonitrile:water, both containing 5 mM ammonium acetate. Using a flow rate of 0.25 mL/min, the LC gradient consisted of: 100% B for 0–2 min, ramp to 0% B at 28 min, 0% B for 28–30 min, ramp to 100% B at 31 min, 100% B for 31–35 min. MS data were acquired using negative and positive ionization in full scan mode over the range of m/z 50–1200. Data were analyzed using Bruker TASQ software version 2.1.22.3. All reported metabolite intensities were normalized to internal standards with comparable retention times and response in the MS. Metabolite identification has been based on a combination of accurate mass, (relative) retention times and fragmentation spectra, compared to the analysis of a library of standards.

Statistical analysis

Data was tested for normality. Normally distributed continuous variables were expressed as mean ± SD, skewed continuous variables were expressed as median (minimum-maximum) and categorical variables were expressed as numbers (percentages). Depending on skewness of the data, a paired-samples T test or Wilcoxon signed-rank test was used to compare HSP levels between each of the three follow-up moments (i.e., baseline, 3-month and 6-month follow-up). Bonferroni correction was applied for comparison of the three measurements; a p-value of < 0.0167 (0.05/3) was considered statistically significant. Correlations between clinical variables were calculated using Pearson's or Spearman's correlation coefficient, depending on skewness of the data. In general, a p-value < 0.05 was considered statistically significant. Metabolite ratios higher than 1.5 were classified as increased, whereas ratios lower than 0.667 were classified decreased. Metabolite ratios between 0.667 and 1.5 were classified as stable. All statistical analyses were performed using R Statistical Software (RStudio, Inc., Boston, MA, USA; version 1.0.153).

Results

Study population

Clinical characteristics of all patients (n = 21, 16 male (76.2%), age 58.7 ± 10.5 years) are presented in *Table 1*. Patients had a history of paroxysmal (n = 13, 61.9%), persistent (n = 6, 28.6%) or longstanding persistent AF (n = 2, 9.5%). The far majority of patients had a normal left ventricular function (n = 18, 85.7%). All patients completed the 3-month follow-up (n = 21, 100%), whereas 20 patients (95.2%) completed the 6-month follow-up.

Table 1 – Patient characteristics

Number of patients	**21**
Male	16 (76.2)
Age (years)	58.7 ± 10.5
BMI	26.7 (22.0-36.3)
Type of AF	
- Paroxysmal	13 (61.9)
- Persistent	6 (28.6)
- Longstanding persistent	2 (9.5)
Time since AF diagnosis (y)	1.8 (0.2-19.5)
Hypertension	6 (28.6)
Dyslipidemia	2 (9.5)
Left ventricular function	
- Normal	18 (85.7)
- Mild impairment	3 (14.3)
Use of anti-arrhythmic drugs (at baseline)	
- Class I	8 (38.1)
- Class II	6 (28.6)
- Class III	7 (33.3)
- Class IV	3 (14.3)
- Class V	1 (4.8)
Follow-up duration	
- Completed 3-month follow-up	21 (100)
- Completed 6-month follow-up	20 (95.2)
Glutamine compliance	
- Baseline to 3-month follow-up (n=20)	0.99 (0.77-1.00)
- 3-month to 6-month follow-up (n=19)	0.97 (0.61-1.00)
- Baseline to 6-month follow-up (n=20)	0.97 (0.69-1.00)
Reduced kidney function (n=17)	1 (5.9)
Reduced liver function (n=17)	0 (0)
Reduced thyroid function (n=17)	0 (0)

Values are presented as N (%) or median (min-max). BMI, body mass index.

Effect of L-glutamine on HSP levels

Median HSP27 level at baseline was 540.39 and ranged from 250.97 to 1315.63. As seen in *Table 2* and *Figure 2*, levels of HSP27 significantly decreased to 380.69 (185.68–915.03) after 3-months of L-glutamine supplementation (p = 0.004). After 6-months of L-glutamine supplementation, the level of HSP27 normalized to baseline levels [634.96 (139.57–3103.61), p < 0.001]. For HSP70, the level at baseline was 548.86 (31.50–1564.51) and decreased to 353.65 (110.58–752.50) after 3-months of L-glutamine supplementation (p = 0.045). The HSP70 level remained low after 6-months of L-glutamine supplementation [309.30 (118.29–1744.19), p = 0.517]. There were no significant differences between the HSP27 and HSP70 levels at baseline and after 6-months of L-glutamine use. Unfortunately, HSP70 levels of patient 8 (baseline, 3-month and 6-month follow-up), patient 14 (6-month follow-up) and patient 15 (3-month follow-up) could not be determined due to poor quality of the sample.

Table 2 – Serum levels of HSP27 and HSP70 at baseline (B), 3-month (3M) and 6-month (6M) follow-up.

Study ID	AF type	HSP27-B	HSP27-3M	HSP27-6M	HSP70-B	HSP70-3M	HSP70-6M
1	L-PER	1315.63	489.79	821.92	751.86	230.31	245.39
2	L-PER	455.71	312.78	571.25	31.50	110.58	118.29
3	PAR	869.73	352.14	441.98	862.09	268.50	565.83
4	PAR	751.50	271.66	278.59	542.14	202.70	120.66
5	PAR	288.50	407.61	769.92	524.28	610.66	463.72
6	PAR	514.07	915.03	1150.48	258.42	353.65	304.15
7	PAR	250.97	516.21	501.01	352.67	555.83	500.92
8	PAR	463.89	319.85	1401.11	NA	NA	NA
9	PAR	1203.41	271.80	1078.15	1564.51	396.58	1027.39
10	PAR	485.48	356.38	-	211.71	752.50	-
11	PER	360.65	332.83	379.69	390.49	382.47	409.58
12	PER	706.81	528.21	3103.61	1149.16	705.89	1744.19
13	PER	423.98	380.69	421.96	365.78	574.18	878.51
14	PER	1305.84	364.30	698.66	555.57	312.52	NA
15	PAR	666.37	629.06	1044.07	1119.96	177.28	179.68
16	PAR	911.61	402.25	929.48	614.61	190.27	314.44
17	PAR	369.99	407.58	139.57	143.11	635.17	142.24
18	PER	550.98	409.01	758.89	735.83	328.16	1182.55
19	PAR	1102.87	394.93	483.66	880.77	304.32	135.65
20	PER	540.39	185.68	192.68	678.67	371.17	208.70
21	PAR	498.64	221.64	437.17	268.38	NA	225.46
median	-	*540.39*	*380.69*	*634.96*	*548.86*	*353.65*	*309.30*
min-max	-	*250.97-1315.63*	*185.68-915.03*	*139.57-3103.61*	*31.50-1564.51*	*110.58-752.50*	*118.29-1744.19*

L-PER, longstanding persistent AF; NA, not available; PAR, paroxysmal AF; PER, persistent AF.

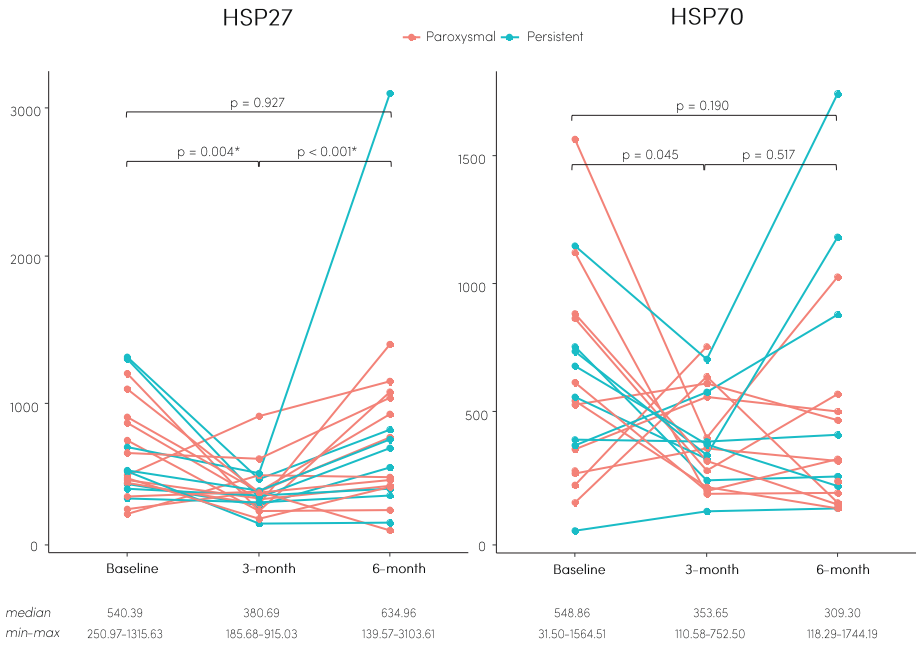

Figure 2 – Effect of glutamine on HSP levels. *A*: levels of HSP27 per patient during the study period. *B*: levels of HSP70 per patient during the study period. Statistical significance is indicated with an asterisk (*, p<0.0167).

The relation between (Δ)HSP27 and/or (Δ)HSP70 levels at baseline and after 3-months and 6-months of L-glutamine supplementation is illustrated in *Figure 3*. The level of HSP27 at baseline showed a strong negative correlation with the ΔHSP27 from baseline to 3-months L-glutamine supplementation (R = -0.86, p < 0.001, upper left panel). Similarly, a strong negative correlation was found between the level of HSP70 at baseline and the ΔHSP70 from baseline to 3-months L-glutamine supplementation (R = - 0.91, p < 0.001, lower left panel). In addition, a strong positive correlation between the ΔHSP27 from 3-months to 6-months L-glutamine supplementation and the HSP27 at 6-month L-glutamine supplementation was found (R = 0.88, p < 0.001, lower right panel). At baseline, levels of HSP27 and HSP70 showed a significant positive correlation (R = 0.7, p < 0.001, upper right panel).

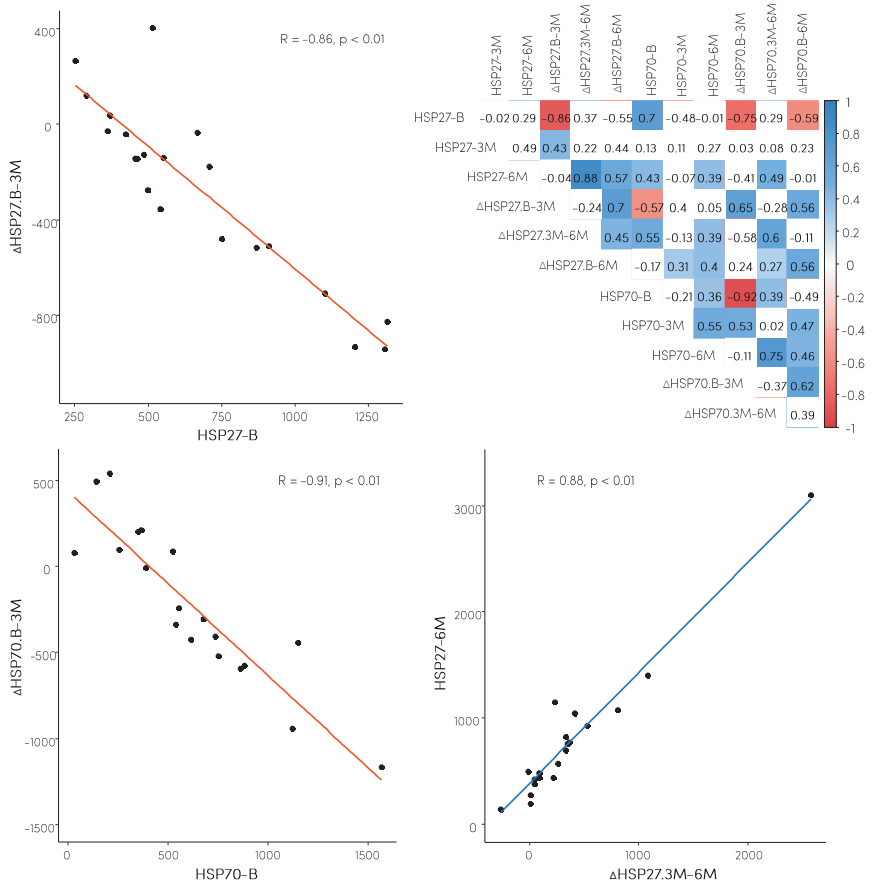

Figure 3 – Relation between (Δ) HSP27 and/or (Δ)HSP70 levels during the study period. *A*: scatterplot with regression line for the relation between HSP27 at baseline and the ΔHSP27 from baseline to 3-month follow-up. The corresponding correlation coefficient and statistical significance are indicated in the graph. *B*: correlogram with correlation coefficients for all possible relations between (Δ) HSP27 and/or (Δ) HSP70. Significant correlations ($p < 0.05$) are colored with either blue (positive correlation) or red (negative correlation). Variables with a strong correlation ($-0.8 < R > 0.8$) are visualized in the other panels. *C*: scatterplot with regression line for the relation between HSP70 at baseline and the ΔHSP70 from baseline to 3-month follow-up. *D*: scatterplot with regression line for the relation between ΔHSP27 from 3-month to 6-month follow-up and HSP27 at 6-month follow-up.

Relation between HSP levels and patient characteristics

Levels of HSP27 and HSP70 did not differ between patients with paroxysmal or (longstanding) persistent AF, as illustrated in *Figure 4*. In addition, no statistical difference was found in HSP27 and HSP70 levels between male and female patients, and HSP27 and HSP70 levels did not correlate with L-glutamine compliance nor with age.

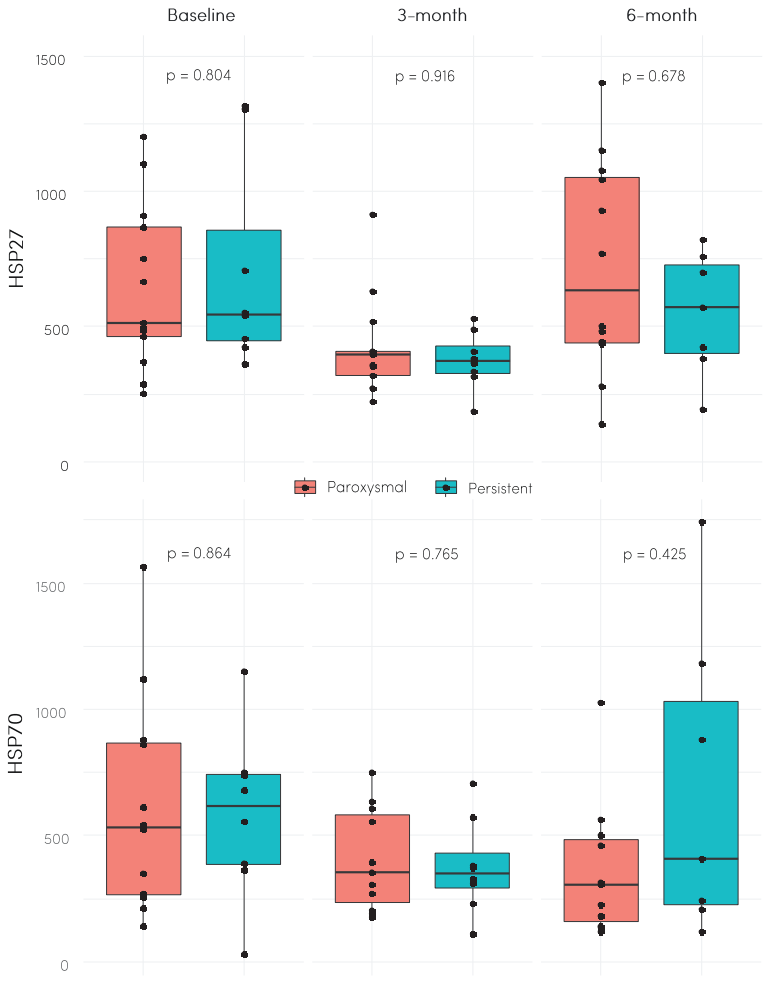

Figure 4 – HSP levels for paroxysmal and (longstanding) persistent AF patients. *A*: boxplots of HSP27 levels for paroxysmal and (longstanding) persistent AF patients separately during the study period. *B*: boxplots of HSP70 levels for paroxysmal and (longstanding) persistent AF patients separately during the study period.

Relation between HSP27 and energy metabolism

A positive correlation between HSP27 and HSP70 levels at baseline was observed. Given the highly significant reduction of HSP27 during 3-months of L-glutamine supplementation, further metabolite analysis was performed based on HSP27 levels. Hereto, the effect of 3-months L-glutamine supplementation on metabolite levels from patients showing high HSP27 levels was contrasted to low HSP27 levels at baseline. Mass spectrometry was utilized in pooled serum samples, as described in the *Methods*.

In total 83 metabolites were identified in the four groups. The derived ratios between the groups are listed in *Supplemental table 1*. A heat map and dendrogram generated from the absolute metabolite levels showed that the group with high HSP at baseline is distinct from the other three groups, suggesting that high HSP levels at baseline represent a different metabolic phenotype compared to low HSP levels at baseline and after 3-months of L-glutamine supplementation (*Figure 5*).

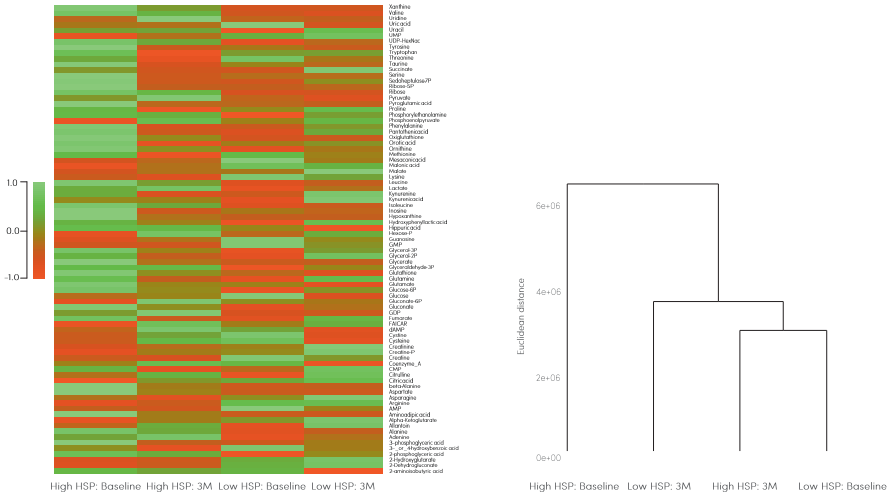

Figure 5 – HSP level and L-glutamine supplementation affects metabolic phenotypes. *A*: heat map of the absolute levels of all 83 metabolites for high HSP: baseline, high HSP: 3-month follow-up (3M), low HSP: baseline and low HSP: 3M. The pooled group high HSP at baseline is distinct from the other groups. *B*: dendrogram showing the hierarchical clustering using the Euclidean distance with average linkage for all four groups.

Based on the ratios (i.e., high HSP: 3M/baseline, low HSP: 3M/baseline, baseline: low HSP/high HSP), metabolites were clustered, as listed in *Table 3*. In total, 55.4% of metabolite levels were comparable between the four groups. In high HSP levels at baseline, seven metabolites (8.43%) showed normalization after 3- months L-glutamine supplementation and were comparable to low HSP levels at baseline and 3- months of L-glutamine supplementation. For both high and low HSP at baseline, two metabolites (2.4%) showed a simultaneous increase (ratios >1.5) and one metabolite (1.2%) showed simultaneous decrease (ratios <0.667) after 3-months L-glutamine supplementation. The remaining metabolites, 31.3%, did show level changes in ratios (<0.667 or >1.5), which could partly explain the hierarchical clustering as observed in *Figure 5*.

By contrasting the metabolic changes between the groups, key metabolites were identified: ribose-5P, aspartate, beta-alanine, hypoxanthine, oxiglutathione,

pyroglutamic acid, citric acid, creatine P, GDP and inosine (*Figure 6*). In *Supplemental table 2*, all human pathways and global pathways related to these metabolites are listed. Findings indicate that 3-months L-glutamine supplementation affect pathways related to carbohydrates, nucleotide, amino acid and vitamin synthesis.

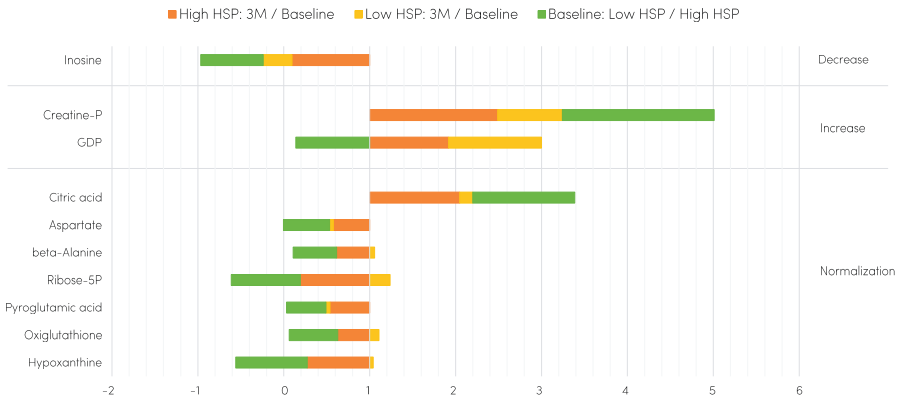

Figure 6 – Metabolite ratios of high HSP: 3M/baseline, low HSP: 3M/baseline and baseline: low HSP/high HSP, grouped on behavior. Inosine showed simultaneous decrease (ratio <0.667), whereas Creatine-P and GDP showed simultaneous increase (ratio >1.5) in both high HSP: 3M/baseline and low HSP: 3M/baseline, representing the effect of L-glutamine supplementation on both. Seven metabolites (8.43%) showed a normalization behavior, in which high HSP: 3M/baseline shows a normalization (either increase or decrease) towards stable levels of low HSP: 3M/baseline.

Table 3 – Clustering of metabolites sharing similar behavior.

	Ratios				
Behavior	**High HSP: 3M/ baseline**	**Baseline: low HSP/high HSP**	**Low HSP: 3M/ baseline**	**Metabolites**	**Percentage**
Normalization	<0.667	<0.667	Stable	Ribose-5P, Aspartate, beta-Alanine, Hypoxanthine, Oxiglutathione, Pyroglutamic acid	8.43%
	>1.5	>1.5	Stable	Citric Acid	
Increase	>1.5	>1.5	>1.5	Creatine P	2.4%
	>1.5	<0.667	>1.5	GDP	
Decrease	<0.667	<0.667	<0.667	Inosine	1.2%
Independent	<0.667	<0.667	>1.5	Sedoheptulose-7P, Fumarate, CMP, 3-phosphoglyceric acid	31.32%
	<0.667	Stable	Stable	3- and 4-hydroxybenzoic acid	
	>1.5	Stable	Stable	Gluconate-6P	
	>1.5	Stable	<0.667	dAMP	
	Stable	Stable	>1.5	Allantoin, Malate	
	Stable	Stable	<0.667	Coenzyme A, Hippuric acid	
	Stable	<0.667	>1.5	Uracil, UDP-HexNac, 2-phosphoglyceric acid, Adenine, Glycerol-3P	
	Stable	<0.667	Stable	Xanthine, Phosphorylethanolanine, Aminoadicpic acid, Glucose 6P, Glutathione, Ribose	
	Stable	>1.5	Stable	Creatine, Guanosine	
	Stable	>1.5	<0.667	AMP, GMP, Mesaconic acid	
Stable	Stable	Stable	Stable	2-aminoisobutyric acid, 2-dehydrogluconate, 2-hydroxyglutarate, Alanine, Alpha, Ketoglutarate, Arginine, Asparagine, Citrulline, Creatinine, Cysteine, Cystine, FAICAR, Gluconate, Glucose, Glutamate, Glutamine, Glyceraldehyde-3P, Glycerate, Glycerol-2P, Hexose-P, Hydroxyphenyllactic acid, Isoleucine, Kynurenic acid, Kynurenine, Lactate, Leucine, Lysine, Malonic acid, Methionine, Ornithine, Orotic acid, Pantothenic acid, Phenylalanine, Phosphoenolpyruvate, Proline, Pyruvate, Serine, Succinate, Taurine, Threonine, Tryptophan, Tyrosine, UMP, Uric acid, Uridine, Valine	55.4%

Ratios between the pooled metabolites of high HSP27 at baseline and 3-month follow-up (high HSP: 3M/baseline), low HSP27 at baseline and 3-month follow-up (low HSP: 3M/baseline) and high HSP27 and low HSP27 at baseline (baseline: low HSP/high HSP) are clustered on behavior. Ratios between 0.667 and 1.5 are classified as stable.

Discussion

Despite many innovative insights and interventions in recent years, still no curative therapy for AF patients exists. Our pilot study is the first to investigate the effect of L-glutamine on HSP27 and HSP70 levels in serum samples of AF patients. After 3-months of L-glutamine supplementation, the level of HSP27 and HSP70 significantly decreased, and HSP27 normalized to baseline levels after 6-months of L-glutamine supplementation. A strong correlation was found between the baseline level of HSP27 or HSP70 and the degree of reduction at 3-months of L-glutamine supplementation: patients with a higher baseline level of HSP27 or HSP70 revealed a large reduction, whereas patients with a low HSP27 or HSP70 level at baseline stayed low after 3-months supplementation. Analysis of metabolites revealed that 3-months of L-glutamine supplementation normalized the levels of metabolites related to the synthesis of carbohydrates, nucleotides and amino acids, compared to non-treated patients with high levels of HSP at baseline. These findings indicate that 3-months L-glutamine supplementation reduces HSP27 and HSP70 levels in serum samples which is accompanied with normalization of metabolites of fundamental pathways within cell function.

Effect of L-glutamine on HSP and metabolite levels

Recent experimental studies by Brundel et al. showed that AF is associated with structural damage in the cardiomyocyte due to derailment in proteostasis (i.e., protein expression, function and clearance), a process which could be normalized by overexpression of HSP27.[6, 7, 10, 27] Various HSPs, including the HSP27 and HSP70, are involved in the protection against different forms of cellular stress by functioning as intra-cellular chaperones for other proteins.[6, 28] In cardiomyocytes, HSP27 can bind to structural proteins and thereby shield them from damage and functional loss.[6, 9, 10] In accordance, upregulation of HSP27 in atrial tissue of dogs protected cardiomyocytes from AF-induced cellular stress and as such contributed to the maintenance of atrial tissue integrity and contractile function.[6, 28] These findings indicate that pharmacological induction of HSPs may be an interesting target to treat AF. Previous studies by Gong and Jing, Hamiel et al. and Hayashi et al. demonstrated L-glutamine to induce expression of HSPs in organs, including the heart.[12-14] The precise interaction between induced levels of HSPs in cardiac tissue and its effect on HSP levels in serum is not fully known. Our data demonstrate HSP27 and HSP70 to decrease from baseline to 3-months of L-glutamine supplementation, followed by a partly increase from 3-months to 6-months of L-glutamine supplementation. Although several studies have detected HSP27 and HSP70 in the extracellular milieu, there is still lack of consensus regarding the exact mechanisms of transmembrane transport, as well as their role outside the cell of origin.[29] Given that HSP's function of protein homeostasis belongs to the intracellular space, L-glutamine administration may firstly increases intracellular

levels of HSPs, thereby promoting enhancement of contractile function during AF. This beneficial state may prevent cellular disruption and subsequent pathological release of HSP from the cardiomyocytes into the circulation as observed in the period from baseline to 3-months. Further studies are necessary to reveal a mechanistic understanding of the interaction between cardiomyocyte and serum levels of HSPs after L-glutamine supplementation and the duration of the potential beneficial effect on HSP levels. Unfortunately, in the current study no atrial tissue samples could be selected, and therefore the effect of L-glutamine on atrial tissue and serum HSP levels could not be studied. Although previous studies indicate an increase in HSPs in serum and tissue after L-glutamine administration[30-33], very few studies measured HSPs in human cardiac tissue, specifically atrial tissue, nor performed long-term usage of L-glutamine.

Interestingly, patients with a higher HSP27 or HSP70 baseline level decreased more in HSP level during 3-months of L-glutamine supplementation in comparison to patients with a low HSP27 or HSP70 baseline level, which stayed low at 3-months L-glutamine supplementation. In correspondence, our findings revealed normalization of several metabolites to levels as observed in patients with low HSP at baseline and over the course of 3-months L-glutamine supplementation. This suggests a beneficial effect of L-glutamine on these metabolites, which may reveal an influence on carbohydrates, nucleotides, amino acids and cofactors and vitamins metabolism. In addition, a simultaneous and parallel variation—increase or decrease—in high HSP and low HSP throughout the 3-months of L-glutamine supplementation was observed for metabolites related to amino acids and nucleotide metabolism. These findings indicate that L-glutamine supplementation reveals an influence on metabolic phenotypes, encouraging further research on its influence on energy metabolic status in AF patients.

Study limitations and future perspectives

The small sample size of this prospective interventional pilot trial disables the formulation of strong conclusions. Also, patients with paroxysmal as well as (longstanding) persistent AF of varying age and co-morbidities participated in this study, potentially leading to (unaccounted) differences in individual responses to administration of L-glutamine. Nevertheless, a (significant) reduction in HSP27 and HSP70 serum levels was observed after L-glutamine supplementation, substantiating a possible effect of L-glutamine on HSP serum levels. Further mechanistic investigation is warranted to elucidate the exact relation between HSPs levels in atrial tissue and in blood. Therefore, it is of interest to mount a future clinical study to test a beneficial effect of L-glutamine on the reduction of AF burden. Hereto, we recommend a large – ideally randomized controlled – trial using continuous rhythm monitoring to determine the AF burden together with a validated patient-observed-effect questionnaire, in order to gain insight into the

(patient-specific) effects of L-glutamine on HSP levels and AF burden. In such a trial, individual metabolomics analyses could be performed to reveal the metabolic phenotype of each patient, allowing accurate correlation with clinical parameters for AF progression.

Conclusions

Our study reveals that the level of HSP27 significantly decreased after 3-months of L-glutamine supplementation, and partly normalized to baseline levels after 6-months of L-glutamine supplementation. A strong correlation was found between the baseline level of HSP27 or HSP70 and the amount of decrease at 3-months of L-glutamine supplementation: patients with a higher baseline level of HSP27 or HSP70 decreased more, whereas patients with a low HSP27 or HSP70 level remained low after 3-months supplementation. Analysis of metabolites revealed that several metabolites related to carbohydrates, nucleotides, amino acids vitamins metabolism pathway are normalized in patients with high level of HSP27 at baseline, indicating a potential beneficial effect of L-glutamine on the metabolic profile. Next step is to mount a clinical trial in AF patients and study the effect of L-glutamine on AF burden.

References

1. Kirchhof P, Benussi S, Kotecha D, Ahlsson A, Atar D, Casadei B, Castella M, Diener HC, Heidbuchel H, Hendriks J, Hindricks G, Manolis AS, Oldgren J, Popescu BA, Schotten U, Van Putte B, Vardas P and Group ESCSD. 2016 ESC Guidelines for the management of atrial fibrillation developed in collaboration with EACTS. *Eur Heart J*. 2016;37:2893-2962.
2. Zoni-Berisso M, Lercari F, Carazza T and Domenicucci S. Epidemiology of atrial fibrillation: European perspective. *Clin Epidemiol*. 2014;6:213-20.
3. Sultan A, Luker J, Andresen D, Kuck KH, Hoffmann E, Brachmann J, Hochadel M, Willems S, Eckardt L, Lewalter T, Senges J and Steven D. Predictors of Atrial Fibrillation Recurrence after Catheter Ablation: Data from the German Ablation Registry. *Sci Rep*. 2017;7:16678.
4. van Marion DM, Lanters EA, Wiersma M, Allessie MA, Brundel BB and de Groot NM. Diagnosis and Therapy of Atrial Fibrillation: The Past, The Present and The Future. *J Atr Fibrillation*. 2015;8:1216.
5. Wiersma M, van Marion DMS, Wust RCI, Houtkooper RH, Zhang D, Groot NMS, Henning RH and Brundel B. Mitochondrial Dysfunction Underlies Cardiomyocyte Remodeling in Experimental and Clinical Atrial Fibrillation. *Cells*. 2019;8.
6. Brundel BJ, Henning RH, Ke L, van Gelder IC, Crijns HJ and Kampinga HH. Heat shock protein upregulation protects against pacing-induced myolysis in HL-1 atrial myocytes and in human atrial fibrillation. *J Mol Cell Cardiol*. 2006;41:555-62.
7. Zhang D, Ke L, Mackovicova K, Van Der Want JJ, Sibon OC, Tanguay RM, Morrow G, Henning RH, Kampinga HH and Brundel BJ. Effects of different small HSPB members on contractile dysfunction and structural changes in a Drosophila melanogaster model for Atrial Fibrillation. *J Mol Cell Cardiol*. 2011;51:381-9.
8. Hoogstra-Berends F, Meijering RA, Zhang D, Heeres A, Loen L, Seerden JP, Kuipers I, Kampinga HH, Henning RH and Brundel BJ. Heat shock protein-inducing compounds as therapeutics to restore proteostasis in atrial fibrillation. *Trends Cardiovasc Med*. 2012;22:62-8.
9. Hu X, Li J, van Marion DMS, Zhang D and Brundel B. Heat shock protein inducer GGA*-59 reverses contractile and structural remodeling via restoration of the microtubule network in experimental Atrial Fibrillation. *J Mol Cell Cardiol*. 2019;134:86-97.
10. Brundel BJ, Shiroshita-Takeshita A, Qi X, Yeh YH, Chartier D, van Gelder IC, Henning RH, Kampinga HH and Nattel S. Induction of heat shock response protects the heart against atrial fibrillation. *Circ Res*. 2006;99:1394-402.
11. Sakabe M, Shiroshita-Takeshita A, Maguy A, Brundel BJ, Fujiki A, Inoue H and Nattel S. Effects of a heat shock protein inducer on the atrial fibrillation substrate caused by acute atrial ischaemia. *Cardiovasc Res*. 2008;78:63-70.
12. Gong J and Jing L. Glutamine induces heat shock protein 70 expression via O-GlcNAc modification and subsequent increased expression and transcriptional activity of heat shock factor-1. *Minerva Anestesiol*. 2011;77:488-95.
13. Hamiel CR, Pinto S, Hau A and Wischmeyer PE. Glutamine enhances heat shock protein 70 expression via increased hexosamine biosynthetic pathway activity. *Am J Physiol Cell Physiol*. 2009;297:C1509-19.
14. Hayashi Y, Sawa Y, Fukuyama N, Nakazawa H and Matsuda H.

Preoperative glutamine administration induces heat-shock protein 70 expression and attenuates cardiopulmonary bypass-induced inflammatory response by regulating nitric oxide synthase activity. *Circulation*. 2002;106:2601-7.
15. Cruzat V, Macedo Rogero M, Noel Keane K, Curi R and Newsholme P. Glutamine: Metabolism and Immune Function, Supplementation and Clinical Translation. *Nutrients*. 2018;10.
16. Ropeleski MJ, Riehm J, Baer KA, Musch MW and Chang EB. Anti-apoptotic effects of L-glutamine-mediated transcriptional modulation of the heat shock protein 72 during heat shock. *Gastroenterology*. 2005;129:170-84.
17. Wu C, Kato TS, Ji R, Zizola C, Brunjes DL, Deng Y, Akashi H, Armstrong HF, Kennel PJ, Thomas T, Forman DE, Hall J, Chokshi A, Bartels MN, Mancini D, Seres D and Schulze PC. Supplementation of l-Alanyl-l-Glutamine and Fish Oil Improves Body Composition and Quality of Life in Patients With Chronic Heart Failure. *Circ Heart Fail*. 2015;8:1077-87.
18. Shahzad K, Chokshi A and Schulze PC. Supplementation of glutamine and omega-3 polyunsaturated fatty acids as a novel therapeutic intervention targeting metabolic dysfunction and exercise intolerance in patients with heart failure. *Curr Clin Pharmacol*. 2011;6:288-94.
19. Ziegler TR, Ogden LG, Singleton KD, Luo M, Fernandez-Estivariz C, Griffith DP, Galloway JR and Wischmeyer PE. Parenteral glutamine increases serum heat shock protein 70 in critically ill patients. *Intensive Care Med*. 2005;31:1079-86.
20. Morrison AL, Dinges M, Singleton KD, Odoms K, Wong HR and Wischmeyer PE. Glutamine's protection against cellular injury is dependent on heat shock factor-1. *Am J Physiol Cell Physiol*. 2006;290:C1625-32.
21. Luo LL, Li YF, Shan HM, Wang LP, Yuan F, Ma YY, Li WL, He TT, Wang YY, Qu MJ, Liang HB, Zhang ZJ, Yang GY, Tang YH and Wang YT. L-glutamine protects mouse brain from ischemic injury via up-regulating heat shock protein 70. *CNS Neurosci Ther*. 2019;25:1030-1041.
22. Boelens PG, van Leeuwen PA, Dejong CH and Deutz NE. Intestinal renal metabolism of L-citrulline and L-arginine following enteral or parenteral infusion of L-alanyl-L-[2,15N]glutamine or L-[2,15N]glutamine in mice. *Am J Physiol Gastrointest Liver Physiol*. 2005;289:G679-85.
23. Shih YM, Shih JM, Pai MH, Hou YC, Yeh CL and Yeh SL. Glutamine Administration After Sublethal Lower Limb Ischemia Reduces Inflammatory Reaction and Offers Organ Protection in Ischemia/Reperfusion Injury. *JPEN J Parenter Enteral Nutr*. 2016;40:1122-1130.
24. Morris CR, Suh JH, Hagar W, Larkin S, Bland DA, Steinberg MH, Vichinsky EP, Shigenaga M, Ames B, Kuypers FA and Klings ES. Erythrocyte glutamine depletion, altered redox environment, and pulmonary hypertension in sickle cell disease. *Blood*. 2008;111:402-10.
25. Forstermann U and Sessa WC. Nitric oxide synthases: regulation and function. *Eur Heart J*. 2012;33:829-37, 837a-837d.
26. Molenaars M, Janssens GE, Williams EG, Jongejan A, Lan J, Rabot S, Joly F, Moerland PD, Schomakers BV, Lezzerini M, Liu YJ, McCormick MA, Kennedy BK, van Weeghel M, van Kampen AHC, Aebersold R, MacInnes AW and Houtkooper RH. A Conserved Mito-Cytosolic Translational Balance Links Two Longevity Pathways. *Cell Metab*. 2020;31:549-563 e7.
27. Lanters EA, van Marion DM, Steen H, de Groot NM and Brundel BJ. The

future of atrial fibrillation therapy: intervention on heat shock proteins influencing electropathology is the next in line. *Neth Heart J*. 2015;23:327-33.
28. Brundel BJ, Ke L, Dijkhuis AJ, Qi X, Shiroshita-Takeshita A, Nattel S, Henning RH and Kampinga HH. Heat shock proteins as molecular targets for intervention in atrial fibrillation. *Cardiovasc Res*. 2008;78:422-8.
29. Batulan Z, Pulakazhi Venu VK, Li Y, Koumbadinga G, Alvarez-Olmedo DG, Shi C and O'Brien ER. Extracellular Release and Signaling by Heat Shock Protein 27: Role in Modifying Vascular Inflammation. *Front Immunol*. 2016;7:285.
30. Leite JS, Raizel R, Hypolito TM, Rosa TD, Cruzat VF and Tirapegui J. l-glutamine and l-alanine supplementation increase glutamine-glutathione axis and muscle HSP-27 in rats trained using a progressive high-intensity resistance exercise. *Appl Physiol Nutr Metab*. 2016;41:842-849.
31. Moura CS, Lollo PCB, Morato PN, Risso EM and Amaya-Farfan J. Modulatory effects of arginine, glutamine and branched-chain amino acids on heat shock proteins, immunity and antioxidant response in exercised rats. *Food Funct*. 2017;8:3228-3238.
32. Andreasen AS, Pedersen-Skovsgaard T, Mortensen OH, van Hall G, Moseley PL and Pedersen BK. The effect of glutamine infusion on the inflammatory response and HSP70 during human experimental endotoxaemia. *Crit Care*. 2009;13:R7.
33. Jordan I, Balaguer M, Esteban ME, Cambra FJ, Felipe A, Hernandez L, Alsina L, Molero M, Villaronga M and Esteban E. Glutamine effects on heat shock protein 70 and interleukines 6 and 10: Randomized trial of glutamine supplementation versus standard parenteral nutrition in critically ill children. *Clin Nutr*. 2016;35:34-40.

Supplemental material

Internal standards for metabolomics

A 75 µL mixture of the following internal standards in water was used: adenosine-15N5-monophosphate (100 µM), adenosine-15N5-triphosphate (1 mM), D4-alanine (100 µM), D7-arginine (100 µM), D3-aspartic acid (100 µM), D3-carnitine (100 µM), D4-citric acid (100 µM), 13C1-citrulline (100 µM), 13C6-fructose-1,6-diphosphate (100 µM), guanosine-15N5-monophosphate (100 µM), guanosine-15N5-triphosphate (1 mM), 13C6-glucose (1 mM), 13C6-glucose-6-phosphate (100 µM), D3-glutamic acid (100 µM), D5-glutamine (100 µM), 13C6-isoleucine (100 µM), D3-leucine (100 µM), D4-lysine (100 µM), D3-methionine (100 µM), D6-ornithine (100 µM), D5-phenylalanine (100 µM), D7-proline (100 µM), 13C3-pyruvate (100 µM), D3-serine (100 µM), D5-tryptophan (100 µM), D4-tyrosine (100 µM), D8-valine (100 µM).

Supplemental table 1 – Pooled levels of 83 metabolites of the four groups; high HSP: baseline, high HSP: 3-month follow-up (3M), low HSP: baseline and low HSP:3M, and the derived ratios; high HSP: 3M/baseline, low HPS: 3M/baseline and baseline: low HPS/high HSP.

Metabolites	Absolute values				Ratios		
	High HSP: baseline	High HSP: 3M	Low HSP: baseline	Low HSP: 3M	High HSP: 3M/baseline	Low HSP: 3M/baseline	Baseline: low HSP / high HSP
2-aminoisobutyric acid	287781,75	277788,47	285416,84	214518,22	0,97	0,75	0,99
2-dehydrogluconate	221990,38	231779,98	263663,53	280698,09	1,04	1,06	1,19
2-hydroxyglutarate	179094,73	184905,70	213122,48	230604,84	1,03	1,08	1,19
2-phosphoglyceric acid	9926,70	8988,38	5199,31	7997,68	0,91	1,54	0,52
3- and 4-hydroxybenzoic acid	10833,38	7093,30	14676,67	10051,74	0,65	0,68	1,35
3-phosphoglyceric acid	6537,20	1955,93	1596,29	2724,92	0,30	1,71	0,24
Adenine	5423,51	6909,21	2816,32	4277,13	1,27	1,52	0,52
Alanine	716595,75	707790,81	691113,69	696588,19	0,99	1,01	0,96
Allantoin	418144,81	577707,25	325782,84	687823,25	1,38	2,11	0,78
Alpha-ketoglutarate	940000,81	1047807,62	1086722,12	1196047,88	1,11	1,10	1,16
Aminoadipic acid	82965,83	59265,31	53330,67	52626,80	0,71	0,99	0,64
AMP	6237,84	4863,07	25807,34	10240,82	0,78	0,40	4,14
Arginine	1202491,38	1264341,62	1447160,88	1451369,12	1,05	1,00	1,20
Asparagine	1169169,62	1128355,62	1191380,50	1270973,12	0,97	1,07	1,02
Aspartate	1950403,00	1124820,12	902401,25	863328,75	0,58	0,96	0,46
beta-Alanine	489070,22	300834,41	241404,47	255252,84	0,62	1,06	0,49
Citric acid	553016,31	1132180,12	1209130,12	1394095,38	2,05	1,15	2,19
Citrulline	784433,75	796071,19	771386,75	802437,19	1,01	1,04	0,98
CMP	2983,49	472,36	1466,52	3696,88	0,16	2,52	0,49
Coenzyme A	1521,25	2052,42	1927,21	919,93	1,35	0,48	1,27
Creatine	245893,25	224660,03	390407,16	299876,72	0,91	0,77	1,59
Creatine-P	2239,47	5574,60	6194,40	10863,28	2,49	1,75	2,77
Creatinine	387146,94	407434,75	415656,44	478292,44	1,05	1,15	1,07
Cysteine	381218,09	479506,28	498019,75	346933,97	1,26	0,70	1,31

Supplemental table 1 – Continued

Metabolites	Absolute values				Ratios		
	High HSP: baseline	High HSP: 3M	Low HSP: baseline	Low HSP: 3M	High HSP: 3M/baseline	Low HSP: 3M/baseline	Baseline: low HSP / high HSP
Cystine	1505512,50	1754215,38	1973982,12	1428263,25	1,17	0,72	1,31
dAMP	1276,62	2460,60	1875,82	925,48	1,93	0,49	1,47
FAICAR	7713,72	9556,80	8597,92	9202,78	1,24	1,07	1,11
Fumarate	154782,72	99075,59	84258,62	141831,33	0,64	1,68	0,54
GDP	892,85	1712,25	125,81	261,81	1,92	2,08	0,14
Gluconate	1508107,75	1249584,62	1022769,06	1180698,50	0,83	1,15	0,68
Gluconate-6P	9953,55	15665,16	12618,45	11933,20	1,57	0,95	1,27
Glucose	15051773,00	15415444,00	17053558,00	14473830,00	1,02	0,85	1,13
Glucose-6P	48728,48	38391,93	27251,93	39509,27	0,79	1,45	0,56
Glutamate	3777537,75	3276630,00	3258287,50	2892569,75	0,87	0,89	0,86
Glutamine	7359593,50	7269876,00	7231684,50	7353338,50	0,99	1,02	0,98
Glutathione	273734,25	197898,98	169461,56	136910,77	0,72	0,81	0,62
Glyceraldehyde-3P	17259,19	17093,24	11644,60	14950,53	0,99	1,28	0,67
Glycerate	2420490,50	1996610,88	1919937,12	1930657,25	0,82	1,01	0,79
Glycerol-2P	23346,77	19750,82	18253,38	24790,04	0,85	1,36	0,78
Glycerol-3P	109429,25	80145,04	55516,98	87604,36	0,73	1,58	0,51
GMP	6084,78	6083,10	32880,94	17010,21	1,00	0,52	5,40
Guanosine	27225,68	32666,48	46811,73	35511,89	1,20	0,76	1,72
Hexose-P	55519,26	62733,46	57668,94	60660,54	1,13	1,05	1,04
Hippuric acid	5122954,00	5001819,50	4068981,75	2557098,75	0,98	0,63	0,79
Hydroxyphenyllactic acid	391409,44	364428,97	316635,09	403702,75	0,93	1,27	0,81
Hypoxanthine	4133240,75	1126731,00	692743,75	721457,81	0,27	1,04	0,17
Inosine	3740350,25	359541,16	1020823,44	678759,94	0,10	0,66	0,27
Isoleucine	951234,81	862355,00	725410,81	758966,81	0,91	1,05	0,76
Kynurenic acid	16246,47	15923,84	13601,25	19662,87	0,98	1,45	0,84

Supplemental table 1 – Continued

Metabolites	Absolute values				Ratios		
	High HSP: baseline	**High HSP: 3M**	**Low HSP: baseline**	**Low HSP: 3M**	**High HSP: 3M/baseline**	**Low HSP: 3M/baseline**	**Baseline: low HSP / high HSP**
Kynurenine	14726,31	11901,50	12381,64	16343,15	0,81	1,32	0,84
Lactate	1753591,50	1876363,75	1455605,00	1610763,62	1,07	1,11	0,83
Leucine	499256,72	437421,78	359404,44	384554,25	0,88	1,07	0,72
Lysine	1479301,25	1461074,00	1580014,50	1528886,38	0,99	0,97	1,07
Malate	109803,13	134011,34	137286,62	225086,86	1,22	1,64	1,25
Malonic acid	584030,38	667470,81	785184,00	749892,31	1,14	0,96	1,34
Mesaconic acid	204886,19	235236,62	414397,53	262510,47	1,15	0,63	2,02
Methionine	1032750,94	824053,00	1030812,00	943850,38	0,80	0,92	1,00
Ornithine	1145510,88	1045397,81	961652,12	1025651,00	0,91	1,07	0,84
Orotic acid	31423,60	25836,63	28049,31	28791,13	0,82	1,03	0,89
Oxiglutathione	6445,94	4046,31	2806,63	3108,22	0,63	1,11	0,44
Pantothenic acid	28282,16	22077,56	21334,92	25665,18	0,78	1,20	0,75
Phenylalanine	432958,88	348660,59	356347,62	386391,44	0,81	1,08	0,82
Phosphoenolpyruvate	72120,92	88755,93	81087,99	87339,29	1,23	1,08	1,12
Phosphorylethanolamine	28125,24	27514,03	18592,93	26249,35	0,98	1,41	0,66
Proline	694712,12	590366,69	660961,19	703327,31	0,85	1,06	0,95
Pyroglutamic acid	3732751,25	2007733,75	2020519,00	1925066,12	0,54	0,95	0,54
Pyruvate	3090132,75	3607122,00	2798369,00	2582617,00	1,17	0,92	0,91
Ribose	78844,84	69713,19	41277,18	42491,13	0,88	1,03	0,52
Ribose-5P	67586,32	13006,05	13230,18	16366,28	0,19	1,24	0,20
Sedoheptulose-7P	9813,83	2893,79	2653,62	5372,14	0,29	2,02	0,27
Serine	2069198,12	1662040,88	1715682,88	1721282,50	0,80	1,00	0,83
Succinate	547055,50	496645,81	498179,00	611279,25	0,91	1,23	0,91
Taurine	7920577,00	6883827,00	7242785,00	7073309,50	0,87	0,98	0,91
Threonine	3028374,75	2603921,50	3203242,75	2857039,75	0,86	0,89	1,06

Supplemental table 1 – Continued

Metabolites	Absolute values				Ratios		
	High HSP: baseline	High HSP: 3M	Low HSP: baseline	Low HSP: 3M	High HSP: 3M/baseline	Low HSP: 3M/baseline	Baseline: low HSP / high HSP
Tryptophan	239878,62	209133,36	230502,98	231175,75	0,87	1,00	0,96
Tyrosine	2083736,50	1488541,62	1578549,38	1490897,12	0,71	0,94	0,76
UDP-HexNac	4607,83	3300,96	804,66	1873,41	0,72	2,33	0,17
UMP	81202,38	89027,72	96067,88	101030,18	1,10	1,05	1,18
Uracil	15774,99	16091,43	8874,64	18312,55	1,02	2,06	0,56
Uric acid	16063145,00	16035150,00	17161386,00	15726882,00	1,00	0,92	1,07
Uridine	797953,38	945954,81	790121,38	788372,06	1,19	1,00	0,99
Valine	2501336,00	2417852,25	2203344,75	2174082,25	0,97	0,99	0,88
Xanthine	2970335,25	2135401,50	1363402,38	1407568,75	0,72	1,03	0,46

Supplemental table 2 – Human pathways of metabolites which show an association between HSP and metabolic energy levels. In addition, the global metabolism pathway which the human pathway corresponds with is denoted (x).

			Global metabolism pathways			
Behavior	**Metabolites**	**Human pathways**	**Carbo-hydrates**	**Nucleotides**	**Amino acids**	**Vitamins & cofactors**
Normalization	Ribose 5P	Pentose phosphate pathway	x			
		Purine metabolism		x		
		Carbon metabolism	x			
		Biosynthesis of amino acids			x	
	Aspartate	Alanine, aspartate and glutamate metabolism			x	
		Arginine biosynthesis			x	
		Biosynthesis of amino acids			x	
		beta-Alanine metabolism			x	
		Pantothenate and CoA biosynthesis				x
		Carbon metabolism	x			
		2-Oxocarboxylic acid metabolism		x		
		Histidine metabolism			x	
	beta-Alanine	beta-Alanine metabolism			x	
		Histidine metabolism			x	
		Pantothenate and CoA biosynthesis				x
		Pyrimidine metabolism		x		
		Propanoate metabolism	x			
	Hypoxanthine	Purine metabolism		x		
	Oxiglutathione	Glutathione metabolism			x	
	Pyroglutamic acid	Glutathione metabolism			x	
	Citric acid	Citrate cycle (TCA cycle)	x			
		2-Oxocarboxylic acid metabolism	x			
		Glyoxylate and dicarboxylate metabolism	x			
		Biosynthesis of amino acids			x	
		Alanine, aspartate and glutamate metabolism			x	
		Carbon metabolism	x			
Increase	Creatine P	Arginine and proline metabolism			x	
	GDP	Purine metabolism		x		
Decrease	Inosine	Purine metabolism		x		

14

General discussion

Roeliene Starreveld

The growing epidemic of atrial fibrillation (AF) should be called to halt rather earlier than later. As delineated in **Chapter 1**, current treatment modalities cannot yet compete with the intricate, multifactorial and patient-specific milieu initiating and persisting AF. In order to improve future patient outcomes, it is of prime importance to gain better insight into the processes underlying pathophysiology of AF. On the one hand, high-resolution mapping can be used to unravel and quantify electrophysiological abnormalities underlying AF. By firstly investigating characteristics during SR, high-resolution mapping can aid in (re)defining what is 'normal' (e.g. physiological conduction). Consequently, the arrhythmogenic substrate that underlies AF initiation and persistence can be uncovered using AF mapping. On the other hand, identifying biological markers of AF remodeling is of relevance, as therapeutic strategies could potentially be directed at these (ongoing) processes. In this thesis, new insights into both electrical and biological characteristics of AF have been introduced, which are discussed and put into perspective in the current chapter.

Electrophysiological mechanisms contributing to pathogenesis of AF: taking a closer look

Cardiac action potentials form the basis of electrical activation of cardiomyocytes and electrical conduction in the human heart. Action potentials are caused by changes in membrane currents, of which the most prominent are the Ca^{2+}, Na^{+} and K^{+} current. In pacemaker cells (i.e. the sinoatrial and atrioventricular node), depolarization is primarily caused by rapid influx of Ca^{2+} ions due to activation of the L-type Ca^{2+} channels. Activation of Na^{+} channels predominantly facilitates depolarization in non-pacemaker cells, such as atrial and ventricular cardiomyocytes. As the membrane potential becomes more positive, Ca^{2+} and Na^{+} channels are inactivated and cannot be opened, regardless of the strength of an arriving stimulus (*absolute refractory period*). All cardiomyocytes are repolarized due to the outward K^{+} current, which slowly makes the membrane potential more negative and reset the Ca^{2+} and Na^{+} channels. It is possible to initiate a new action potential during this *relative refractory period*, yet a stronger stimulus than normal is required. Action potentials transfer from one cell to the neighboring cell by gap junctions, facilitating conduction. These intercellular connections are densely arranged longitudinally, connecting end-to-end, whereas sparse junctions connect in the transverse, side-to-side, direction.[1] Together with the elongated parallel arrangement of atrial cardiomyocytes, this promotes action potentials to conduct in the longitudinal direction, leading to a higher conduction velocity (CV) along this axis.[1, 2] Conceptually, the minimal activating current or charge that is necessary to sustain action potential propagation is termed the *safety factor* for cardiac conduction. It is generally assumed that the safety factor in the longitudinal direction is lower than in the transverse direction. The direction-dependency

of atrial conduction is called *anisotropy*. In 1988, Spach et al. demonstrated longitudinal CV to reach 0.57m/s, whereas transverse CV is 0.12m/s.[3]

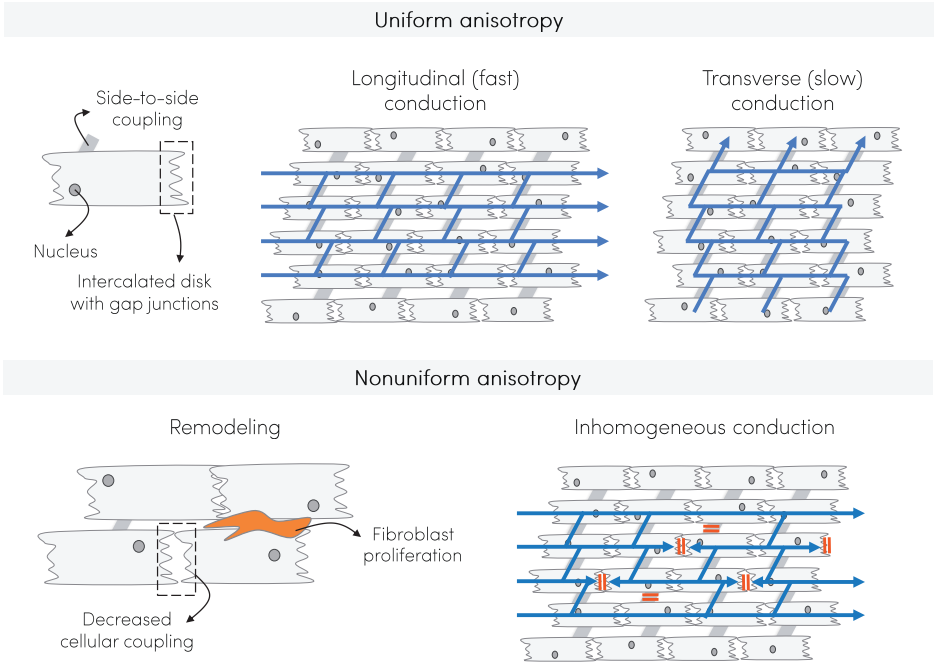

Figure 1 – Uniform and nonuniform anisotropy. *Upper panel:* propagation of action potentials along cardiomyocytes is faster in the longitudinal than in the transverse direction, i.e. uniform anisotropy. *Lower panel:* decreased cellular coupling and proliferation of fibroblasts due to remodeling of cardiac tissue causes nonuniform anisotropy and facilitates inhomogeneous conduction.

Though anisotropy is a physiologic characteristic of atrial tissue, AF-initiated structural remodeling, such as decreased cell-to-cell coupling in combination with formation of fibrosis, facilitates *nonuniform anisotropy* (*Figure 1*).[2,4,5] In 1994, Spach et al. characterized nonuniform anisotropy by a 'sparsity or the infrequent presence of side-to-side electrical connections between cells and small groups of cells'.[5] This spatial nonuniformity causes asymmetry in excitability, so that unidirectional conduction block can occur in one pathway while conduction is maintained in a second pathway, providing a stage for reentry to occur.[5] Similarly, spatial dispersion in refractory periods, decreased cellular coupling and deposition of (micro)fibrosis have been shown to facilitate inhomogeneous conduction and – consequently – reentry.[5] As asynchronous activation of cardiomyocytes results in morphological alterations in extracellular electrograms, such as multiphasic fractionated electrograms[2], high-density mapping can aid in locating arrhythmogenic structural discontinuities (**Chapter 2**).

Analyzing electrogram morphology: what does it add?

The potential of especially unipolar electrogram morphology to reflect underlying conduction processes has been distinguished for years. During normal conduction, due to homogeneously activated cardiomyocytes, a single, biphasic RS-wave is observed. In contrast, multiple positive and negative peaks in the unipolar electrogram (i.e., fractionation) arise from action potentials in (groups of) cardiomyocytes that are activated asynchronously.[6, 7] Using high-resolution unipolar mapping, such asynchronous activation can be uncovered and localized. Corresponding with the fundamental studies of Spach et al. [2, 3], **Chapter 3** elucidated direction- and rate-dependent fractionation, reflecting nonuniform anisotropy. Throughout sinus rhythm (SR) mapping, several premature atrial complexes occurred and exposed highly irregular potentials with low-amplitude deflections and prolonged duration. Due to the short coupling interval, the area at which the premature impulse arises is still partly refractory. This induced multiple areas of local conduction block around which the activation front slowly propagated, as visualized in the long duration potential with low-amplitude fractionation. We believe these potentials characterize *slow conduction* [8], an important pathological mechanism in the initiation and perpetuation of AF. Direction-dependent nonuniform anisotropy is provoked by the premature impulse and leads to slow conduction, as previously described in bipolar recordings by Jadidi et al. in the left atrium (LA).[9] After SR recordings, programmed electrical stimulation was performed. Increasing the pacing frequency resulted in similar low-amplitude, fractionated atrial potentials with prolonged duration, again reflecting discontinuous, slow conduction in underlying myocytes.[10, 11] In this example, rate-dependent nonuniform anisotropy is provoked with the increased pacing rate, again leading to slow conduction. The underlying mechanisms of direction-dependent and rate-dependent nonuniform anisotropy are however believed to be distinct. Whereas premature stimulation provokes especially longitudinal block with preserved transverse conduction, increasing the pacing rate causes an increase in intercellular coupling resistance and decreases transverse conduction exponentially.[10, 12] These examples illustrate the unique capacity of high-resolution unipolar mapping, yet also reveal its challenges, as morphological characteristics within electrograms often represent intertwined underlying electrophysiological and/or structural mechanisms, which cannot always be distinguished based on electrogram morphology alone.

In addition to slow conduction, areas of *wave collision*, *lines of block*, *pivot sites* and *endo-epicardial dissociation* have been identified as important contributors to arrhythmogenesis and AF maintenance.[8, 13, 14] Primarily experimental animal studies have investigated the effects of conduction patterns – mostly slow conduction, wave collision, lines of block and pivot sites – on morphology of unipolar [7, 15-17] and bipolar electrograms [6, 18, 19]. In addition, computer model studies [20, 21] and

bipolar measurements during atrial flutter [22-25], atrial tachycardia [8] and ventricular tachycardia [26, 27] have been performed. However, it was still largely unknown to what extent these various conduction patterns contribute to the temporal and spatial variations in electrogram morphology as observed during AF. In 1977, Konings et al. firstly studied this and described morphological characteristics of rapid uniform conduction, wave collision, conduction block, pivot sites and slow conduction during induced AF (as illustrated in *Figure 2*), as well as during SR and atrial pacing.[13]

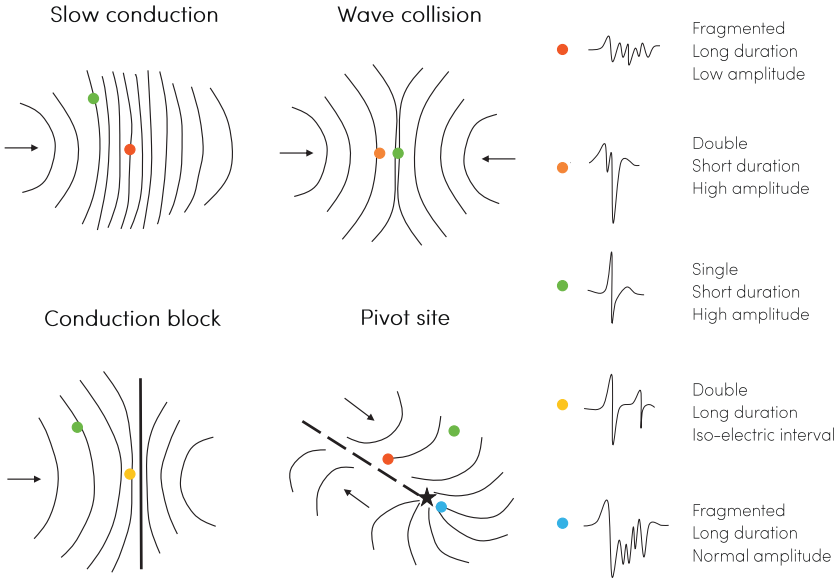

Figure 2 – Unipolar electrogram morphology during different activation patterns. Long duration, low-amplitude fractionated potentials are primarily found at areas of slow conduction. At the borders of slow conduction zones, normal (single) potentials have also been observed. Short-double potentials mainly appear in the vicinity of colliding waves, whereas long-double potentials with an iso-electric interval characterize conduction block and reflect asynchronous activation of tissue at both sides of the blocked area. Fragmented potentials with long duration, but normal amplitude, are found at pivoting points (star). In the friction area of a pivot site (dashed line), fragmented potentials with long duration and low-amplitude deflections can be observed. Based on findings of Konings et al.[13]

Using a 244-unipolar electrode array, the epicardial surface of the right atrium (RA) was mapped in 25 Wolff-Parkinson-White patients undergoing cardiac surgery. During induced AF, 77±12% of potentials were single, 7±3% short-doubles (two deflections, <10 ms apart), 10±7% long-doubles (two deflections, 10-50 ms apart) and 6±4% fragmented (>2 deflections within 50 ms). Of all electrograms, 79±11% were recorded at sites showing rapid uniform conduction, 3±2% during wave collision, 15±8% during conduction block, 2±2% at areas of slow conduction, and 2±1% at pivot sites. During wave collision, conduction block, slow conduction

or pivoting, proportion of single potentials was only 22±13%, 14±7%, 33±27%, and 17±12%, respectively. In contrast, 94±4% of potentials were single during fast uniform conduction. Further investigating the relation between activation patterns and morphology of electrograms, Konings et al. found high sensitivity (0.95) and specificity (0.84) of single potentials for rapid uniform conduction, with a positive predicting value (PPV) of 0.96.[13]

Single potentials: simple or misunderstood?

Though most single potentials represent normal conduction, asymmetry of unipolar single potentials has been linked to areas of wave collision and conduction heterogeneity in computer studies.[21] In the clinical mapping study performed in **Chapter 6**, (a)symmetry of unipolar single potentials was studied in patients with mitral valve disease during SR. In general, amplitude of unipolar single potentials was mainly determined by the amplitude of the S-wave. As wave activation during SR generally originates from the sinoatrial node in the upper RA, monophasic S-waves were preliminary found there, evolving to biphasic RS-waves when the wavefront propagates away from the excitation site in the lower RA and Bachmann's Bundle (BB). In turn, R-wave predominance was found in the pulmonary veins (PVs) and the left atrium (LA), corresponding with wavefront collision and termination[13, 21, 28-30]. The PVs and the roof of the LA are also known to have heterogeneity in myocardial cell size, fiber orientation and cell-to-cell coupling, promoting nonuniform anisotropic, discontinuous conduction leading to wave collisions.[6, 31] Even though Spach et al. observed single monophasic R-waves at the exact site of wave collision in thin in vitro preparations[17], recordings performed in intact hearts exhibited biphasic potentials with R-wave predominance[13, 30], probably due to depolarization waves propagating in deeper layers of the atrial wall generating the far-field negative part of the biphasic potential. In addition, decreased unipolar single potential amplitudes in combination with a decreased conduction velocity (CV) were found in patients in patients with a history of paroxysmal AF (PAF) compared to patients without a history of AF (**Chapter 6**), especially in BB. Whereas areas of fast, normal conduction along the longitudinal axis of myocardial fibers would be characterized by high amplitude RS-waves, these lower amplitude single potentials can be observed in areas with colliding waves and slow conduction, due to the loss of primarily S-wave amplitude.[32] Patients with PAF are prone to structural and electrophysiological remodeling, increasing susceptibility to altered wavefront conduction. So, whereas the typical biphasic RS-wave evidently represents normal, fast conduction, asymmetrical single potentials can reflect sites of wavefront collisions in unipolar recordings.

Double potentials: double the trouble?

Single potentials at the exact sites of collision (22±13%) were flanked by short-double potentials (65±15%) in the study of Konings et al.[13] Short-double potentials were most

present during wave collision, yet PPV only yielded 0.33, as short-doubles were also rather frequently observed during conduction block (15±6%). Most common in areas of conduction block were long-double potentials (71±8%), showing a sensitivity of 0.75, specificity of 0.99 and PPV of 0.84. The two distinct deflections within the long-double potential represent depolarization of myocytes at both sides of the intra-atrial blockade. Wavefront collision is the most frequently observed phenomenon underlying fractionation during SR[9], pacing[9], atrial tachycardia[8], and is often functional and passive in nature. Even though it is hypothesized that collisions can ease initiation of AF, it is unlikely that areas of wavefront collision play a critical role in maintenance of AF[33, 34]. Arcs of intra-atrial conduction block are theorized to be more important, considering that they facilitate re-entry and initiate AF, while also promoting separation of wavelets and inhomogeneous conduction maintaining AF.[13] In transitioning from organized to fractionated potentials during (induced) AF, Atienza and colleagues showed increased presence of functional block and slow conduction[35], indicating an important role for these abnormal conduction patterns. Though Frontera et al. did not define *bipolar* long-double potentials as fractionation[8], we do believe *unipolar* long-doubles (partly) reflect functional lines of local intra-atrial blockades.

Increased morphology complexity: depiction of the arrhythmogenic substrate?
In general, there is consensus that the higher the complexity of fractionation, the more deteriorated underlying atrial conduction properties are. Highest percentages of fractionation were found during slow conduction and pivoting of AF waves (58±21% and 80±10%, respectively).[13] In these areas, severely fragmented potentials with long-duration were observed. Sensitivity and specificity of such potentials was 0.61 and 0.98 for slow conduction, and 0.85 and 0.99 for pivot sites, respectively.[13] When combined, the PPV of fragmented potentials for slow conduction or pivot sites was 0.87. Importantly, Konings et al. concluded that in the absence of a fragmented electrogram, the chance of slow conduction or pivot sites is practically zero. Areas of slow conduction progressively shorten the wavelength of meandering AF waves, thereby increasing complexity, and thus persistence, of AF.[13] Pivot sites are also believed vital during AF, as non-pivoting waves will die out at the boundaries of the atria.[13] However, whereas slow conduction is believed to be of structural nature, pivoting is considered more functional, facilitated by anisotropy and wavefront curvature.[8, 36] As such, it is hypothesized that slow conduction plays a more crucial role in maintaining the arrhythmia.[8]

As the electrogram represents the summation of extracellular currents, the different components of fractionated electrograms represent disparate activation of (adjacent) cardiomyocytes.[6] Where one would expect a prolonged, yet smooth, low-amplitude biphasic potential during homogeneous slow conduction, the fractionated component within the observed potentials suggests slow activation

in combination with inhomogeneities.[6] Such inhomogeneities include localized increases in intra- or extracellular resistance, abrupt changes in cell size or surface-to-volume ratios, alterations in cell-to-cell coupling, abrupt cell branching and (micro)fibrosis, as discussed in **Chapter 1**.[6, 11, 36] Particularly fractionated potentials with long-duration and low-voltage deflections are associated with (inhomogeneous) slow conduction. During SR and pacing, Jadidi et al. showed "dyssynchronous" activation around a zone of slow conduction to represent 24% of fractionation.[9] As described in **Chapter 7**, potentials in areas of slowed conduction (local CV <28 cm/s) and conduction block (local conduction delay <18 cm/s) had lower voltages than during normal conduction in SR. In addition, fractionated potentials (>2 deflections), had significantly lower amplitudes compared to single potentials (2.05 [1.04 – 3.75] mV vs. 5.16 [2.85 – 8.01] mV, p<0.001) and a clear inversely proportional relationship between unipolar voltage and the number of additional deflections was observed. These observations in SR largely correspond with those of Konings et al. during AF and Frontera et al. during AT.[8, 13] In addition to our findings, Frontera et al. objectified a significant inverse relationship between electrogram duration and voltage.[8] Atrial potentials longer than 63 ms had a 0.99 sensitivity and specificity for identification of pathological mechanisms, including slow conduction and pivoting points.[8] Though these analyses were performed in bipolar recordings, duration of AF potentials is not expected to differ substantially in unipolar recordings. Electrogram amplitude <0.3 mV showed a 0.88 specificity and 0.97 sensitivity for identification of pathological mechanisms. Despite these promising numbers, slow conduction could not be distinguished based on amplitude and duration of electrograms alone.[8]

(Re)defining targets for ablative therapy

Considering the suboptimal success rates of pulmonary vein isolation (PVI) alone in primarily non-paroxysmal AF patients[37], it remains an ongoing challenge to find the adequate therapy for these patients. The discovery that especially low-amplitude fractionated potentials with long-duration reflect critical conduction abnormalities during AF has therefore led to the introduction of new, morphology-based targets during ablative therapy. Several mapping systems developed automatic algorithms to quantify electrogram morphology of bipolar recordings during ablation. The pioneering study of Nademanee et al. firstly performed ablation of complex fractionated atrial electrograms (CFAEs), using the automatic algorithm of CARTO for its analyses.[38] In this study, CFAEs were defined as: 1) atrial electrograms that have fractionated electrograms composed of two deflections or more, and/or perturbation of the baseline with continuous deflection of a prolonged activation complex over a 10-s recording period; 2) atrial electrograms with a very short cycle length (≤120 ms) averaged over a 10-s recording period. Ablation of these CFAEs resulted in termination of AF in 95% of patients, including 58 (longstanding) persistent AF patients (success rate: 91%).[38] Unfortunately, these extraordinary results

could never be reproduced in randomized controlled trials, as listed in *Table 1*. Also, PVI has been shown to significantly reduce fractionation and prolong the AF cycle length[39], suggesting a non-primary, more passive role in AF for CFAEs. Considering the mixed outcomes, in addition to the prolonged procedural time and increased exposure to fluoroscopy, CFAE ablation is nowadays only advised in patients in whom other ablative therapies fail (i.e. recurrence of AF).[40]

Failure of current CFAE-guided ablative strategies could lie in the fact that not all fractionated electrograms represent slow conduction, presumed to be crucial in maintenance of AF, and vice-versa. In the search for a possible anatomic predilection site for low-voltage and/or fractionated potentials, we studied regional differences in voltages and fractionation in both patients with and without PAF (**Chapter 7)**. The highest percentage of fractionated potentials was found at BB in both groups. This region also yielded the lowest potential voltages in patients with PAF, whereas the PV area had the lowest amplitudes in the no AF group. Low-voltage areas (<1.0 mV) were more frequently observed in BB in the PAF group compared to the no AF group. Though these findings stress the intricate relation between unipolar voltage and fractionation with arrhythmia-induced remodeling (PAF), and indicate important regional differences, it remains difficult to find clear predilection sites. This was also objectified in **Chapter 4**, where we found pre-ablation fractionation in high proportions (>60% of patients or electrograms) in almost all regions of both atria. Though we do believe areas of slow conduction are meaningful targets for ablation, identification based on electrogram morphology alone is not yet feasible. Atrial electrogram fractionation can have multiple causes of both pathologic (e.g. slow conduction due to structural abnormalities) and nonpathologic origin (e.g. wave collisions). Furthermore, several technical aspects of ablative systems have been identified as influencers of signal morphology, such as interelectrode spacing[41, 42], distal electrode size[43] and also filter settings (**Chapter 5**). The latter impacted not only the number of deflections (fractionation), but also altered the deflection amplitude, potential duration (fractionation delay time) and local activation time. In addition, as no uniform definition or methodology is used for measuring fractionated electrograms[44] (**Chapter 4**), identification of true pathologic fractionation is compromised. Targeting all areas with fractionation is unnecessary and can even cause harm to the patient, as risk of iatrogenic atrial tachyarrhythmia might increase due to extensive scarring of atrial tissue[45].

Table 1 - Efficacy of (additional) complex fractionated atrial electrograms ablation

Author (year)	Sample size			Persistent AF			Ablation procedures per patient	Follow-up (months)	Freedom of AF/AT		
	PVI	CFAE	PVI + CFAE	PVI	CFAE	PVI + CFAE			PVI	CFAE	PVI + CFAE
Elayi et al. (2008)	48	-	49	100%	-	100%	1	16±1	40%	-	61%
Deisenhofer et al. (2008)	48	-	50	0%	-	0%	1.3	19±8	74%	-	83%
Di Biasi et al. (2009)	35	34	34	0%	0%	0%	1	12	89%	23%	91%
Oral et al. (2009)	50	-	50	100%	-	100%	1	10±3	38%	-	36%
Verma et al. (2010) *STAR-AF*	32	34	34	34%	38%	35%	1	12	48%	29%	74%
Chen et al. (2011)	35	24	58	0%	0%	0%	1	22.6±6.4	77%	38%	69%
Dixit et al. (2011) *RASTA*	55	-	51	100%	-	100%	1	22±9	49%	-	29%
Nürich et al. (2014)	33	-	35	0%	-	0%	1.4	21±1	88%	-	86%
Verma et al. (2014) *STAR-AF 2*	61	-	244	100%	-	100%	1	18	59%	-	49%

AF, atrial fibrillation; AT, atrial tachycardia; CFAE, complex fractionated atrial electrograms; PVI, pulmonary vein isolation

Existence of pre-ablation scarring, due to interstitial fibrosis by AF-induced structural remodeling, has been linked to ablation outcomes. Multiple studies have indicated presence of low-voltage areas (LVAs), hypothesized to reflect fibrosis and highly-remodeled tissue, to predict AF recurrence after PVI.[46-52] As such, targeting of LVAs has recently been introduced. Subsequent to CFAE ablation, this substrate-guided ablation strategy is based on the concept of detecting abnormal atrial tissue that is related to AF initiation and persistence. In general, LVAs are defined as areas with a *bipolar* voltage ≤0.5 mV. In paroxysmal AF patients with pre-existing LVAs, ablation of these areas did not improve AF-recurrence-free survival in the recently published randomized controlled trial of Masuda et al.[52] In persistent AF patients, no randomized controlled trial has been performed comparing PVI plus LVA ablation with PVI alone. Without randomization, it has been shown that freedom from AT/AF at 18 months after procedure improved with additional LVA ablation (72% PVI±LVA vs. 58% PVI, p=0.02, respectively) in patients with persistent AF.[53] Importantly, mapping of LVAs is based on the *conception* that low-voltage reflects scarred tissue and thus arrhythmia substrate. Bipolar voltage, however, should be used with caution, as it is influenced by numerous factors, including wavefront of activation, tissue contact and characteristics of the recording catheter and mapping system (i.e., electrode size, interelectrode spacing, filtering, mapping density and resolution).[54, 55] Cut-off values for abnormal low-voltage in *unipolar* electrograms have not yet been defined, but could potentially further enhance voltage-guided ablation.

Endo-epicardial dissociation: new player in the field

Usually, mapping of the atria is performed from either the endocardium or epicardium, assuming that atrial conduction is mostly confined to the two-dimensional plane. However, structural and electrophysiological inhomogeneities can facilitate dissociation of the endo- and epicardial layer, which was firstly identified during AF in humans by de Groot and van der Does et al. in 2016 (*Figure 3*).[14] The asynchronous activation of the endo- and epicardial layers provide opportunity for fibrillation waves to travel transmurally and thereby cause new breakthrough waves on the opposite side of the wall. Incidence of endo-epicardial asynchrony was shown to range between 0.9 to 55.9%, without preference for the endo- or epicardial layer to be firstly activated.[14] Furthermore, non-transmural conduction block has recently been illustrated using simultaneous endo-epicardial mapping[56], indicating that arrhythmia-substrate is not limited to the two-dimensional plane.

Whether local endo-epicardial asynchrony (EEA) causes fractionated electrograms was investigated in **Chapter 8**. In patients undergoing cardiac surgery, endo- and epicardial unipolar electrograms were simultaneously recorded at the inferior-, mid- and superior-RA during SR. Incidence of fractionation was comparable between the endo- and epicardial layer at all locations (inferior-RA 17% vs. 15%, mid-RA 22% vs. 21%, superior-RA 38% vs. 33%, p=NS for all, respectively). The vast

majority of fractionated electrograms (95%) had deflections that corresponded with local activation (i.e., deflection) in the surrounding tissue of the same or the opposite layer. Of these electrograms, in 4% a matching local activation was present in the opposite plane, corresponding with EEA (Δ≥15ms between layers) and 9% in the same plane, corresponding with delayed, discontinuous activation (Δ≥12 ms) within that layer. In 83% a matching local activation was present in both layers, whereas in the remaining 5% of fractionated deflections no matching local activation was found. This study elucidates that fractionated potentials during SR only represent EEA in a limited percentage, whereas small conduction disorders within the same plane are a more common cause of fractionation. Importantly, due to the relative scarcity of inhomogeneous conduction, SR recordings generally exhibit less EEA in comparison to premature stimulation and atrial arrhythmias.[14, 30] The incidence of EEA based fractionation is therefore expected to increase during AF. This study furthermore shows that EEA-based fractionation can even be discovered when measured from only one side of the atrial wall by relating unipolar electrogram morphology to spatial patterns of activation.

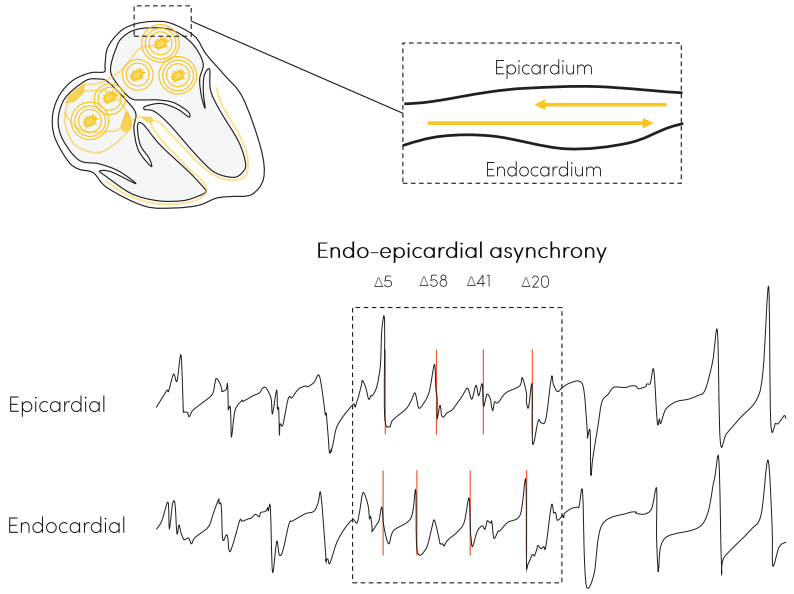

Figure 3 – Endo-epicardial asynchrony and fractionated electrograms. Asynchronous activation of the epicardium and endocardium can be elucidated using unipolar electrograms.

In clinical practice, electrophysiological studies commonly record electrical activity from the endocardial side. During these studies, bipolar recordings are often preferred above unipolar recordings given their ability to reduce far-field influence.[57] However, bipolar measurements are susceptible to changes in interelectrode

distance, electrode size and, most importantly, wavefront direction.[57-59] As multiple wavefronts collide and coincide during AF, bipolar recordings fail to identify and represent these waves. Unipolar recordings can safely identify local activation time during colliding and coinciding wavefronts, and reflect underlying conduction processes better, which is why currently emerging ablative systems focus more on unipolar measurements [60, 61]. Whether unipolar or bipolar electrograms are better suited for detection of fractionation-based EEA from only one side of the atrial wall was discussed in **Chapter 9**. During SR (n=14), atrial extrasystoles (n=7) and atrial pacing (n=1), EEA was studied in unipolar maps and derived bipolar maps (bipolar-x and bipolar-y). Given its ability to remove far-field influence, bipolar recordings were hypothesized to not include EEA based fractionation. Nonetheless, fractionation corresponding to EEA did appear on bipolar electrograms, indicating the asynchronous activity was locally enough to observe. Unipolar recordings yielded less noise and thus better signal-to-noise ratios, emphasizing superiority of unipolar electrograms for mapping of AF than bipolar electrograms.

A short detour into postoperative AF: whom is at risk?

Postoperative AF (PoAF) is the most commonly encountered complication after cardiac surgery, occurring in up to 44% of patients.[62] Although considered a transient and predominantly mild complication occurring especially in the early recovery period after surgery, PoAF is associated with an increased risk of mortality and morbidity, longer hospitalization and higher costs of post-operative care.[63-65] Advanced age, male gender, hypertension, diabetes and combined valvular and coronary artery surgery have been consistently identified as predictors for PoAF.[65] In addition to these risk factors, obesity (body mass index (BMI) ≥ 30 kg/m^2) predisposed to a larger number of prolonged PoAF episodes in the first five postoperative days (**Chapter 10**). Obese patients showed a higher PoAF burden (i.e., the ratio between total duration of all PoAF episodes and total recording time), more frequent prolonged PoAF episodes (i.e., lasting more than one hour). Prolonged episodes of PoAF have been associated with increased risk of stroke[66]. Furthermore, a significant relation between BMI and PoAF burden was objectified. For both obese and non-obese patients, PoAF particularly occurred on the third postoperative day and the majority of PoAF episodes lasted less than five minutes, which has been described in previous literature.[64] The precise interplay between obesity, the arrhythmogenic substrate and initiation of PoAF are not fully understood, but increased depositions of epicardial adipose tissue promoting interstitial fibrosis might play a role.[67, 68] In addition, left atrial enlargement, inducing stretch-related functional remodeling, can be a crucial mechanism underlying the relation between (Po)AF and obesity.[69-71] In patients with a bicuspid aortic valve (BAV), one of the most common types of congenital heart disease, left atrial enlargement was also found an important predictor of PoAF (**Chapter 11**). In contrast to the rather fixed effects of congenital abnormalities on left atrial dimensions, the effects of

obesity are (partly) reversible with weight control[71]. As such, preventive lifestyle measures before cardiac surgery could aid in reversing the pre-existing substrate in these patients. Based on the strong association between complexity of surgery and development of PoAF, however, we believe the AF substrate develops during and after the surgery as well, e.g. due to surgery-related edema and inflammation on short-term and development of fibrosis and scar on the long-term. By characterizing unipolar electrogram morphology and conduction abnormalities with high-resolution epicardial mapping during cardiac surgery, but before commencement to extra-corporeal circulation, the pre-existent atrial substrate underlying PoAF can be uncovered. (*van Schie and Starreveld et al., in preparation)* To elucidate surgery-related development of AF substrate, non-invasive approaches that can quantify electropathological measures in the postoperative period, such as body-surface mapping, should be developed further.

Biological mechanisms contributing to pathogenesis of AF: root cause or bystander?
Electro-anatomical remodeling, including left atrial dilatation, contractile dysfunction and interstitial fibrosis, has been widely recognized crucial in pathogenesis and persistence of AF. Nevertheless, pharmaco-therapeutic strategies for AF are not yet directed at potential drivers of these mechanisms, such as cardiomyocyte damage, derailment of proteostasis and mitochondrial dysfunction.[72] As cardiomyocytes are highly sensitive to changes in the intra- and extracellular milieu, the AF-induced cellular calcium overload causes cardiomyocyte stress, consequently inducing derailment of proteostasis within weeks after AF onset. Proteostasis literally is the homeostasis of proteins, maintaining the balanced cycle of protein synthesis, protein translation, chaperone assisted protein folding and degradation of proteins. Within the heart, heat shock proteins (HSPs) act as chaperones to ensure healthy cardiomyocyte proteostasis during stressful conditions (i.e. AF), by assisting in the refolding of unfolded proteins[73, 74], preventing damage to contractile proteins[75, 76] and attenuation of protein degradation[77]. HSPs protect cardiomyocytes against AF-induced remodeling and, consequently, progression and persistence of AF. Whereas HSPs immediately increase in response to acute stress, they eventually get depleted during chronic stress, as shown in heart failure and non-paroxysmal AF patients.[75, 78] As such, compounds that could induce HSPs back to normal, healthy, levels have great potential to restore proteostasis, and potentially reverse stress-induced structural remodeling.[79] The semi-essential amino acid L-glutamine has demonstrated ability to induce HSPs in organs, including the heart.[80-82] In **Chapter 13**, we therefore investigated the effect of daily supplementation of the semi-essential amino acid L-glutamine as a HSP-inducing compound in AF patients. We found HSP27 and HSP70 *serum* levels to decrease in the first three months of L-glutamine supplementation, and HSP27 levels to normalize to baseline levels after six months of L-glutamine supplementation. As the precise mechanisms of transmembrane transport between the intracellular and extracellular milieu are

not fully understood, we can only hypothesize about the interaction between HSP levels in cardiomyocytes and serum. On the one hand, (1) high levels of HSPs in cardiomyocytes could prevent cellular stress from occurring and thereby leak less HSPs to the external milieu, leading to decreased levels of HSP in the blood, (2) while on the other hand (too) high levels of HSPs in cardiomyocytes could cause leakage of HSPs to the extracellular matrix and thereby increase HSP levels in the serum. Patients with a higher HSP27 or HSP70 start level decreased more in HPS level during three months of L-glutamine supplementation, which was in correspondence with the normalization pattern we observed in metabolites related to carbohydrates, nucleotides, amino acids and cofactors and vitamins. Though uncertain about the precise interplay and protective effect, these findings indicate an influence of L-glutamine on HSP levels and metabolic phenotypes, and encourage further mechanistic studies on this topic.

Both cellular and blood-based biomarkers have great potential as therapeutic targets for AF, but also for diagnostics and disease-progression prediction (**Chapter 12**). Novel insights into the mechanisms facilitating development of the arrhythmogenic substrate are warranted to fuel the search for non-invasive AF-specific biomarkers.

Future perspectives

Probably, *the* arrhythmogenic substrate of AF does not exist. Pathophysiology of AF rather seems pluriform, sophisticated and patient-specific, which also calls for highly individualized diagnostics, prognostics and, consequently, therapy. Considerable steps still have to be made to enhance our understanding of AF, ultimately going from research to renewed practice. Translational research is key to identify the different components contributing to pathogenesis and maintenance of AF. On the one hand, studies focusing on biological processes such as (loss of) proteostasis are necessary, while on the other hand, high-resolution epicardial mapping studies should be performed to uncover electrical processes. During these mapping studies, it is of prime importance to discard any technical influence on signal morphology. As such, uniform mapping settings should be defined and used clinically, in order to increase comparability and compatibility, which could strengthen identification of new morphology-based targets. To improve discrimination of pathological and physiological processes, a combination of imaging (e.g. high frame rate echocardiography) and high-resolution mapping could be examined. Furthermore, technical innovations are necessary to go from the golden standard of *invasive* high-resolution epicardial mapping to high-resolution mapping with a *minimal invasive* character, for example using newly established endocardial catheters or body surface mapping.

References

1. Wit AL, Dillon SM, Coromilas J, Saltman AE and Waldecker B. Anisotropic reentry in the epicardial border zone of myocardial infarcts. *Ann N Y Acad Sci*. 1990;591:86-108.
2. Spach MS. Anisotropy of cardiac tissue: a major determinant of conduction? *J Cardiovasc Electrophysiol*. 1999;10:887-90.
3. Spach MS, Dolber PC and Heidlage JF. Influence of the passive anisotropic properties on directional differences in propagation following modification of the sodium conductance in human atrial muscle. A model of reentry based on anisotropic discontinuous propagation. *Circ Res*. 1988;62:811-32.
4. Spach MS, Heidlage JF, Dolber PC and Barr RC. Changes in anisotropic conduction caused by remodeling cell size and the cellular distribution of gap junctions and Na(+) channels. *J Electrocardiol*. 2001;34 Suppl:69-76.
5. Spach MS and Josephson ME. Initiating reentry: the role of nonuniform anisotropy in small circuits. *J Cardiovasc Electrophysiol*. 1994;5:182-209.
6. Gardner PI, Ursell PC, Fenoglio JJ, Jr. and Wit AL. Electrophysiologic and anatomic basis for fractionated electrograms recorded from healed myocardial infarcts. *Circulation*. 1985;72:596-611.
7. Spach MS and Dolber PC. Relating extracellular potentials and their derivatives to anisotropic propagation at a microscopic level in human cardiac muscle. Evidence for electrical uncoupling of side-to-side fiber connections with increasing age. *Circ Res*. 1986;58:356-71.
8. Frontera A, Takigawa M, Martin R, Thompson N, Cheniti G, Massoullie G, Duchateau J, Wielandts JY, Teijeira E, Kitamura T, Wolf M, Al-Jefairi N, Vlachos K, Yamashita S, Amraoui S, Denis A, Hocini M, Cochet H, Sacher F, Jais P, Haissaguerre M and Derval N. Electrogram signature of specific activation patterns: Analysis of atrial tachycardias at high-density endocardial mapping. *Heart Rhythm*. 2018;15:28-37.
9. Jadidi AS, Duncan E, Miyazaki S, Lellouche N, Shah AJ, Forclaz A, Nault I, Wright M, Rivard L, Liu X, Scherr D, Wilton SB, Sacher F, Derval N, Knecht S, Kim SJ, Hocini M, Narayan S, Haissaguerre M and Jais P. Functional nature of electrogram fractionation demonstrated by left atrial high-density mapping. *Circ Arrhythm Electrophysiol*. 2012;5:32-42.
10. Spach MS, Kootsey JM and Sloan JD. Active modulation of electrical coupling between cardiac cells of the dog. A mechanism for transient and steady state variations in conduction velocity. *Circ Res*. 1982;51:347-62.
11. Spach MS, Miller WT, 3rd, Geselowitz DB, Barr RC, Kootsey JM and Johnson EA. The discontinuous nature of propagation in normal canine cardiac muscle. Evidence for recurrent discontinuities of intracellular resistance that affect the membrane currents. *Circ Res*. 1981;48:39-54.
12. Valderrabano M. Influence of anisotropic conduction properties in the propagation of the cardiac action potential. *Prog Biophys Mol Biol*. 2007;94:144-68.
13. Konings KT, Smeets JL, Penn OC, Wellens HJ and Allessie MA. Configuration of unipolar atrial electrograms during electrically induced atrial fibrillation in humans. *Circulation*. 1997;95:1231-41.
14. de Groot N, van der Does L, Yaksh A, Lanters E, Teuwen C, Knops P, van de Woestijne P, Bekkers J, Kik C, Bogers A and Allessie M. Direct Proof of Endo-Epicardial Asynchrony of the Atrial Wall During Atrial Fibrillation in Humans. *Circulation: Arrhythmia and Electrophysiology*. 2016;9(5).

15. Schalij MJ, Lammers WJ, Rensma PL and Allessie MA. Anisotropic conduction and reentry in perfused epicardium of rabbit left ventricle. *Am J Physiol*. 1992;263:H1466-78.
16. Spach MS, Dolber PC and Heidlage JF. Interaction of inhomogeneities of repolarization with anisotropic propagation in dog atria. A mechanism for both preventing and initiating reentry. *Circ Res*. 1989;65:1612-31.
17. Spach MS, Barr RC, Serwer GS, Johnson EA and Kootsey JM. Collision of excitation waves in the dog Purkinje system. Extracellular identification. *Circ Res*. 1971;29:499-511.
18. Kadish A, Shinnar M, Moore EN, Levine JH, Balke CW and Spear JF. Interaction of fiber orientation and direction of impulse propagation with anatomic barriers in anisotropic canine myocardium. *Circulation*. 1988;78:1478-94.
19. Kadish A and Spear J. Identification of conduction block in cardiac muscle: in vitro observations in canine epicardium. *Cardiovasc Res*. 1994;28:259-69.
20. Jacquemet V and Henriquez CS. Genesis of complex fractionated atrial electrograms in zones of slow conduction: a computer model of microfibrosis. *Heart Rhythm*. 2009;6:803-10.
21. Jacquemet V, Virag N, Ihara Z, Dang L, Blanc O, Zozor S, Vesin JM, Kappenberger L and Henriquez C. Study of unipolar electrogram morphology in a computer model of atrial fibrillation. *J Cardiovasc Electrophysiol*. 2003;14:S172-9.
22. Schoels W, Restivo M, Caref EB, Gough WB and el-Sherif N. Circus movement atrial flutter in canine sterile pericarditis model. Activation patterns during entrainment and termination of single-loop reentry in vivo. *Circulation*. 1991;83:1716-30.
23. Shimizu A, Nozaki A, Rudy Y and Waldo AL. Multiplexing studies of effects of rapid atrial pacing on the area of slow conduction during atrial flutter in canine pericarditis model. *Circulation*. 1991;83:983-94.
24. Cosio FG, Arribas F, Barbero JM, Kallmeyer C and Goicolea A. Validation of double-spike electrograms as markers of conduction delay or block in atrial flutter. *Am J Cardiol*. 1988;61:775-80.
25. Cosio FG, Arribas F, Palacios J, Tascon J and Lopez-Gil M. Fragmented electrograms and continuous electrical activity in atrial flutter. *Am J Cardiol*. 1986;57:1309-14.
26. Kay GN, Epstein AE and Plumb VJ. Region of slow conduction in sustained ventricular tachycardia: direct endocardial recordings and functional characterization in humans. *J Am Coll Cardiol*. 1988;11:109-16.
27. Dillon SM, Allessie MA, Ursell PC and Wit AL. Influences of anisotropic tissue structure on reentrant circuits in the epicardial border zone of subacute canine infarcts. *Circ Res*. 1988;63:182-206.
28. Mouws E, Kik C, van der Does L, Lanters EAH, Teuwen CP, Knops P, Bogers A and de Groot NMS. Novel Insights in the Activation Patterns at the Pulmonary Vein Area. *Circ Arrhythm Electrophysiol*. 2018;11:e006720.
29. Mouws E, Lanters EAH, Teuwen CP, van der Does L, Kik C, Knops P, Yaksh A, Bekkers JA, Bogers A and de Groot NMS. Impact of Ischemic and Valvular Heart Disease on Atrial Excitation:A High-Resolution Epicardial Mapping Study. *J Am Heart Assoc*. 2018;7.
30. Schuessler RB, Kawamoto T, Hand DE, Mitsuno M, Bromberg BI, Cox JL and Boineau JP. Simultaneous epicardial and endocardial activation sequence mapping in the isolated canine right atrium. *Circulation*. 1993;88:250-63.

31. Park J, Park CH, Lee HJ, Wi J, Uhm JS, Pak HN, Lee M, Kim YJ and Joung B. Left atrial wall thickness rather than epicardial fat thickness is related to complex fractionated atrial electrogram. *Int J Cardiol*. 2014;172:e411-3.
32. Spach MS, Miller WT, 3rd, Miller-Jones E, Warren RB and Barr RC. Extracellular potentials related to intracellular action potentials during impulse conduction in anisotropic canine cardiac muscle. *Circ Res*. 1979;45:188-204.
33. Konings KT, Kirchhof CJ, Smeets JR, Wellens HJ, Penn OC and Allessie MA. High-density mapping of electrically induced atrial fibrillation in humans. *Circulation*. 1994;89:1665-80.
34. Ortiz J, Niwano S, Abe H, Rudy Y, Johnson NJ and Waldo AL. Mapping the conversion of atrial flutter to atrial fibrillation and atrial fibrillation to atrial flutter. Insights into mechanisms. *Circ Res*. 1994;74:882-94.
35. Atienza F, Calvo D, Almendral J, Zlochiver S, Grzeda KR, Martinez-Alzamora N, Gonzalez-Torrecilla E, Arenal A, Fernandez-Aviles F and Berenfeld O. Mechanisms of fractionated electrograms formation in the posterior left atrium during paroxysmal atrial fibrillation in humans. *J Am Coll Cardiol*. 2011;57:1081-92.
36. Spach MS, Miller WT, 3rd, Dolber PC, Kootsey JM, Sommer JR and Mosher CE, Jr. The functional role of structural complexities in the propagation of depolarization in the atrium of the dog. Cardiac conduction disturbances due to discontinuities of effective axial resistivity. *Circ Res*. 1982;50:175-91.
37. Gaita F, Caponi D, Scaglione M, Montefusco A, Corleto A, Di Monte F, Coin D, Di Donna P and Giustetto C. Long-term clinical results of 2 different ablation strategies in patients with paroxysmal and persistent atrial fibrillation. *Circ Arrhythm Electrophysiol*. 2008;1:269-75.
38. Nademanee K, McKenzie J, Kosar E, Schwab M, Sunsaneewitayakul B, Vasavakul T, Khunnawat C and Ngarmukos T. A new approach for catheter ablation of atrial fibrillation: mapping of the electrophysiologic substrate. *J Am Coll Cardiol*. 2004;43:2044-53.
39. Roux JF, Gojraty S, Bala R, Liu CF, Dixit S, Hutchinson MD, Garcia F, Lin D, Callans DJ, Riley M, Marchlinski F and Gerstenfeld EP. Effect of pulmonary vein isolation on the distribution of complex fractionated electrograms in humans. *Heart Rhythm*. 2009;6:156-60.
40. Kirchhof P, Benussi S, Kotecha D, Ahlsson A, Atar D, Casadei B, Castella M, Diener HC, Heidbuchel H, Hendriks J, Hindricks G, Manolis AS, Oldgren J, Popescu BA, Schotten U, Van Putte B, Vardas P and Group ESCSD. 2016 ESC Guidelines for the management of atrial fibrillation developed in collaboration with EACTS. *Eur Heart J*. 2016;37:2893-2962.
41. Lau DH, Maesen B, Zeemering S, Kuklik P, van Hunnik A, Lankveld TA, Bidar E, Verheule S, Nijs J, Maessen J, Crijns H, Sanders P and Schotten U. Indices of bipolar complex fractionated atrial electrograms correlate poorly with each other and atrial fibrillation substrate complexity. *Heart Rhythm*. 2015;12:1415-23.
42. Nagashima K, Okumura Y, Watanabe I, Nakai T, Ohkubo K, Kofune T, Kofune M, Mano H, Sonoda K and Hirayama A. Effects of inter-electrode spacing on complex fractionated atrial electrograms and dominant frequency detection. *J Interv Card Electrophysiol*. 2012;34:51-7.
43. Correa de Sa DD, Thompson N, Stinnett-Donnelly J, Znojkiewicz P, Habel N, Muller JG, Bates JH, Buzas JS and Spector PS. Electrogram fractionation: the relationship between spatiotemporal variation of tissue excitation and electrode spatial resolution. *Circ Arrhythm Electrophysiol*. 2011;4:909-16.
44. van der Does LJ and de Groot NM. Inhomogeneity and complexity in

defining fractionated electrograms. *Heart Rhythm*. 2017;14:616-624.
45. Wu SH, Jiang WF, Gu J, Zhao L, Wang YL, Liu YG, Zhou L, Gu JN, Xu K and Liu X. Benefits and risks of additional ablation of complex fractionated atrial electrograms for patients with atrial fibrillation: a systematic review and meta-analysis. *Int J Cardiol*. 2013;169:35-43.
46. Verma A, Wazni OM, Marrouche NF, Martin DO, Kilicaslan F, Minor S, Schweikert RA, Saliba W, Cummings J, Burkhardt JD, Bhargava M, Belden WA, Abdul-Karim A and Natale A. Pre-existent left atrial scarring in patients undergoing pulmonary vein antrum isolation: an independent predictor of procedural failure. *J Am Coll Cardiol*. 2005;45:285-92.
47. Jadidi AS, Lehrmann H, Keyl C, Sorrel J, Markstein V, Minners J, Park CI, Denis A, Jais P, Hocini M, Potocnik C, Allgeier J, Hochholzer W, Herrera-Sidloky C, Kim S, Omri YE, Neumann FJ, Weber R, Haissaguerre M and Arentz T. Ablation of Persistent Atrial Fibrillation Targeting Low-Voltage Areas With Selective Activation Characteristics. *Circ Arrhythm Electrophysiol*. 2016;9.
48. Rolf S, Dagres N and Hindricks G. Voltage-Based Ablation: The Growing Evidence for the Role of Individually Tailored Substrate Modification for Atrial Fibrillation. *J Cardiovasc Electrophysiol*. 2016;27:31-3.
49. Rolf S, Kircher S, Arya A, Eitel C, Sommer P, Richter S, Gaspar T, Bollmann A, Altmann D, Piedra C, Hindricks G and Piorkowski C. Tailored atrial substrate modification based on low-voltage areas in catheter ablation of atrial fibrillation. *Circ Arrhythm Electrophysiol*. 2014;7:825-33.
50. Kottkamp H, Berg J, Bender R, Rieger A and Schreiber D. Box Isolation of Fibrotic Areas (BIFA): A Patient-Tailored Substrate Modification Approach for Ablation of Atrial Fibrillation. *J Cardiovasc Electrophysiol*. 2016;27:22-30.
51. Masuda M, Fujita M, Iida O, Okamoto S, Ishihara T, Nanto K, Kanda T, Tsujimura T, Matsuda Y, Okuno S, Ohashi T, Tsuji A and Mano T. Left atrial low-voltage areas predict atrial fibrillation recurrence after catheter ablation in patients with paroxysmal atrial fibrillation. *Int J Cardiol*. 2018;257:97-101.
52. Masuda M, Asai M, Iida O, Okamoto S, Ishihara T, Nanto K, Kanda T, Tsujimura T, Matsuda Y, Okuno S, Hata Y and Mano T. Additional Low-Voltage-Area Ablation in Patients With Paroxysmal Atrial Fibrillation: Results of the Randomized Controlled VOLCANO Trial. *J Am Heart Assoc*. 2020;9:e015927.
53. Nery PB, AlQarawi W, Nair GM, Sadek MM, Redpath CJ, Golian M, Al Dawood W, Chen L, Hansom SP, Klein A, Wells GA and Birnie DH. Catheter Ablation of Low-Voltage Areas for Persistent Atrial Fibrillation: Procedural Outcomes Using High-Density Voltage Mapping. *Can J Cardiol*. 2020.
54. Anter E and Josephson ME. Bipolar voltage amplitude: What does it really mean? *Heart Rhythm*. 2016;13:326-7.
55. Josephson ME and Anter E. Substrate Mapping for Ventricular Tachycardia: Assumptions and Misconceptions. *JACC Clin Electrophysiol*. 2015;1:341-352.
56. Kharbanda RK, Wesselius FJ and de Groot NMS. Three-dimensional visualization of atrial conduction disorders using simultaneous endo-epicardial mapping. *European Heart Journal - Case Reports*. 2020.
57. Venkatachalam KL, Herbrandson JE and Asirvatham SJ. Signals and signal processing for the electrophysiologist: part II: signal processing and artifact. *Circ Arrhythm Electrophysiol*. 2011;4:974-81.
58. Stevenson WG and Soejima K. Recording techniques for clinical electrophysiology. *J Cardiovasc Electrophysiol*. 2005;16:1017-22.
59. de Bakker JM and Wittkampf FH. The pathophysiologic basis of fractionated and complex electrograms and the

impact of recording techniques on their detection and interpretation. *Circ Arrhythm Electrophysiol*. 2010;3:204-13.
60. Zaman JAB, Schricker A, Lalani GG, Trikha R, Krummen DE and Narayan SM. Focal Impulse And Rotor Mapping (FIRM): Conceptualizing And Treating Atrial Fibrillation. *J Atr Fibrillation*. 2014;7:1103.
61. Grace A, Willems S, Meyer C, Verma A, Heck P, Zhu M, Shi X, Chou D, Dang L, Scharf C, Scharf G and Beatty G. High-resolution noncontact charge-density mapping of endocardial activation. *JCI Insight*. 2019;4:e126422.
62. D'Agostino RS, Jacobs JP, Badhwar V, Fernandez FG, Paone G, Wormuth DW and Shahian DM. The Society of Thoracic Surgeons Adult Cardiac Surgery Database: 2019 Update on Outcomes and Quality. *Ann Thorac Surg*. 2019;107:24-32.
63. LaPar DJ, Speir AM, Crosby IK, Fonner E, Jr., Brown M, Rich JB, Quader M, Kern JA, Kron IL, Ailawadi G and Investigators for the Virginia Cardiac Surgery Quality I. Postoperative atrial fibrillation significantly increases mortality, hospital readmission, and hospital costs. *Ann Thorac Surg*. 2014;98:527-33; discussion 533.
64. Aranki SF, Shaw DP, Adams DH, Rizzo RJ, Couper GS, VanderVliet M, Collins JJ, Jr., Cohn LH and Burstin HR. Predictors of atrial fibrillation after coronary artery surgery. Current trends and impact on hospital resources. *Circulation*. 1996;94:390-7.
65. Echahidi N, Pibarot P, O'Hara G and Mathieu P. Mechanisms, prevention, and treatment of atrial fibrillation after cardiac surgery. *J Am Coll Cardiol*. 2008;51:793-801.
66. Boriani G, Diemberger I, Ziacchi M, Valzania C, Gardini B, Cimaglia P, Martignani C and Biffi M. AF burden is important - fact or fiction? *Int J Clin Pract*. 2014;68:444-52.
67. Rabkin SW. The relationship between epicardial fat and indices of obesity and the metabolic syndrome: a systematic review and meta-analysis. *Metab Syndr Relat Disord*. 2014;12:31-42.
68. Csige I, Ujvarosy D, Szabo Z, Lorincz I, Paragh G, Harangi M and Somodi S. The Impact of Obesity on the Cardiovascular System. *J Diabetes Res*. 2018;2018:3407306.
69. Aiad NN, Hearon C, Jr., Hieda M, Dias K, Levine BD and Sarma S. Mechanisms of Left Atrial Enlargement in Obesity. *Am J Cardiol*. 2019;124:442-447.
70. Movahed MR and Saito Y. Obesity is associated with left atrial enlargement, E/A reversal and left ventricular hypertrophy. *Exp Clin Cardiol*. 2008;13:89-91.
71. Garza CA, Pellikka PA, Somers VK, Sarr MG, Seward JB, Collazo-Clavell ML, Oehler E and Lopez-Jimenez F. Major weight loss prevents long-term left atrial enlargement in patients with morbid and extreme obesity. *Eur J Echocardiogr*. 2008;9:587-93.
72. Henning RH and Brundel BJJM. Proteostasis in cardiac health and disease. *Nat Rev Cardiol*. 2017;14:637-653.
73. Ke L, Meijering RA, Hoogstra-Berends F, Mackovicova K, Vos MJ, Van Gelder IC, Henning RH, Kampinga HH and Brundel BJ. HSPB1, HSPB6, HSPB7 and HSPB8 protect against RhoA GTPase-induced remodeling in tachypaced atrial myocytes. *PLoS One*. 2011;6:e20395.
74. Meijering RA, Henning RH and Brundel BJ. Reviving the protein quality control system: therapeutic target for cardiac disease in the elderly. *Trends Cardiovasc Med*. 2015;25:243-7.
75. Brundel BJ, Henning RH, Ke L, van Gelder IC, Crijns HJ and Kampinga HH. Heat shock protein upregulation protects against pacing-induced myolysis in HL-1 atrial myocytes and in human atrial fibrillation. *J Mol Cell Cardiol*. 2006;41:555-62.
76. Zhang D, Ke L, Mackovicova K, Van Der Want JJ, Sibon OC, Tanguay RM, Morrow G, Henning RH, Kampinga

HH and Brundel BJ. Effects of different small HSPB members on contractile dysfunction and structural changes in a Drosophila melanogaster model for Atrial Fibrillation. *J Mol Cell Cardiol*. 2011;51:381-9.
77. Zhang D, Wu CT, Qi X, Meijering RA, Hoogstra-Berends F, Tadevosyan A, Cubukcuoglu Deniz G, Durdu S, Akar AR, Sibon OC, Nattel S, Henning RH and Brundel BJ. Activation of histone deacetylase-6 induces contractile dysfunction through derailment of alpha-tubulin proteostasis in experimental and human atrial fibrillation. *Circulation*. 2014;129:346-58.
78. Knowlton AA, Kapadia S, Torre-Amione G, Durand JB, Bies R, Young J and Mann DL. Differential expression of heat shock proteins in normal and failing human hearts. *J Mol Cell Cardiol*. 1998;30:811-8.
79. Hoogstra-Berends F, Meijering RA, Zhang D, Heeres A, Loen L, Seerden JP, Kuipers I, Kampinga HH, Henning RH and Brundel BJ. Heat shock protein-inducing compounds as therapeutics to restore proteostasis in atrial fibrillation. *Trends Cardiovasc Med*. 2012;22:62-8.
80. Gong J and Jing L. Glutamine induces heat shock protein 70 expression via O-GlcNAc modification and subsequent increased expression and transcriptional activity of heat shock factor-1. *Minerva Anestesiol*. 2011;77:488-95.
81. Hamiel CR, Pinto S, Hau A and Wischmeyer PE. Glutamine enhances heat shock protein 70 expression via increased hexosamine biosynthetic pathway activity. *Am J Physiol Cell Physiol*. 2009;297:C1509-19.
82. Hayashi Y, Sawa Y, Fukuyama N, Nakazawa H and Matsuda H. Preoperative glutamine administration induces heat-shock protein 70 expression and attenuates cardiopulmonary bypass-induced inflammatory response by regulating nitric oxide synthase activity. *Circulation*. 2002;106:2601-7.

15

English summary

Roeliene Starreveld

The pathophysiology of atrial fibrillation (AF) – the most common cardiac arrhythmia worldwide – remains insufficiently understood. As a general introduction to this thesis, **Chapter 1** provides background information on the etiology of atrial fibrillation, therapeutic options and current extraordinary challenges. As the risk of developing AF strongly increases with age and the presence of underlying heart disease, the growing epidemic of AF should be called to halt rather than later. This thesis aims to further characterize electrophysiological and structural alterations underlying onset and persistence of AF in patients undergoing cardiac surgery, as such mechanistic insights can aid in optimizing treatment strategies and enhance outcomes for AF patients.

In **Chapter 2** we outline our atrial fibrillation fingerprinting (AFFIP) project that aims to exploit markers of both electrophysiological and structural remodelling during AF. Intra-operative high-resolution mapping studies are performed to identify the patient-specific electrical profile, whereas the patient-specific biological profile is assessed by evaluating proteostasis markers in blood samples and atrial appendage tissue samples. The findings will elucidate whether electrophysiological and structural characteristics represent a novel diagnostic tool (the 'AF fingerprint') to predict onset and early progression of AF in cardiac surgery patients.

Electrical markers of atrial fibrillation

In the first part of this thesis, the focus lies on discovering electrical markers of AF. The human case presented in **Chapter 3** is the first to illustrate morphological manifestations of direction- and rate-dependent anisotropic conduction in high-resolution unipolar atrial potentials. Premature impulses and an increased pacing rate induced low-amplitude, fractionated potentials with exceptional prolongation of potential duration, reflecting nonuniformity of anisotropic cardiac tissue. These findings cohere with the hypothesis that unipolar potential morphology can aid in identifying the substrate of AF. Specifically, pacing with different rates and from different sites could be used to uncover remodeled and arrhythmogenic tissue.

The impact of atrial anatomy on electrogram (EGM) morphology is investigated in **Chapter 4**, reviewing the pre-ablation distribution of fractionated electrograms within the left and right atrium. High proportions of fractionated EGMs were found within all regions of both atria, without a clear preference for specific sites. In the left atrium (LA), 60.8% (48.5-72.5%) of all patients had fractionated EGMs and 55.4% (38.9-71.2%) of all EGMs were fractionated. In addition, no differences were observed in fractionation proportions between paroxysmal AF (PAF) patients and persistent AF patients in any of the LA regions. Our findings – summarizing all studies performed on this topic – indicate that high occurrence rates of complex

fractionated electrograms (CFEs) are not restricted to the interatrial septum, pulmonary veins (PVs), LA roof and coronary sinus, but can be found abundantly within all areas of both atria. Aside from fractionation due to artifacts, the anatomic nature of atrial tissue itself seems an inherent hotspot for fractionation. Simply targeting all fractionated electrograms would be very extensive, would unnecessarily increase scarring of healthy atrial tissue and thereby increase the risk of post-ablative iatrogenic atrial tachyarrhythmias. Although still used in clinical practice, automated fractionation detection algorithms are unable to distinguish "physiologic CFEs" from "pathologic CFEs", with only the latter reflecting potential targets for ablative therapy of AF.

In order to gain more insight into the "fact or artifact" of fractionated atrial electrograms, the impact of filtering on unipolar fibrillation potentials was investigated in **Chapter 5**. In total, 3000 seconds of AF recordings were analyzed, containing 2,557,045 pulmonary vein fibrillation potentials. High-pass filtering ranging from 0.5 to 100 Hz decreased the number of detected potentials, deflection amplitude, percentage of double potentials (DPs) and complex fractionated potentials (CFPs) as well as the fractionation delay time (FDT, interval first to last deflection) and increased percentage of single potentials (SPs) (all $p<0.01$). Low-pass filtering ranging from 400 to 200 Hz decreased the number of potentials, percentage of DPs and CFPs, whereas deflection amplitude, percentage of SPs and FDT increased (all $p<0.01$). Notch filtering at 50 Hz decreased the number of potentials and deflection amplitude (both $p<0.01$), whereas the percentage of CFPs increased ($p=0.016$). Notch filtering did not impact percentage of SPs and DPs, nor FDT (p=NS). In addition, filtering induced the local activation time (LAT) of fibrillation potentials to shift, especially with more aggressive low-pass filtering. Although filtering impacted LATs of all potential types (i.e. SPs, DPs and CFPs), more complex and long fractionated potentials had a greater ΔLAT and shifted more than potentials with simpler morphology. Thus, filtering choices have significant impact on unipolar fibrillation signal morphology. Attempts to correct for noise or baseline drift can easily result in erroneous (under)detection of fractionation and/or low-voltage areas and thus ablative targets during mapping. These results stretch the importance of adequate (i.e. as minimal as possible) filtering during clinical mapping.

The morphology of unipolar single potentials (SPs), represented by the relative positive (R-wave) and negative (S-wave) components, contains information on intra-atrial conduction and possibly the substrate underlying AF. In **Chapter 6** we demonstrate a clear predominance of S-waves at Bachmann's bundle (BB) and the right atrium (RA) in both patients without and with a history of PAF (BB 88.8% vs. 85.9%, RA: 92.1% vs. 85.1%, respectively). Potential voltages at the RA, BB and the pulmonary vein area (PVA) were significantly lower in the PAF group ($p<0.001$

for each) and were mainly determined by the size of the S-waves amplitudes. The largest difference in S-wave amplitudes was found at BB, where the S-wave amplitude was lower in the PAF group (4.08 [2.45–6.13] mV vs. 2.94 [1.40–4.75] mV; p<0.001). In addition, conduction velocity (CV) at BB was lower as well in PAF patients (0.97 [0.70–1.21] m/s vs. 0.89 [0.62–1.16] m/s, p<0.001). Though excitation of the atria during SR is heterogeneously disrupted, a history of AF is characterized by decreased SP amplitudes at BB due to loss of S-wave amplitudes and decreased CV. This suggests that SP morphology could provide additional information on wavefront propagation.

Unipolar voltage mapping is increasingly used for guiding ablative therapy of AF as unipolar electrograms – in contrary to bipolar electrograms – are independent of electrode orientation and atrial wavefront direction. **Chapter 7** illustrates individual, high-resolution unipolar SR voltage fingerprints in order to identify low voltage areas and study the effect of AF episodes on unipolar voltages in patients with mitral valve disease (MVD). A total of 600,722 potentials were analyzed out of 829 SR recordings of 5-seconds duration. There was no significant correlation between unipolar voltage and conduction velocity (CV), though smaller voltages were recorded in areas of conduction slowing (<28cm/s; 1.74 [0.88–3.53] mV vs. 4.72 [2.46–7.61] mV, p<0.001), and in areas surrounding conduction block (<18cm/s; 1.22 [0.69–2.26] mV vs. 4.79 [2.55–7.65] mV, p<0.001) compared to areas with normal conduction (≥28 cm/s). Fractionated potentials had lower voltages compared to single potentials (2.05 [1.04–3.75] mV vs. 5.16 [2.85–8.01] mV, p<0.001) and a clear decrease in unipolar voltage was found with a larger number of deflections (1: 5.16 [2.85–8.01] mV; 2: 2.20 [1.14–3.95] mV; 3: 1.21 [0.68–2.26] mV; ≥4: 0.94 [0.52-1.71] mV, p<0.001 for all). Areas with low voltage potentials were present in all patients and no predilection sites for low voltage potentials were found. Patients with PAF had lower voltages at BB (no AF: 4.92 [3.45–6.09] mV, PAF: 2.95 [2.24–4.57] mV, p=0.007) and a higher number of low voltage potentials (no AF: 2.13 [0.52–7.68] %, PAF: 12.86 [3.18–23.59] %, p=0.001). In the no AF group, BB yielded a higher number of fractionated potentials (19.58 [12.40–31.72] %) compared to the RA, PVA and LA. As low unipolar voltages are even present in patients without a history of AF and do not automatically indicate 'diseased' atrial tissue, they should carefully be used as an indicator for ablative therapy.

Endo–epicardial asynchrony (EEA) and the interplay between the endocardial and epicardial layers could be of great importance in the pathophysiology of AF. Electrogram morphology is often used for the identification of structural or electrical remodeled areas with arrhythmogenic properties, yet morphologic differences between epicardial and endocardial atrial electrograms were not described. In the study described in **Chapter 8**, unipolar electrograms were simultaneously recorded from the epicardium and endocardium at the RA during

SR in 26 patients. A total of 102,129 potentials were analyzed in 16,954 electrograms, including 50,714 potentials of 8,423 electrograms recorded at the epicardium and 51,415 potentials of 8,531 electrograms recorded at the endocardium. Especially the superior RA was predisposed for delayed activation, EEA and fractionation. Unipolar voltage decreased with more fractionated potentials at both the epi- and endocardium. Both epicardial and endocardial electrograms demonstrated an S-predominance, indicating that the RS-ratio cannot be used to identify the leading layer during SR. Incidence of fractionated potentials (>1 deflection) demonstrated an increasing trend from the inferior-RA (16%) towards the mid-RA (22%, p=0.136) and was highest at the superior-RA (36%, p<0.001). Fractionation was mostly similar between the two sides, yet the superior-RA demonstrated a trend towards more fractionated potentials at the endocardium: 33 vs. 38% (p=0.09). Local epi-endocardial differences in the number of detected deflections occurred in 6.6%. EEA occurred at the inferior-RA in 12% of the patients, the mid-RA in 19% and the superior-RA in 57% (p=0.001). The far majority of fractionated deflections (95%) were attributable to remote activation, as a corresponding LAT was present in the surrounding tissue of the same or opposite layer, of which 4% could be attributed to EEA. So, if a potential is fractionated during SR, most additional deflections can be explained by conduction disorders in the same or opposite layer and in a small percentage they represent EEA. Particularly interesting, especially for clinical practice, is the observation that the morphology of unipolar electrograms could potentially be a tool to identify areas of EEA when electrograms are recorded on only one side of the wall.

Although bipolar electrogram recordings are often preferred in electrophysiological studies, unipolar electrograms may be better suited to detect EEA when recording electrograms from only one side. In **Chapter 9** we demonstrate that fractionation corresponding to EEA is present in both unipolar and bipolar electrograms at both the epi- and endocardium (epi: 75% vs 65% (bi-x) and 69% (bi-y), endo: 72% vs 78% (bi-x) and 72% (bi-y)). Using the bipolar recording mode, signal-to-noise ratio of EEA corresponding fractionation decreased (from 11 (6-25) to 4 (2-7) in bi-y, p<0.001) and additional fractionation increased for electrograms recorded at the endocardium (53% (10-86) to 82% (52-100) in bi-x, p=0.019). Therefore, better signal-to-noise ratio of EEA corresponding fractionation and less additional fractionation make unipolar electrograms better suited for detection of EEA based on electrogram fractionation.

Early postoperative AF (EPoAF) is the most frequently encountered postoperative complication after cardiac surgery. EPoAF does not only increase the length and hence costs of hospitalization, but is also associated with poorer long-term prognosis.[1] Aiming to identify patients at risk of developing EPoAF, **Chapter 10** describes characteristics of EPoAF in obese (BMI ≥30) and nonobese patients

(BMI <30). Obesity predisposed to a larger number of prolonged atrial fibrillation episodes in the early postoperative period (first five postoperative days) after cardiac surgery for coronary artery disease or valvular heart disease. The higher atrial fibrillation burden (i.e. ratio between total duration of all AF episodes and total recording time) in the early postoperative period occurred particularly on the third day. Because the effects of obesity on the AF substrate are reversible with weight control, preventive lifestyle before cardiac surgery may play an invaluable role.

A cohort of 154 bicuspid aortic valve (BAV) patients was investigated in **Chapter 11** for EPoAF characteristics (e.g. incidence, duration, burden), as well as preoperative risk factors (e.g. gender, age, BMI, history of AF) and long-term follow-up (e.g. AF recurrence, survival). EPoAF occurred in 28% of BAV patients and had a burden of 13.2%, and significantly reduced AF-free survival, yet not impacted overall survival. EPoAF burden was significantly correlated with median and longest EPoAF episode duration (r=0.66 and r=0.89, respectively), and men had a higher overall burden than women (p=0.03). Older age, left atrial enlargement and rethoracotomy were independent risk factors for EPoAF. Rhythm monitoring during follow-up of BAV patients with a high burden is recommended to detect AF-recurrences.

Biological markers of atrial fibrillation

In the second part of this thesis, the focus is shifted towards biological markers of AF. Even though mechanisms responsible for progression of AF are still of key debate, atrial electro-anatomical remodeling (e.g. left atrial dilatation, atrial interstitial fibrosis or scarring) is a widely-recognized factor in the pathogenesis of AF. Based on the conception that low bipolar voltage (≤0.5mV) implies presence of scar tissue, and thus arrhythmia substrate, multiple studies have found a significant correlation between presence of low-voltage areas (LVA) and progression of AF.[2] As detection of LVA is only possible periprocedural, Büttner et al. propose using natriuretic peptides to phenotype AF progression and remodeling noninvasively.[3] In **Chapter 12** we comment on their valuable work. Biomarkers in the blood have great potential to be included within the treatment chain of AF, since they are relatively easy accessible and can be of great diagnostic and predictive value. Unfortunately, the association between atrial natriuretic peptide and LA diameter and LVA was found only weak to moderate, indicating that more larger studies should be performed to validate the outcomes.

All current pharmaco-therapeutic strategies are not yet directed at mechanistic root causes of AF that drive structural cardiomyocyte damage, mitochondrial dysfunction and consequently electro-anatomical remodeling, and are thus not able to prevent AF onset and progression. Emerging evidence indicate that heat

shock proteins (HSP) mitigate AF onset and progression in experimental model systems for AF. An HSP inducing compound is L-glutamine. The clinical pilot study performed in **Chapter 13** therefore investigated the effect of L-glutamine on cardio-protective heat shock proteins (HSPs) and metabolite levels in serum levels of patients with AF (N=21). Hereto, HSP27 and HSP70 levels were determined by ELISAs and metabolites with LC-mass spectrometry. HSP27 levels significantly decreased after 3-months of L-glutamine supplementation [540.39 (250.97-1315.63) to 380.69 (185.68-915.03), p=0.004] and normalized to baseline levels after 6-months of L-glutamine supplementation [634.96 (139.57-3103.61), p<0.001]. For HSP70, levels decreased after 3-months of L-glutamine supplementation [548.86 (31.50-1564.51) to 353.65 (110.58-752.50), p=0.045] and remained low after 6-months of L-glutamine supplementation [309.30 (118.29-1744.19), p=0.517). In contrast to patients with low HSP27 levels at baseline, patients with high HSP27 levels showed normalization of several metabolites related to the carbohydrates, nucleotides, amino acids, vitamins and cofactors metabolic pathways after 3-months L-glutamine supplementation. Though the small sample size of this prospective interventional pilot trial disables the formulation of strong conclusions, L-glutamine supplementation reduces serum levels of HSP27 and HSP70 within 3-months and normalizes metabolite levels in this cohort. Therefore, it is of interest to mount a future, large and ideally randomized controlled, clinical study to test a beneficial effect of L-glutamine on the reduction of AF episodes.

References

1. LaPar DJ, Speir AM, Crosby IK, Fonner E, Jr., Brown M, Rich JB, Quader M, Kern JA, Kron IL, Ailawadi G and Investigators for the Virginia Cardiac Surgery Quality I. Postoperative atrial fibrillation significantly increases mortality, hospital readmission, and hospital costs. *Ann Thorac Surg*. 2014;98:527-33; discussion 533.
2. Kogawa R, Okumura Y, Watanabe I, Nagashima K, Takahashi K, Iso K, Watanabe R, Arai M, Kurokawa S, Ohkubo K, Nakai T, Hirayama A, Sonoda K and Tosaka T. Left atrial remodeling: Regional differences between paroxysmal and persistent atrial fibrillation. *J Arrhythm*. 2017;33:483-487.
3. Buttner P, Schumacher K, Dinov B, Zeynalova S, Sommer P, Bollmann A, Husser D, Hindricks G and Kornej J. Role of NT-proANP and NT-proBNP in patients with atrial fibrillation: Association with atrial fibrillation progression phenotypes. *Heart Rhythm*. 2018;15:1132-1137.

16

Nederlandse samenvatting

Roeliene Starreveld

De pathofysiologie van boezemfibrilleren (AF), de meest voorkomende hartritmestoornis wereldwijd, blijft onvoldoende begrepen. **Hoofdstuk 1** geeft een algemene inleiding op dit proefschrift en beschrijft de etiologie van AF, de therapeutische opties en de huidige uitdagingen. Aangezien het risico op het ontwikkelen van AF sterk stijgt naarmate de leeftijd toeneemt en indien er onderliggende hartaandoeningen aanwezig zijn, is het belangrijk om de groeiende AF-epidemie zo snel mogelijk een halt toe te roepen. Dit proefschrift heeft als doel om zowel elektrofysiologische als structurele veranderingen die ten grondslag liggen aan het ontstaan van persistentie van AF te karakteriseren bij patiënten die een openhartoperatie ondergaan. Deze inzichten kunnen helpen bij het optimaliseren van behandelmethodes en het verbeteren van resultaten voor AF-patiënten.

In **Hoofdstuk 2** beschrijven we ons AFFIP project, dat tot doel heeft markers van zowel elektrofysiologische als structurele remodelling tijdens AF te ontrafelen. Intra-operatieve mapping met een hoge resolutie wordt uitgevoerd om het patiëntspecifieke elektrische profiel te identificeren, terwijl het patiëntspecifieke biologische profiel wordt beoordeeld door proteostase-markers in bloed- en weefselmonsters te evalueren. De bevindingen zullen uitwijzen of deze kenmerken een nieuw diagnostisch hulpmiddel vormen (de 'AF-vingerafdruk') om zowel het ontstaan als progressie van AF bij patiënten die een openhartoperatie ondergaan te voorspellen.

Elektrische markers van boezemfibrilleren

In het eerste deel van dit proefschrift ligt de focus op het ontdekken van elektrische markers van AF. De casus die in **Hoofdstuk 3** wordt gepresenteerd is de eerste die de morfologische manifestaties illustreert van richting- en snelheidsafhankelijke anisotrope geleiding in unipolaire atrial potentialen met een hoge resolutie. Premature atriale slagen en een verhoogde pacingfrequentie veroorzaakten gefractioneerde potentialen met een lage amplitude en een uitzonderlijke verlenging van de potentiaalduur, wat een weerspiegeling geeft van de inhomogeniteit van anisotroop hartweefsel. Deze bevindingen komen overeen met de hypothese dat unipolaire potentiaalmorfologie kan helpen bij het identificeren van het substraat van AF. Pacing met verschillende snelheden en van verschillende locaties kan worden gebruikt om geremodelleerd en aritmogeen weefsel te ontdekken.

De relatie tussen atriale anatomie en morfologie van electrogrammen is onderzocht in **Hoofdstuk 4**, waarbij de verdeling van gefractioneerde electrogrammen in het linker- en rechteratrium voorafgaand aan ablatie is beoordeeld. Grote hoeveelheden gefractioneerde electrogrammen werden gevonden in alle regio's van beide boezems, zonder een specifieke voorkeurslocatie uit te wijzen. In de linkerboezem (LA) had 60,8% (48,5-72,5%) van alle patiënten gefractioneerde

electrogrammen en was 55,4% (38,9-71,2%) van alle electrogrammen gefractioneerd. In geen van de LA regio's werden bovendien verschillen gevonden in de hoeveelheid fractionatie tussen patiënten met paroxysmaal AF (PAF) en patiënten met persisterend AF. In deze studie zijn alle onderzoeken uitgevoerd op dit onderwerp samengevat. Hoge percentages van complex gefractioneerde electrogrammen blijken niet beperkt tot het interatriale septum, de longaderen, het dak van de LA en de sinus coronarius, maar zijn overvloedig aanwezig in alle gebieden van beide boezems. Los van fractionatie als gevolg van artefacten lijkt de anatomische structuur van de boezems zelf een brandhaard voor fractionatie. Het simpelweg ableren van alle gefractioneerde electrogrammen zou niet alleen zeer veel tijd kosten, maar zou ook onnodige littekens in gezond boezemweefsel veroorzaken en het risico op post-ablatie iatrogene atriale tachycardieën vergroten. Geautomatiseerde detectie algoritmes voor fractionatie, alhoewel nog steeds gebruikt in de klinische praktijk, blijken geen onderscheid te kunnen maken tussen 'fysiologische fractionatie' en 'pathologische fractionatie', waarbij alleen de laatste een doel voor ablatietherapie van AF is.

Om meer inzicht te krijgen in het 'feit of fabel' van gefractioneerde atriale electrogrammen werd in **Hoofdstuk 5** de invloed van filteren op unipolaire fibrillatiepotentialen onderzocht. In totaal werden 3000 seconden aan AF-opnames geanalyseerd, die 2.557.045 boezemfibrillatie-potentialen uit het pulmonaal vene gebied bevatten. Een hoogdoorlaatfilter variërend van 0,5 tot 100 Hz verminderde zowel het aantal gedetecteerde potentialen, deflectie amplitude, percentage van dubbele potentialen (DP's) en complex gefractioneerde potentialen (CFP's), als de potentiaalduur (FDT, interval van eerste tot laatste deflectie) en verhoogde het aantal enkelvoudige potentialen (SP's) (alle p-waardes <0.01). Laagdoorlaatfiltering variërend van 400 tot 200 Hz verminderde het aantal potentialen, percentage van DP's en CFP's, terwijl deflectie amplitude, percentage SP's en FDT toenam (alle p-waardes <0.01). Een smal stopbandfilter (ofwel 'notch' filter) van 50 Hz verminderde eveneens het aantal potentialen en deflectie amplitude (beide p-waardes <0.01), terwijl het percentage CFP's toenam (p=0.016) Het notch filteren had geen invloed op het percentage SP's, DP's en FDT. Bovendien veroorzaakte filtering dat de lokale activatie tijd (LAT) van de fibrillatiepotentialen verschoof, vooral wanneer er een strikt laagdoorlaatfilter werd gebruikt. Filteren beïnvloedde de LAT's van alle potentiaaltypes (d.w.z. SP's, DP's en CFP's), maar potentialen die complex en relatief lang van duur waren lieten een grotere verschuiving zien in LAT dan potentialen met een eenvoudigere morfologie. Keuzes in filtering hebben dus aanzienlijk invloed op de signaalmorfologie van unipolaire fibrillatiepotentialen. Pogingen om te corrigeren voor ruis of baseline-drift kunnen gemakkelijk resulteren in foutieve detectie van fractionatie en/of lage amplitude gebieden en belemmeren daardoor dus het in kaart brengen van ablatiedoelen. Deze resultaten benadrukken het belang van adequate (d.w.z. zo min mogelijk) filtering tijdens klinische mapping procedures.

De morfologie van unipolaire SP's, bestaande uit de positieve R-golf en de negatieve S-golf, bevat informatie over intra-atriale geleiding en mogelijk het onderliggende substraat van AF. In **Hoofdstuk 6** demonstreren we een duidelijke dominantie van S-golven bij Bachmann's bundel (BB) en het rechter atrium (RA), bij zowel patiënten zonder en met een voorgeschiedenis van PAF (BB 88.8% vs. 85.9%, RA: 92.1% vs. 85.1%, respectievelijk). Amplitudes op RA, BB en in het longvenengebied (PVA) waren significant lager in de PAF-groep en werden voornamelijk bepaald door de amplitude van de S-golf. Het grootste verschil in S-golf amplitudes werd gevonden bij BB, waar de S-golf lager was in de PAF groep (4.08 [2.45–6.13] mV vs. 2.94 [1.40–4.75] mV; p<0.001). Bovendien was de geleidingssnelheid (CV) ook lager in BB in PAF patiënten (0.97 [0.70–1.21] m/s vs. 0.89 [0.62–1.16] m/s, p<0.001). Alhoewel activatie van de boezems tijdens sinusritme (SR) heterogeen wordt verstoord, kenmerkt een voorgeschiedenis met AF zich door verminderde SP-amplitudes op BB als gevolg van amplitudeverlies van de S-golf en verminderde CV. Dit suggereert dat morfologie van SP's aanvullende informatie kan geven over geleiding van het activatiefront.

Mapping van unipolaire voltages wordt in toenemende mate gebruikt voor het begeleiden van ablatie therapie van AF, aangezien unipolaire electrogrammen – in tegenstelling tot bipolaire electrogrammen – onafhankelijk zijn van elektrode-oriëntatie en de richting van het atriale activatiefront. **Hoofdstuk 7** illustreert individuele unipolaire voltage 'vingerafdrukken' tijdens SR met hoge resolutie om lage voltage gebieden te identificeren en het effect van AF-episodes op unipolaire amplitudes te bestuderen, specifiek bij patiënten met een mitralisklep aandoening (MVD). In totaal werden 600.722 potentialen geanalyseerd uit 829 SR opnames van 5 seconden. Er was geen significante correlatie tussen unipolaire voltage en CV, hoewel kleinere voltages werden geregistreerd in gebieden met geleidingsvertraging (<28cm/s; 1,74 [0,88–3,53] mV vs. 4.72 [2,46–7,61] mV, p<0,001) en in gebieden rond geleidingsblok (<18cm/s; 1,22 [0,69–2,26] mV vs. 4,79 [2,55–7,65] mV, p<0,001), vergeleken met gebieden met normale geleiding (≥28 cm/s). Gefractioneerde potentialen hadden lagere voltages dan enkelvoudige potentialen (2,05 [1,04–3,75] mV vs. 5,16 [2,85–8,01] mV, p<0,001) en er werd een duidelijke afname in unipolair voltage gevonden naar mate het aantal deflecties in een potentiaal toenam (1: 5,16 [2,85–8,01] mV; 2: 2,20 [1,14–3,95] mV; 3: 1,21 [0,68–2,26] mV; ≥4: 0,94 [0,52-1,71] mV, alle p-waardes <0,001). Gebieden met lage voltage potentialen waren aanwezig bij alle patiënten en er werden geen voorkeurslocaties gevonden. Patiënten met PAF hadden lagere voltages op BB (geen AF: 4,92 [3,45–6,09] mV, PAF: 2,95 [2,24–4,57] mV, p=0,007) en een hoger aantal lage voltage potentialen (geen AF: 2,13 [0,52 - 7,68]%, PAF: 12,86 [3,18-23,59]%, p = 0,001). In de groep zonder AF was er in BB een hoger aantal gefractioneerde potentialen (19,58 [12,40–31,72]%) in vergelijking met RA, PVA en LA. Aangezien lage unipolaire voltages zelfs aanwezig zijn bij patiënten zonder voorgeschiedenis van AF en dus niet altijd

'ziek' boezemweefsel aantonen, moeten ze zorgvuldig gebruikt worden tijdens ablatie therapie.

Endo-epicardiale asynchronie (EEA) en de samenhang tussen de endocardiale en epicardiale lagen kunnen van groot belang zijn in de pathofysiologie van AF. Electrogram-morfologie wordt veelal gebruikt voor de identificatie van structurele of elektrisch geremodelleerde gebieden met aritmogene eigenschappen, maar de morfologische verschillen tussen epicardiale en endocardiale electrogrammen waren nog niet onderzocht. In de studie beschreven in **Hoofdstuk 8** werden unipolaire electrogrammen van het epicardium en het endocardium gelijktijdig geregistreerd op het RA tijdens SR bij 26 patiënten. Een totaal van 102.129 potentialen werden geanalyseerd in 16.954 electrogrammen, waaronder 50.714 potentialen van 8.423 epicardiale electrogrammen en 51.415 potentialen van 8.531 endocardiale electrogrammen. Vooral het bovenste deel van de RA liet vertraagde activatie, EEA en fractionatie zien. Unipolaire voltages namen af met de mate van fractionatie in het epicardium en het endocardium. Zowel epicardiale als endocardiale electrogrammen toonden een S-golf predominantie, wat aangeeft dat de RS-ratio niet kan worden gebruikt om de leidende laag tijdens SR te identificeren. Incidentie van gefractioneerde potentialen (>1 deflectie) toonde een stijgende trend van het onderste deel van de RA (16%) naar het middelste deel van de RA (22%, p=0,136) en was het hoogst in het bovenste deel van de RA (36%, p<0,001). Fractionatie was grotendeels vergelijkbaar tussen de beide lagen, al liet het bovenste deel van de RA een trend zien naar meer gefractioneerde potentialen in de endocardiale laag (33 vs. 38% (p = 0,09). Lokale epi-endocardiale verschillen in het aantal gedetecteerde deflecties traden op bij 6,6%. In 12% van de patiënten was EEA te zien in het onderste deel van de RA, bij 19% in het middelste deel van de RA en bij 57% in het bovenste deel van de RA (p=0,001). Het overgrote deel van de gefractioneerde deflecties (95%) kon worden toegeschreven aan activatie op afstand, aangezien een overeenkomstige LAT aanwezig was in het omringende weefsel van dezelfde of de tegenoverliggende laag. Slechts 4% hiervan kon aan EEA worden toegeschreven. Als een potentiaal tijdens SR gefractioneerd is kunnen dus de meeste extra deflecties worden verklaard door geleidingsstoornissen in hetzelfde of tegenoverliggende vlak, en in een klein percentage vertegenwoordigen ze EEA. De waarneming dat morfologie van unipolaire electrogrammen mogelijk een hulpmiddel zou kunnen zijn om EEA te identificeren is interessant voor de klinische praktijk, omdat er dan slechts aan één kant van de atriale wand gemeten kan worden.

Alhoewel bipolaire opnames vaak de voorkeur krijgen in elektrofysiologische studies, zijn unipolaire electrogrammen mogelijk beter geschikt om EEA te detecteren bij het opnemen van electrogrammen aan slechts één kant van de atriale wand. In **Hoofdstuk 9** laten we zien dat fractionatie die overeenkomt met EEA aanwezig is in unipolaire en bipolaire electrogrammen in zowel het epi-

als het endocardium (epi: 75% vs 65% (bi-x) en 69% (bi-y), endo: 72% vs 78% (bi-x) en 72% (bi-y)). In bipolaire metingen nam de signaal-ruisverhouding van EEA-overeenkomstige fractionatie af (van 11 (6-25) tot 4 (2-7) in bi-y, p <0,001) en nam de fractionatie in elektrogrammen opgenomen op het endocardium toe (53% (10-86) tot 82% (52-100) in bi-x, p = 0,019). De betere signaal-ruisverhouding van EEA-overeenkomstige fractionatie en de minder aanwezige fractionatie maken unipolaire electrogrammen beter geschikt voor detectie van EEA op basis van electrogram fractionatie dan bipolaire elektrogrammen.

Vroeg postoperatief AF (EPoAF) is de meest voorkomende complicatie na hartchirurgie. EPoAF verhoogt niet alleen de duur en de kosten van de ziekenhuisopname, het gaat ook gepaard met een slechtere prognose op de lange termijn.[1] Om de patiënten met risico op het ontwikkelen van EPoAF te kunnen identificeren, beschrijft **Hoofdstuk 10** kenmerken van EPoAF bij obese patiënten (BMI ≥30) en niet-obese patiënten (BMI <30). Obesitas verhoogde het aantal langdurige AF episodes in de vroege postoperatieve periode (eerste vijf postoperatieve dagen) na hartchirurgie voor zowel patiënten met coronarialijden als hartklepaandoeningen. De hogere EPoAF last (d.w.z. de verhouding tussen de totale duur van alle AF-episodes en de totale opnametijd) in de vroege postoperatieve periode trad vooral op de derde dag op. Omdat de effecten van obesitas op het AF-substraat omkeerbaar zijn met gewichtsbeheersing, kan een preventieve levensstijl vóór de operatie een belangrijke rol spelen.

Een cohort van 154 bicuspide aortaklep (BAV) patiënten werd in **Hoofdstuk 11** onderzocht op EPoAF-kenmerken (bijv. incidentie, duur en last), evenals preoperatieve risicofactoren (bijv. geslacht, leeftijd, BMI en voorgeschiedenis van AF) en lange termijn follow-up (bijv. recidief AF, overleving). EPoAF kwam voor bij 28% van de BAV-patiënten, had een last van 13,2% en verminderde de AF-vrije overleving significant, maar had geen invloed op de algehele overleving. EPoAF-last was significant gecorreleerd met de mediane en langste EPoAF-episodeduur (r=0,66 en r=0,89, respectievelijk), en mannen hadden een hogere algehele last dan vrouwen (p=0,03). Oudere leeftijd, vergroting van het LA en rethoracotomie waren onafhankelijke risicofactoren voor EPoAF. Ritmecontrole tijdens follow-up van BAV-patiënten met een hoge EPoAF-last wordt aanbevolen om AF-recidieven te detecteren.

Biologische markers van boezemfibrilleren

In het tweede deel van dit proefschrift wordt de focus verlegd naar biologische markers van AF. Alhoewel de onderliggende mechanismen die verantwoordelijk zijn voor de progressie van AF nog steeds niet helemaal duidelijk zijn, wordt atriale

elektro-anatomische remodelling (bijv. LA dilatatie, atriale interstitiële fibrose of littekens) algemeen erkend als een belangrijke factor in de pathogenese van AF. Gebaseerd op de opvatting dat lage bipolaire voltages (≤0,5mV) de aanwezigheid van littekenweefsel en dus aritmogeen substraat impliceert, hebben meerdere studies een significante correlatie gevonden tussen de aanwezigheid van gebieden met lage voltages (LVA) en de progressie van AF.[2] Gezien detectie van LVA momenteel alleen mogelijk is periprocedureel, stellen Büttner et al. voor om natriuretische peptiden te gebruiken om AF-progressie en remodelling middels non-invasieve methodes te fenotyperen.[3] In **Hoofdstuk 12** geven we commentaar op hun waardevolle werk. Biomarkers in het bloed hebben een groot potentieel om te worden opgenomen in de behandelingsketen van AF, gezien ze relatief gemakkelijk toegankelijk zijn en van grote diagnostische en voorspellende waarde kunnen zijn. Helaas was de associatie tussen atriaal natriuretische peptiden en LA-diameter en LVA slechts zwak tot matig, wat aangeeft dat er grotere onderzoeken uitgevoerd moeten worden om de uitkomsten te valideren.

Alle huidige farmacotherapeutische strategieën zijn nog niet gericht op mechanistische hoofdoorzaken van AF die structurele schade aan cardiomyocyten, mitochondriële dysfunctie en vervolgens elektro-anatomische remodelling aansturen, en kunnen daardoor dus ook het ontstaan en de progressie van AF niet voorkomen. Recente experimentele studies laten zien dat heat shock eiwitten (HSP's) de initiatie en progressie van AF kunnen matigen. Een HSP-inducerende stof is L-glutamine. In **Hoofdstuk 13** onderzochten we daarom het effect van L-glutamine op HSP waardes en metabolietniveaus in het bloed van patiënten met AF (N=21). De HSP27 en HSP70 niveaus werden bepaald door middel van ELISA's en de metabolieten met LC-massaspectrometrie. HSP27-niveaus namen significant af na drie maanden suppletie met L-glutamine [540,39 (250,97-1315,63) tot 380,69 (185,68-915,03), p=0,004] en normaliseerden na zes maanden suppletie met L-glutamine [634,96 (139,57-3103,61), p<0,001]. Voor HSP70 daalden de niveaus na drie maanden suppletie met L-glutamine [548,86 (31,50-1564,51) tot 353,65 (110,58-752,50), p=0,045] en bleven laag na zes maanden suppletie met L-glutamine [309,30 (118,29- 1744,19), p=0,517). In tegenstelling tot patiënten met lage HSP27-niveaus bij aanvang van de studie vertoonden patiënten met hoge HSP27-niveaus na drie maanden L-glutamine suppletie normalisatie van verschillende metabolieten, welke verband houden met de metabolisatie van koolhydraten, nucleotiden, aminozuren, vitamines en cofactoren. Alhoewel de kleinschaligheid van deze prospectieve interventiestudie de formulering van sterke conclusies bemoeilijkt, verlaagt suppletie van L-glutamine de serumspiegels van HSP27 en HSP70 binnen drie maanden en normaliseert het de metabolietniveaus in dit cohort. Het is daarom van belang om in de toekomst een grotere en idealiter gerandomiseerde klinische studie uit te voeren om een effect van L-glutamine op de vermindering van AF-episodes te testen.

References

1. LaPar DJ, Speir AM, Crosby IK, Fonner E, Jr., Brown M, Rich JB, Quader M, Kern JA, Kron IL, Ailawadi G and Investigators for the Virginia Cardiac Surgery Quality I. Postoperative atrial fibrillation significantly increases mortality, hospital readmission, and hospital costs. *Ann Thorac Surg*. 2014;98:527-33; discussion 533.
2. Kogawa R, Okumura Y, Watanabe I, Nagashima K, Takahashi K, Iso K, Watanabe R, Arai M, Kurokawa S, Ohkubo K, Nakai T, Hirayama A, Sonoda K and Tosaka T. Left atrial remodeling: Regional differences between paroxysmal and persistent atrial fibrillation. *J Arrhythm*. 2017;33:483-487.
3. Buttner P, Schumacher K, Dinov B, Zeynalova S, Sommer P, Bollmann A, Husser D, Hindricks G and Kornej J. Role of NT-proANP and NT-proBNP in patients with atrial fibrillation: Association with atrial fibrillation progression phenotypes. *Heart Rhythm*. 2018;15:1132-1137.

Financial support for the publication of this thesis was generously provided by:

Erasmus Medisch Centrum Rotterdam
Afdeling Cardiologie, Erasmus Medisch Centrum Rotterdam
Abbott Medical Nederland BV
Fresenius Kabi Nederland BV
Boehringer Ingelheim BV
Chipsoft BV
Pfizer BV